AN INVESTIGATION INTO THE LOSS MECHANISMS ASSOCIATED WITH A PUSHING METAL V-BELT CONTINUOUSLY VARIABLE TRANSMISSION

Submitted by Sam Akehurst
For the degree of PhD of the University of Bath 2001

COPYRIGHT

_____

SUMMARY

Over the last decade or so the environmental pressures of the modern world have been dictating the work of the automotive engineer. Governments, under the pressure of the environmental lobby, have had to increase the constraints which modern motor vehicle must meet, in terms of emissions and fuel consumption.

As the pressures of these constraints mount, the focus of the engineer has concentrated on improving the efficiency of the automobile. Most of the work has concentrated on the vehicle prime mover, the internal combustion engine. However, to date little of the work has concentrated on the transmission of the vehicle and improving its efficiency.

This thesis details the work undertaken in a project to investigate and model the loss mechanism that exist in an automotive pushing metal V-belt continuously variable transmission (CVT). The aim of the project was to investigate the magnitude of inefficiency associated with each of the transmission components, particularly those associated with the belt itself, and develop an understanding of the effects of temperature on these loss mechanisms.

The work entailed the development of a transmission test rig capable of measuring the losses through the transmission at very low power levels. The test rig developed is capable of testing the transmission at controlled low temperatures, with a high degree of accuracy and repeatability. The experimental work carried out on the transmission test rig is also supported with data from a further variator test rig, designed to measure belt slip, and with complete vehicle testing performed on a chassis dynamometer facility.

The thesis introduces a number of new models for predicting both the torque losses and slip losses present in the transmission. Torque loss models are developed based upon the interactions of belt segments and bands and pulley deflections at belt entry and exit conditions. Slip is predicted due to the existence of gaps in the belt. A high degree of interaction between the slip and torque loss models is displayed, whilst both models are validated individually using the collected experimental data. Finally some proposals are made to improve the efficiency of the pushing metal V-belt CVT, based upon the findings of the modelling work.

_____

_____

ACKNOWLEDGEMENTS

_____

TABLE OF CONTENTS

INDEX OF FIGURES

_____

_____

_____

INDEX OF TABLES

_____

_____

NOMENCLATURE

A	Cross sectional area	(m^2)
B	Width of Hydrodynamic contact	(m)
C_x	Segment compressive force	(N)
D	Pump Displacement	(m^3/rad)
E	Youngs Modulus	(N/m^2)
F	Force	(N)
F_R	Band friction force on pulley shoulder and between bands	(N)
F_T	Tractive force on side of segment	(N)
F_{rad}	Radial friction force acing on side of segment	(N)
I	Geometric belt ratio	
L	Length	(m)
M_{seg}	Mass of one segment	(kg)
N	Segment Side Normal Force* or Pulse Counts	(N)*
$\dot{N}_{seg}$	Rate of segments passing a point per second	(s^{-1})
P	Pressure	(N/m^2)
Q	Segment shoulder force	(N)
$\hat{Q}$	Summation of segment shoulder forces	(N)
R	Ideal Radius	(m)
R'	Actual entrance/exit radius	(m)
R''	Radius of maximum penetration	(m)
T	Tension* or Temperature	(N)* or (°C)
Tq	Torque	(Nm)
U	Sliding speed	(m/s)
V	Absolute velocity	(m/s)
$Vrel$	Relative velocity	(m/s)
$Vreq$	Required velocity for no relative motion to occur	(m/s)
W	Power	(J/s)
X	Pulley centre distance	(m)
e	Extension or compression	(m)
h	Oil film thickness	(m)

_____

i	Band number	
m_{belt}	Mass of belt per unit length	(kg/m)
n	Number	
t	Time	(s)
t_{band}	Thickness of an individual band	(m)
t_{seg}	Thickness of one segment	(m)
v	Velocity	(m/s)
x	x direction of co-ordinate system	
y	y direction of co-ordinate system	
α	Inclusive angle of belt	(rad)
β	Angle of wrap	(rad)
ΔP	Pressure difference	(N/m^2)
ΔT	Torque difference	(Nm)
δ	Radial displacement of inner band from segment rocking edge	(m)
δ_{pri}	Axial deflection of primary pulley	(m)
δ_{sec}	Axial deflection of secondary pulley	(m)
δC_x	Change in compression per segment	(N)
δT	Change in band tension across one segment shoulder	(N)
δV	Difference in absolute velocities	(m/s)
δx	Linear displacement of belt components	(m)
ϕ	Angle of action between neighbouring segment	(rad)
η	Efficiency or viscosity*	(kg/ms)*
φ	Pulley exit/entrance wedge angle	(rad)
λ	Coefficient of traction	
μ	Coefficient of friction	
π	Pi	
θ	Half pulley wedge angle	(rad)
τ	Time in a sector of the pulley	(s)
ν	Kinematic viscosity	(m^2/sec)
ω	Rotational speed	(rad/s)
ψ_{act}	Active angle	(rad)

ψ_{idle} Idle angle   (rad)

Subscripts

act	Active angle
actual	Actual operating conditions
axial	Axial
band	Per band
belt	Whole belt assembly
CL	Clutch
complete	Complete transmission
FD	Final drive
Ideal	Ideal operating conditions
idle	Idle angle
loss	Loss
LVDT	Derived from LVDT data
pen	Penetration
pri	Primary
pulley	Pulley
pulse	Derived from pulse count data
pump	Pump
rel	Relative
removed	Component removed
sec	Secondary
seg	Per segment
shear	Oil film shearing
slip	Slip
strut	Strut
wedge	In pulley wedge zone
x	x direction
y	y direction

_____

1   Introduction

Over the last decade or so the environmental pressures of the modern world have dictated the work of the automotive engineer. Governments, under pressure from the environmental lobby, have had to increase the severity of the constraints imposed upon motor vehicles, in terms of both emissions and fuel consumption. Year on year, legislation controlling vehicle emissions has increased, and at the same time governments throughout the world have increased vehicle and fuel taxes in an attempt both to move the population onto forms of public transport and reduce the average engine size in vehicles. As the pressures of these constraints has increased, engineers have concentrated on improving the efficiency of the automobile. Most of this work has been on the vehicle prime mover, the internal combustion engine. However, to date little of the work has concentrated on the transmission of the vehicle and in particular improving its efficiency.

The efficiency of any vehicle transmission system is an important factor in the overall efficiency of the vehicle. With the increased environmental requirements described above it is important to understand where the inefficiencies lie within a transmission design. Continuously variable transmissions (CVTs) have been on the market for a number of years now, and should in principle offer increased fuel efficiency over similarly sized fixed ratio transmissions. By having effectively an infinite number of gear ratios the CVT should allow better matching of the engine operating conditions to the variable driving conditions experienced. For example, Figure 1-1 below shows how a typical CVT system might be controlled so that the engine can be constrained to operate as near as possible to its maximum efficiency point.

It can be seen that this CVT strategy aims for the engine to operate as near to the minimum Specific Fuel Consumption (SFC) region as possible. The vertical part of the CVT running line is set at the minimum engine speed that gives satisfactory engine performance, in terms of acceleration and drivability. It can also be seen that for a large range of intermediate vehicle speeds the transmission is able to maintain the engine in the low SFC regions of the fuel consumption map, in contrast to the typical running lines of a fixed ratio transmission. By operating in this region the vehicle fuel consumption should be reduced. In reality few CVT controllers are optimised purely for SFC; other considerations in controller strategy might

_____

include vehicle emissions and vehicle drivability. In these cases a weighted ideal engine operating line is generated, based upon the perceived importance of each output to the overall vehicle performance.

Despite these theoretical predictions to date reduced fuel consumptions and emissions have not been realised by production cars fitted with CVTs. Rather fuel economy figures compared to equivalent fixed ratio vehicles have been at best equal and in most cases considerably lower. Since the control strategy for reduced fuel consumption is well founded; it must be concluded that existing CVT systems have a lower efficiency than their fixed ratio counterparts.

This inefficiency has been linked to a number of possible inherent parasitic losses associated with CVTs, namely torque losses within the belt mechanism itself, belt slip and hydraulic control system pumping losses. These losses exist alongside the normal losses associated with a standard fixed ratio transmission, namely gear meshing losses, bearing losses, oil churning and windage.

1.1 The Pushing V-belt CVT

1.1.1 A Brief History of the CVT

CVTs are not actually a recent invention; they were in fact first patented as early as the 1850s, but it is only recently that the engineer has begun to realise the benefits that might be available from their use. The term CVT may be adopted for a number of different types of transmission, including hydrostatic and electrical drives, but the pushing metal V-belt drive investigated here is effectively a mechanical traction drive. Within the group name of mechanical traction drives there are a number of different sub-groups, which are now being investigated as viable future forms of CVT. Two such sub-groups are V-belt drives and rolling traction drives. A good overview of rolling traction drive technology is given by Lubomyr [1].

The transmission being tested for this work is based on the Van Doorne pushing V-belt transmission, which is a relatively new design. The complete transmission is the same as that operating in Rover 200 and 400 Series (now 25 & 45 Series) automatic vehicles, and in the MGF sports car as a 'selectronic' derivative of the same transmission.

_____

An overview of the Van Doorne belt is given by Hendriks et al. **[2 & 3]**. Similar transmissions to the one under test have been fitted to small cars such as the Ford Fiesta and Subaru Justy since the mid 1980s. To date there are well over a million of the units operating worldwide. The transmission design has even undergone testing in a Williams Renault Formula 1 racing car, during the early 90s, with successful results.

1.1.2 How the Belt Drive Functions

The main components of the pushing metal V-belt CVT are the belt and the primary and secondary pulleys, shown schematically in Figure 1-2; these three components together may be termed the 'variator'. The ratio at which the transmission is operating can be varied by changing the radius at which the belt rotates on each of the two pulleys. Thus for a low ratio the radius on the primary pulley will be small and the radius on the secondary pulley large, while for maximum over drive ratio the other extremes of belt radius on each pulley are adopted. The variation in belt radius is achieved by changing the axial spacing between the pulley halves. On each pulley set one half of the pulley (sheave) is fixed and the opposing half free to move axially under the influence of a hydraulic actuator. The moveable sheaves of the primary and secondary pulleys are diagonally opposite to each other, such that the belt always maintains a nominal straight line between the pulley pairs. Since the belt is of a fixed length any increase in radius on one pulley dictates a similar, though not equal, reduction in radius on the opposing pulley.

A pictorial section view of the complete transmission, as tested, is shown in Figure 1-3. The transmission is packaged for close coupling to an engine in a transverse front wheel drive arrangement. Power enters the transmission from the engine crankshaft via a torsion damper, to absorb shock loads. This in turn drives a combined hydraulic clutch pack and epicyclic gear set, which is controlled to give either forward or reverse drive directions. Power then passes to the primary pulley, which drives the V-belt. The V-belt then drives the secondary pulley, itself connected to the output differential via two step-down helical gear pairs. An external gear pump is driven directly by the input shaft of the transmission at engine speed and this supplies both the hydraulic clamping pressures and the lubrication oil.

_____

Modulating the pressure to each pulley controls the position of each of the pulleys and thus the transmission ratio, as described above. The ratio at which the transmission operates is implemented by the transmission control system, a complex manifold of hydraulic valves situated in the sump of the transmission. By decreasing the ratio of secondary to primary pressure the drive ratio is decreased, i.e. a higher gear is selected. The secondary pressure is controlled so that the tension in the belt and clamping force on the secondary pulley are high enough to prevent excessive belt slip, while the volume of oil in the primary actuator is controlled to dictate the position of the primary pulley and thus the ratio. The system controls the transmission ratio as a function of gear selector position, engine throttle position and engine speed. Within the controller manifold there are two main control valves, the primary valve and the secondary valve. In addition there are also valves to control clutch modulation at launch, although these are not significant in this work.

The metal V-belt itself is constructed from approximately 400 steel segments held together by two sets of steel bands, running in slots in the segments as shown in Figure 1-4. Each of the sets of bands (band pack) is made up of a number of individual bands, but generally between 8 & 12. A peg on the front of each segment engages in a hole on the back of the preceding segment, thus ensuring the segments run perpendicular to the direction of motion. In operation the pressures applied to the pulleys causes a tension to exist in the steel band packs; this tension acts to prevent the compressed segments from buckling out from their lines of travel. Under certain conditions the bands assist in the torque transfer process alongside the compressive force built up between the belt segments. This is discussed in more detail in future sections of this thesis, dealing with the modelling of the transmission.

The hydraulic control manifold is shown pictorially in Figure 1-5, in which the inputs to the controller can clearly be seen. The kickdown cable is effectively the driver demand or input to the system, along with the selector shaft position determined by the gear stick position. The sensor shoe closes the loop of the controller by feeding back the position of the primary pulley, and thus the actual ratio, to the system. The controller also has inputs of engine speed from hydraulic pitot tube assemblies on the input shaft of the transmission. From an engine speed input and throttle position input the controller modulates the secondary pressure to cope with the expected input torque. Similarly the throttle position also gives an indication of the driver's wishes and the change up and change down decisions are made by the controller.

_____

The effect of a typical controller on the driving characteristic of the vehicle is shown in Figure 1-6, which plots engine speed vs. vehicle speed for a number of operating conditions. At the point (A) drive is engaged, at low engine speed. As the engine speed increases the automatic wet clutch begins to engage (B). The vehicle then continues to accelerate steadily (C→D) at a constant engine speed, approximately 1700 rev/min, until the high ratio limit is reached (D). The vehicle then continues to accelerate to (E) the maximum cruising speed. Point (F) is the maximum speed point. Route (G→H→F) is the maximum power route, using the kick down facility. Operating the kick down at any other point will result in a jump horizontally to the maximum power route (I). The more acceleration demanded, via throttle position, the further to the right the graph moves (J).

1.2 Definition of Parasitic Losses

Work by Simner **[4]** defines the losses that occur within a transmission into four distinct areas: parasitic losses, power proportional losses, weight and inertia, and transmission configuration and control. A number of papers have been written on the subject of CVT control strategy and a number of models have been produced analysing ratio change for the metal pushing V-belt CVT design. However, to date little work has been undertaken to investigate the parasitic or the power proportional losses in CVTs, even though the parasitic losses are becoming steadily more important.

By definition, parasitic losses are those that occur under no-load conditions and are independent of the power being transmitted by the transmission. Parasitic losses are mainly speed dependent, but due to the effects of viscosity, they are also highly temperature dependent. In a manual transmission parasitic losses are simple to define, namely oil churning and seal and bearing drag. However, within a CVT it becomes harder to define parasitic losses. For the purpose of this project it is assumed that parasitic losses will include the above mentioned losses, plus pumping losses in the control system, drag losses in the clutch packs and any belt-dependent losses.

The work described in this thesis concentrated essentially on the no-load losses that occur within the transmission, and the effects of low loads through the transmission. Throughout the work, the losses will be described in terms of torque loss rather than efficiency. This method

_____

has been chosen since the efficiency calculation can vary considerably depending on the amount of power being transmitted, despite the fact that the energy loss from the transmission is the same. This can be shown clearly by examining two extreme scenarios. Consider a transmission with a torque loss of 1 Nm at all operating conditions; firstly with a 2 Nm torque input the transmission the efficiency would be 50% and secondly with 100 Nm torque input into the transmission the efficiency would be 99%. This is the same transmission with the same losses, yet for two different test conditions the efficiency varies by nearly 100%.

It is useful to look at the low power torque losses for two reasons. Firstly, it allows the parasitic losses to be isolated from the power proportional losses and secondly, it gives useful data around the real operating conditions that a vehicle will experience. A considerable amount of the operating cycle for a car is actually at very low torque levels, compared to the maximum torque available from the engine. Figure 1-7 shows the proportion of time that a vehicle spends over a range of different torque levels while undertaking a standard FTP75 drive cycle. It can be seen that nearly 50% of the cycle time is spent at torque level of 10-19%, and some 90% of the drive cycle is spent below 50 % of maximum engine torque. This would therefore indicate that any reduction in parasitic losses would greatly reduce fuel consumption and emissions over a similar drive cycle test. In addition there is the fact that drive cycle test legislation now requires ambient temperature starts to tests, and that future legislation will include a sub zero start condition. These reduced temperatures will only lead to an increase in the parasitic losses and so it can be seen that the development of an understanding of these losses is essential in order that they might be reduced. This would help improve the performance of CVTs, both in legislative tests and more importantly everyday driving conditions.

_____

1.3 Objective

The work described in this thesis aims to identify the parasitic loss mechanisms associated with a pushing metal V-belt CVT. The transmission was tested on a specially developed test rig under controlled conditions, which resulted in the development of a second test rig. The results from both test rigs were then used in the development and validation of mathematical models of the losses occurring in the transmission. In particular the work on the original test rig aimed to investigate the effects of lubricant temperature on the losses in the transmission, especially those of low temperatures. This was planned to replicate conditions similar to those experienced on short journeys, in cold morning start up situations or in future cold start legislative emissions tests.

1.4 Layout of the Thesis

This thesis has been split in to a number of different sections in an attempt to make its navigation a simpler task. Chapter 1 introduces the project and the pushing metal V-belt CVT concept, with a brief history of CVTs and the fundamentals of the transmission function. This is followed, in chapter 2, by a review of the existing work that has been undertaken in the field of this research. Chapter 3 introduces some experimental work performed on a chassis dynamometer facility to assess the performance of the belt drive CVT, compared to a manual transmission vehicle. This includes some cold ambient temperature studies of transmission warm up times and the collection of a range of transmission operating parameters over standard European drive cycles. Chapter 4 is dedicated to describing the transmission test rig, which was developed as part of this project. This rig was used to collect a vast amount of data on the torque losses occurring in the transmission as a whole and for individual components. Chapter 5 describes these experimental results. Chapter 6 introduces a second test rig developed for this work and the experimental results therefrom. This second test rig was developed to test the variator in isolation and investigate in more detail the existence of belt slip losses. The results as analysed in chapters 5 and 6 constitute experimental data suitable for validation with the mathematical models developed in chapters 7 & 8.

_____

_____

Chapter 7 describes the modelling of the other components in the transmission such as the pump, clutch and final drive. Chapter 8 concentrates on analysing the belt losses mathematically, models for both torque losses and belt slip are introduced and validated against experimental data. Chapter 9 & 10 discusses methods for improving the efficiency of the belt drive transmission. Finally chapter 10 contains conclusions drawn from this work and proposals for possible future work respectively. A number of appendices are included at the end of the thesis including computer model print outs and data collected from the chassis dynamometer test work.
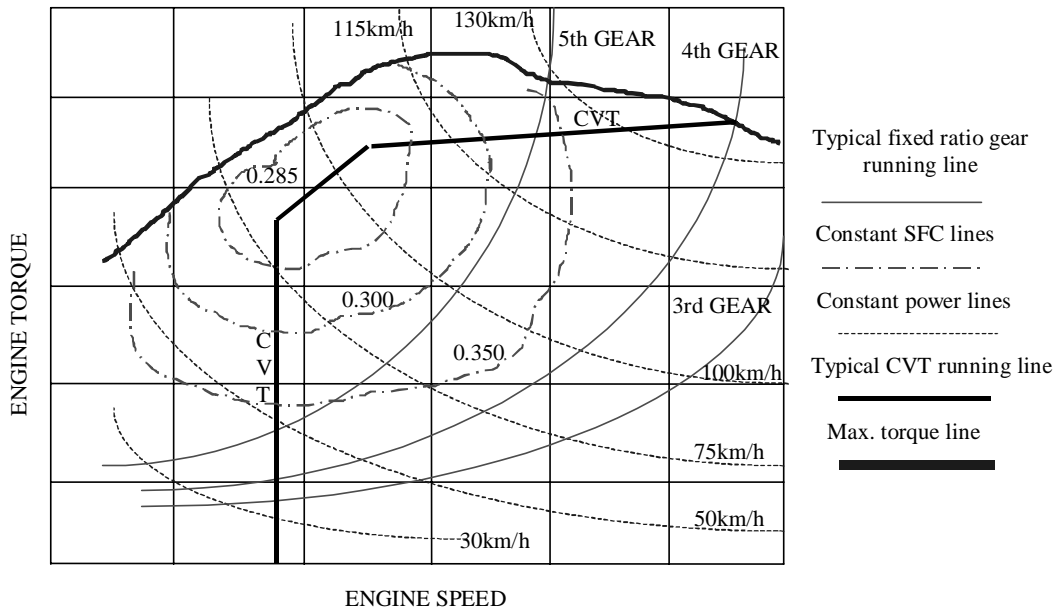
Figure 1-1 A Typical CVT Driving Strategy for Fuel Economy
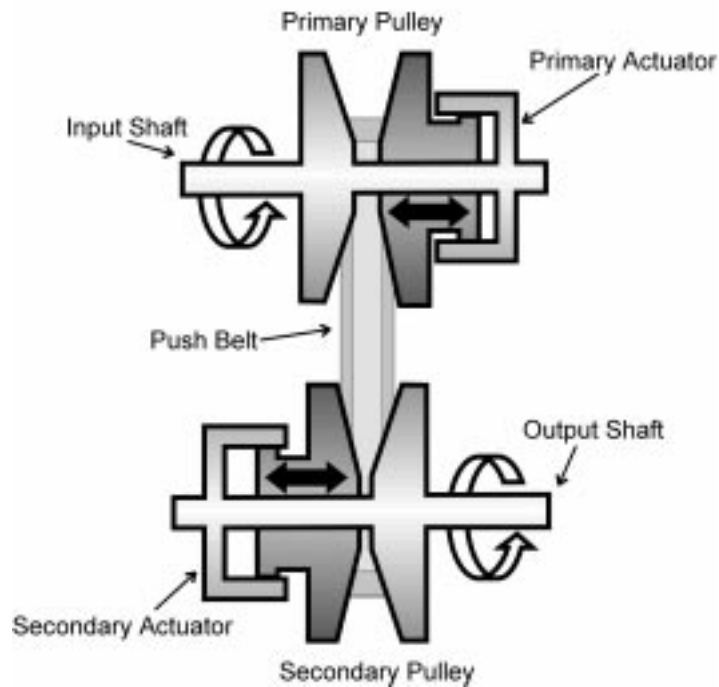
Figure 1-2 Function of the Van Doorne Variator (Brace [5])
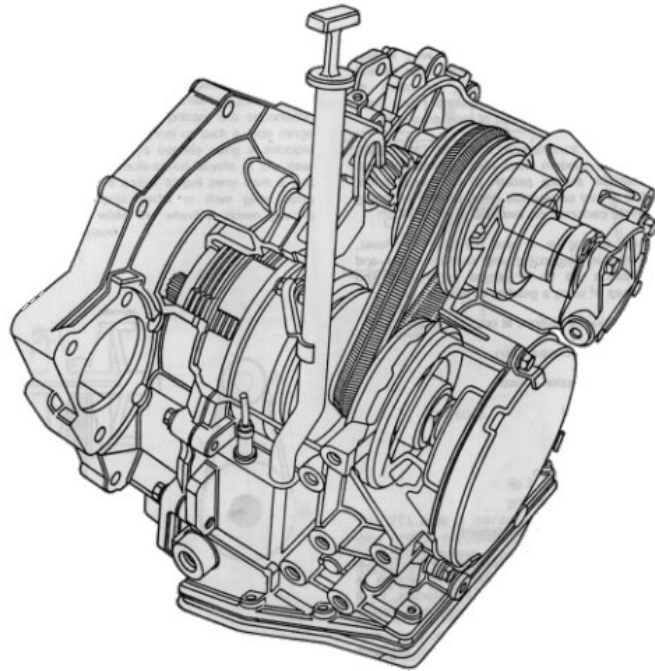
Figure 1-3 Section of the Transmission (Rover Group [6])

Each band pack contains 12 separate bands

Direction of Travel

Direction of Travel

Rocking Edge

Socket

A

Peg

Belt Segment

Rocking Edge

A

Section A-A
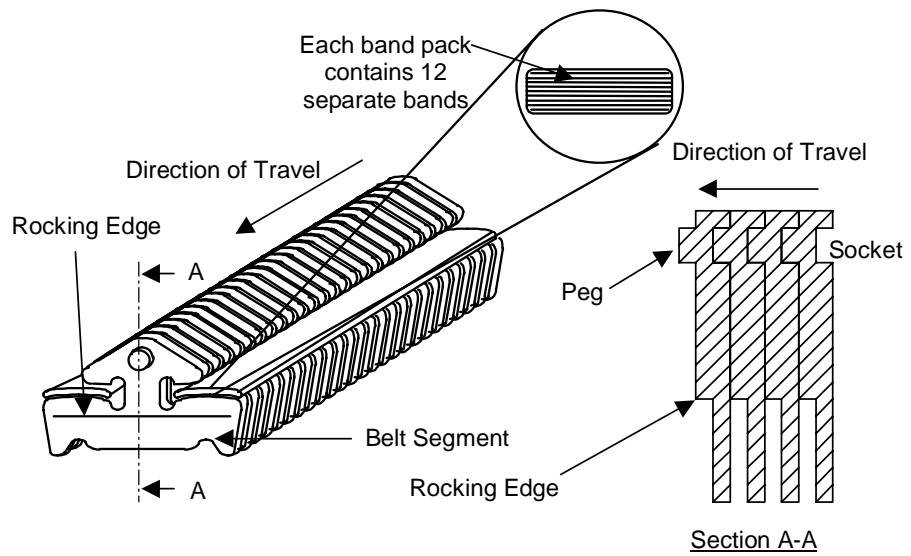
Figure 1-4 The Metal Pushing V-belt
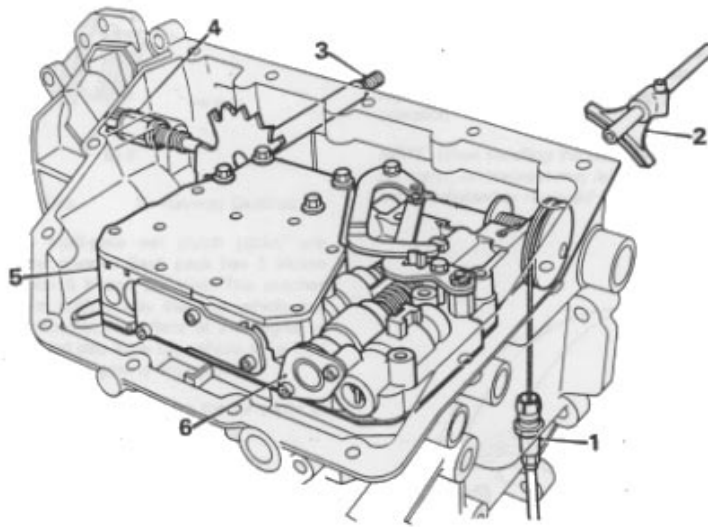
Figure 1-5 Transmission Controller Manifold (Rover Group [6])

1. Kickdown cable from engine throttle assembly
2. Sensor shoe for feedback of primary pulley position
3. Selector Shaft for Park, Drive, Low, Reverse Selection
4. Starter inhibitor switch
5. Hydraulic controller manifold
6. Primary control valve
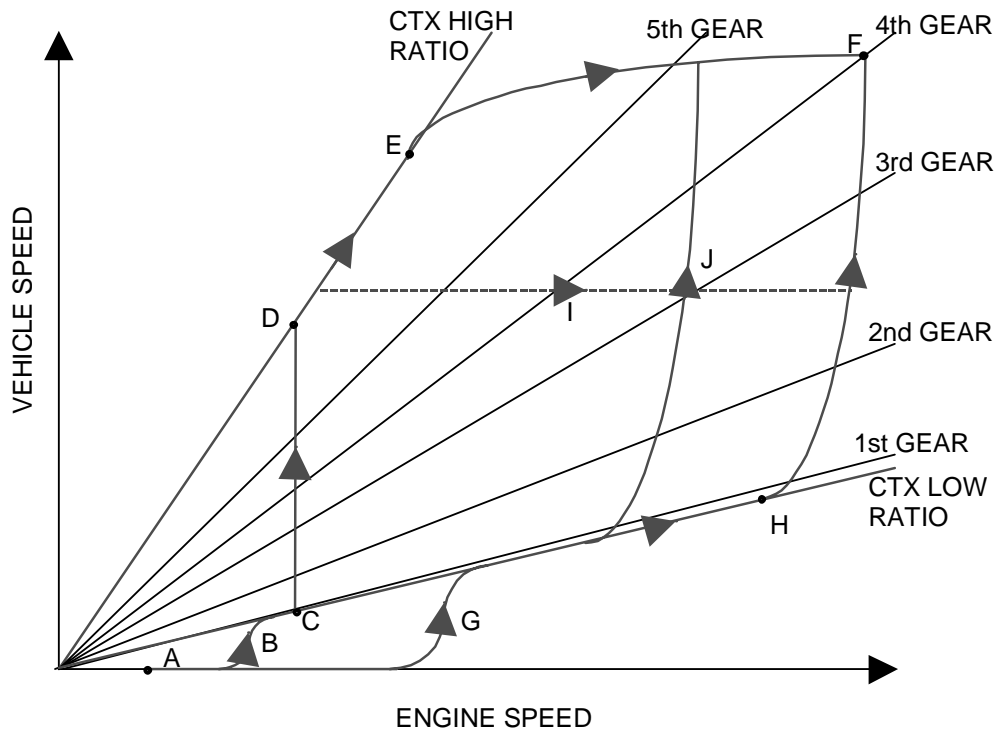
Figure 1-6 Variogram of the Control Strategy Associated with the Transmission.
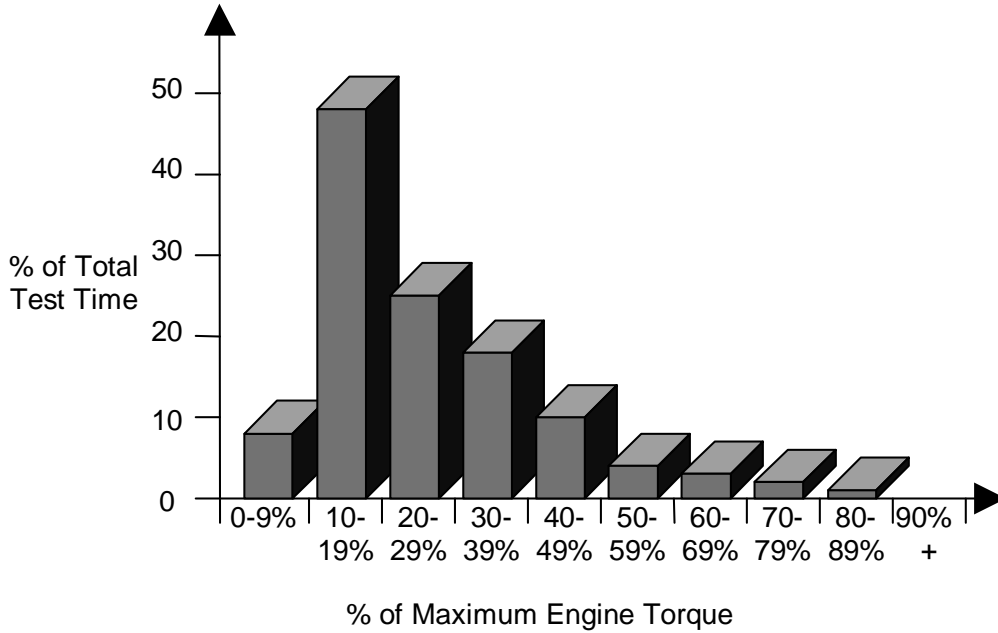
Figure 1-7 Percentage of Time Spent at Torque Levels on FTP75 Drive Cycle (Simner [4])

2   Existing Work

This section reviews previously published work related to the objectives outlined above. It has been split into a number of areas: metal pushing V-belt mechanics, clutch drag losses, pump losses, general transmission losses, lubricant modelling and CVT control strategies. The latter of these is reviewed in less detail, as in general CVT control strategy is well founded. However, the subject does have a bearing on the fundamentals of CVT operation, while the control pressures, the output of any control strategy, are a major input to many of the likely loss mechanisms.

2.1 Losses in CVTs

Very little research has been published specifically regarding the efficiency of CVTs. Of the work that has been produced, much is aimed at the traction drive toroidal CVT system, which as a mechanism is considerably different to the multi-component belt drive CVT.

Ide **[7]** produced an interesting study of the effect of various components in the metal V-belt CVT on the fuel economy of a vehicle. The author identifies the major power loss mechanism as the hydraulic pump and the belt. At low speeds the major loss mechanism is the pump, while at higher vehicle speeds the belt loss becomes greater. The paper details complete vehicle simulation work performed using measured loss data. It concludes that for improved performance in all speed ranges both the hydraulic pump losses and the belt losses need to be reduced. The author performs some simulation based on theoretical improvements in pump and belt efficiency. For example a 50% reduction in belt torque loss results in approximately 5% improvement in vehicle fuel consumption, while a 50% reduction in the hydraulic pump torque loss produces nearly 4% improvement in vehicle fuel consumption. These results are compared to the necessary reduction in vehicle weight to achieve similar fuel economy improvements. Both these results are based on the Japanese 10-15 mode drive cycle. At higher average vehicle speeds the effect of belt torque loss is much greater. For example a 50% improvement in belt efficiency at 60 km/h results in a 6% improvement in vehicle fuel consumption.

_____

The author proposes a number of methods for reducing the loss mechanisms. These include marginal control of the secondary pressure and increasing the effective friction coefficient between the belt and pulley, by oil formulation design, so that lower clamping pressures may be used. However, the author expresses concern over the effect an increase in friction coefficient may have on moving parts in the belt mechanism, in that the belt torque loss could actually increase. Interestingly, the author shows that a very good relationship exists between steady state torque loss values and those recorded during ratio change transients.

Abo et al. **[8]** researched the loss mechanism in the metal V-belt CVT from a different perspective. The aim of their research was to investigate the rate of heat generation in the transmission with respect to slip speeds between mating components. The authors model a slip speed between the belt and pulley using a gap closure method as proposed by Kobayashi et al **[9]**, which is discussed later in this chapter. Any slip speed between the segments and bands was assumed to occur only on the pulley with the smallest radius. The slip between neighbouring bands in the band packs is calculated in a similar way. All the energy loss due to the slipping contacts was assumed to be converted into heat energy, since noise and vibration energy are likely to be small.

Simulation results indicated that at constant belt speeds belt heat generation is greatest when the belt ratio is low (high loads between components). Losses also increase if the input torque is large (more slip likely) or the belt speed is high. The simulation results were validated using a test rig facility. The heat generation measured experimentally, by recording the temperature rise of a known volume of lubricant, is assumed to be due to the bearings and the belt mechanism. Due to stable temperatures in the laboratory, heat losses to the laboratory are assumed to be negligible.

2.1.1 Metal V-belt Mechanics

A number of papers have been published over the last two decades, attempting to model the mechanisms and events that occur within a pushing V-belt CVT. These papers vary greatly in their level of complexity and their mode of analysis. They also vary according to which specific aspect of the transmission they model. Many papers simply analyse the force

_____

_____

distributions in the transmission, while others target the loss mechanisms and some concentrate solely on generating models to describe the torque capacity of the belt.

The original pushing V-belt models were often derived from existing models and the principles of rubber tension V-belts. However, due to the considerable differences in the construction and operation of the two types of belt, this approach acts only as a starting point.

Two of the earliest models for the metal compression belt are the works by Gerbert **[10]** and Becker **[11]**. Becker in particular produced a fundamental analysis of the forces acting within the belt mechanism, which is the basis to many other papers discussed here. The work by Becker is in no way flawed but the end results were not developed to produce useful information such as torque losses, while belt slip was not investigated or discussed. Much of the work by Gerbert & Becker was the basis for that undertaken at the University of Bath by Micklem et al. **[12,13 & 14]**, who produced some quasi-empirical models for losses that exist in the belt system.

Micklem produced a number of models to describe torque loss in the belt system, and a number of papers were published on the subject. The first of these papers, **[12]**, introduces a number of models of the steel pushing V-belt. These include models of viscous shear losses between the bands and a belt slip model based upon Elastohydrodynamic Lubrication (EHL) theory, which predicted an EHL regime existing between the belt segments and pulley contacts. An empirical model predicting a torque loss mechanism due to the belt wedging into and out of the pulleys is also developed. The modelling work undertaken by Micklem was adopted by Guebeli **[15 & 16]** for his work on optimising the efficiency of a CVT by optimisation of the hydro-mechanical controller. This work highlighted the flexibility of reducing the pump losses in the transmission by reducing the clamping pressures; however, this must be balanced against the increasing rates of belt slip that occur. A similar optimisation scheme is also discussed in a further paper, Vaughan et al. **[17]**, to which Guebeli is a co-author.

The second paper by Micklem et al. **[13]** describes in more detail the empirical torque loss models, due to the pulley wedge effect, introduced in the first paper. While the final paper Micklem et al. **[14]** describes all the additional losses in the transmission and methods of reducing the losses associated with the metal V-belt drive.

_____

_____

Since this work was performed by Micklem a number of changes have been made to the design of the metal V-belt, in particular the design of the segment has been changed (Liebrand [18]). In addition to these design changes, more research has been performed, which has proven a number of Micklem's modelling assumptions to be inaccurate. This research is discussed in more detail in the remainder of this section. The design changes to the segment of the belt are twofold. Firstly the segments have been made thinner in the force transfer direction, thus increasing the number of segments in the belt. This was done primarily to reduce a number of noise problems that existed with the original belt design and allow tighter curvature of the belt around the minimum radius operating condition. The second modification to the belt segment is the design of the contact side with the pulley. This has been changed from the original shot blasted design with irregular deep pits to a regular profiled section with grooves running in the travel direction of the segment. The original design of the segment was often proposed to hold oil deep in the cavities so that there was always a supply available for lubrication during the contact period. The new segment design appears to have been designed specifically to break down the formation of any lubricant layer. In his work Micklem made a number of assumptions the validity of which are now suspect. These included uniform band tension throughout the variator, uniform loading and unloading arcs about the complete angles of wrap and his assumptions of the distribution of band speeds within the band pack.

More recently research has been performed by Asayama [19], Karam & Play [20] and Fujii & Kanehara [21,22,23 & 24]. Experimental work by Fujii & Kanehara has shown that both the belt tension and compressive forces between sequential belt segments will vary within the wrap angles on both the driving and the driven pulleys, in a non uniform way. This is a factor not considered in any of the work by Micklem et al.

Based on these original experimental findings Fujii & Kanehara have produced a number of subsequent publications each expanding to a degree on the previous work. The original work Fujii et al. [21] was a simple experimental analysis of the pulley clamping force ratios required to maintain a fixed belt ratio at a variety of different torque levels and input speeds. The effect of speed on the pulley clamping force was found to be much more significant than the torque load effects. In their second paper, Fujii et al. [22], the authors introduce some experimental techniques to measure the band tension and segment compression forces. Experimental

_____

_____

results are introduced showing the distribution of segment compressive force and band tension about the contact arcs, which differ considerably between the driving pulley and the driven pulley. The authors draw a number of conclusions, including the existence of active and idle angles on the driving pulley and the magnitude of torque transmission by the bands, which may be up to 40~45% under some operating conditions. The authors also proposed that the band tension distributions are due to the speed differences that must exist between the bands and segments. Tension distributions are shown to decrease around the smaller of the two pulleys in the direction of belt travel.

The third work of Fujii & Kanehara [23], is of particular interest. The authors produced a number of strain gauged segments to measure forces acting in a number of directions on the segment. In general, the results from the test work should be used only to assess trends occurring in the variator and not quantitative values for the forces. It should also be noted that the tests were performed under less than realistic test conditions so that the instrumentation could function. Specifically belt speeds were very slow (1.1 m/s), which negates significantly the effects of centrifugal forces. In addition very low clamping pressures were used (6 bar), thus reducing the gross forces acting in the transmission. The results from this experimental work are discussed below in more detail due to their significance for this work. The forces discussed are defined in detail in Figure 2-1.

Pulley Normal Force (N):

Measurements by the authors indicate that the pulley normal force is not evenly distributed about the contact arcs. As expected the normal force per segment is lower on the pulley with the larger angle of wrap but on both pulleys the segment normal force peaks at the entry and exit locations. This can be assumed to result in higher losses associated with pulley bending around the entrance and exit conditions. The author proposes that the force spikes were due to elastic deformations of the pulley surfaces around the exit and entry locations. Quantitative results were not produced as the author believes that the design of the sensor block for this measurement may have resulted in a less stiff segment, thus reducing its loading.

Segment Compression Force (C_x):

Compressive force results show clear evidence of the compressive strut changing sides in low ratio, and a much faster build up of compressive force in a loading arc, when compared to the rate of force unloading on the opposing pulley. Due to the nature of the measurement

_____

_____

technique used, compressive force distributions could not be measured in the straight section of strut. The authors made approximations of a straight line fit between the exit and entry conditions on each of the pulleys, which appears to be a satisfactory assumption.

Segment Transmitting Force (F_T):

The transmitting force on the side of the segment was also measured experimentally. In low ratio this force was shown to act in a positive sense at the primary pulley (i.e. the pulley driving the segment), while the force is reversed at the secondary pulley with the segment effectively driving the pulley. In low ratio the transmitting force was always larger at the secondary pulley than the primary pulley. Similar results were achieved in high ratio, but with evidence of 'idle' and 'active' sectors existing on the primary pulley. In general measurements of the transmitting force were poor compared to the other results presented in the paper and the author expresses a concern that there might be other forces interacting with the chosen measurement method.

Radial Friction Force (F_{rad}):

The radial force acting on a segment was also measured. This appears to act mainly in the outward radial direction (i.e. restricting penetration of the segment into the pulley), except at the point of exit from each pulley, where the force acts to retain the segment in the pulley wedge. No scale is given on the radial force results and therefore assessing the magnitude of the force is difficult. However, if the forces were large there would be a significant effect of these forces visible on the segment shoulder force results. Since no large effect is seen it can be assumed that the radial friction force is not significant when compared to the other forces. The large radial force associated with the pulley exit appears to coincide with the large increase seen in pulley normal force at the same location. The existence of this force would seem to justify the pulley wedge loss proposed by Micklem et al. [12] discussed earlier.

Segment Shoulder Force (Q) and Shoulder Traction Force (F_R):

Segment shoulder traction force is shown to act in the opposite direction on opposing pulleys and also swap direction between high and low ratio. These forces are coincidental with the changes in band tension measured by the authors and others. The segment shoulder normal force appears directly proportional to the band tension and the radius on each pulley. This is confirmed as measurements of the segment shoulder forces are used by the authors to

_____

_____

derive the values for band tension. Fujii et al. propose the following equation to calculate the band tension -

$$T = \frac{QR}{t_{seg}}$$

where T is the band tension, Q is the segment shoulder force, t_{seg} is the thickness of a segment and R is the belt radius. Hence in high ratio the force is lower on the primary pulley and increases towards the exit of the pulley and on the secondary pulley the force is higher and reduces towards the exit of the secondary pulley. Conversely in low ratio the segment shoulder normal force is higher on the primary pulley and reduces towards its exit, while at the secondary pulley the force is less, but it increases in the direction of travel around the pulley.

The fourth paper in the series, Fujii et al. **[24]**, details similar experimental force measurements but in this case recorded while the belt ratio is changing. The paper does, however, introduce in detail the experimental methods for recording the forces. In general the conclusions from the work are that the force distributions during ratio change are considerably different to those seen under steady state test conditions. In particular the radial force component becomes more significant during ratio changes.

None of the Fujii papers described above includes theoretical modelling of the events measured experimentally. However, Fujii & Kanehara have co-authored a further paper, Kuwabara et al. **[25]**, which produces some numerical models to analyse the power transmitting mechanisms of the metal V-belt. A number of assumptions were made in the modelling; these included the neglecting of pulley bending, radial friction forces and centrifugal force effects. In general the results compare reasonably well with the experimental measurements (with some of the phenomena not being modelled). However, as discussed previously the Fujii experimental data was collected under low speed conditions. Therefore, the assumption of ignoring centrifugal effects is probably not valid for modelling the belt under normal operating conditions.

Asayama et al. **[19]** produced a theoretical model to describe variations in band tension and segment compression force that were measured experimentally. The belt tension model shows good correlation with their experimental results. However, the compressive force model appears to be less accurate. The authors introduce the existence of relative motion

_____

_____

between the bands and segments, as they have a different radius of rotation, and use this to predict changes in band tension. Some experimental measurements of band tension and segment compression forces were performed in a similar method to that used by Fujii et al. The main aim of the theoretical analysis was to produce a prediction for clamping pressures, such that no gross belt slip would occur. A form of 'micro-slip' between segment and pulley is predicted based upon elastic strain of the segments. However, it appears that elastic deformation of the bands is ignored. The authors improved the accuracy of their simulation by including an arbitrary deflection in the pulley sheaves, resulting in a non-circular travel path for a segment around the contact arc. In general the experimental results in the work of Asayama et al. are very similar to those shown in the work of Fujii et al. thus increasing confidence in the validity of their measurements.

Kim et al. [26] investigated the belt behaviour and slip characteristics both analytically and experimentally. The authors propose a radial movement of the belt within the contact arc, thus making the belts trajectory noncircular, which adds radial friction force components to the loss mechanisms. It is proposed that the belt radial motion is a contributory factor in explaining the active and inactive areas within the contact arc, and that the magnitude of the active area is integral to the design of the torque capacity of the transmission. The paper assumes that band tension is constant, an assumption that has been disproved by the experimental work of Fujii et al. [22]. It is also assumed that the inertia forces can be neglected and that the coefficient of friction remains constant. The theory derived in the paper produces radial displacement several magnitudes smaller than the experimental apparatus is able to measure, and the experimental results indicate that the analysis is inaccurate at the inlet and exit conditions of the pulley. In general the paper appear to derive a number of theories from poor assumptions and validate these using experimental results which show nothing as the phenomena predicted are too small to be measured with the experimental apparatus.

Karam & Play [20] also modelled the metal V-belt mechanism. Due to the large number of parts, they adopted a numerical approach to derive global equilibrium equations from the elemental part equations. The model proposes that the steel bands actively function in the power transmission mechanism of the drive. The model takes into account a number of hypotheses and assumptions in its development. It is assumed that the segments are always in compression and thus an initial tension exists in the steel bands when at rest, the bands

_____

_____

are also assumed to be rigid and so their length may not change and that the flanges of the pulleys are also rigid. Many of the simplifying assumptions made in this work have been shown to be significant by other authors.

Karam & Play also subdivide the contact arc about each pulley into two zones, the adherence zone and the sliding zone. The adherence zone is defined as that where the segment and pulley forces remain constant, while the sliding zone is the region where the compressive forces between segments are either built up (driving pulley) or unloaded (driven pulley). The authors draw a number of conclusions from their work. The relative motions of the many elements that exist within the belt mechanism add to the difficulties in modelling its mechanical behaviour. The distribution of the power transfer between the different mechanisms is governed by the coefficients of friction used. Belt efficiency is at a maximum at a ratio of 1, the steel bands aid power transmission for low ratio conditions, but act against power transmission in high ratio conditions. Extending the modelling to include pulley flange deformation increased the calculated axial force values by more than 10%, but made insignificant changes to other calculations. It did however, remove some existing discontinuity problems.

Lee & Kim **[27]** have very recently produced an analysis of the metal V-belt. Like many other authors the aim of their work was to further understand the clamping pressures required on the V-belt system to transmit torque. From the theoretical modelling it is proposed that the hydraulic system clamping forces may be optimised to improve the efficiency of the transmission. Therefore the analysis performed by the authors leads to calculations of the required clamping forces for specific torque and ratio combinations. The authors derive these equations for a number of different conditions, namely low ratio low load, low ratio high load, high ratio and as a special case at a belt ratio of one. For each condition above the authors have split each of the pulley contact arcs into three distinct regions in which

1. The segment compressive force and band tensions remain constant
2. The band tension only changes
3. Both the band tension and segment compressive force vary

For each of these regions and for each pulley an axial compressive force requirement is calculated. The total axial force at each pulley is then the sum of each of these component parts. The authors found that for their derived theory to fit experimental data it was necessary to implement a variable coefficient of friction between the segments and the pulleys which

_____

increases linearly as the speed ratio decreases. Lee & Kim thus appear to have derived interesting proposals based upon variations in band tensions and segment compression forces similar to those described by other authors such as Fujii et al. **[22]**.

Sato & Kato **[28]** produced a paper analysing the torque transmitting forces in a steel pushing V-belt. The analysis is similar to that performed by many other authors, including Becker **[11]**. The results from the simulation are interesting, but concentrate on examining force distributions around the contact arcs using a segment by segment method. The results tend to agree with other work, with changes in tension and active and idle angles appearing in the results, but no validation is performed against experimental data and the aim of the analysis is rather unclear.

Kanehara et al. **[29]** introduced models of the belt drive to investigate the effects of the coefficient of friction acting between the bands and segments of the belt. The paper is co-authored by Fujii and identifies 6 coefficients of friction that may be varied to achieve a good modelling fit to experimental results. These include radial segment friction, tangential segment friction and friction between the bands and segments. The simulation in effect concentrates on changes in ratio and the effect of up-shift and downshift conditions on the friction coefficients between the components. A later and paper investigating the same shift effects, and also co-authored by Fujii exists, Fujimura et al. **[30]**.

2.1.2 Belt Slip Modelling

A paper by Kobayashi et al. **[9]** investigates the mechanisms causing micro slip in the metal V-belt. The analysis focuses on the distribution of gaps between the segments of the belt. It is hypothesised that gaps exist between the segments and these gaps cause slip to occur between the segments and the pulley in order that the gaps may be closed to generate compression force between them. Experimental measurements of belt slip through the whole transmission were recorded as well as experimental measurements of the friction vs. slip speed characteristic between segment and pulley. A simulation method was then developed to predict the slip-limit torque of the belt. The simulation also allowed the analysis of different ratios and clamping forces on the slip limit, such that it could be used to determine suitable pulley clamping forces for a range of operating conditions. Slip ratios of 3~4% were measured

prior to the slip-limit torque being reached. The slip hypothesis made a number of assumptions; these included the slip only occurring on the pulley where the gaps were present and that the gaps present are distributed evenly in an idle sector at the entrance to the loading pulley. The paper presents experimental validation for the gap theory by using a high speed camera to photograph a belt in operation with 26 mm of segments removed from it. A number of models were built up based upon the modes of belt operation proposed by others, and performing a force analysis on the segment and band similar to that of Becker [11]. The mean gap was calculated in terms of any initial gap plus segment compression and band extension. Experimental data were collected at fixed ratio conditions by mechanically restraining the axial displacement of the movable half on the primary pulley, a factor that could influence the function and mechanisms of the transmission. Initial simulation results showed favourable comparison to micro-slip, but failed to predict accurately the slip-limit torque. This was overcome by including the effects of a slip speed dependent friction coefficient, as measured experimentally. The results from the work were used to predict required clamping forces rather than loss mechanisms that might occur in the transmission. The test method used did not measure any changes in actual belt ratio or investigate the occurrence of slip at individual pulleys.

2.1.3 Belt Misalignment & Pulley Deflection Effects

Kobayashi [9] also co-authored a later paper, Shimizu et al. [31], investigating the dynamic behaviour of the metal pushing V-belt. The theory models the variator mechanism as a whole using Finite Element Analysis (FEA). The aim of the research was to study the forces acting on the belt components and quantify the stresses occurring within the components. The downside of this complex modelling was CPU run times of approximately 100 hours per operating condition. The simulation work showed a reasonably good fit to experimental data for the band tensions. The authors then added to the simulation the effects of belt misalignment as described by Robertson & Tawi [32] and Hendriks [2]. The authors used this to investigate the effects of the misalignment on the band tension distribution and the belt torque capacity. The results of the simulation indicated that with increased misalignment the maximum tension in the bands would increase. The simulation also indicated that the active arc, in which segment compression force changes, on the primary pulley increases as the

_____

belt misalignment is increased. This indicates that increased belt misalignment effectively reduces the torque capacity of the belt drive.

A number of the papers discussed previously have shown that the addition of a simple pulley bending model can improve the fit of a model to the experimental data. A number of authors have investigated this aspect of the metal V-belt CVT, using pulley deflection methods to model the transmission and understand its function. One such paper is the analysis provided by Sorge [33], who investigates the effect of pulley bending on V-belt mechanics. The author applies the virtual displacement approach to give approximations to belt trajectories, tension distributions, axial thrust and slip. Unlike rubber belts the elastic deformation of metal belts is small, and generally may be neglected in comparison to the flexural deformation of the pulley, especially for large wrap radii. The paper analyses the bending of the pulley halves, as annular plates fixed at the inner edge, and assumes the belt to have infinite rigidity in both the longitudinal and transverse directions. The author concludes that the influence of pulley deflection is important when the belt trajectory is close to the outer radius. The influence decreases near the middle radius and becomes negligible near the inner clamped radius. Therefore at large radii the assumption of high belt stiffness is apt, but at smaller radii a mixed model should be adopted accounting for the deformation of both components. Although the analysis is an interesting approach to the problem from a new angle, the results and significance of the findings appear to be lost, with insignificant variables, such as sliding direction vs. pulley angle, being the validated output of the simulation.

A similar investigation of pulley deformation was performed by Sattler [34], analysing the mechanics of the belt drive considering both longitudinal and transverse belt stiffness, belt misalignment and pulley deformation. The author however opted to use an FEA approach to the modelling of the pulley deformations. The pulley is considered to deform in two ways, purely axial deformation and a skew deformation. The belt radius within the pulley is then determined by the addition of a local transverse compression of the chain and the shape of the pulley groove. Power losses in the wrap angle were predicted although, validation to experimental data was difficult as no internal losses in the belt were modelled. The sliding motion on the pulley is predicted to cause a 2% power loss at rated torque using ideal clamping forces, but this can double with some of the clamping pressures actually implemented. Under optimal force conditions the pulleys of the variator should exceed 97% efficiency, although additional losses exist associated with events within the belt itself.

_____

_____

Gerbert **[35 & 36]** also investigated pulley deformations. The author identifies three types of pulley flexibility, namely local deflections, plate deflections and skew pulleys. Local deflections are defined as local elastic deflections of the pulley surface and belt, while plate deflections are those associated with the properties of the pulleys, which produce global deflections not associated with localised forces. Finally the skew pulley effect is due to tolerances in the manufacture of the two pulley halves allowing them to move relative to each other. The author indicates the difficulty in modelling the final phenomena, as it is possible for these tolerances to change throughout the life of the transmission. Thus a pulley pair originally assembled such that only small skewness levels existed could end up displaying high levels of skewness later in its life.

On a similar subject, Robertson & Tawi **[32]** produced a model to describe the misalignment of the belt and pulleys over the ratio range of the transmission. They investigated the effects of the ratio at which zero misalignment occurs and how this ratio can be optimised to reduce maximum misalignment over the transmission ratio range. Hendriks et al. **[2]** developed a simple approximation to this misalignment problem and the complexity of 3D modelling used by the authors of this paper seems excessive in an effort to achieve very similar results. It is possible that these misalignment effects could influence the efficiency of the transmission. However implementing a model of the misalignment would be difficult due to the difficulty of measuring the position of zero misalignment, and effects are likely to be minimal compared to those of pulley deflection and skewness.

2.1.4 Summary of Existing Belt Modelling Work

In general the quantity of previously published work relating to the functioning of the metal V-belt CVT has been small. A number of good experimental papers do exist notably (Fujii et al **[22]** and Kanehara **[23]**) and some good theoretical analyses (Becker **[11]**), although none of these consider the efficiency of the belt drive. The only existing work clearly devoted to efficiency is that of Micklem **[12 & 13]**, which it has been shown to have some fundamental flaws in its assumptions.

_____

It is clear from some of the more recent papers (notably Fujii et al **[22]**) that progress has been made in to understanding the function of the pushing metal V-belt CVT. Analysis of the belt mechanism will require a detailed understanding of all the forces and tension distribution identified by Fujii and how these will interact with relative motions occurring in the belt. It is also clear that belt slip has been identified and modelled in a number of different ways, although the 'gap' theory appears to be favoured by a number of authors (Kobayashi **[9]**, in particular). Significantly it would appear that if the gap theory is the cause of slip in the belt there is likely to be considerable interaction between the slip events and the tension distribution phenomena proposed by Fujii et al.

2.2 Automatic and Manual Transmissions Losses

Many of the components found in the belt drive CVT are also found in manual and automatic transmissions, such as wet clutch units, bearings, pumps, gears and seals. A number of papers have been produced modelling automatic and manual transmissions in a component by component method, and these are discussed in more detail here.

Park et al. **[37]** performed a detailed theoretical analysis, modelling mathematically the power losses of all the major automatic transmission components. Detailed models were introduced for components common to the belt drive CVT such as hydraulic pumps, clutches, bearings, seals and gears. Many of the models have parametric constants, which were varied by the authors to give a good fit to the experimental data available. A simple analysis was then performed investigating the percentage contribution of each component to the overall losses in a complete automatic transmission. This was followed by some theoretical proposals to improve the efficiency of a transmission. A number of the models used in this paper will be discussed in more detail in the modelling chapter of this thesis, (Chapter 7).

A similar analysis is provided by Kluger **[38]**, which investigates automatic transmission parasitic losses and efficiency characteristics. The author identifies a number of loss mechanisms, and predicts their overall influence on transmission efficiency. A number of the losses are identified specifically as parasitic losses. These include pump losses, clutch pack drag, gear losses and bearing and seal drag. No theoretical models to predict the losses were produced in this paper. Van Dongen **[39]** performs a very similar analysis investigating

_____

experimentally the efficiency characteristics of both a manual and an automatic transmission. The primary effect causing differences in efficiency between manual and automatic transmissions was identified as the hydraulic pump unit, which increases no load parasitic losses considerably. In conclusion the automatic transmission was found to be 10% less efficient than the manual transmission across all operating conditions.

An incredibly detailed theoretical model of manual transmission losses is provided by Roulet & Briec [40]. In general the models produced are too detailed, with individual models of sliding friction, rolling friction, bearing friction, seal friction and oil churning used to generate the overall losses in a gear mesh. The complexity of the models introduces a huge array of parametric constants, all of which need experimental data to assist in their prediction. In conclusion the models are highly complex yet they are not validated accurately by the experimental data produced. A less complex model would probably generate results of a similar, if not improved, accuracy. The authors do however identify the most critical parameters that influence oil churning losses as oil viscosity, radii of gears, immersion height and oil flow characteristic (laminar or turbulent). More simple analysis of gear losses from first principles is available from Tuplin [41] and Buckingham [42], both of whom introduce a number of simple models to predict gear efficiency.

2.3 Lubricant Property Modelling

This section of the literature review has been dedicated to discussing the contribution of the CVT lubricant to its performance, since this is a critical factor affecting the temperature dependence of the loss mechanisms. It is also important to develop an understanding of the likely contact conditions that exist between the neighbouring components in the belt. A number of the authors discussed in this section propose likely sliding speeds, contact pressures and friction coefficients, that can be used to help in the development of the belt models discussed in chapter 8. The CVT fluid has to perform many tasks in the transmission, from lubrication and heat removal to a signal transfer mechanism in the hydro-mechanical controller. It is also a critical component of the belt mechanism, having to lubricate the assembly but at times permit a high coefficient of friction through which the torque may be transmitted.

_____

_____

Fewkes et al. **[43]** produced a study of the function of the lubricant in a CVT. In particular the study aimed to investigate the phenomena of 'scratch noise' associated with the original derivatives of the Van Doorne belt. The authors predict levels of pressure and relative velocities for a number of contact points within the variator, as tabulated in Table 2-1. It can be seen from these predictions that a vast range of different operating conditions exist between locations and the conditions that occur at any one location may vary considerably as well. The authors tested a number of different fluids under lab test conditions and are able to predict from these results the suitability of the fluid to prevent the 'scratch noise' phenomena. In general the stick slip characteristic of the CVT fluid needs to be one where the friction coefficient of the fluid increases with sliding speed rather than decreasing.

Ishikawa et al. **[44]** studied the effects of CVT fluid on the friction coefficients between metal components. The authors performed experimental friction test methods using a block-on-ring wear test machine to simulate the friction between the belt and pulley on the transmission. The effect of oil detergent additives was also investigated; it was found that the additives deposit a film of 80-90 nm on the sliding surfaces, which acts to increase the friction coefficient between the two surfaces. Two additives were tested, a calcium (Ca) detergent and a zinc dialkyldithiophosphate (ZDDP); both additives were shown to increase the coefficient of friction between two sliding surfaces. The friction coefficient was also shown to decrease again as the additive levels began to deteriorate

Similarly, Ichihashi et al. **[45]** have also investigated CVT fluid friction properties; they have simulated the belt pulley contact using a test rig applying a 100 MPa load at a sliding speed of 0.1m/s, based on the values proposed by Fewkes et al. **[43]**. The authors then investigated the effects of blending several different additives with the base oil. Generally calcium containing detergents gave improved friction coefficients, and reduced noise problems, while amide and ester based additives reduced the friction coefficient. However, the calcium detergents had a detrimental effect on the clutch judder tests. It was concluded that the best results were achieved using a blend of both calcium detergents, for improved traction, and phosphate detergents to improve clutch judder performance. Measured coefficients of friction ranged from approximately 0.09 to 0.135. All the fluids tested displayed an increase in friction coefficient, by as much as 30%, as the fluid temperature was increased.

_____

_____

Peiffer et al. **[46]** describe a range of methods developed by Shell for testing that different blends of CVT fluids have the correct performance characteristics. The paper discusses the conflicting requirements, of a CVT lubricant and how these requirements affect the efficiency of the variator mechanism itself.

The authors note that CVT transmissions need to achieve a wide acceptance with the end user, the driver, and in order to do this they must achieve these performance characteristics with the same standard as would be expected of a manual or automatic transmission. All CVT fluids must therefore have a fill for life performance similar to all modern manual and automatic transmission fluids. The CVT fluids also have to perform many tasks in the transmission, allowing judder free clutch performance, good low temperature pumpability and starting performance, low losses in gears and bearings, high pump efficiency, and high variator efficiency. High pump efficiency requires the fluid to have almost constant viscosity/temperature behaviour, and excellent air release properties, so that the pumped volume does not change due to excessive leakage or changes in the fluid density. The variator efficiency demands on the fluid are more contradictory; a fluid capable of giving high metal to metal friction characteristics allows the clamping pressure to be reduced, thus reducing the pump losses, but at the same time this may increase the power loss due to friction within the other belt components. The authors have developed a test to approximate the power loss in the belt mechanism by measuring the stable temperature difference between the transmission, run at a set condition, and the ambient temperature. The smaller the temperature difference measured the lower the power loss that exists in the belt. A number of the fluids tested produced friction vs. slip characteristics that increase with sliding speed, a beneficial characteristic in the functioning of the variator.

Similar conclusions and desired fluid characteristics are also proposed by Watts et al. **[47]**. The authors also note the importance of differentiating between dynamic and static coefficients of friction. A high dynamic coefficient is desirable in CVT applications to transmit the torque at the pulley face. However, fluids which display static coefficients significantly higher than their dynamic coefficients are more likely to exhibit noise-inducing stick-slip behaviour.

_____

_____

2.4 CVT Control

This section of the thesis will give a brief overview of the effects of CVT control on the functioning of the belt drive variator. Although controlling the transmission relative to the engine and driving conditions is not directly related to the work undertaken in this study it is important to understand the benefits that are achievable with CVTs. It is also important to understand how the actions of the control strategy might impinge on the loss mechanisms within the transmission.

A poorly developed control strategy might demand clamping pressures above the level needed to achieve the required level of traction. This would effectively increase both the pump losses in the transmission and the belt torque losses. In recent years some work has been undertaken to optimise the control of the clamping pressure within a belt drive CVT. There can be a trade-off between acceptable belt slip and reduction in clamping pressure levels. However, the slip limit that may be acceptable is still 'unknown' since long term operation of a CVT at higher slip levels could lead to possible failures of the belt components. A number of papers have been written on this subject including Guebeli **[15 & 16]** and Vaughan et al. **[17]**, of which Guebeli is a co-author.

_____

_____

Contact	Pressure Range (bar)	Velocity (m/s)
Pulley to segment	100-1000	Unmeasurable tangential slip
Segment to band	20-100	0.05-0.5 sliding
Band to band	20-100	0.01-0.1 sliding
Segment to segment	0-10000	1-10 rolling

Table 2-1 Velocities and Pressures in Belt Contacts (Fewkes et al. [43])
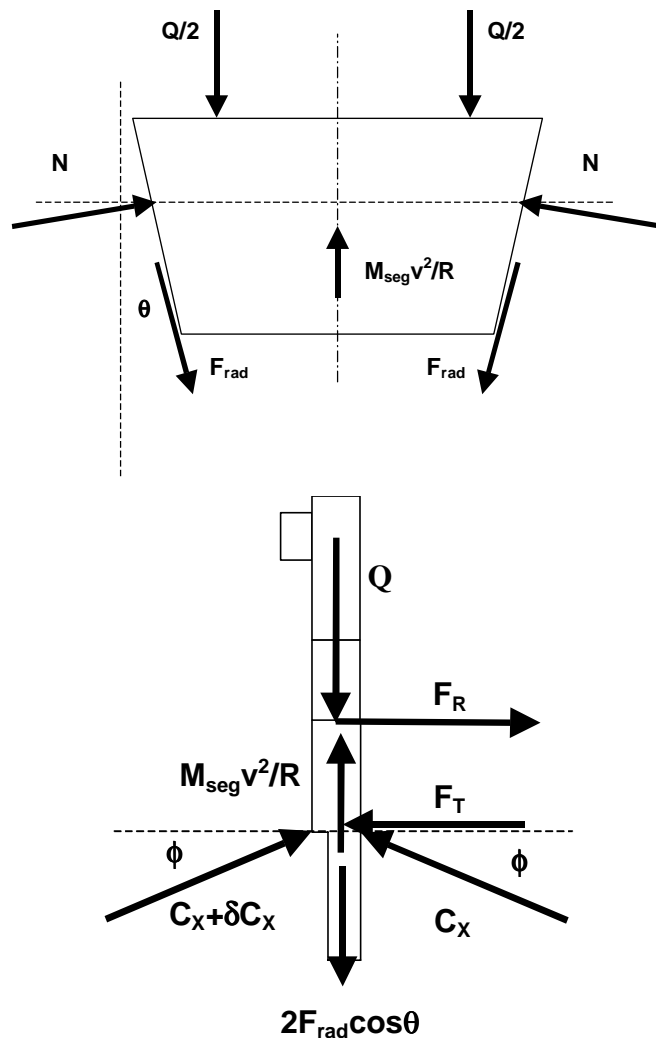
Figure 2-1 Forces Acting on a Segment

_____

_____

3   Chassis Dynamometer Testing

3.1 Introduction & Objectives

This chapter of the thesis details some preliminary vehicle testing undertaken on a Rover 216GSi car equipped with the belt drive CVT. The vehicle was tested using a chassis dynamometer facility at the University of Bath. The objectives for this work were twofold. Firstly, the results would give an understanding of the significance of the cold start investigations being undertaken on the transmission test rig, and in addition the work would give an insight into the load, ratio and control pressure conditions that occur in the transmission during a standard European drive cycle. A range of experimental data were collected, namely vehicle emissions measurement using the facilities available with the chassis dynamometer, and transmission and engine monitoring using an in-vehicle data acquisition system described later in this chapter. The in-vehicle data acquisition would provide scheduled data for the control pressures, ratios, and temperatures acting on the transmission over a standard European drive cycle.

This data acquired from this work had a number of uses. Firstly the speed and pressure data would generate information as to how the CVT functions and the load conditions under which it works during a typical drive cycle, as at present models for the transmission controller do not exist. From these data a belt ratio for the transmission could also be derived for use as simulation input. Secondly the temperature data could be analysed to give typical warm up times for the transmission under a range of ambient conditions.

3.2 The Chassis Dynamometer

The Chassis Dynamometer is equipped with two independent AVL Zöllner 126 kW DC machines driving 48" diameter rollers. The dynamometer is capable of simulating the inertia of any vehicle with mass between 454 kg and 2722 kg. This is achieved with a base inertia of the rollers equivalent to 1360 kg. Higher effective inertias are achieved by the motors absorbing more power and lower inertias by the motors assisting in driving the rollers.

_____

_____

The whole test facility is environmentally controlled to regulate the internal temperature of the cell between −10°C and +40°C. Vehicle cooling is achieved using a variable speed engine cooling fan which tracks the dynamometer road speed to simulate road speed cooling. The test vehicle is shown in the test facility in the photograph of Figure 3-1.

The test facility is equipped with a range of emissions equipment, based on the Horiba MEXA 7000 Series analysers. Emissions recorded included Total Hydrocarbons, Oxides of Nitrogen, Carbon Monoxide, Carbon Dioxide and Oxygen (THC, NO/NOx, CO, CO_2 and O_2). The emissions data were collected continually from the tailpipe of the test vehicle post catalyst, via a constant volume sampling unit (CVS). The emissions were also recorded using a standard bag system to measure total emissions levels over the standard phases of the European drive cycle and extra urban drive cycle (ECE15 +EUDC). All the data acquisition and control of the chassis dynamometer and emissions equipment was performed using the Horiba PC VETS system.

3.3 Emissions Testing

Testing was undertaken to investigate the effects of ambient temperature conditions on the emissions and fuel consumption of a CVT equipped vehicle: a similar range of tests was also undertaken on a vehicle equipped with a manual transmission for comparison purposes. The tests were performed over a standard ECE15 + EUDC cycle as in Figure 3-2. The tests were carried out at ambient temperatures of −10, 0, 10, 25 and 40°C. An initial test was performed with the test vehicles soaked overnight to the ambient temperature. The tests were then repeated under 'warmed' conditions, but with the same ambient temperature.

Table 3-1 shows the specifications of the two vehicles used during the emissions test program. The vehicles were not compared directly with each other; rather the comparison was between the different levels of performance of each vehicle over the chosen range of test conditions. Significant differences between the vehicles other than the transmission system were the ratio ranges available from the transmission and the engine capacities.

_____

_____

3.4 Vehicle Instrumentation

The Rover 216 CVT vehicle was instrumented with a number of transducers to obtain critical control pressures, speeds and temperature data during the drive cycle tests that were performed. The variables that were measured are highlighted in Table 3-2.

The in-vehicle data acquisition was carried out using the arrangement shown schematically in Figure 3-3. The installation of the data acquisition hardware in the boot of the vehicle can be seen pictorially in Figure 3-4. The main components are a desktop PC supporting a PC226 A/D converter data acquisition card, a breakout box to connect to the PC226 and a card frame into which a number of signal conditioning cards are mounted. The desktop PC was set up as a remote host using pcAnywhere ™ software, which allows the operation of the PC to be controlled remotely, in this case by a laptop PC on the passenger seat of the test vehicle. The data acquisition software (LABTECH NOTEBOOKpro) runs on the desktop unit alongside pcAnywhere, while the laptop runs a second copy of pcAnywhere to communicate with the desktop. This installation allowed the convenience of running both a high quality and a readily available data acquisition card with a compact laptop as the operator interface within the vehicle. The ECU in the Rover vehicle was adapted, by Rover technicians, to supply the required ECU data through standard BNC connectors to the data acquisition system.

3.5 Complete Drive Cycle Results

The emissions test results for the complete drive cycle were analysed to investigate the effects of ambient temperature and vehicle soak temperature on emissions and fuel consumption. Identical tests were carried out on both the manual vehicle and the CVT equipped vehicle. The results can be analysed over the complete drive cycle (ECE15 + EUDC), or as individual phases for the ECE15 part of the test or the EUDC part in isolation.

The overall fuel consumption rates for the complete drive cycle and for the individual phases are shown graphically in Figure 3-5 to Figure 3-7, comparing the performance of the manual transmission equipped Mondeo and the CVT equipped Rover 216GSi. Figure 3-5 shows the fuel consumption results (in L/100 km) for the whole ECE15 + EUDC drive cycle. In general

_____

the results show the CVT equipped vehicle to be ~5% less efficient than the manual equipped vehicle despite the Mondeo having a larger capacity engine (2.0 L vs. 1.6). This clearly indicated that despite the theoretical improvement in efficiency that should be available from a CVT, a current production model is in fact less efficient than a manual vehicle. A more detailed analysis is seen when exploring the results for the two individual phases of the drive cycle. Also indicated in this figure is that in relative terms the efficiency of the CVT system is worse than that of the manual in the warm tests compared to the soak test conditions. This is indicative that the parasitic losses of the CVT system are still affecting fuel consumption levels in the warm tests whereas the transmission losses of the manual vehicle are negligible.

Figure 3-6 shows the results over the first phase (ECE15) of the drive cycle. Under these conditions the CVT equipped vehicle is considerably less efficient than its manual counter part. Typically fuel consumption is at least 10% worse than that of the manual transmission vehicle. This characterises the high parasitic losses in the CVT under low load conditions such as those found in the ECE15 cycle. It also indicates that, particularly under the cold soak test conditions, these parasitic losses are even higher in comparison to standard transmission losses. One characteristic of the CVT function under the ECE15 driving conditions is the high clamping pressures used by the variator to maintain torque transfer, see Figure 3-8 compared to Figure 3-9, where during the EUDC the secondary pressure is much lower. These conditions increase considerably the hydraulic system losses in the CVT during the EC15 phase of the tests.

In comparison to Figure 3-6, Figure 3-7 shows the results of the second phase or EUDC drive cycle characterised by higher speed driving conditions. Under these conditions the fuel consumption results are reversed and the CVT equipped vehicle is up to 7% more efficient than the manual transmission vehicle. This is indicative of the high ratio range available from the CVT vehicle, which allows the engine to operate at a lower and more efficient speed for higher road speeds. The higher CVT efficiency under these conditions is also due to the reduction in hydraulic system pressures, and thus losses, seen under these operating conditions for the CVT vehicle.

3.6 Real Time Emissions Results

The real time emissions testing allows the results to be analysed in more detail, since concurrent sets of data from the repeat sections of the ECE15 testing could be compared from the same drive cycle. This also enabled the emissions data to be cross-referenced to the transmission and engine temperatures measured during the same tests. The complete emissions profiles can be found in Appendix A of this thesis for completeness. However, they are not discussed here in detail, as the main consideration of this test program was fuel consumption results and CVT performance.

3.7 Transmission and Engine Data

The data collected from the in-vehicle data acquisition system was analysed to provide information for the modelling work to be undertaken. The engine speed and vehicle speeds were used to calculate the overall transmission ratio.

Figure 3-8 shows a set of typical vehicle data from the first quarter of the ECE15 drive cycle. From these data it can be seen that the transmission ratio during the ECE15 drive cycle is often at intermediate ratios rather than at the two extremes at which the test rig work could be undertaken. The secondary pressure appears to vary considerably from maximum peaks of nearly 40 bar during pulling away manoeuvres, to as small as 12 bar in the fastest part of the cycle. The trace shows clearly the relationship between the secondary clamping pressure and the transmission ratio. Another characteristic of the CVT is the de-coupling of the engine speed relative to the vehicle speed. This is seen typically at the end of acceleration manoeuvres, where the engine speed decelerates at a constant vehicle speed, as the CVT continues to perform an up-shift.

Figure 3-9 shows a comparable set of data for the EUDC phase of the drive cycle. In this case the vehicle speed is much higher and the control pressures lower at around 10~15 bar. The CVT is characterised by a very high overdrive ratio compared to a manual (2.65 vs. 3.47) which is also indicated by the very low engine speeds of less than 3000 rev/min even at 120

_____

km/h road speeds. During most high speed manoeuvres the transmission appears to operate very near to the high extreme ratio conditions.

The two sets of data shown in Figure 3-8 & Figure 3-9 were collected at standard ambient temperature conditions of 25°C. Further sets of data were collected at the other ambient temperature test conditions and these did show some change in the function of the CVT controller and the magnitude of the secondary pressures. The secondary pressure was found to increase at lower temperature operating conditions. However the purpose of this part of the work was to investigate general function of the CVT while more detailed measurements of the temperature effects on clamping pressure are found in the steady state torque loss results shown in chapter 5 of this thesis.

3.8 Transmission Warm up Times

An important part of the chassis dynamometer testing was to record the transmission temperatures during the drive cycle tests, and to gain an understanding of how ambient temperature affects the warm up times for the transmission. Although a temperature survey had been performed on the transmission on the test rig to determine local temperature variations with respect to the bulk fluid temperature, little data were available to describe the warm up process in the transmission. A typical temperature trace for the transmission is shown in Figure 3-10. Temperatures recorded include the engine and CVT sump temperatures and the temperature to and from the CVT oil cooler. The result shown is for a -10°C ambient temperature on a soaked vehicle. A complete range of warm up cycles are shown for completeness in Appendix B of this thesis for all the ambient temperature conditions and for soaked and warm tests.

The results in Figure 3-10 show one of the major problems with the CVT. Over a 20 minute drive cycle the lubricant temperature of the transmission has only risen to 30°C, a condition where the lubricant is still highly viscous. In comparison the engine oil temperature has risen considerably more to a value of 90°C. The effect of the engine thermostat is clearly visible at around 70 to 80 °C. An improvement in the warm up time of the CVT could be achieved by isolating the cooler intelligently to prevent any unnecessary heat rejection. These results

_____

clearly indicate the necessity to understand the losses of the transmission over a range of lower temperature conditions.

	Rover 216 GSi	Ford Mondeo
Engine	1.6 litres	2.0 litres
	Fuel injection	Fuel injection
	16 valves	16 valves
Transmission	Metal pushing belt CVT	Manual (5 gears)
	Ratio range: 2.65 to 15.48	Ratio range: 3.47 to 13.12
Catalysts	3 way catalyst	3 way catalyst

Table 3-1 Specification of Emissions Test Vehicles

Measurement	Data Source	Conditioning Card
Inlet Manifold Pressure	ECU transducer	From Engine ECU
Throttle Position	ECU transducer	From Engine ECU
8 thermocouples for 8 temperatures	1. Engine sump 2. CVT sump 3. Ambient 4. Air Filter Box 5. To CVT Cooler 6. From CVT Cooler 7. Air Pre CVT Cooler 8. Air Post CVT Cooler	K-type (4 channels per card)
Clutch pressure	Pressure transducer installed on CVT	DC amplifier
Secondary pressure	Pressure transducer installed on CVT	DC amplifier (2 channels per card)
Engine Speed	Clamp detector on HT lead	Frequency to Voltage Converter
Vehicle Speed	Rotary encoder fitted to speedometer drive	Frequency to Voltage Converter

Table 3-2 Variables Measured During Chassis Dynamometer Testing

_____

Figure 3-1 The CVT Equipped Rover 216GSi on the Chassis Dynamometer
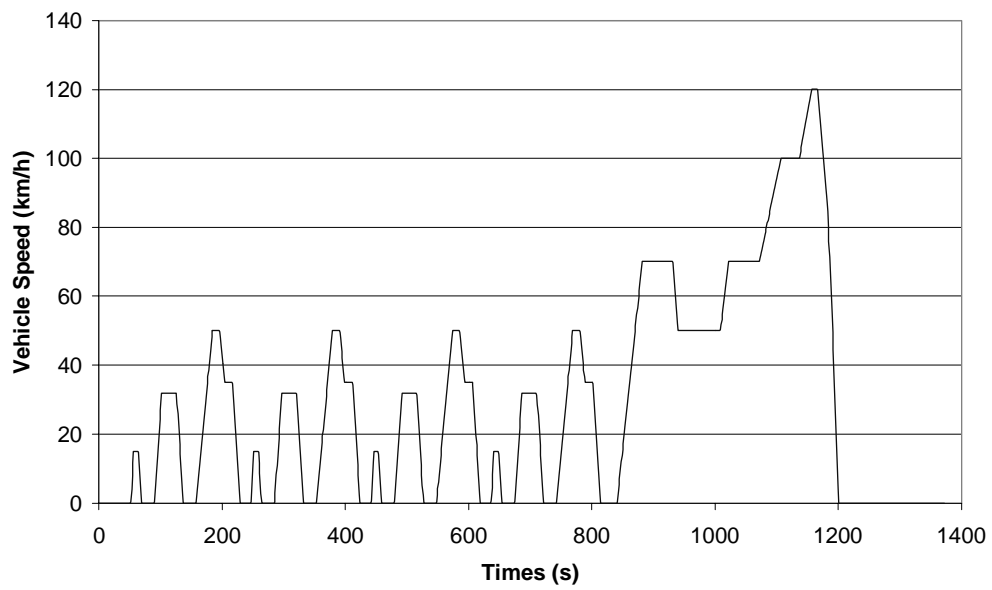
Figure 3-2 Vehicle Speed Trace for ECE15 + EUDC Test

_____
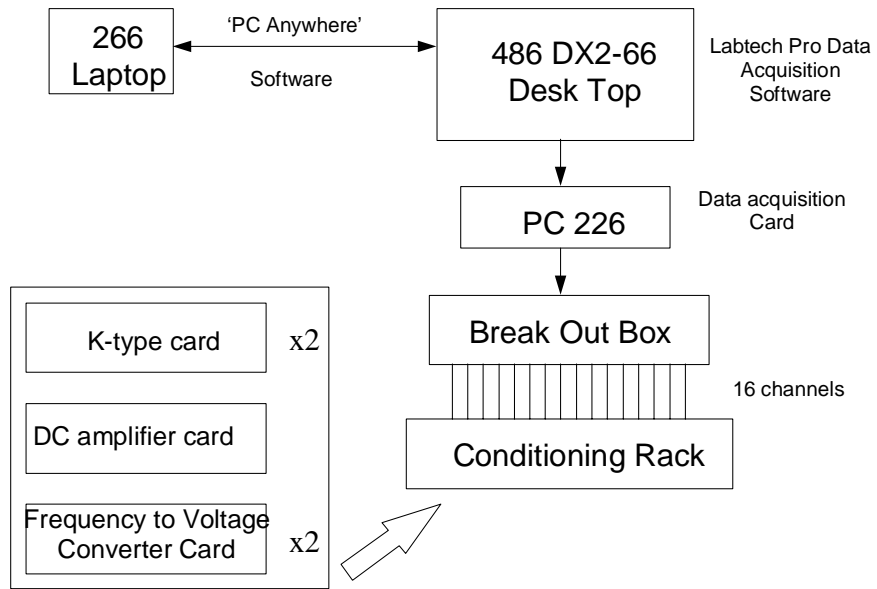
Figure 3-3 Schematic of in-Vehicle Data Acquisition System
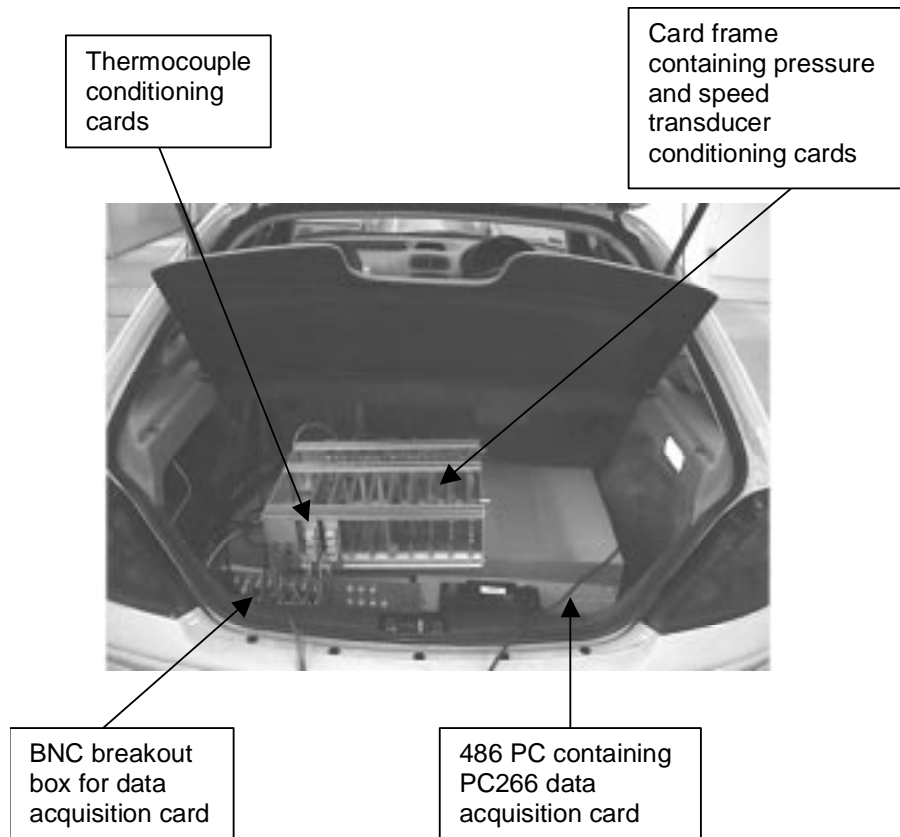
Figure 3-4 Installation of Instrumentation in Rover 216 Boot
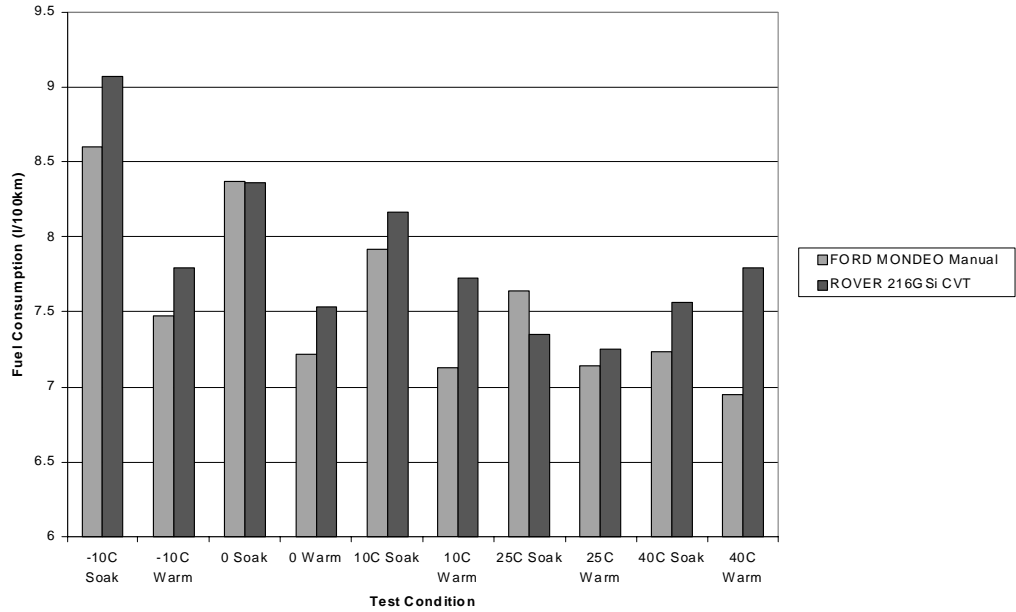
Figure 3-5 Total Fuel Consumption Results for ECE15 + EUDC (Mondeo Manual and Rover CVT)
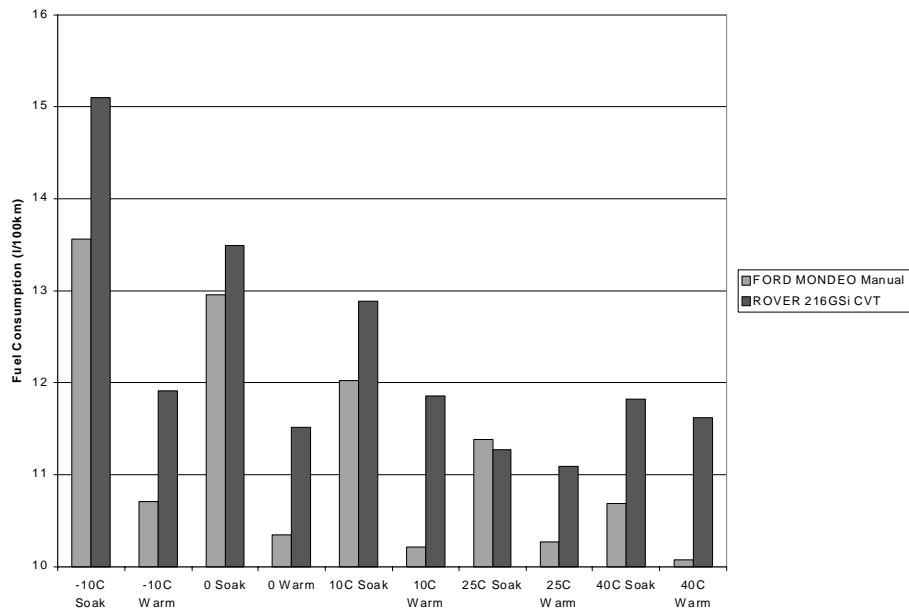
Figure 3-6 Total Fuel Consumption Results for ECE15 Phase Only (Mondeo Manual and Rover CVT)

_____
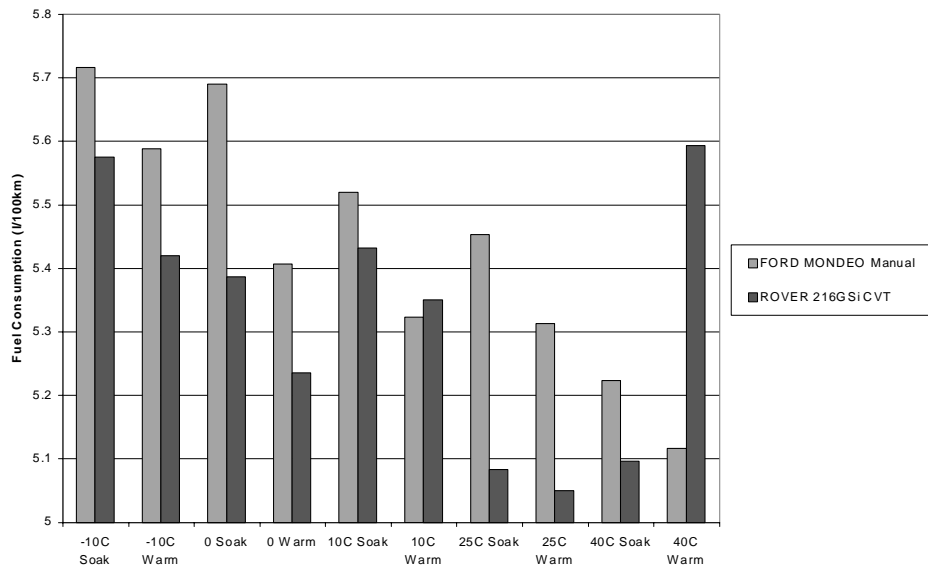
Figure 3-7 Total Fuel Consumption Results for EUDC Phase Only (Mondeo Manual and Rover CVT)
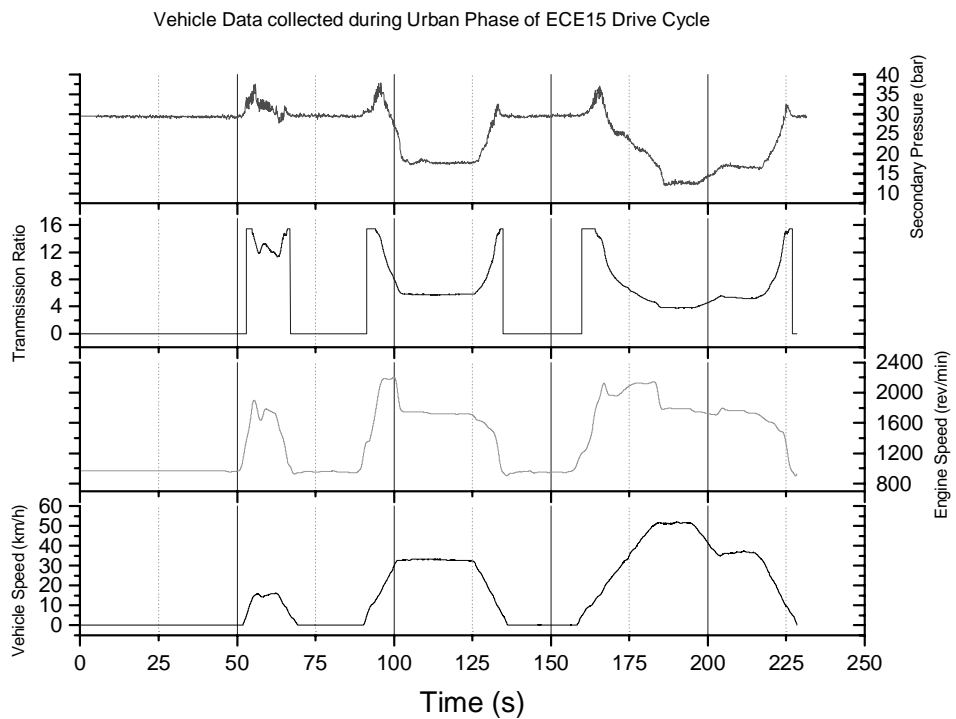
Figure 3-8 Vehicle Data from 1ˢᵗ Quarter of ECE15 Drive Cycle

_____
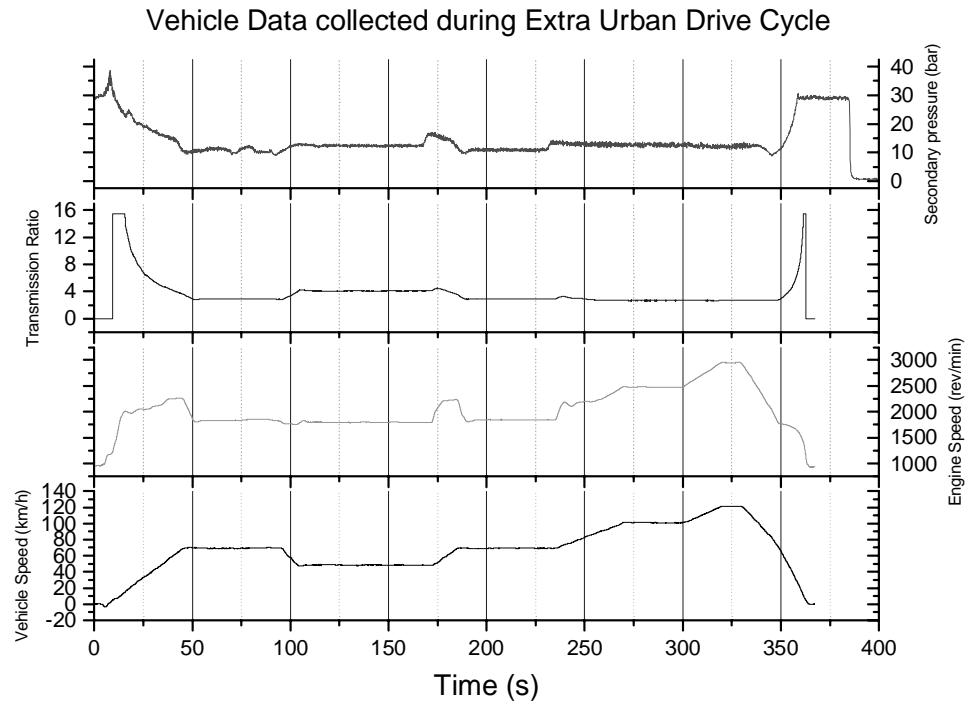
Figure 3-9 Vehicle Data from the EUDC Phase
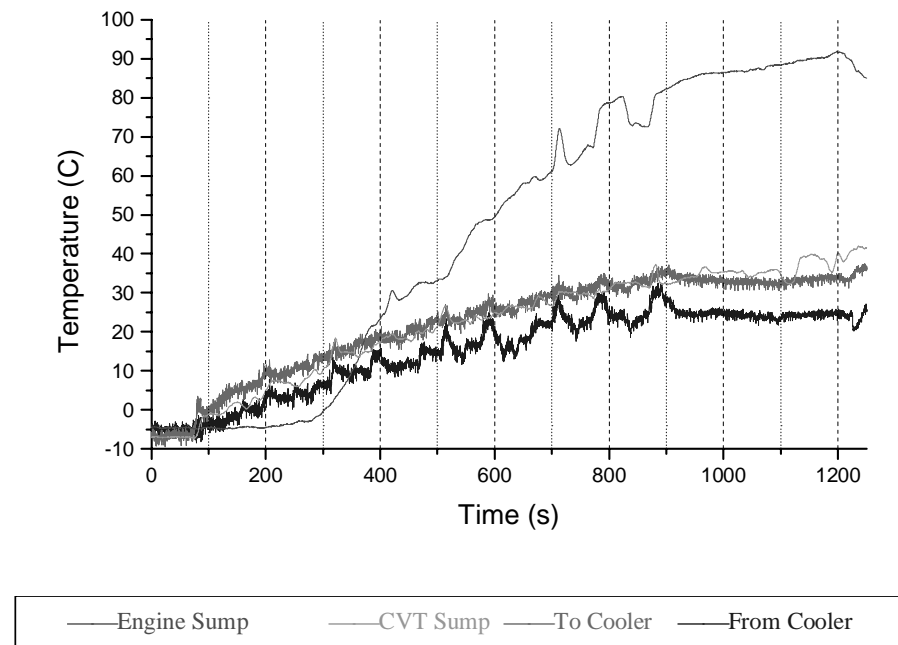
Figure 3-10 Typical Temperature Profiles for a Cold Start Drive Cycle Test (-10°C Ambient Temperature)

4   The Transmission Test Rig

4.1 Introduction

This section of the thesis introduces the transmission test rig developed to measure the torque losses through the test transmission. These data are presented in chapter 5; they are used to provide the foundation for the theoretical work undertaken later in the project and also described in chapters 7 & 8 of this thesis.

Figure 4-1 shows a schematic diagram of the transmission test rig, in side elevation and plan elevation, while Figure 4-2 shows a pictorial view of the same. The rig was built around a standard Van Doorne pushing metal V-belt CVT unit, as fitted to the then current Rover 200 Series automatic cars (now 25 Series). The three main components of the test rig are the hydraulic driving motor, the test transmission and the hydraulic loading pump. The transmission is driven by the hydraulic motor and loaded by the hydraulic pump circuit so as to control the input speed of the transmission and the torque at the output shaft of the transmission respectively. The hydraulic motor is powered from a hydraulic ring main facility available at the University of Bath. The outlet flow from the hydraulic motor acts as a boosted supply to the loading pump to prevent cavitation.

The design specifications for the transmission test rig were an input speed range from 750 rev/min (equivalent to engine idle) to 4000 rev/min (typical maximum steady state engine speed) and an output torque load variable between 0 (no load) and 100 Nm. These design specifications further dictated the output speed range of the transmission (60-1750 rev/min) and the maximum input torque likely to be required (85 Nm). Figure 4-3 shows the torque speed envelopes over which the test rig is able to operate the transmission, compared with the envelope expected from a typical vehicle application. From the graphs it can be seen that the test rig operates the transmission at a much lower torque load, than an in-vehicle situation, but the rig is still able to operate over most of the speed range that would be seen in-vehicle.

This range of testing allows the torque transducer to be sized with a small measurement range to measure accurately the very small torque losses expected, but at the same time it allows investigation into the load dependency of any of the losses. The large speed

_____

range of the transmission test rig allows detailed investigations into the speed dependency of any losses.

4.2 Instrumentation

The main purpose of developing the transmission test rig was to investigate experimentally performance phenomena of the belt drive CVT and to acquire data to validate any mathematical models. Therefore, the test rig was fully instrumented to record information from a range of transducers. All the transducers were linked to a PC based data acquisition system via the necessary signal conditioning cards and two DT3001 16 channel, analogue to digital data acquisition cards, (see Figure 4-4 and Figure 4-5). The variables measured and the conditioning cards used are presented in Table 4-1.

4.2.1 Torque Measurement

Both the input shaft and the output shaft torque loads were measured with non-contacting HBM T10f flange torque transducers, rated to 100 Nm. The torque transducers are each connected to HBM MC10 amplifier cards, which are controlled by a HBM AB12 display and control panel. The torque transducers are full bridge strain gauge units. The AB12 unit allows the implementation of low and high pass filters, to improve the output signal quality prior to data acquisition.

The torque transducer units give particularly accurate measurements of the low torque levels being used. This is due in part to the relative sizing of the transducers and the low noise characteristics achieved by the non-contacting telemetry. Traditional torque transducers as used by Chan **[48]** and Valenta **[49]**, on a project preceding this work, use brushes to transmit the signals from the rotating shaft; this can introduce high frequency electrical noise into the signal. The telemetry on the HBM system is based on a stator hoop around the torque transducer that is excited by a high frequency supply from the conditioning amplifier. This induces a voltage in the transducer to energise the strain gauges, which in turn transmit the strain signals back to the stator and conditioning amplifier. The torque transducers have an analogue ±10 volts output for a full scale ±100 Nm torque loading; these signals were recorded directly by the data acquisition system.

_____

4.2.2 Speed Measurement

The input and output speeds were measured using toothed gear wheels and magnetic pickups. The gear teeth induce a voltage in the magnetic pickup which is conditioned using an in house frequency to voltage (F to V) conditioning card. The F to V card first conditions the irregular voltage characteristic from the pickup into a signal of uniform magnitude and duration; this is then "averaged" by an integrator to produce an analogue voltage output proportional to the frequency of the pulses. The analogue voltage is then fed directly to the data acquisition system.

4.2.3 Belt Position Measurement

To understand in more detail the belt mechanics, the belt radius around both the primary and secondary pulleys was measured using radial probes (see Figure 4-6), similar to those used by both Micklem **[12 & 13]** and Guebeli **[15]**. The probes were fitted with linear variable differential transformer (LVDT) displacement transducers. From these the actual belt ratio can be compared to the ratio of input to output speeds to determine the magnitude of any belt slip that may exist.

The LVDT measurement system has a number of advantages. The resolution of the system is effectively infinite and there are no contacting parts to wear; the transducers are also very rugged, being unaffected by vibration and contamination. The probes were also fitted with magnetic pick-ups to measure the belt speed (see section 4.2.4 below). The only apparent disadvantage of this measuring system appeared to be some temperature sensitivity, due in part to the LVDTs and also due to thermal expansion in the probe assemblies.

4.2.4 Belt Speed Measurement

The magnitude of any belt slip can be further quantified from measurement of the belt speed; this is done using a magnetic pickup on each of the radial probes to count the number of belt segments passing. To allow accurate slip measurements the input speed, belt speed and output speed were monitored using 3 counter/timer units. A rotary encoder was fitted to the output shaft, using 1000 pulse/rev, to improve the resolution of the results obtained using the standard 60 tooth gear wheel originally fitted. In high ratio the counter timers were triggered simultaneously using a 10 second duration square wave generated by one of the PC Digital to Analogue output channels.

It was not possible to detect all the belt segments in low ratio due to the slower belt speeds producing too weak an output from the magnetic pick-ups. Therefore the test method had to be modified. To test in low ratio the tip of one segment on the belt was ground off. This produced one pulse per revolution of the belt. This signal was used as the trigger for the input and output counter timers. A frequency divider card was developed to produce a square wave with a period equal to 100 belt pulses. Thus the input and output counter timers could acquire shaft rotations equivalent to 100 belt revolutions.

4.2.5 Control Pressure Measurement

The control pressures in the transmission influence the belt torque loss and may affect any belt slip that exists. Therefore, the primary pulley, secondary pulley and clutch control pressures were all recorded. The primary and secondary pressure transducers were sized at 40 bar to cope with the maximum working pressures foreseen, while the clutch pressure transducer was sized as 10 bar for similar reasons.

All the pressure transducers were calibrated using a dead weight tester at regular intervals throughout the test period, and additionally if any anomalies were detected as the results were processed. All the transducers were conditioned using standard in house DC amplifier cards. The calibrations were performed such that the output from the conditioning cards was 10 volts at the full-scale pressure, for maximum resolution.

_____

4.2.6 Throttle Position Measurement

The throttle position was measured since it is an input variable to the hydromechanical controller fitted to the transmission. A system was required to measure the effective pull on the kick-down cable. This was achieved by using the appropriate throttle body from in-vehicle applications. The throttle butterfly valve is fitted with a rotary potentiometer, which normally interfaces with the engine management system. This was calibrated in house, using a standard DC Amplifier conditioning card, to supply $\pm$ 5 volts from fully closed to 100% throttle. The throttle position data were then recorded by the data acquisition system.

4.2.7 Temperature Measurement

Up to 16 temperatures throughout the transmission were available for recording at any one time, as one of the main objectives of the investigation was to determine the temperature dependence of any parasitic losses. The temperatures recorded also allowed monitoring of the temperature control system described later in this section. All the thermocouples used on the test rig were of the T-type. This was due to the range of temperatures over which they had to measure. The thermocouple channels were conditioned using a stand-alone conditioning box situated near the rig. The box contains two conditioning cards each capable of conditioning 8 thermocouples including the necessary cold junction compensation using PRT transducers. This effectively reduces the measured temperature channels to 14. The locations of the temperatures measured are given in Table 4-2.

The thermocouple conditioning cards are controlled by DTVEE data acquisition software controls the conditioning cards (see section 4.3 & Figure 4-4). By locating the conditioning box near the rig the length of thermocouple cables was minimised, thus reducing the chance of erroneous electrical noise entering the system at the micro-volt level produced by thermocouples. Each conditioning card is connected to the data acquisition system via a 24 pin D-connector, which also carries the configuration signals to the cards.

_____

_____

4.3 DTVEE Data Acquisition Software

DTVEE data acquisition software is an icon based program that runs in the Windows environment. The software allows data acquisition systems to be constructed by simply arranging individual blocks and linking them together in a similar fashion to a flow diagram. One of the main advantages of the Windows environment is the graphical display facility, which enables recorded data to be displayed on the PC monitor in a number of different gauge formats.

The DTVEE software operates both DT3001 data acquisition cards sampling at 1000 Hz; all the data is averaged every second and then written to a data file at a frequency of 1 Hz. All configuration of the A/D conversion is carried out within DTVEE, as is the thermocouple card configuration and cold junction correction. Within the software it is also possible to insert formulas to scale all the data inputs into SI units and perform pre acquisition calculations.

4.4 Output Load Control

The output shaft loading system had to be able to control the torque on the output shaft of the transmission accurately to a pre-set value between 0 Nm and 100 Nm. The system was developed on the basis of using a hydraulic pump to produce the load. No-load conditions could be investigated by disconnecting the output drive shaft from the hydraulic load system. The use of a hydraulic pump was convenient due to the hydraulic system being used to drive the rig and the availability of the Department's hydraulic ring main facility.

A schematic of the hydraulic circuit is shown in Figure 4-7. One of the problems encountered with the design of the system was the large range of speeds at which the output pump would be driven, a problem magnified by the large ratio range of the CVT unit. The pressure relief valve selected requires a minimum flow rate to function correctly and therefore a large pump has to be selected to supply this flow at very low speeds.

For convenience the load pump is boosted by the outlet flow from the drive motor, to prevent cavitation. Although the pump displacement is considerably larger than that of the

_____

_____

drive motor, the flow requirement is similar, since the ratio of the transmission always ensures that the pump speed is considerably less than that of the motor.

The pump load torque was controlled by modulating the pressure at the outlet to the pump. This is achieved by using a Vickers proportional pressure relief valve driven by an in house developed control card. The valve is a two-stage pressure relief valve rated to a maximum pressure of 200 bar. The control card allows simple open loop control of the output torque by setting a demand to the valve via a multi-turn potentiometer dial. The card also has the facility to adopt closed loop PID control of the output torque and then implement external command signals. This allows the output shaft torque to be controlled by a PC, for example to simulate load steps. A hydraulic accumulator unit, charged with nitrogen gas, is fitted between the pump and the pressure relief valve to smooth out some of the pressure ripple from the pump, and effectively reduce the torque fluctuations in the output shaft. These fluctuations were particularly noticeable at low speeds, when they have a very low frequency.

4.5 Drive Control System

A hydraulic motor was used to drive the test rig and Figure 4-7 shows a schematic diagram of the hydraulic control circuit. The hydraulic motor is a Linde HMF28, a fixed swash plate axial piston design with a displacement of 28 cm^3/rev. It is rated to a maximum continuous speed of 4500 rev/min and continuous pressure of 250 bar. The motor was sized to prevent any possible overload occurring to the input shaft torque transducer.

The input speed to the test rig is simply controlled by throttling the hydraulic supply using an electrical proportional flow control valve. The valve is a Vickers 2 stage proportional valve with integral amplifier electronics. The valve requires a $\pm$ 15 volt supply to drive the valve and the control signal is $\pm$ 10 Volts, which is approximately proportional to the flow characteristics of the valve. The control signal is supplied by an in house developed control card, which allows the speed to be set by adjusting an electrical potentiometer circuit.

The system was developed with the option of closed loop PID speed control. This would allow speed data to be supplied from an external source, for example by a PC to perform

_____

_____

a drive cycle. However, for the purpose of this work the control was performed open loop as all of the work was steady state.

4.6 Low Temperature Testing Facility

One of the main objectives of the project was to investigate the effect of the transmission lubricant temperature on the losses. Therefore, the test rig was developed to facilitate low temperature testing of the transmission. This required some form of temperature control system.

From simple preliminary tests carried out with an earlier transmission test rig used by Chan **[48]** and Valenta **[49]**, some basic values for the rate of heat rejection by the transmission could be calculated. Initial costs of environmental control systems for the test cell were too high and therefore an alternative and more economic solution to the problem had to be found.

Initial design calculations were based on the heat rejection values and the specific heat capacities of a number of fluids. From these values it was possible to calculate the volumes of fluid required to act as a heat sink for the transmission, based upon a minimum time period to perform the tests. Once a fluid had been chosen a temperature control system was developed to transfer the heat from the transmission fluid to the heat sink fluid efficiently and with some means of control.

It was planned that if a large heat sink capacity could be cooled over a long period of time it would allow testing to be carried out for a comparatively short period. Initial aims were to chill the heat sink overnight to allow for 30 minutes testing each morning. The temperature control circuit, see Figure 4-8, was based upon a standard domestic deep freezer unit, acting as an insulated reservoir, filled with approximately 100 litres of a 50% water and 50% ethylene glycol mixture. The ethylene glycol mixture acts as the heat sink of the system. The mixture was chosen since it has both a high specific heat capacity and a very good heat transfer coefficient.

A Flowcool industrial water chiller unit, rated at 0.4 kW, is used to chill the fluid. The chiller uses R404a refrigerant, which is pumped on the low pressure side through a plate heat exchanger to extract heat from the ethylene glycol mixture. On the high pressure side of

_____

_____

the compressor the refrigerant enters an air cooled condenser with a fan unit to force convection.

An electrically driven centrifugal pump draws the ethylene glycol mixture from the reservoir and pumps it around the chiller circuit. A three way valve in the ethylene glycol circuit allows the circuit to be used in two configurations. In one position the circuit simply circulates the flow though the chiller and back to the reservoir for cooling. In the second position, the fluid is pumped through a further oil to water heat exchanger in which the glycol/water mixture extracts heat from the transmission fluid. At this point the chilled water glycol mixture meets the transmission fluid.

The internal transmission pump, assisted by an independent hydraulic pump driven by an electric motor circulates the transmission fluid. With the two pumps running simultaneously a flow rate of up to 20 L/min can be achieved, thus circulating the 5 litre volume of the transmission sump four times per minute. The independent pump also allows the facility of pre-cooling the transmission prior to a test, without any heat generation from the transmission.

Within the oil circuit there is also an additional oil to water heat exchanger, which can be bought online using the 3 way valve. This heat exchanger is connected to the departmental cooling water supply and can be used when testing at higher temperatures or as a preliminary form of heat removal prior to the oil passing through the chilling circuit. The heat exchanger can therefore be bypassed if the cooling water temperature is above the temperature of the oil exiting the transmission. In effect the oil to water cooler system represents the oil to air cooler that is used for in-vehicle applications.

The amount of heat rejected to the chiller system is controlled by modulating the flow of transmission fluid through the main heat exchanger. This is achieved by controlling two proportional electro-hydraulic throttle valves. To reject more heat the oil flow through the heat exchanger is increased, by opening the inlet valve (A) and restricting the bypass valve (B). Conversely to slow the rate of heat rejection valve A is restricted and valve B is opened.

A temperature control module monitors the transmission return line oil temperature and varies the flow through the proportional throttle valves A and B. Each valve is driven by an individual Vickers amplifier card which is in turn controlled by an off the shelf temperature

_____

_____

controller incorporating a PID controller module, which was tuned to achieve accurate temperature control.

In addition to the low temperature test apparatus, the transmission also needed a facility to warm the oil. During normal testing the transmission warmed up due to the inherent losses. However, during the strip down tests the number of loss mechanism were reduced and thus an oil heater had to be fitted to warm the fluid for the higher temperature work. The oil heater was a simple electrical immersion heater unit with a built in thermostatic control.

4.7 Transmission Modifications

A number of modifications had to be made to the transmission to allow for the fitting of measurement transducers. A radial hole had to be bored through the transmission casing, about each of the pulleys, into which an aluminium sleeve and flange were fitted. This allowed mounting of the radial probes to measure the radial position of the belt on each pulley. A window was also machined into the side of the transmission enabling the primary pulley and belt to be viewed. Other modifications included the locking of the transmission differential, so as to allow output drive along one shaft, and the machining of thermocouple entry points and oil drain ports for the cooling system.

4.8 Test Program

Once the test rig was developed a test program was designed so that as much relevant information as possible could be acquired without resorting to excessive testing times.

It should be noted that previous work using the transmission had justified the assumption that the transmission had reached its 'run in' state. A base line test was adopted to pick up any variation in the properties of the transmission fluid, or to indicate the possibility of further 'bedding in' of the belt during the period of the test program.

_____

Variable measured	Transducer	Signal Conditioning Card
Input Torque (T_{in})	HBM T10f torque flange (0-100 Nm)	HBM MC60 Amplifier plug-in unit
Output Torque (T_{out})	HBM T10f torque flange (0-100 Nm)	HBM MC60 Amplifier plug-in unit
Input Speed (ω_{in})	Magnetic pick-up (0-4500 rev/min)	Frequency to Voltage converter
Output Speed (ω_{out})	Magnetic pick-up (0-1750 rev/min)	Frequency to Voltage converter
Output Speed (ω_{out})	Rotary Encoder 720 pulse/rev	Frequency to Voltage converter
Primary Pulley Pressure (P_{prim})	0-40 bar	DC. Amplifier
Secondary Pulley Pressure (P_{sec})	0-40 bar	DC. Amplifier
Clutch Pressure (P_{clutch})	0-40 bar	DC. Amplifier
Primary Pulley Radius (R_{pri})	Radial probe LVDT $\pm$ 50 mm	Carrier frequency card
Secondary pulley Radius (R_{sec})	Radial probe LVDT $\pm$ 50 mm	Carrier frequency card
Belt Speed (V_{belt})	Magnetic pick-up	Frequency to Voltage converter
Primary Pulley Speed (ω_{pri})	Magnetic pick-up	Frequency to Voltage converter
Throttle Position (X)	Potentiometer	DC. Amplifier

Table 4-1 Variables and Transducers Used on the Test Rig

_____

Thermocouple Channel	Thermocouple card	Thermocouple Location
1	A	Room Temperature
2	A	Sump 1
3	A	Clutch Side
4	A	Clutch Front
5	A	Differential
6	A	Gear Spray
7	A	Above Differential
8	A	**Cold Junction Compensation**
9	B	Sump 2
10	B	Belt Spray
11	B	To Cooler
12	B	From Cooler
13	B	Under Belt
14	B	Under Clutch
15	B	Spare
16	B	**Cold Junction Compensation**

Table 4-2 Thermocouple Locations

_____
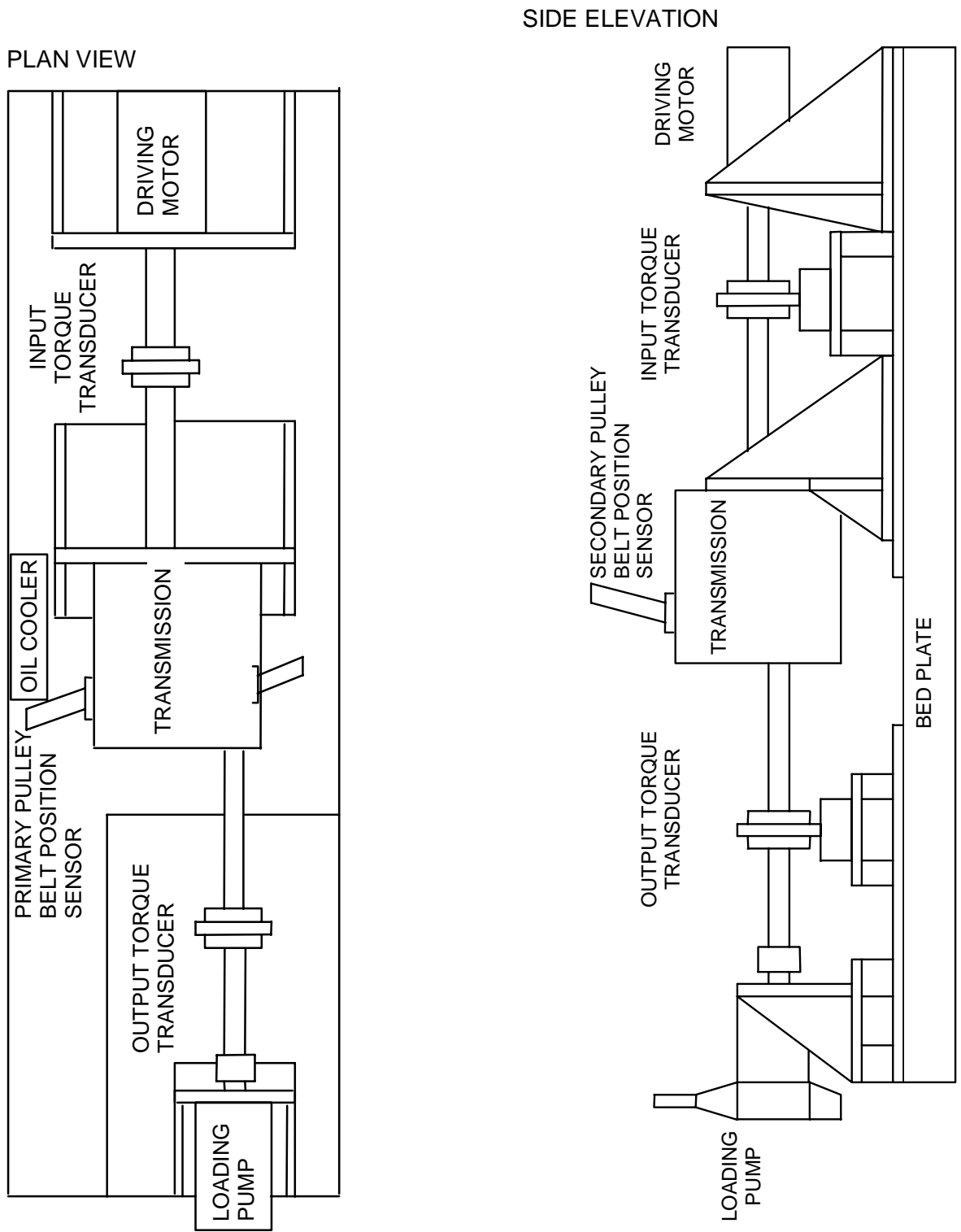
Figure 4-1 Schematic of Transmission

Test Rig

_____

Test Transmission

Input Torque Transducer

Motor Speed Control Valve

Hydraulic Drive Motor

Hydraulic Loading Pump Assembly

Primary Pulley Position Sensor

Oil to Water Heat Exchanger
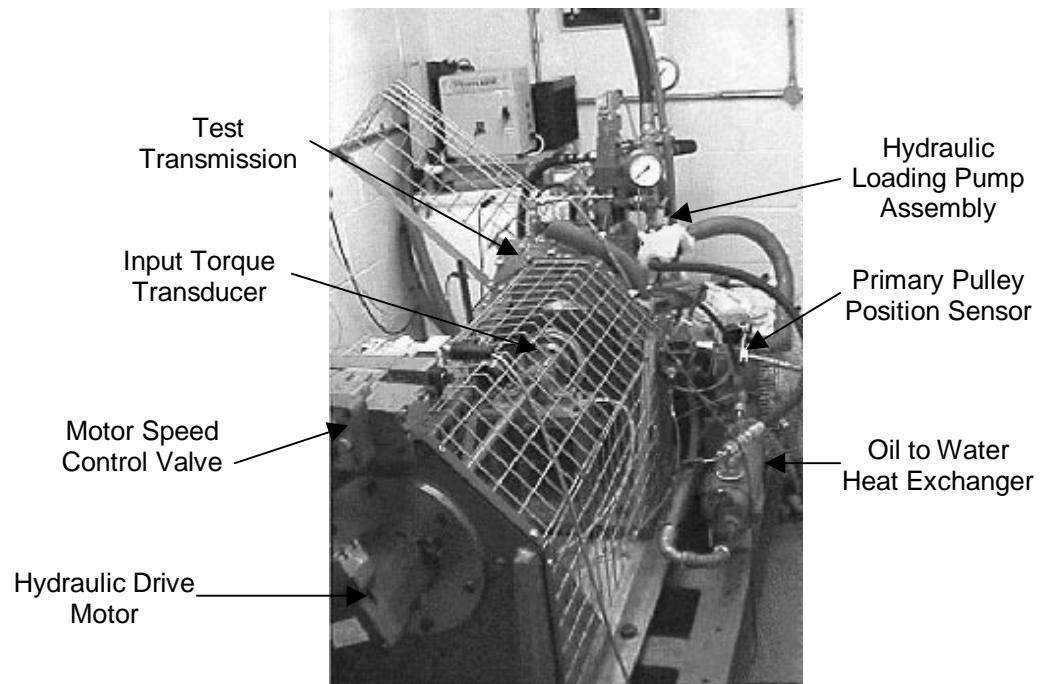
Figure 4-2 Pictorial View of the Transmission Test Rig

_____

(a) Test Rig at Minimum Throttle

(b) Test Rig at Maximum Throttle

(c) Transmission and Engine Operating at Maximum Throttle

(d)Transmission and Engine Operating at Minimum Throttle
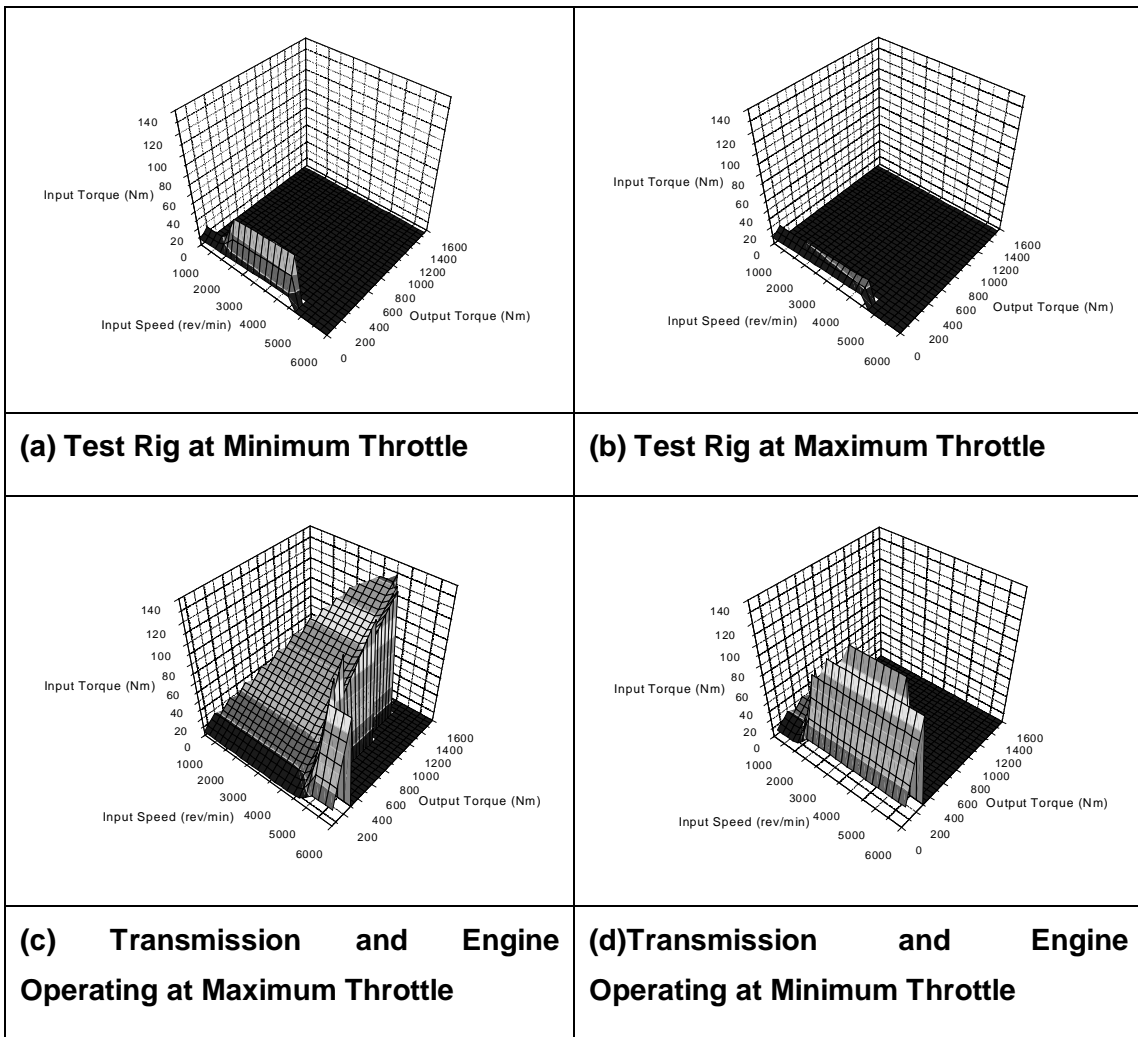
Figure 4-3 Typical Operating Envelope of Test Rig Compared to the Transmission Operating with an Engine

PC running
Windows based
DTVEE data
acquisition
software

2 x DT3001 16
channel data
acquisition cards

2 x 8 channel t-type
thermocouple
conditioning cards

Standard Euro card
frame containing 16
channels of conditioning
cards
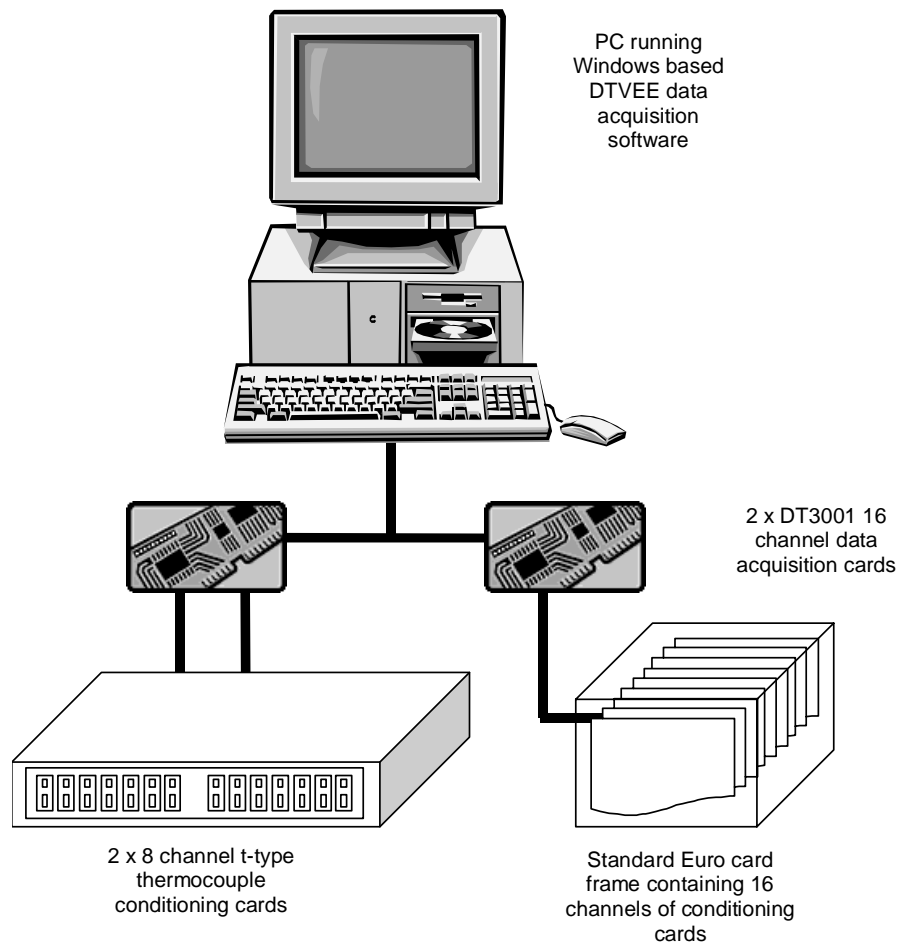
Figure 4-4 Schematic of Rig Instrumentation

HBM Torque Transducer
Conditioning Amplifiers

PID Temperature
Control Module

Input Speed
Control Card

Output Torque
Control Card

Conditioning Card
Frame

BNC Breakout
Monitoring Panel

Data Acquisition
PC Monitor
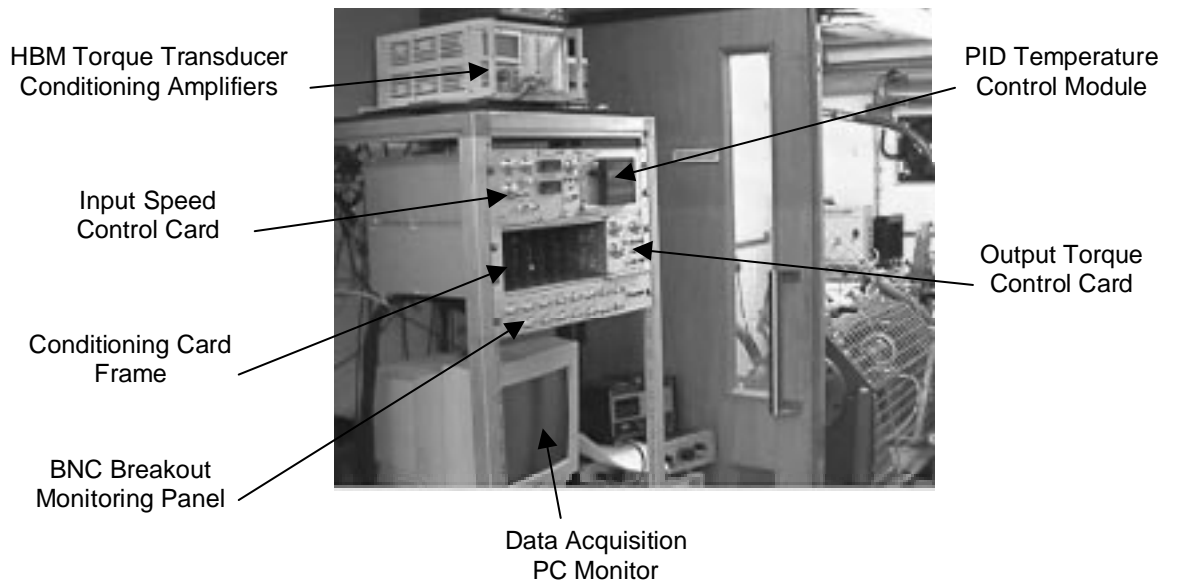
Figure 4-5 The Test Cell and Instrumentation Rack

Pulleys Ride on 'Band Packs'

X-Y Positioning Plate

Spring Pre-loading

Magnetic Belt Speed Sensor

LVDT Assembly
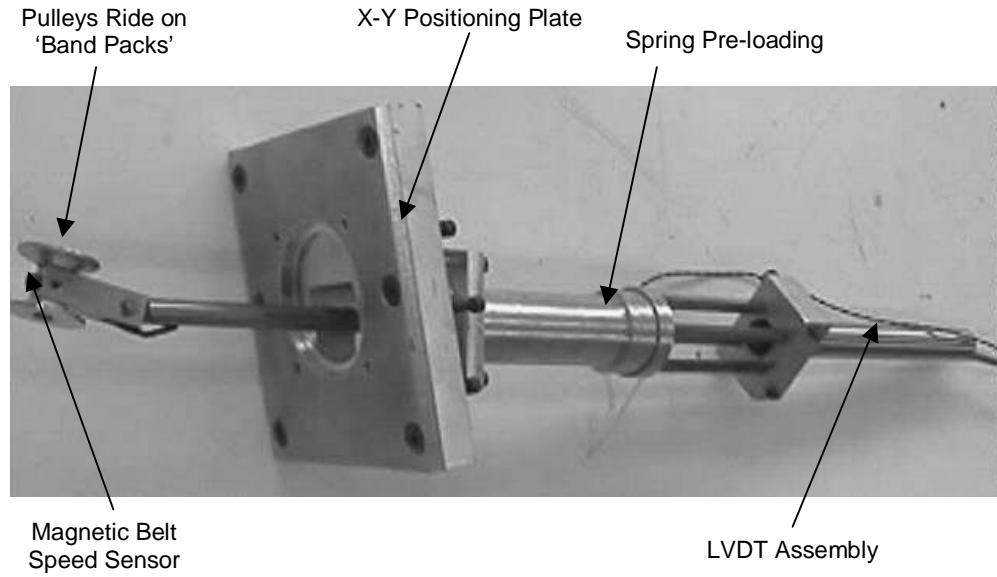
Figure 4-6 The Belt Radial Position Sensor

Supply from Hydraulic Ring Main Facility

Return to Hydraulic Ring Main Facility

Vickers 2-stage Proportional Directional Control Valve

Vickers 2-stage Proportional Pressure Relief Valve

Input Speed and Output Torque Control Inputs (0-10v)

Linde HMF28 Hydraulic Drive Motor (750-4500 rev/min)

Smoothing Accumulator

Bypass Flow Return to Ring Main

Variable Displacement Loading Pump

Transmission at Ratio (I) I≈2.5~13

Boosted Supply to Loading Pump

Figure 4-7 Schematic of Hydraulic Motor and Pump Circuit
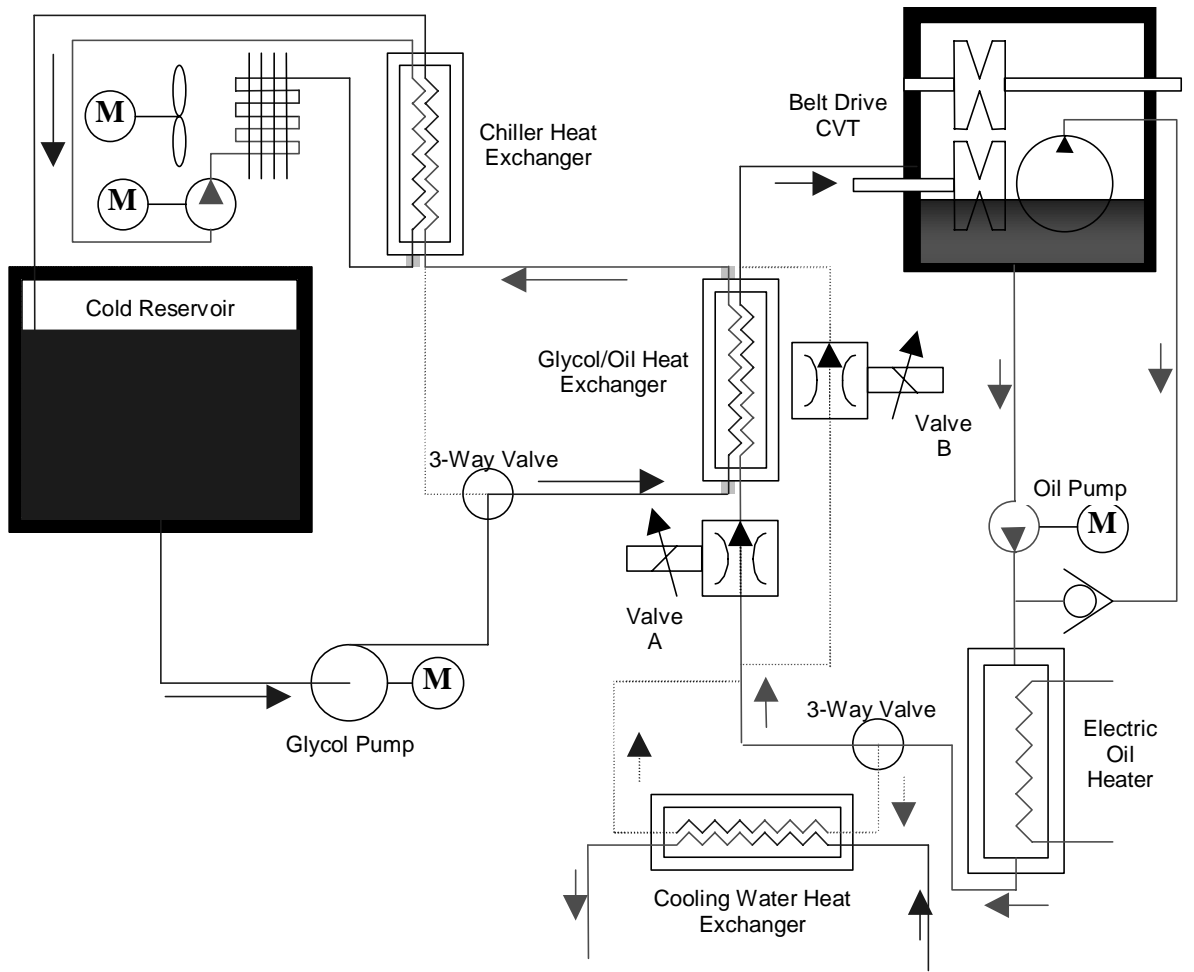
Figure 4-8 Transmission Test Rig Temperature Control System

_____

5   Experimental Torque Loss Results

5.1 Introduction

This chapter of the thesis details the experimental results collected solely on the transmission test rig, which was described previously in chapter 4. Detailed explanations are provided for the method of data collection, the accuracy of the results and methods of processing the acquired data into useful material for interpretation. Typical test results are presented in this chapter, with some initial observations being made. A more detailed analysis of the critical results is performed in chapters 7 & 8, where the experimental data is compared to the results of theoretical modelling.

5.2 Rig Calibration/Validation

Before any results from the rig could be used reliably the transducers had to be calibrated accurately and monitored for errors and repeatability. Some initial problems were discovered and rectified. Both input and output torque transducer signals required low pass filtering to remove noise from the excitation frequency of the hydraulic drive motor and load pump respectively. A range of different filter cut off frequencies were tested to find the most satisfactory solution. This was done by carrying out FFT (Fast Fourier Transform) analysis on the transducer output signals until the higher frequencies were attenuated satisfactorily. Since all the testing was to be steady state or slow transient in nature there were no implications of these filter settings for dynamic response.

The torque transducers were also found to be susceptible to temperature induced zero errors, although very small in magnitude (~0.5%). It was therefore necessary to check the transducer calibration regularly throughout a period of testing. During temperature transient tests, where temperatures might change considerably, the zero error was assumed to change linearly and was compensated for during the analysis of the experimental results.

It was also found that the calibration on the radial probes drifted as the transmission temperature changed. It was concluded that this was due to the expansion of the components of the probe and transmission casing as the temperature increased. The experimental data from the radial probes fitted to the transmission test rig was not

_____

_____

accurate enough to perform a satisfactory results analysis in the case of the temperature transient tests. However, the temperature drift experienced under temperature transient conditions did not exist during the steady state tests on either the transmission or the variator test rig (described in chapter 6).

5.3 Data Collection Methods

Experimental work with the transmission test rig was undertaken in two ways; steady state tests and temperature transient tests. For the steady state test conditions the rig was run for a suitable period of time for the transmission to stabilise at the required steady state testing temperature. Once the operating condition was achieved, the data was acquired once every second over a period of 30 seconds and then averaged. For each of the acquired data points the data acquisition system samples at 1000 Hz and averages the results. Therefore, the final value for a steady state test is effectively the average of 30000 samples. For the temperature transient tests the test rig was started and data were similarly acquired every second over a period of time while the transmission moved towards a steady state condition.

5.3.1 Steady State Rig Testing

Initial testing of the transmission was carried out under steady state conditions. Typically a temperature for testing was chosen and the rig run until that temperature was reached. To produce an overall map of results, tests were made in both high and low ratio extremes. In low ratio, tests were carried out at input speeds between 1000 and 4000 rev/min in nominal 250 rev/min steps. In high ratio the testing was carried out at input speeds between 1750 and 4000 rev/min, again in 250 rev/min steps. A number of standard bulk oil temperatures were eventually selected, for performing complete test matrices. These were 25, 50, 75 and 95°C. The first three temperatures were selected as nominal 25°C steps, while 95°C was selected as the expected maximum operating temperature of the transmission under standard driving conditions. Typical steady state torque loss results are shown in Figure 5-1 & Figure 5-2 for a low and high ratio test respectively. Corresponding sets of secondary pressure results are shown in Figure 5-3 & Figure 5-4

Referring to both figures the low ratio torque loss (Figure 5-1) ranges between 8.5 and 13 Nm, over a speed range of 1000 to 4000 rev/min. While the high ratio torque loss (Figure

_____

_____

5-2) varies between 9 and 13 Nm over a reduced speed range of 2000 to 4000 rev/min. The low ratio torque loss increases rapidly between 1000 and 2000 rev/min due to increases in the secondary pressure caused by the hydromechanical controller (Figure 5-3). After 2000 rev/min there is a lower gradient to the results, under conditions where the clamping pressure is nominally constant. This indicates a small speed dependency to the losses in low ratio, and a high dependency due to the clamping pressures in the variator. The losses in high ratio are obtained at a more constant clamping pressure, which is much lower than that seen in low ratio conditions, and decreases very gradually with speed (Figure 5-4). The results thus show a much greater speed dependency to the losses as the torque loss increases significantly over a speed range of 2000 rev/min. As both ratio extremes result in nominally equal torque losses it indicates that the losses in the other components of the transmission tend to be higher in high ratio, as the hydraulic pump losses should be reduced under this operating condition.

All of the torque loss and secondary pressure plots discussed above show results for a range of steady state temperature conditions. Both the torque losses and pressure levels are shown to vary with temperature and thus the results have to be corrected to compensate for this. The method for doing this is discussed on more detail in Section 5.4.

5.3.2 Temperature Transient Testing

Initial work acquiring the steady state test results indicated some unusual torque loss phenomena occurring as the transmission warmed up to steady state operating conditions, with the torque loss through the transmission increasing with respect to temperature under a number of test conditions. This was contrary to many of the initial model indications, which predicted torque losses decreasing as the viscosity of the lubricant decreases. To further investigate this discrepancy it was decided to measure the transmission performance under transient temperature conditions. For these tests the transmission input speed and output torque are set to pre-desired levels and the transmission is allowed to warm up from its starting temperature to a predetermined final temperature, nominally 95°C. At the final temperature condition the test rig cooling system is turned on and used to cool the rig down to its starting temperature, thus resulting in a complete temperature loop.

_____

_____

Typical temperature transient results are shown in Figure 5-5 & Figure 5-6 for low and high ratios respectively. The temperature hysterisis effect is clearly visible in both cases, as is a definite increase in torque loss at the higher temperatures in low ratio. During the warm up phase the low ratio case shows the torque loss decreasing from approximately 12.5 Nm to 11 Nm, at 80°C, before increasing by a further 0.25 Nm as the temperature rises to 100°C. As the transmission is cooled the torque loss increases rapidly, presumably due to increased viscous losses in certain transmission components. The torque loss in the cooling phase then matches the warm up phase torque loss at approximately 40°C. The result in high ratio shows less of a hysterisis affect and a minimal increase in torque loss. However, the torque loss does reduce from approximately 11 Nm to as low as 9.25 Nm showing significant temperature dependency.

5.3.3 Reduced Temperature Testing

One of the main aims of the investigation was to gain an understanding of the effects of temperature on the loss mechanisms within the transmission. Experimental results were taken at a number of reduced temperature conditions. In addition to the full matrices of steady state results that were recorded at 25, 50, 75 and 95°C, further results were also recorded at –5, 0, 5 and 10°C. Test results at these conditions were limited due to the performance of the cooling system on the transmission test rig, which was highly dependent on low ambient temperatures and low losses from the transmission to maintain low transmission temperatures for a period long enough to collect satisfactory data. In general trends from the few lower temperature results available indicated that the trends seen at 25°C and in the temperature transient tests simply continued, detailed analysis of the results was only performed in areas where complete data sets were available.

5.3.4 2nd Transmission Testing

A second transmission nominally identical to the original was tested after the original transmission to check for the variance between two builds of the same transmission. A difference in torque loss of around 1 Nm was found between the two test transmissions, with the original transmission having the slightly higher loss under all test conditions. While some of the discrepancy may be due to differences in build clearances etc., most of the difference is believed to be associated with differences in the clamping pressure

_____

demanded by the hydromechanical controller. The pressures were recorded and found to be nominally higher in the original transmission, by between 5 and 10%. The results from the back to back test of the second transmission are shown graphically in Figure 5-7 to Figure 5-14 for the two extreme ratio conditions and for all four temperature set points. In conclusion the testing of the 2nd transmission indicated a high level of confidence in the results from the original transmission, with no clear anomalies apart from those explainable by the hydromechanical controller affects.

5.3.5 Transmission Strip Down Tests

Following the tests on the complete transmission, a number of tests were performed stripping sequential components from the transmission to enable the contributions of individual components to the overall losses to be isolated. This was carried out in a number of stages listed below.

1. Final drive removed (final drive losses isolated)
2. Belt removed (belt losses isolated)
3. Clutch removed (clutch losses isolated)
4. Pump removed (input shaft losses tested in isolation)
5. Pump reinstalled for testing (pump torque loss isolated)

The method of testing at each part of this sequence is described in detail and then the results of these tests presented later in this chapter.

5.3.5.1 Final Drive Removed

The initial stage of the strip down test involved removing the final drive components from the transmission. The transmission then underwent steady state testing in both low and high ratio and at 25, 50, 75, and 95°C. The transmission was also tested at 2500 rev/min in each ratio for temperature transient results, which could be compared to those taken with the complete transmission.

The steady state results can be subtracted from the corresponding complete transmission results to obtain a measurement of the torque loss due to the final drive, referred to the input shaft of the transmission. This value in turn can be factored by the transmission ratio to indicate the torque loss occurring at the final drive itself. Figure 5-15 & Figure 5-16 show typical steady state and temperature transient results for both the complete

_____

transmission and the transmission with the final drive removed. The gap between the two results being the loss due to the final drive, although this does need to be corrected for different pressure levels as discussed in Section 5.4. Complete results for these tests are shown in Figure 5-17 to Figure 5-20.

5.3.5.2 Belt Removed

The second stage of the strip down procedure was to test with the belt removed from the transmission. Again the transmission underwent the same steady state and temperature transient tests as described above. With the belt removed the losses being measured are due to the reverse clutch drag, the hydraulic pump, and the bearing and seal drag on the input shaft. These results enabled the torque loss component due to the belt to be isolated. The complete results from the belt removal test are shown in Figure 5-21 to Figure 5-24.

5.3.5.3 Clutch Removed

This stage involved the removal of the reverse clutch plates so that the clutch torque loss component could be deduced from the difference between this stage and the previous stage results. Ideally the clutch packs would have been removed after the pump. However, removing the pump could invalidate the results as the pump supplies a fluid flow to lubricate the clutch plates, and any drag component to the clutch losses is due to the shearing of this oil film. The clutch losses were assumed to be independent of ratio and therefore these tests were performed only in low ratio, which allowed the maximum speed range to be investigated. Torque loss results with the clutch removed and the associated secondary pressures are shown in Figure 5-25 and Figure 5-26 respectively.

5.3.5.4 Pump Removed / Input Shaft Only

The next stage was to remove the hydraulic pump so that the losses for just the input shaft could be deduced. The input shaft was tested across the complete speed range and at the four standard steady state temperature conditions. Oil was circulated through the transmission by an independent pump to create operating conditions as normal as possible. The torque loss measured in this test gives a good indication of the input shaft losses, although it does not include the effects of bearing friction that may occur due to

_____

bearing load as the belt which normally loads the bearings has been removed. However, it is considered that this load dependent friction is likely to be insignificant compared to the speed dependent friction term, SKF **[50]**. The results from testing the input shaft in isolation are shown in Figure 5-27.

5.3.5.5 Pump Testing

To test the pump the original pump unit was reinstalled into the transmission. The transmission was then operated with the throttle in the fully open position to maintain high secondary pressures. An independently controllable pressure relief valve was then fitted to the secondary actuator tapping allowing the secondary pressure to be controlled to lower values, the return from this valve being returned to the sump of the transmission. The pump was then tested across the complete range of speeds, and temperature and pressure operating conditions to develop a torque demand map for the pump and input shaft. The results from these tests are shown in Figure 5-28 to Figure 5-31. The results from the input shaft testing were then subtracted from these results to provide the torque required for the pump in isolation.

5.4 Calculating the Torque Losses

It can be seen clearly from examples such as those in Figure 5-18 & Figure 5-22 that for each temperature test condition and independent test performed the secondary pressure at which the transmission operates is variable. Therefore to calculate the torque losses from individual components this effect must be taken into account, see Figure 5-32.

The ideal torque loss for a component, assuming that all pressures are equal, may be calculated by simply subtracting the two torque values for a corresponding speed condition-

$$T_{FDideal} = T_{complete} - T_{FDremoved}$$

But for this speed condition there is a secondary pressure difference given by-

$$\Delta P_{FD} = P_{complete} - P_{FDremoved}$$

Which corresponds to an approximate torque correction value for the hydraulic pump losses given by-

$$\Delta T_{FD} = D.\Delta P_{FD}$$

Thus the actual torque loss for the final drive is given by-

_____

$$T_{FDactual} = T_{FDideal} - \Delta T_{FD}$$

Similarly the equations below can be used to find the losses due to the belt mechanism and the clutch.

$$T_{BELTideal} = T_{FDremoved} - T_{BELTremoved}$$

$$T_{CLideal} = T_{BELTremoved} - T_{CLremoved}$$

$$T_{BELTactual} = T_{BELTideal} - \Delta T_{BELT}$$

$$T_{CLactual} = T_{CLideal} - \Delta T_{CL}$$

5.5 Magnitude of Individual Torque Loss Contributors

The results of the individual strip down tests are shown compiled in Figure 5-33 to Figure 5-36 and Figure 5-37 to Figure 5-40 for low and high ratios respectively, at the four steady state temperature test conditions. These plots allow simple comparisons to be made between the magnitudes of each contribution to the overall losses and how these contributions are affected by speed and ratio conditions.

Examining first the low ratio test conditions, shown in Figure 5-33 to Figure 5-36. The losses due to the hydraulic pump and the belt appear to be of a similar magnitude (approximately 3 & 4 Nm each), while the input shaft losses can vary between 1 & 2 Nm and the final drive losses appear to range between 0.25 & 1 Nm. Clutch losses are shown to be minimal. Total torque losses for the transmission appear to range between 8 & 13 Nm depending on operating conditions and lubricant temperature. The same general trends are seen across all the different temperature conditions.

Comparing the high ratio test conditions, Figure 5-37 to Figure 5-40, the total torque loss appears to peak at a similar value (13 Nm) to that seen in low ratio, but the distribution of the torque losses and characteristics of the torque loss curves change considerably. Pump torque loss is reduced considerably to between 1 & 2 Nm. Input shaft losses remain as they were in low ratio, while belt torque loss increases considerably to between 4 & 8 Nm approximately. The final drive torque loss also increases to up to 3 Nm. It should be noted however, that all these results are the torque losses referred to the input shaft of the transmission and some of the changes in magnitude are due to the change in effective ratio of the transmission rather than a change in the magnitude of the actual loss components.

_____

The individual contributions of each torque loss were then extracted from the complete data sets discussed in Sections 5.3.5.1 through to 5.3.5.5. These results were then corrected using the method described in Section 5.4. Results from these corrected torque loss figures are presented and discussed in more detail in the following sections of this chapter.

5.5.1 Final Drive Torque Loss

The corrected final drive torque losses are shown in Figure 5-41 & Figure 5-44 for the cases of low and high ratio respectively. The results displayed are for the torque loss referred to the input shaft of the transmission.

Low ratio results (Figure 5-41) show a small loss due to the final drive, typically <1 Nm referred to the input shaft, with a considerable amount of variance due to the errors introduced by adopting multiple sets of experimental data to calculate the losses. The loss at 25°C is consistently greater than that seen at any of the other temperatures indicating a possible viscous churning effect in the more viscous fluid. Losses at the other temperatures appear to average around a constant 0.5 Nm allowing for the expected errors, whereas the 25°C condition appear to average around 0.8 Nm. Speed dependence of the results appears to be minimal.

High ratio results (Figure 5-44) do not appear to follow any particular pattern, but are significantly higher with the 25°C result averaging at just below 3 Nm and all the other conditions averaging around 1 Nm. Taking into consideration the ratio effect the torque loss levels occurring at the final drive approximate to 1.5 Nm at 25°C in high ratio reducing to 0.5 Nm at other temperatures. Whereas in low ratio they equate to 2 Nm at 25°C, reducing to 1.25 Nm at the higher temperature conditions. This is unusual as the final drive losses are predicted to increase with speed and these results indicate the reverse occurring. The final drive speed in low ratio varies between 60 & 250 rev/min, but in high ratio the speed may vary between 400 & 1750 rev/min. This indicates that the speed dependent effects are very unpredictable.

5.5.2 Belt Torque Loss

The torque losses in the belt mechanism are shown in Figure 5-42 & Figure 5-45 for low and high ratios respectively. The torque losses in both cases appear to rise with respect to temperature in the steady state tests. These steady state results appear to indicate a possible mechanism for the torque loss increase phenomenon experienced in the earlier temperature transient tests performed on the complete transmission (Figure 5-5).

From some initial temperature distribution work that was performed on the transmission test rig, it was found that during the steady state temperature tests the temperature of the lubricant spray is generally 20°C higher than the bulk oil temperature. It can also be assumed that the temperature of the belt components is at a nominally similar temperature, since the temperature of the transmission has been allowed to stabilise. However, during the transient temperature tests, when the overall temperature is rising, the temperature of the internal components of the transmission can be assumed to lag behind both the bulk oil temperature and the lubricant spray temperature, due to the heat capacity of the components.

It is believed that the steady state belt torque loss results show the torque loss mechanism goes through an effective phase change as the lubrication regimes between contacting components vary from hydrodynamic lubrication to a boundary lubrication regime, as the temperature of the lubricant increases.

Studying Figure 5-42 in more detail, the low ratio belt torque loss is shown to be highly pressure dependent, considering the corresponding pressure profile (Figure 5-22), but with minimal speed effects present in the losses. However, in high ratio, Figure 5-45, where the clamping pressure on the belt is nominally constant or reducing, Figure 5-24, the losses appear to be clearly speed dependent.

5.5.3 Clutch Torque Loss

Figure 5-43 shows the calculated clutch drag torque for the four different temperatures and at all the speed conditions. The clutch was originally identified, from theory (see

_____

further details Section 7.6), as a significant contributor to the overall transmission losses. However, experimental measurements appear to indicate that this is not the case. Examination of the complete strip down tests in low ratio (clutch torque loss is independent of ratio condition), Figure 5-33 to Figure 5-36, show that the clutch torque loss is barely identifiable except possibly at the 25°C temperature condition. For completeness the clutch torque losses were calculated, Figure 5-43; it can be seen that the results are small. A maximum of 0.7 Nm torque loss was calculated at 25°C and at most of the other test conditions the losses are of the order of 0.2~0.3 Nm. This puts the result within the same order of magnitude as the error which can be expected from the experimental data, especially after the number of calculations performed on the multiple sets of data to arrive at this final result.

Therefore the only conclusions that can be drawn from these results is that the torque loss due to clutch drag is very small. Under most conditions the losses can be ignored, except at temperatures lower than 25°C, where they are best approximated as a small constant loss of approximately 0.5 Nm.

5.5.4 Pump Torque Loss

The measured hydraulic pump torque losses for the four different temperature test conditions are shown in Figure 5-28 to Figure 5-31. It should be noted that the results shown in these figures include the input shaft losses, which were measured afterwards, (see section 5.5.5). Therefore, the latter losses should be subtracted if a net measurement of the pump torque loss is desired. The plots show the variation in the torque loss with respect to both pump speed and the secondary pressure that the pump is supplying.

In general the pump torque loss appears to increase approximately linearly with the secondary pressure, as expected. There is also a small speed dependent effect on the pump torque, although this will be reduced slightly when the speed dependent effects of the input shaft losses are also removed. This small speed dependent term is likely to be associated with viscous friction in the pump mechanism. This theory is further supported by the reduction in pump torque loss seen at each incremental temperature condition. The pump relies on leakage flows to lubricate the moving components and at lower temperatures the fluid will have a higher viscosity resulting in more drag between the moving components.

_____

_____

5.5.5 Input Shaft Torque Loss

Figure 5-27 shows the results from the input shaft testing. It can be seen that generally the torque loss varies linearly with respect to the input speed, and that the torque appears to drop consistently as the lubricant viscosity decreases due to the increasing temperature. The loss mechanisms expected at the input shaft are derived from bearing friction and seal friction and suggest hydrodynamic oil films. Most bearing manufacturers produce formulae with which to calculate the bearing losses. However, these tend to rely on a number of coefficients, all of which vary over a large range of values, depending on the loading, sealing and lubrication regimes under which they are used.

5.6 Effective Ratio Change Measurements

Initial measurements made using the radial position probes and belt speed measurement system were inconclusive in indicating any belt slip. Although both systems were measuring effective ratio changes, the accuracy achievable between the many sets of experimental data was not sufficient to be reliable.

Both the radial position measurements and the belt speed vs. input and output speed appeared to show a torque dependent change in the transmission ratio. However, due to the low torque capacity of the test rig (max 100 Nm) the measurements were never large enough to quantify accurately. It was, however, considered important to be able to measure any belt slip that might be occurring, as this could be indicative of the torque transfer mechanism taking place between the belt/ pulley interfaces.

It was therefore decided to increase the torque envelope of the test rig. This was performed by mapping the speed and pressure effects on the torque requirement of the load pump using the existing 100 Nm torque transducer. The results showed that the pump was highly linear in both speed and torque effects and thus the load pump torque could be calculated by extrapolating the map to higher pressures, and measuring the pump speed and input and output pressures. However, even with this increase in torque envelope the slip test results were not conclusive. Therefore, it was decided to investigate slip phenomena using a different test rig facility, discussed in more detail in chapter 6 of this thesis.

_____
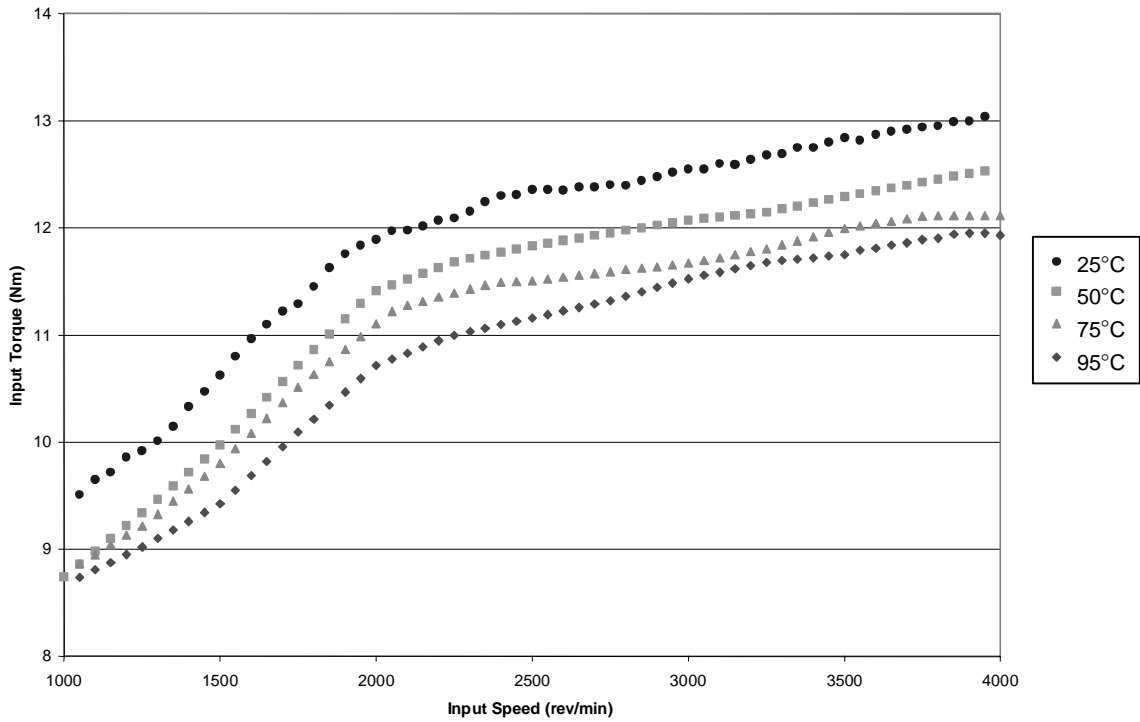
Figure 5-1 Typical Steady State Torque Loss Result in Low Ratio
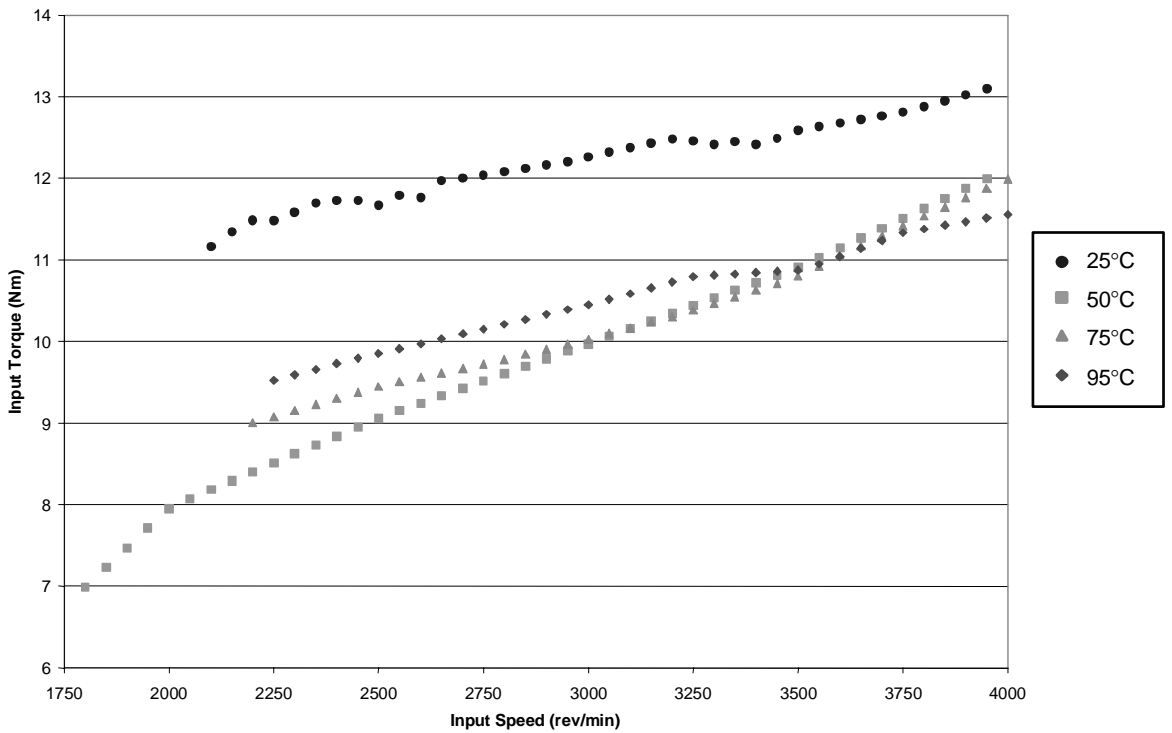
Figure 5-2 Typical Steady State Torque Loss Result in High Ratio
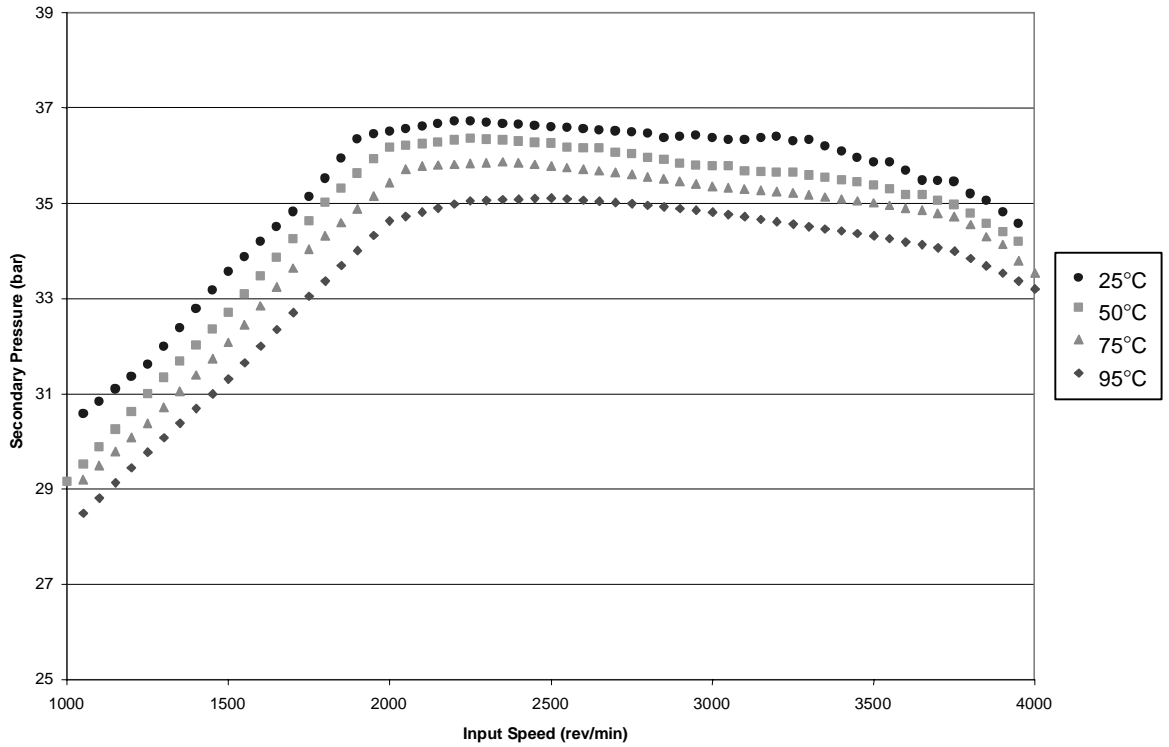
Figure 5-3 Typical Steady State Secondary Pressure Results in Low Ratio
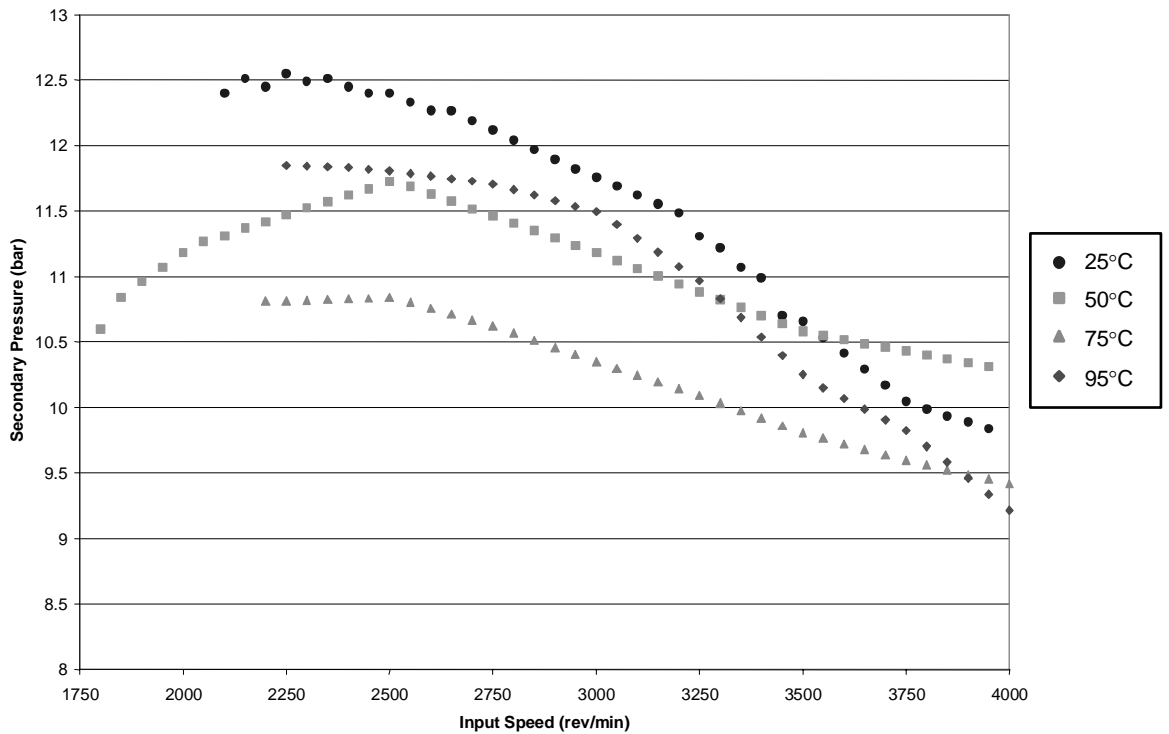
Figure 5-4 Typical Steady State Secondary Pressure Results in High Ratio
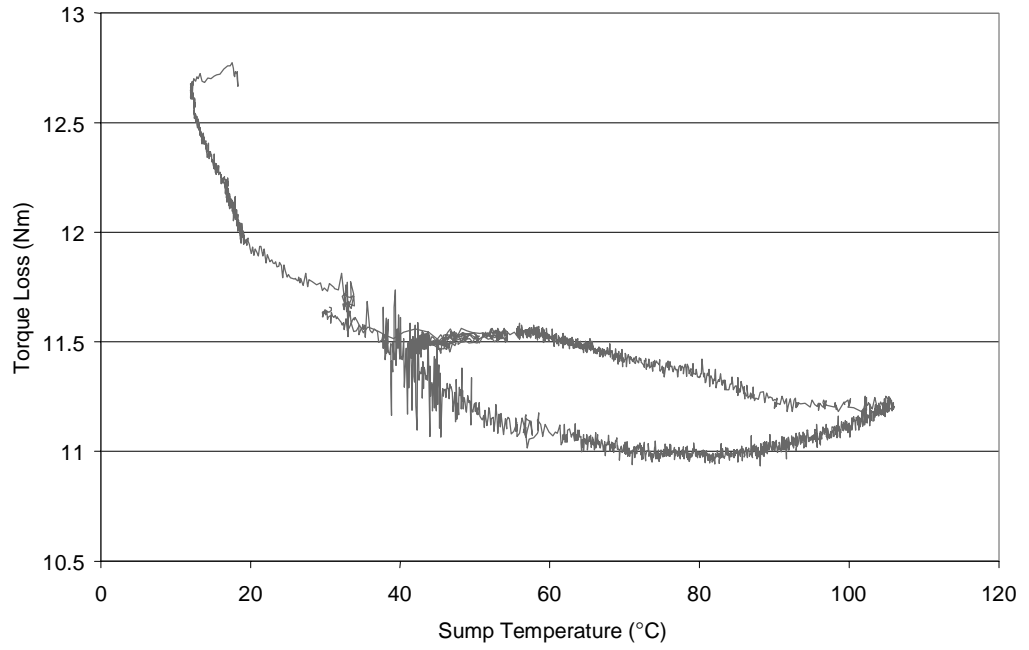
Figure 5-5 Typical Temperature Transients at 2500 rev/min in Low Ratio
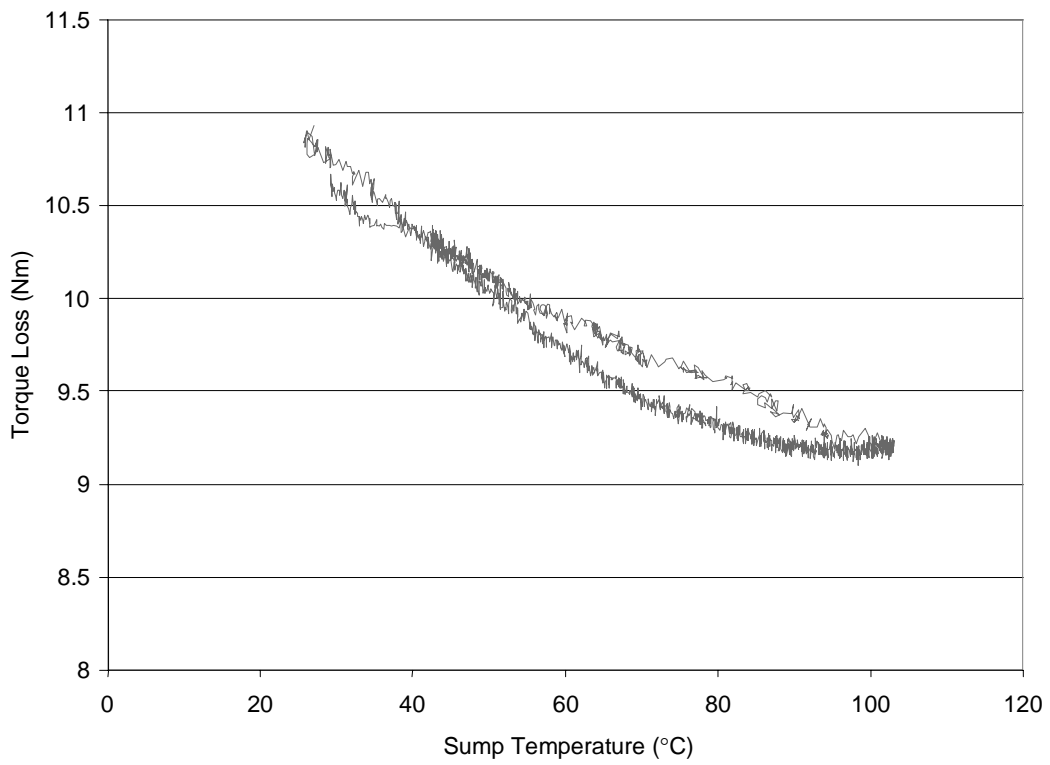
Figure 5-6 Typical Temperature Transients at 2500 rev/min in High Ratio

_____

Figure 5-7 Comparing 2nd Transmission in Low Ratio 25°C

Figure 5-8 Comparing 2nd Transmission in Low Ratio 50°C

Figure 5-9 Comparing 2nd Transmission in Low Ratio 75°C

Figure 5-10 Comparing 2nd Transmission in Low Ratio 95°C

_____

_____

Figure 5-11 Comparing 2ⁿᵈ Transmission in High Ratio 25°C

Figure 5-12 Comparing 2ⁿᵈ Transmission in High Ratio 50°C

Figure 5-13 Comparing 2ⁿᵈ Transmission in High Ratio 75°C

Figure 5-14 Comparing 2ⁿᵈ Transmission in High Ratio 95°C

_____

_____
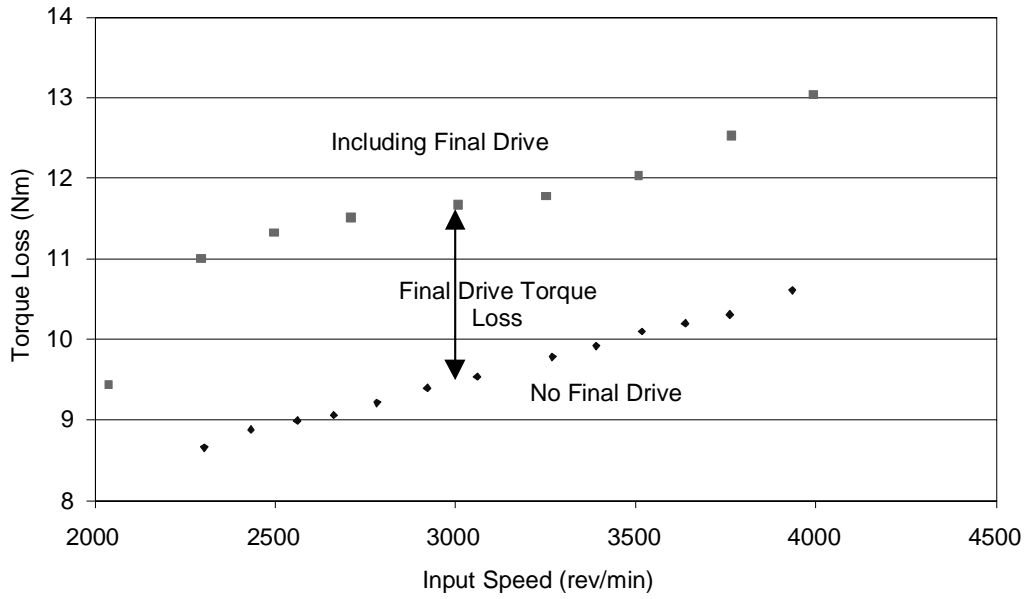
Figure 5-15 Effect of Final Drive Removal at 50°C in High Ratio
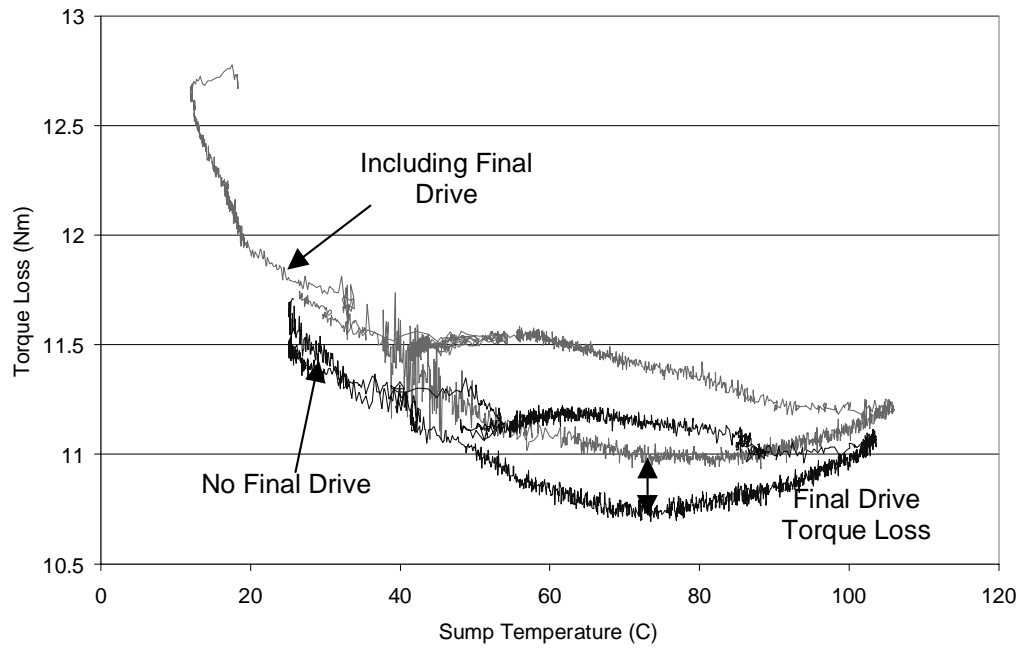
Figure 5-16 Comparing Temperature Transients at 2500 rev/min in Low Ratio, Before and After Final Drive Removal

_____

Figure 5-17 Measured Torque Loss, Final Drive Removed, Low Ratio

Figure 5-18 Measured Secondary Pressure, Final Drive Removed, Low Ratio

Figure 5-19 Measured Torque Loss, Final Drive Removed, High Ratio

Figure 5-20 Measured Secondary Pressure, Final Drive Removed, High Ratio

_____

● 25°C	■ 50°C	▲ 75°C	◆ 95°C

Figure 5-21 Measured Torque Loss, Belt Removed

Figure 5-22 Measured Secondary Pressure, Belt Removed

Figure 5-23 Measured Torque Loss, Belt Removed

Figure 5-24 Measured Secondary Pressure, Belt Removed

Figure 5-25 Measured Torque Loss, Clutch Removed

Figure 5-26 Measured Secondary Pressure, Clutch Removed

_____

Figure 5-27 Torque Loss at Input Shaft, all Other Components Removed
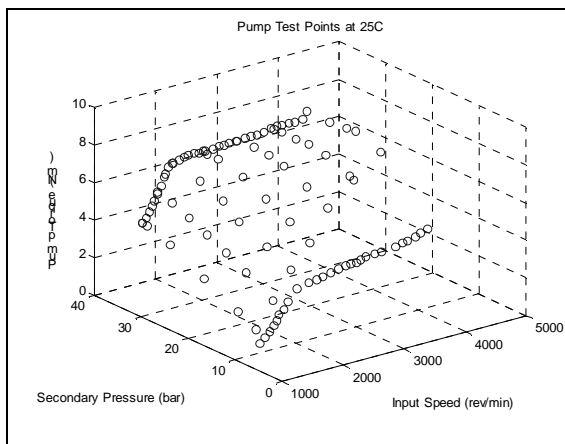
Figure 5-28 Pump Torque Loss at 25°C with Input Shaft Losses Included	**Figure 5-29 Pump Torque Loss at 50°C with Input Shaft Losses Included**
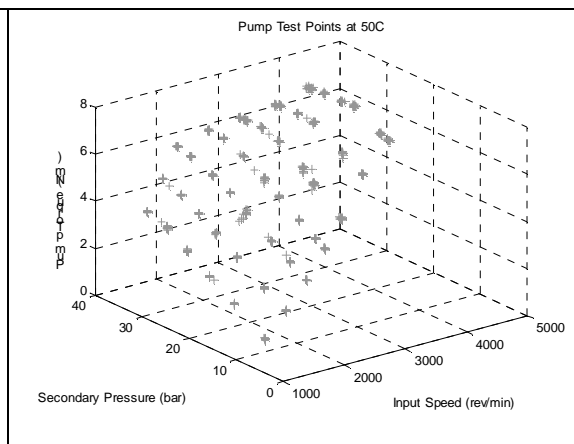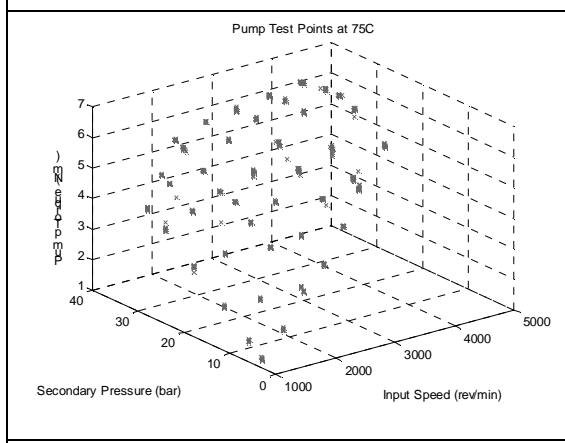
Figure 5-30 Pump Torque Loss at 75°C with Input Shaft Losses Included	**Figure 5-31 Pump Torque Loss at 95°C with Input Shaft Losses Included**
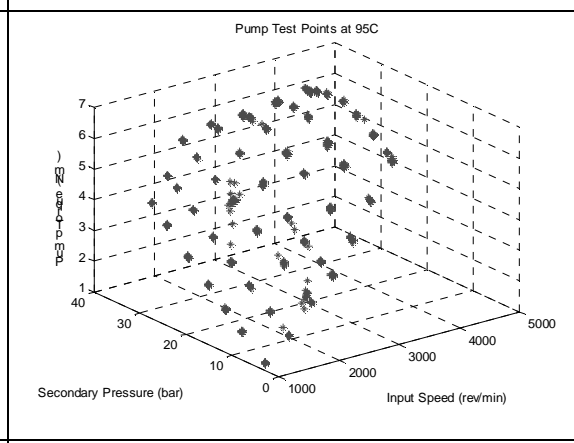
Figure 5-32 Method for Calculating Corrected Torque Losses

_____

Figure 5-33 Complete Strip Down Results in Low Ratio 25°C

Figure 5-34 Complete Strip Down Results in Low Ratio 50°C

Figure 5-35 Complete Strip Down Results in Low Ratio 75°C

Figure 5-36 Complete Strip Down Results in Low Ratio 95°C

_____

Figure 5-37 Complete Strip Down Results in High Ratio 25°C

Figure 5-38 Complete Strip Down Results in High Ratio 50°C

Figure 5-39 Complete Strip Down Results in High Ratio 75°C

Figure 5-40 Complete Strip Down Results in High Ratio 95°C

_____

Figure 5-41 Corrected Final Drive Torque Loss, Low Ratio

Figure 5-42 Corrected Belt Torque Loss, Low Ratio

Figure 5-43 Corrected Clutch Torque Loss

_____
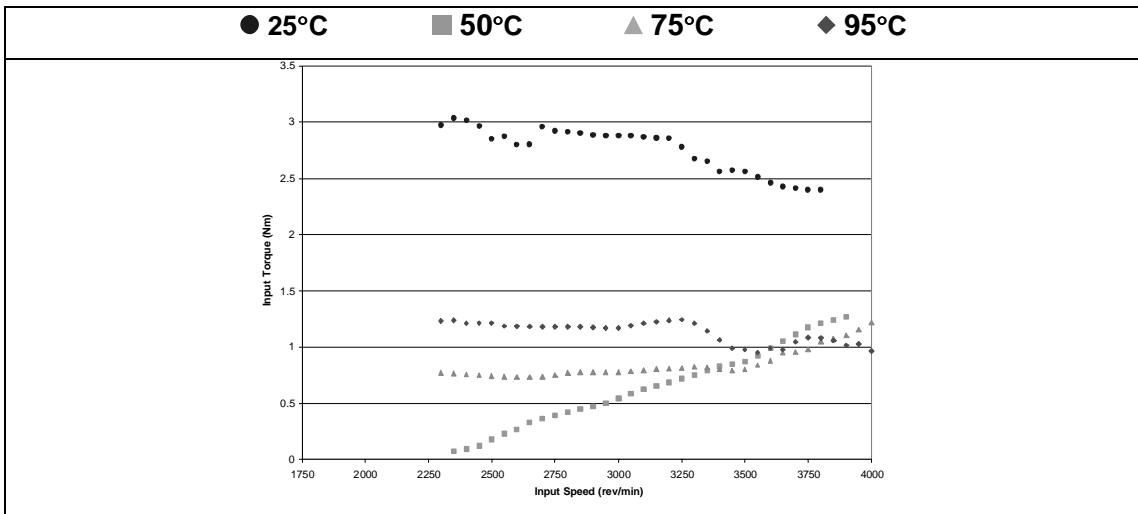
Figure 5-44 Corrected Final Drive Torque Losses, High Ratio
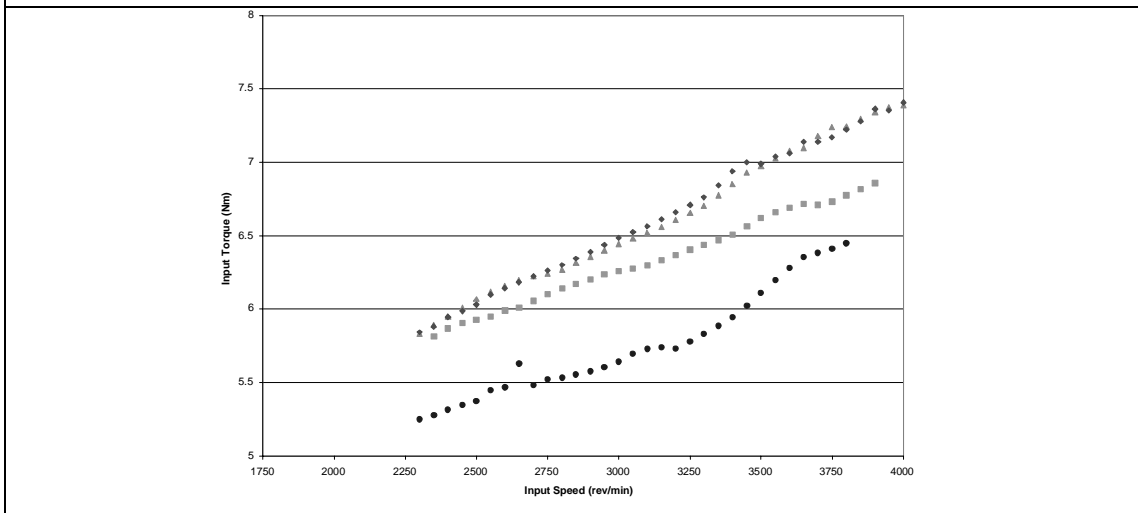
Figure 5-45 Corrected Belt Torque Losses, High Ratio

_____

6   The Belt Variator Test Rig

6.1 Introduction

Following analysis of the work carried out with the original transmission test rig it was clear that further work needed to be undertaken to investigate the effects of belt slip that may be occurring in the belt mechanism. The reasoning behind this is two-fold. Firstly, any belt slip is an inefficiency that may be as great as any of the torque loss mechanisms and it is therefore essential to model. Secondly, a knowledge of the functioning of any belt slip might well lead to an understanding of the fundamental torque transfer mechanisms occurring in the belt. Therefore this section of the thesis details the development of a second test rig. The rig is based upon the belt variator only and was designed primarily to investigate the effects of belt slip. This chapter details the instrumentation techniques developed to measure the slip, the calculations performed to process the collected data and presents results from the test rig.

6.2 The Variator Test Rig

In order to investigate the slip losses occurring in the metal V-belt testing at higher torque levels in a new test rig was necessary. The rig was designed and built to test the variator mechanism of the belt in isolation, with independent control over the belt ratio and primary and secondary pulley clamping pressures. The new rig also allowed testing to much higher output torques than were possible on the original transmission test rig, in order to instigate higher levels of belt slip and recreate more realistic drive line torque levels.

The variator rig is shown schematically in Figure 6-1, and pictorially in Figure 6-2. Due to budgetary restrictions the instrumentation and choice of components on the rig were very limited. A hydraulic axial piston motor, powered from a hydraulic ring main facility, drives the rig, while a variable displacement axial piston pump unit loads the output shaft of the variator. As with the original rig the outlet from the drive motor acts as a boost supply for the load pump. Two hand operated flow control valves arranged in parallel control the input speed, and a simple hand operated pressure relief valve controls the output torque.

The rig was instrumented to record torques up to 400 Nm at the secondary pulley and 250 Nm at the primary pulley, while the maximum speed was limited to 3000 rev/min at the

_____

_____

input shaft. The performance characteristics of the original transmission test rig vs. the new variator test rig are highlighted in Table 6-1.

6.3 Variator Rig Instrumentation

The aim of the variator test rig was primarily to measure the slip losses that might exist in the metal V-belt. Therefore the rig was instrumented accordingly. The variables measured and recorded are shown in Table 6-2.

The torque transducers selected were those available in the Department that fitted the torque loads at which testing was intended. Due to the type of transducer (brush contacts) and the large torques being measured, the results were not satisfactory enough to calculate the torque loss through the variator. However, the output torque transducer gave a reliable enough output to record the output torque to within ±2 Nm.

The pressure transducers acted primarily as a method of setting the primary and secondary clamping pressures prior to a test, while the LVDT probes were the units from the original transmission test rig transferred across to perform this work.

6.3.1 Variator Speed Ratio Measurement

The variator test rig allowed highly accurate measurements to be made of the speed ratio through the variator. Magnetic pickup speed sensors were used on the input shaft, output shaft and to detect the belt speed by counting the segments on the belt as they passed. To increase the accuracy the speed data were collected in a pulse format using digital counter timer units. Each of the magnetic pickup devices was conditioned using in house frequency to voltage cards; the input stages of these conditioning cards produce more uniform pulses than those received directly from the output of the magnetic pickup. These conditioned pulses were then counted using the counter timers and the results recorded manually.

Each test condition was repeated three times, giving highly repeatable results. The counter timer units were triggered to start counting in two different ways. Figure 6-3 shows the data collection technique in high ratio; here the counter timers are triggered by a square wave output from a PC D to A card, of 10 seconds duration. However, in low ratio

_____

_____

the belt speed is very low and the magnetic pickup cannot detect the individual belt segments. Therefore the counter timers are triggered by a once per rev signal from the belt (Figure 6-4). This was achieved by grinding the tip from one belt segment and configuring the F to V card so that it could only detect the pulse from that segment. A frequency divider was then used to trigger the counter timers every 100 belt revolutions.

From the data recorded on the counter timers belt and pulley speeds could be calculated. For example using the high ratio data acquisition method the speed of the belt is given by

$$v_{belt} = \frac{(N_{seg} \times t_{seg})}{10} \qquad \text{(m/s)}$$

Where t_{seg} is the thickness of a belt segment in metres, which is the measured average of 50 belt segments. The speed of each pulley is calculated thus

$$\omega_{pri} = \frac{2\pi \times N_{pri}}{10.n_{pri}} \qquad \text{(rad/s)}$$

$$\omega_{sec} = \frac{2\pi \times N_{sec}}{10.n_{sec}} \qquad \text{(rad/s)}$$

Where N is the number of pulses counted and n is the number of teeth per revolution on the respective shafts. Similarly, using the low ratio data acquisition method, described above, the speed of the belt is given by

$$v_{belt} = \frac{(100 \times L_{belt})}{T}$$

Where, L_{BELT} and T are the length of the belt in metres and the time in seconds required for 100 belt revolutions respectively. The speed of each pulley is given by-

$$\omega_{pri} = \frac{2\pi \times N_{pri}}{T.n_{pri}} \qquad \text{(rad/s)}$$

$$\omega_{sec} = \frac{2\pi \times N_{sec}}{T.n_{sec}} \qquad \text{(rad/s)}$$

6.3.2 Variator Actual Ratio Measurement

The actual belt ratio was measured by recording the LVDT data from the radial probe units transferred form the original transmission test rig. The LVDTs were re-scaled so that they were operating around their most linear region and so that they were highly sensitive. For each of the ratio conditions tested, the LVDTs were relocated to operate around their

_____

_____

central position. LVDT signal conditioning was performed using an off the shelf oscillator demodulator card scaled to give a full range 0 to 10 V output for an LVDT travel of +/- 2.5 mm. The accuracy of calibration was checked repeatedly. Output from the LVDT conditioning card was recorded in voltage format into a PC based data acquisition system with data from all the other transducers.

The raw voltages from the LVDTs were post-processed after data acquisition to represent actual belt radii. This was achieved by assuming that the variator slip at zero output torque would be zero. Thus, initial belt radii can be calculated from the belt geometry and the speed ratio at zero torque conditions. From these conditions relative changes and thus actual belt radii can be calculated directly from the LVDT data.

6.3.3 Calculating Slip Speeds

The data collected from the counter timer units and the PC based data acquisition system had to be manipulated to derive the slip speed occurring in the variator. The total slip through the variator may be calculated as follows

$$\%_{SLIP} = \frac{(I_{pulse} - I_{LVDT})}{I_{LVDT}} \times 100$$

Where I_{pulse} is the pulse derived speed ratio while I_{LVDT} is the actual position ratio of the belt, derived from the LVDT data. Such that

$$I_{pulse} = \frac{n_{pri}}{n_{sec}}$$

$$I_{LVDT} = \frac{R_{sec}}{R_{pri}}$$

Similarly, the primary and secondary pulley slip speeds may be derived as follows

$$v_{slip,pri} = R_{pri}\omega_{pri} - V_{belt}$$

$$v_{slip,sec} = R_{sec}\omega_{sec} - V_{belt}$$

Where R_{pri} and R_{sec} are derived from LVDT data and ω_{pri}, ω_{sec} and V_{belt} are derived from pulse count data.

6.4 Variator Rig Results

_____

_____

Initial results from the variator test rig for low and high ratio can be seen in Figure 6-5 & Figure 6-6 respectively. Both of the plots show primary and secondary radii derived from pulse data and LVDT data. The LVDT radii are derived directly from the calibration values of the transducers and the recorded voltages, while the pulse radii are defined as follows.

$$R_{pri\_pulse} = \frac{V_{belt}}{\omega_{pri}}$$

$$R_{sec\_pulse} = \frac{V_{belt}}{\omega_{sec}}$$

Examining the LVDT derived plots in Figure 6-5, it can be seen that as the torque load on the output shaft is increased the actual ratio of the belt changes. The primary pulley moves to a smaller radius and the secondary pulley moves to a larger radius, i.e. the belt moves further towards low ratio. A similar phenomenon is seen in high ratio (Figure 6-6), with the belt again moving towards low ratio.

However, if the results from the pulse count data are plotted against these results they show an even larger change in the expected radii calculated from the speed ratios of belt relative to each of the pulleys. This difference in actual radius and radius calculated from speed data at the secondary pulley is indicative of the belt having a higher speed than the secondary pulley. Similarly at the primary pulley the difference is indicative of the primary pulley moving faster than the belt. In low ratio (Figure 6-5) it can be seen that the LVDT data tracks the pulse data on the primary pulley at torques less than ~75 Nm indicating that slip does not occur at the primary pulley below this torque level.

It should be noted that the results for the high ratio test are presented over a smaller range of output torques than the low ratio tests. This was due to a limitation in the available torque at the input shaft of the test rig. The analysis of the slip speeds was performed at low ratio since this would be the situation in a vehicle in which the transmission would see the highest output torque loads.

The results in low ratio were repeated at a range of secondary clamping pressures from 15 to 35 bar and the differences between the speed ratios and position ratios were calculated to give a percentage slip through the variator system, as in section 6.3.3. The results of these tests are shown in Figure 6-7. It can be seen that as the output torque is increased initially the slip is zero until a breakpoint occurs and the slip through the variator begins to increase; the increase in slip with load seems to be relatively linear. However, as the clamping pressure on the secondary pulley is reduced the torque at which the

_____

_____

breakpoint occurs is reduced. Thus in the region where slip is occurring, the slip will be nominally higher for an identical output torque with a lower clamping pressure. The results show slips up to 3% and under most test conditions slip is in the 1~2% range. This makes the existence of slip significant and worthy of consideration in relation to the overall losses in the belt drive.

The results appear to show that for a given clamping force there is a maximum limit due to friction at which no slip occurs. If this frictional force is overcome then the belt begins to slip over the pulley surface. Further increasing the torque continues to increase the rate of slip.

To understand how this slip was occurring and where, it was decided to split the slip into the components occurring about each of the pulleys and to express them as a slip speed. The results from this can be seen in Figure 6-8 and Figure 6-9 for the primary and secondary pulley respectively. The maximum slip speed about the primary pulley is approximately 0.14m/s, while at the secondary pulley the slip speeds of 0.04m/s are considerably lower. The difference in slip speeds between the two pulleys is significant and can thus lead to some deductions about the mechanism causing the slip in the belt drive. These are discussed in more detail in the modelling section (chapter 8) of this thesis.

_____

	Original Transmission Test Rig	New Variator Test Rig
Input Torque	Max. 100 Nm	Max. 250 Nm
Output Torque	100 Nm at Output Shaft	400 Nm at Secondary Pulley (equivalent 2000 Nm at Output Shaft)
Input Speed	Up to 4500 rev/min	Max. 3000 rev/min
Output Speed	50-1750 rev/min	Up to 3000 rev/min
Pressures	No control due to integral CVT controller	Primary max. 40 bar
		Secondary max. 40 bar

Table 6-1 Comparing Original and Variator Rig Performance

Variable Measured	Transducer/ Range	Signal Conditioning Card
Input Torque (T_{in})	Vibrometer 250 Nm Shaft Torque transducer	Vibrometer conditioning amplifier and display.
Output Torque (T_{out})	Hovercraft 400 Nm Shaft Torque transducer	DC amplifier Card
Input Speed (ω_{in})	Magnetic pick-up (0-3000 rev/min)	Frequency to Voltage converter
Output Speed (ω_{out})	Magnetic pick-up (0-3000 rev/min)	Frequency to Voltage converter
Belt Speed	Magnetic pick-up	Frequency to Voltage converter
Primary Pulley Position	Radial probe LVDT	Carrier frequency card
Secondary Pulley Position	Radial probe LVDT	Carrier frequency card
Primary Pulley Pressure	0 – 40 bar	DC amplifier card
Secondary Pulley Pressure	0 – 40 bar	DC amplifier card

Table 6-2 Variables Measured on Variator Rig
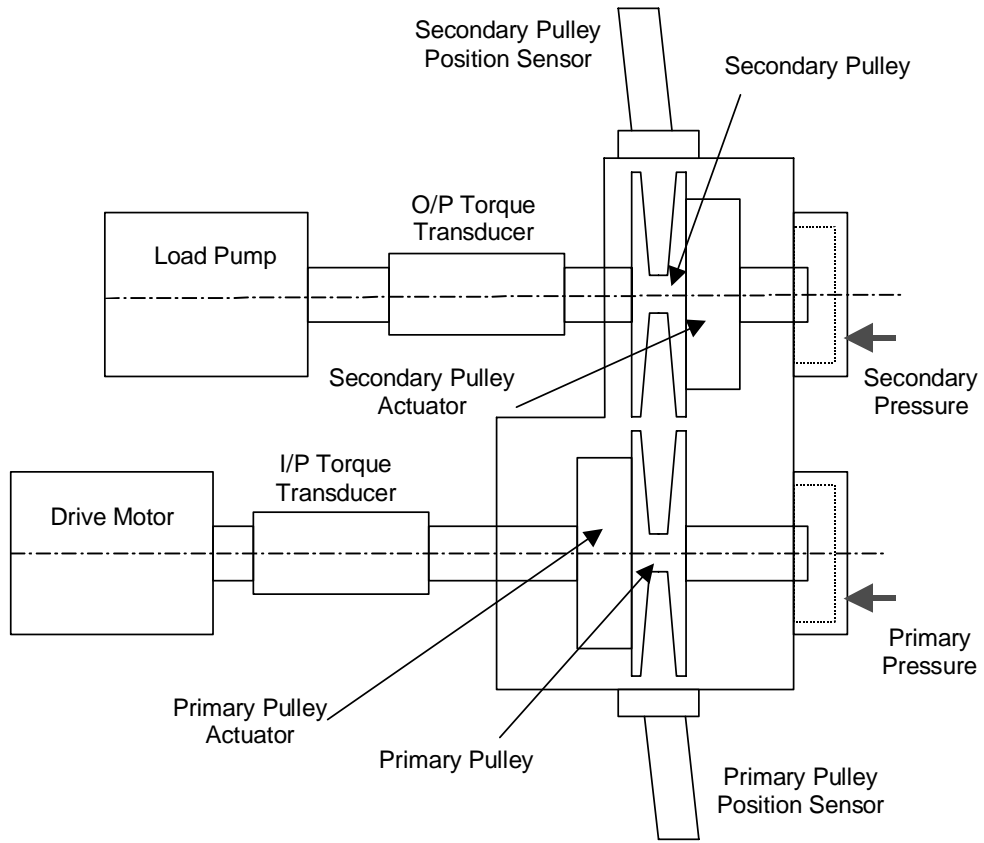
Figure 6-1 Schematic of the Belt Variator Test Rig
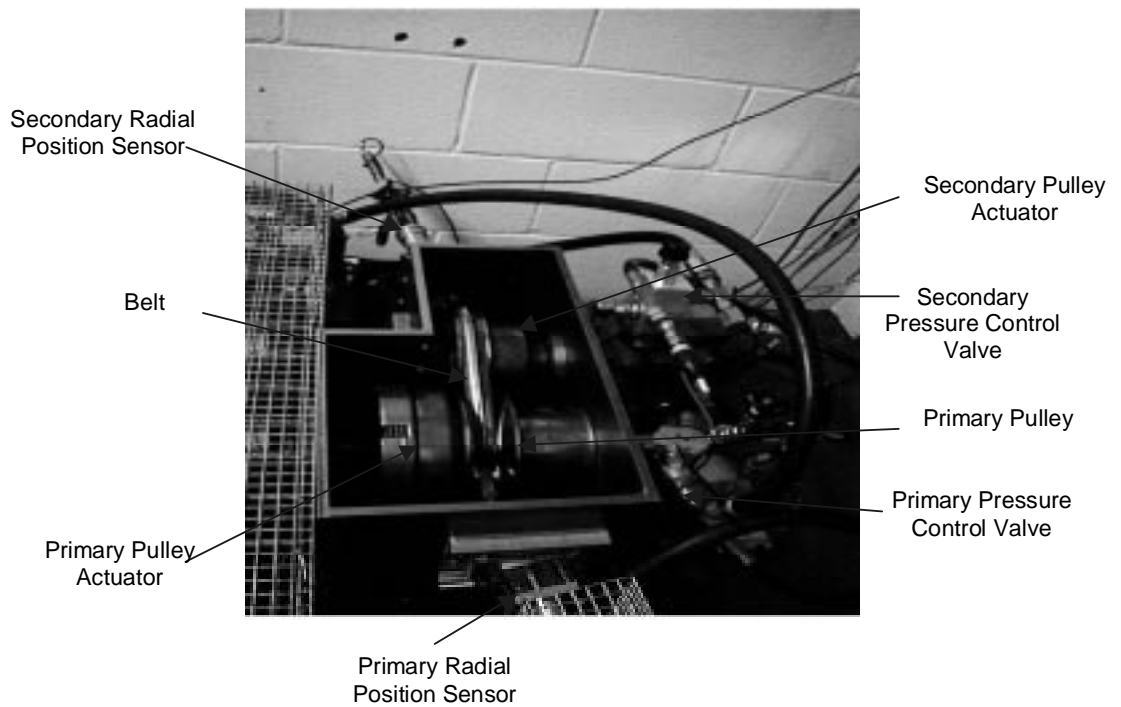
Figure 6-2 The Variator Test Rig
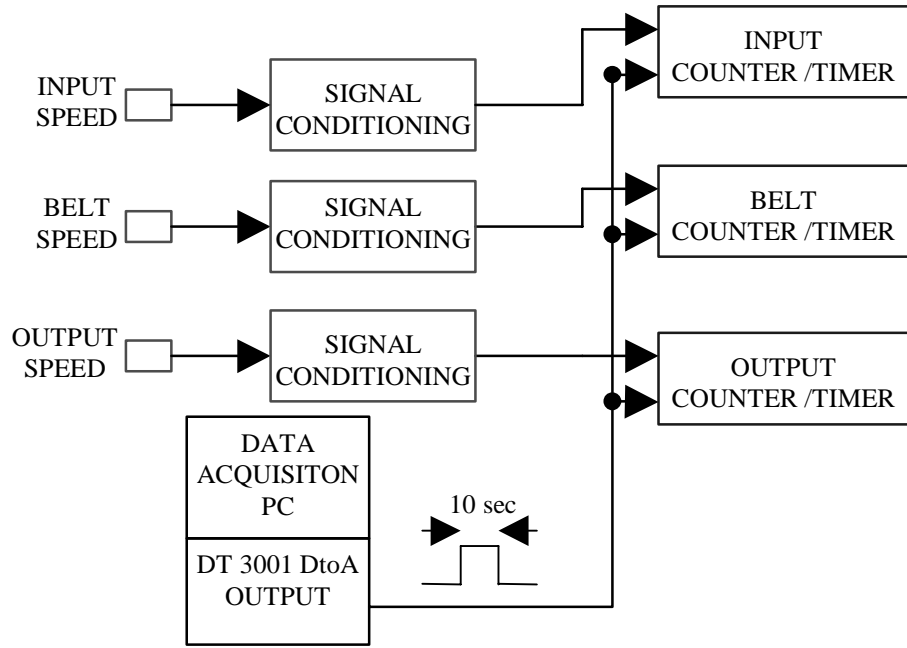
Figure 6-3 Pulse Data Collection Method in High Ratio
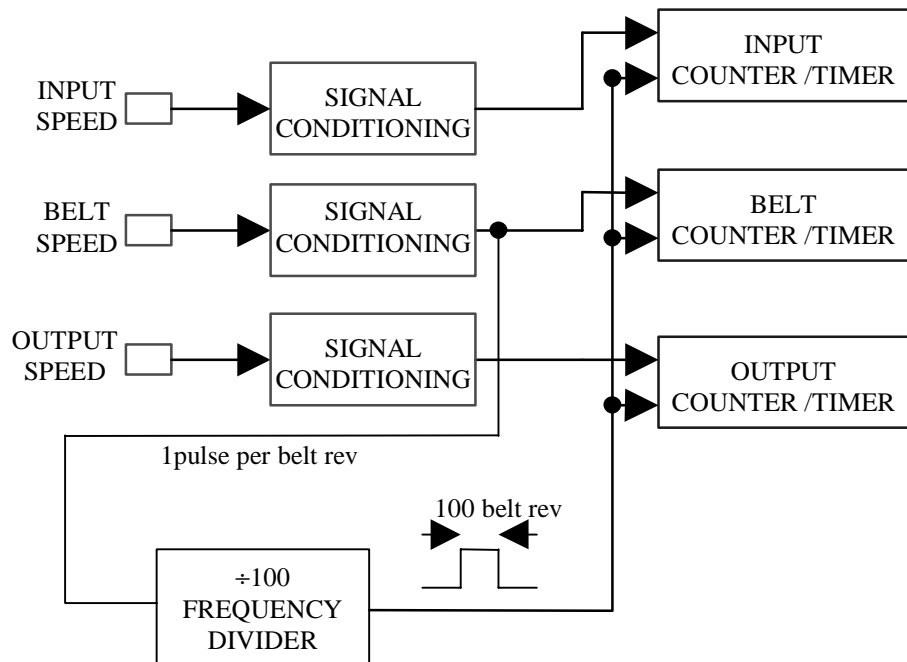
Figure 6-4 Pulse Data Collection Method in Low Ratio

_____
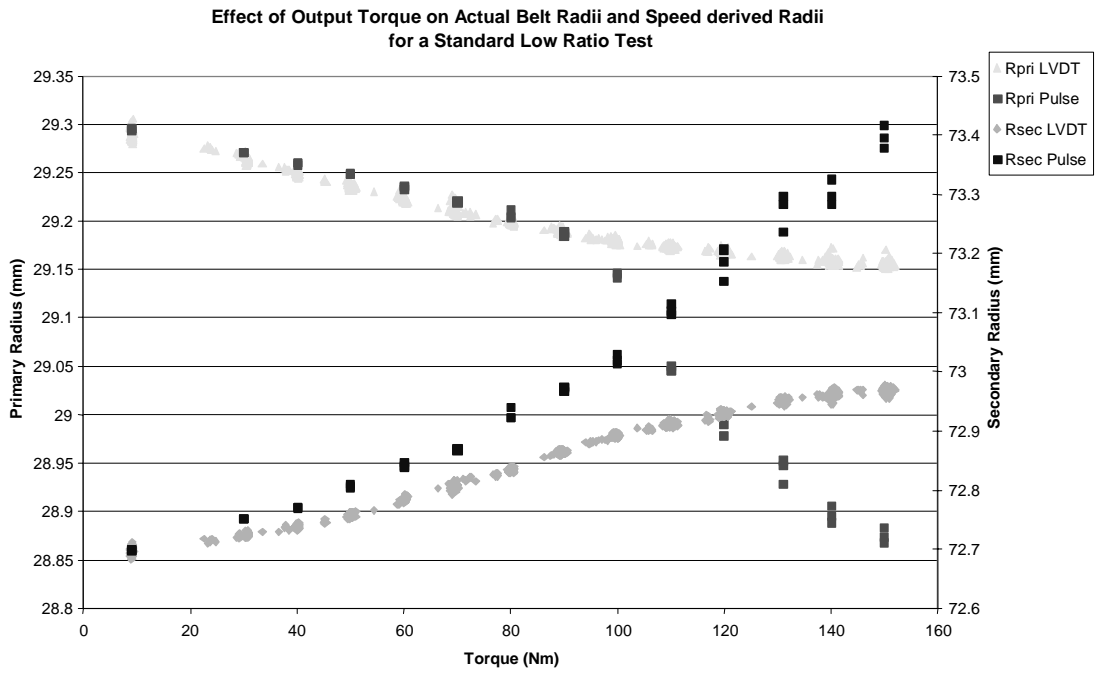
Figure 6-5 Typical Ratio Change Effects in Low Ratio
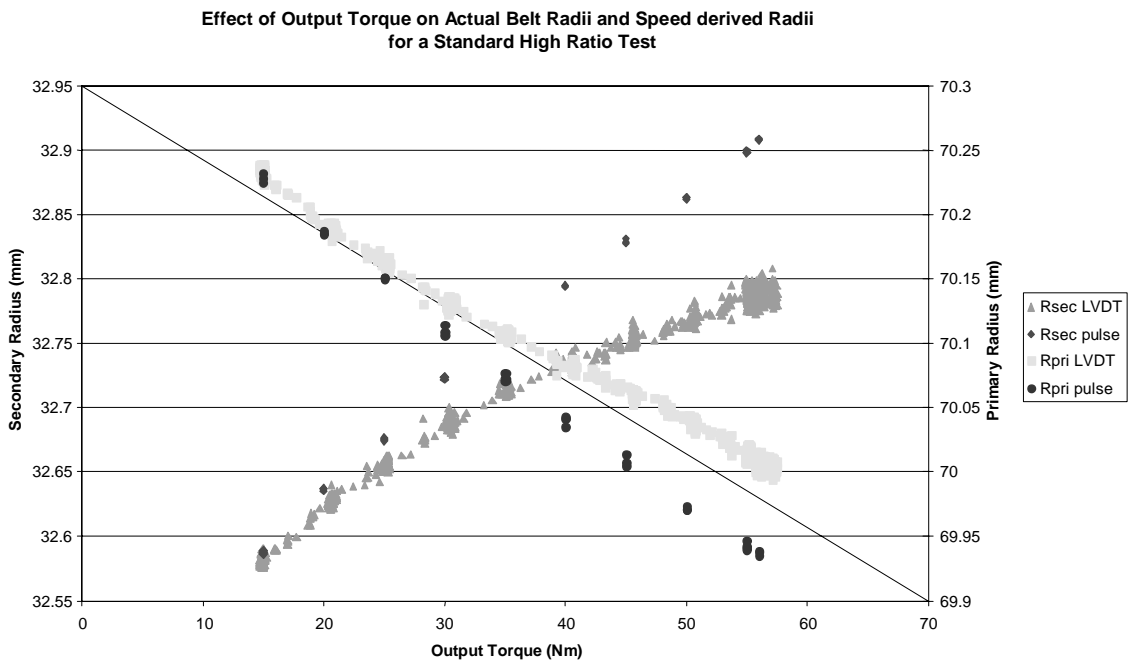
Figure 6-6 Typical Ratio Change Effects in High Ratio

_____

Effect of Clamping Pressure on % Slip in Low Ratio Tests
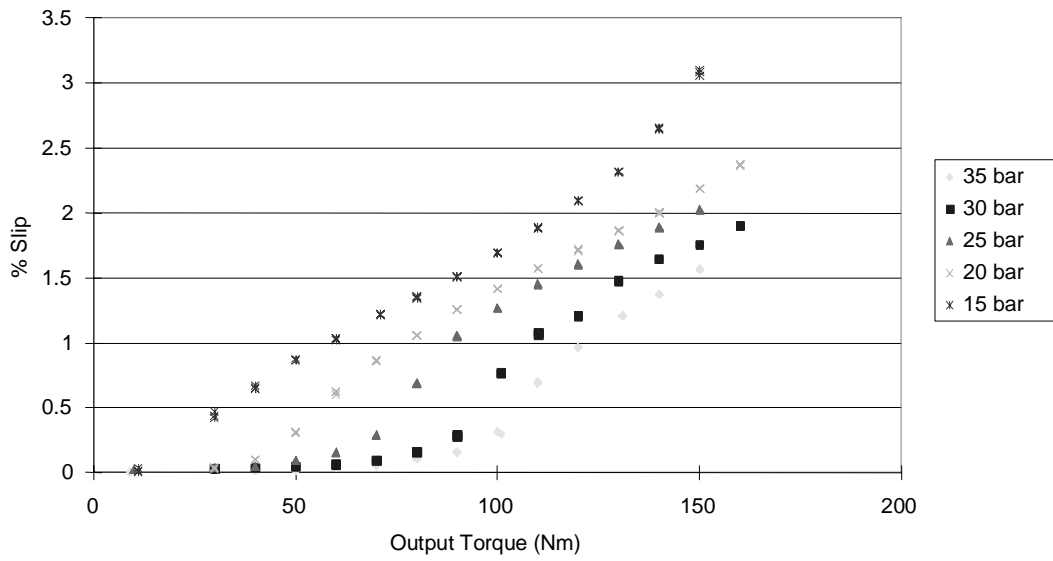
Figure 6-7 Effect of Clamping Pressure on Belt Slip in Low Ratio Tests

_____
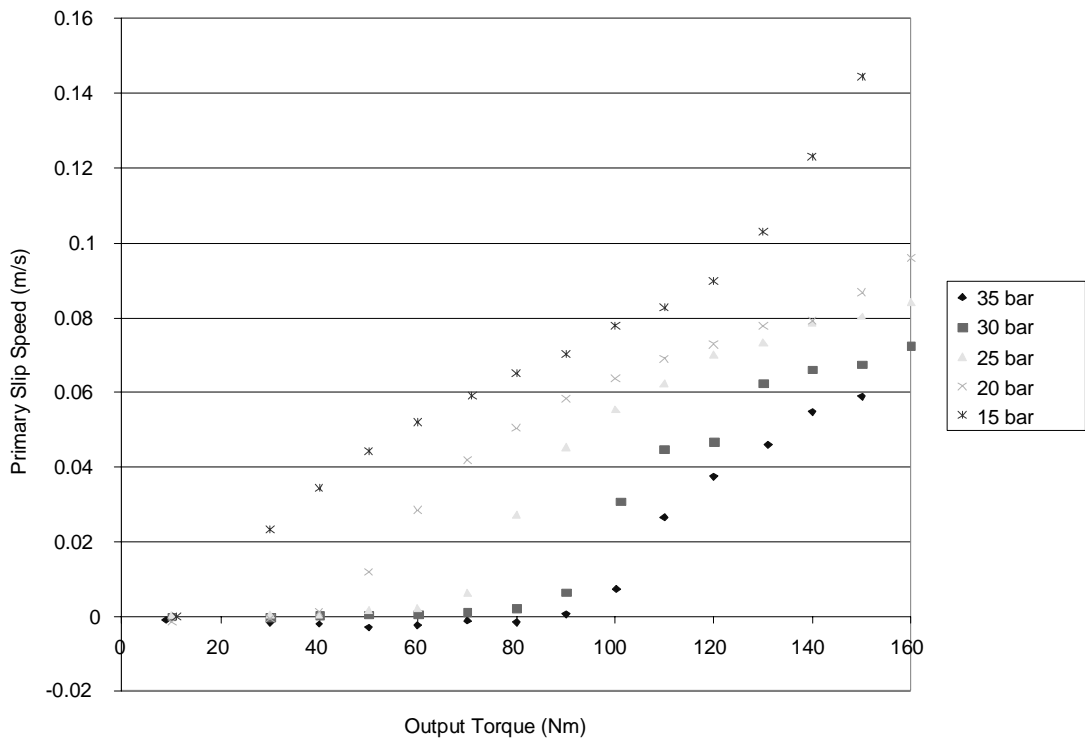
Figure 6-8 Primary Slip Speeds with Respect to Output Torque in Low Ratio
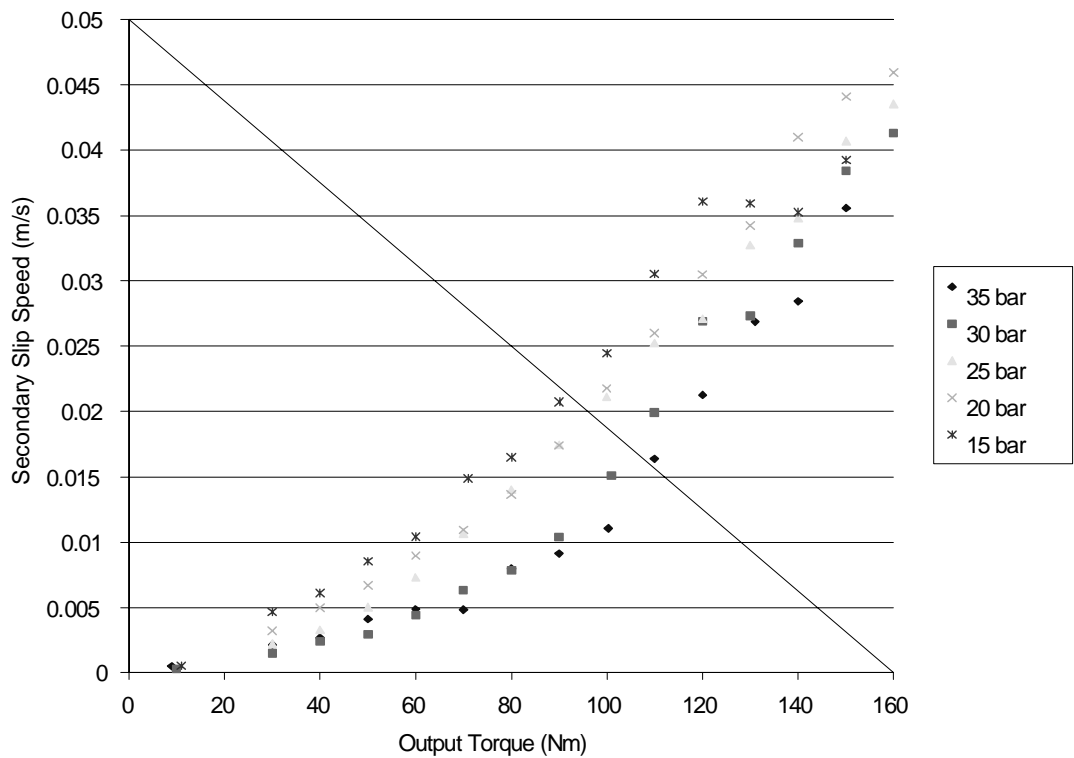
Figure 6-9 Secondary Slip Speeds with Respect to Output Torque in Low Ratio

_____

_____

7 Modelling Non-Belt Loss Mechanisms

This section of the thesis discusses the modelling of the other loss mechanisms that occur in the transmission that are not associated directly with the belt. These include the input shaft losses, pump losses, clutch drag and final drive. It should be noted that these losses and their validation are not discussed in as much detail as the losses that occur in the belt (chapter 8). This is due primarily to their lower significance in terms of losses, greater simplicity in terms of function and modelling, and the fact that in general detailed modelling has been performed before.

7.1 Modelling

The simulation work undertaken in this project was performed in the MATLAB software environment. This software is now becoming an industry standard amongst scientists and engineers of all fields of study. The environment allows simple coding of mathematical expressions with the minimum of syntax requirements. At its most basic level MATLAB operates from simple command line instructions. For more complex programming these commands are simply strung together in M-files (with a .m postfix) and then each M-file is run from the command line prompt. Copies of the code produced for the modelling work undertaken can be found in the Appendix C at the rear of this thesis.

7.2 Temperature Effects on Lubricant Viscosity

The viscosity of the lubricating fluid interacts with many of the models proposed in this section. Therefore manufacturers data, **[51]**, for the transmission lubricant were plotted in terms of temperature vs. viscosity and a polynomial characteristic was derived as shown in Figure 7-1.

The equation of the polynomial derived to fit the visocosity data is shown below-

$$\eta = 0.00000000000131x10^{-03}T^6 - 0.00000000049527x10^{-03}T^5 + 0.00000007686534x10^{-03}T^4 - 0.00000643904577x10^{-03}T^3$$
$$+ 0.00032256104367x10^{-03}T^2 - 0.01002702487252x10^{-03}T + 0.17338402608095x10^{-03}$$

The large number of significant figures has to be maintained to retain accuracy with the fit, due to the large scale range between the SI units used in the plot.

_____

_____

7.3 Input Shaft Losses

The input shaft losses are associated with the seal and bearing drag losses that act on the input shaft. The results shown in Figure 7-2 were obtained experimentally by testing the input shaft of the transmission in isolation, but whilst maintaining realistic lubrication conditions (section 5.3.5.4).

The experimental results show a linear increase in drag torque with speed and an increase in torque loss proportional to the viscosity of the lubricant. A curve fitting routine was applied to the experimental data in order to achieve a description of the input shaft losses in terms of input speed and viscosity, see Figure 7-3.

This process is highly empirical, since the use of standard bearing models, like those proposed by SKF **[50]** overestimate the losses considerably. Therefore these models were used merely to generate characteristics with the correct shape, while the coefficients of fit were chosen to fit the experimental data with no reference to the bearings included in the input shaft assembly.

7.4 Hydraulic Pumping Losses

A number of previous papers notably Micklem et al. **[14]**, Vaughan at al. **[17]** and Bishop et al. **[52]**, stated that a major contributor to power losses in an automatic transmission or CVT was the driving torque required by the hydraulic pump for the control system. Vaughan concludes that pump power losses are at least 10% of the input power and can be up to 25% at low torque levels. This has been further quantified by the experimental work discussed earlier in section 5.5.4 of this thesis, where the hydraulic pump losses were shown to be up to 40% of the total losses in some circumstances. Kluger et al. **[53]** describes a performance comparison experiment on a number of different pumping systems fitted to a range of automatic transmissions. The paper presents details of a number of comparably sized pump configurations, and the range of driving toques for each configuration are displayed graphically. Bishop et al. **[52]** conclude that pumping torque losses can be from 1.5 to 2 times greater with a fixed displacement pump than with a variable displacement unit.

_____

More generic pump models have been produced by authors operating in the fluid power sector of engineering such as McCandlish et al. **[54]**. In its simplest form a pump may be modelled as an ideal unit. This model may then be developed with the addition of simple mechanical and volumetric efficiencies. However, a more detailed analysis and more accurate model can be achieved by further developing the loss terms of the model. Therefore, the volumetric efficiency may be replaced by a leakage flow loss calculation including viscosity and pressure terms, while the mechanical efficiency can be improved by substituting coulomb and viscous friction models into the equations.

The paper by McCandlish et al. **[54]** carried out a study into steady state losses in hydraulic pumps; their paper details two pump torque models, namely the Wilson model and the Schlosser model. Both these models are based on loss coefficients for viscous friction and coulomb friction that are variable with the pump operating conditions.

The Wilson model for pump torque requirements is-

$$T_p = xDP + C_v \left(\frac{\mu\omega}{P} \right) DP + C_f DP + T_c$$

The Schlosser model for pump torque requirements including a hydrodynamic torque loss which allows for fluid acceleration is-

$$T_p = xDP + C_v \left(\frac{\mu\omega}{P} \right) DP + C_f DP + C_h \omega^2 \rho D^{5/3}$$

This can be simplified to-

$$T_p = xDP + C_v * \left(\frac{\mu\omega}{P} \right) DP + C_f * DP$$

Where-

$$C_v * = C_v f(x)f(p)$$

$$C_f * = C_f f(x)f(\omega)f(p)$$

C_v is derived from $\dfrac{\Delta T}{\Delta \omega}$

C_f is derived from $\dfrac{\Delta T}{\Delta P}$

Micklem et al. **[14]** derived their pump torque model using the secondary pulley clamping force as shown below,

$$T_{PUMP} = \frac{2V_p(F_s - F_{sp})}{\eta_{mp}\pi^2(D_{s1}^2 - D_{s2}^2)}$$

where F_s is the clamping force on the secondary pulley, F_{sp} is the pulley spring force and D_{s1} and D_{s2} are the outer and inner diameters of the pulley cylinder. V_p is the volumetric flow through the pump and η_{mp} is the pump mechanical efficiency.

Figure 7-4 below shows some typical pump torque loss data acquired during the experimental work, discussed in section 5.5.4 of this thesis, where a number of additional plots of pump torque loss are available for a range of different temperatures. In general the pump torque loss results show the losses to be as expected, with a large linear fit term varying with respect to pressure with a smaller speed dependent pump loss being present. Since the losses in the pump appear to have been well modelled and understood it was decided to concentrate on modelling the losses in the belt mechanism in more detail, (chapter 8).

7.5 Bearing Losses & Gear Losses

The losses due to gears can be treated, as they would be in a conventional transmission, using conventional gear meshing loss theory as described by Buckingham **[42]** and Tuplin **[41]**. The gear losses can be broken down into three distinct areas, namely meshing losses, churning losses and windage losses. Due to the relatively low rotational speeds occurring within the transmission, it can be assumed that the windage losses are negligible and can thus be ignored. In fact, when compared to theoretical pumping losses and belt torque losses, it is questionable whether gear torque losses are required for an accurate model. However, since existing well proven models already exist and are reasonably simple to implement it seemed logical that these should be included in any overall model.

The bearing losses can be based on conventional bearing theory as described in roller and ball bearing models. Such models are proposed by both Harris **[55]** and Palmgren **[56]**. Most bearing manufacturers also offer torque loss models using friction factors for their bearings. Such models can be found in the SKF catalogue **[50]**, However accuracy of these particular models with respect to the input shaft modelling have been shown to have a very poor.

_____

7.6 Clutch Drag Losses

It is possible that some of the losses at the input shaft of the transmission will be associated with drag torques in the disengaged reversing clutch. Very few published papers could be found that investigated the losses in wet clutch packs when they are disengaged. Fish **[57]** has published a paper detailing some test work using the SAE #2 machine to evaluate disengaged wet clutch drag. The testing was carried out by recording coast down times with a known inertia and thus deriving both the average and instantaneous drag torques. The individual bearing and component losses could be identified by running empty and partially built clutches. Fish studied the effects of individual variables such as plate geometry, surface finish, groove design, pack clearance, oil flow and oil temperature. The effect of clutch speed on the power losses was also investigated.

Fish identified a number of possible drag mechanisms in the clutches; incomplete release, fluid film shear and/or vibration contact between plates. The experimental work drew a number of conclusions; firstly the drag torque loss can be decreased by increasing the pack clearance, and this effect is noticed particularly at low temperatures. Secondly, the oil level and clutch oil flow should be low to decrease the drag torque, while the losses are lower at increased fluid temperatures due to the reduced fluid viscosity. Thirdly, higher rotational speed is shown to increase the clutch drag torque, while friction plate wave can significantly reduce the drag losses by braking up fluid film formation.

Many of the findings by Fish are backed up by the findings from earlier work by Lloyd **[58]**. Although both Fish and Lloyd investigated the effects of the various mechanisms within the clutch assembly, neither of them produced any mathematical models to describe the losses. Both papers are simple parametric studies.

The proposed clutch losses are associated with the viscous drag between each adjacent clutch plate and the oil film separating the plates. Viscous friction would normally suggest a linear function of speed. However, experimental results from Guebeli's work **[15]** showed the losses varied as a quadratic function of speed. Other models also exist such as one proposed by Vahabzadeh **[59]**, which is based on the assumption of Couette flow between the disengaged clutch plates. The torque loss based on Couette flow is given by the expression

_____

_____

$$T_{cl} = \nu \Delta \omega n_i A r_m^2 \frac{1}{S}$$

where ν is kinematic viscosity (m^2/sec), $\Delta\omega$ is the speed differential between clutch plates (rad/sec), n_i is the number of clutch plates, A is the area of clutch the plates (m^2), r_m is the mean clutch plate radius (m) and S is the plate separation (m).

Figure 7-5 shows a cross section through a wet clutch pack, and the variables effecting the drag torque through the clutch.

A more detailed analytical model is given by Park et al. **[37]**, where the torque loss is given by a complex equation including pressure distributions across the clutch faces. Despite the detail included in the modelling work above the clutch drag losses in the test transmission were shown to be minimal under all test conditions except the 25°C case, where they were still only of 0.25~0.5 Nm magnitude. Therefore the models are included here only for completeness, as it was not deemed necessary to investigate the clutch losses any further.

_____

_____
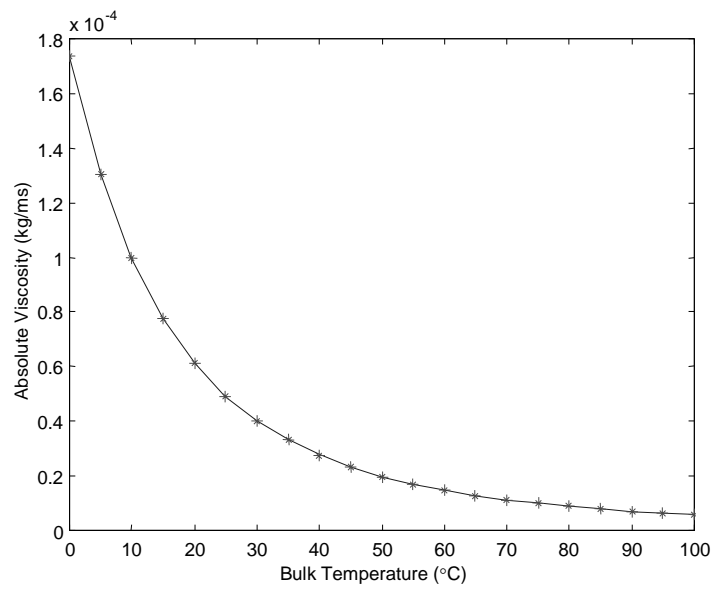
Figure 7-1 Lubricant Temperature vs. Viscosity Characteristic
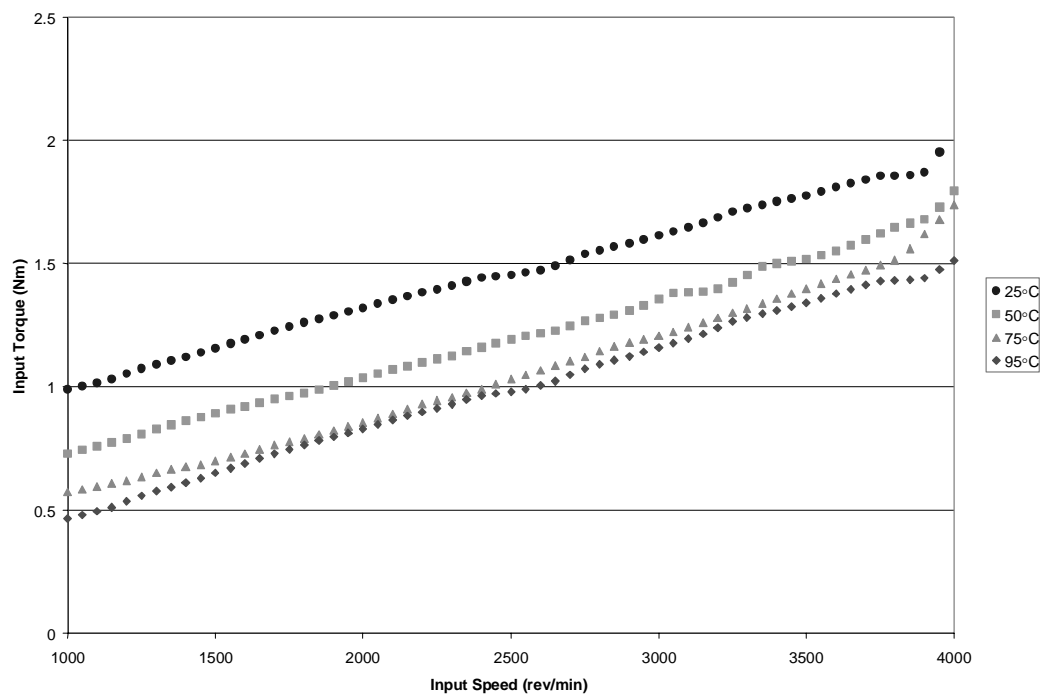
Figure 7-2 Experimental Results of Input Shaft Torque Losses

_____

_____
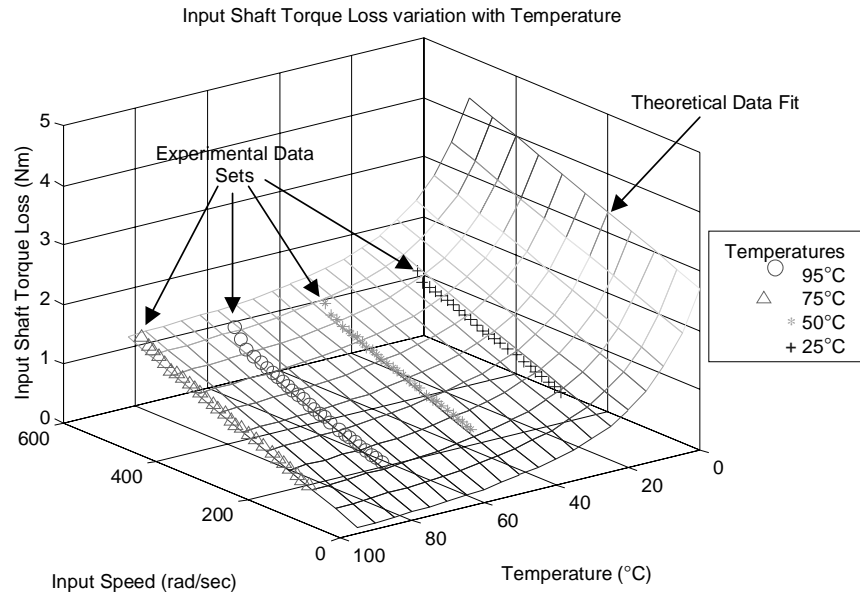
Figure 7-3 Model Predictions of Input Shaft Torque losses Compared with Experimental Results
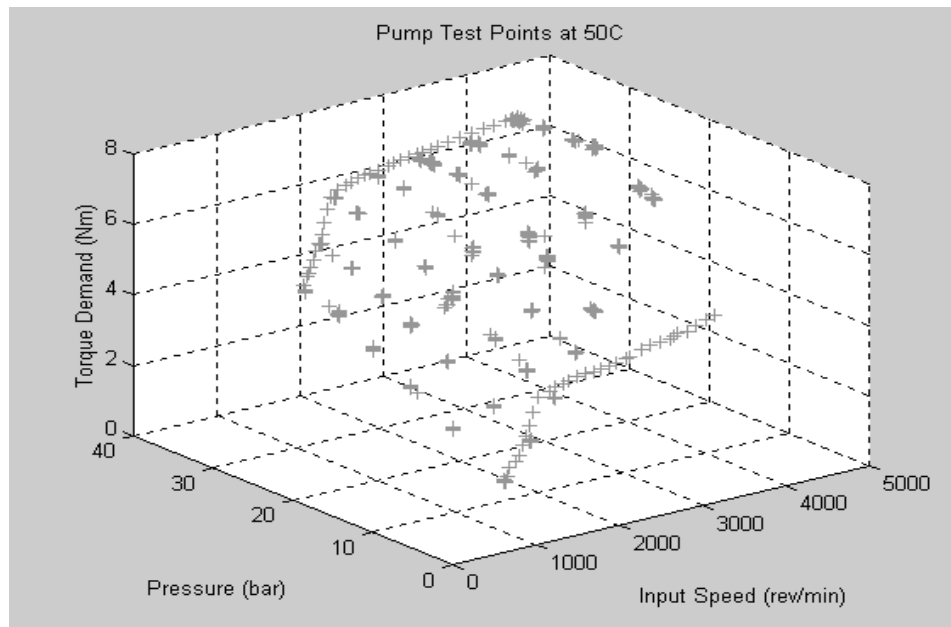
Figure 7-4 Typical Experimental Measurement of Pump Torque Loss

_____
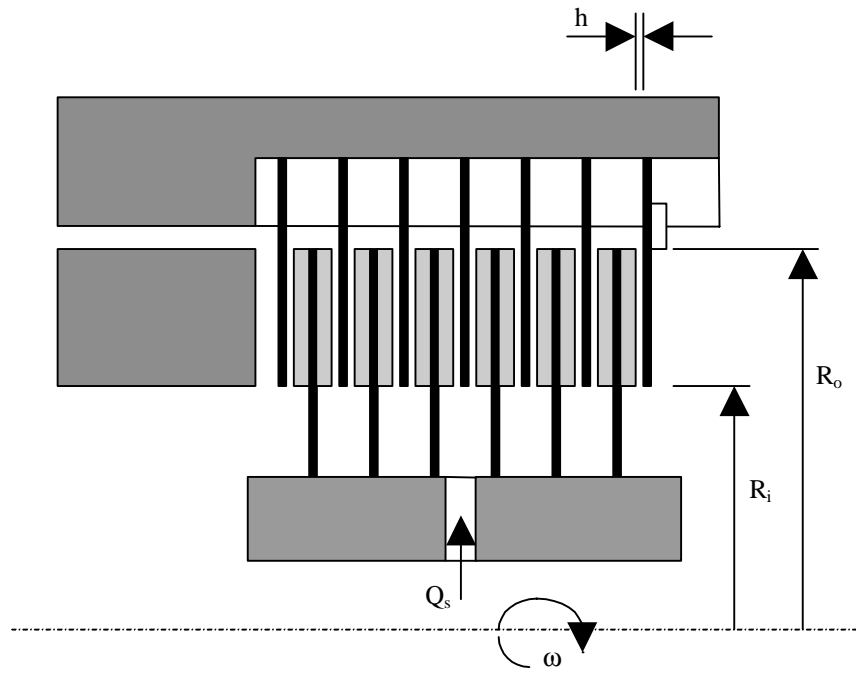
Figure 7-5 Cross Section Through a Wet Clutch Pack

_____

8   The Belt Losses

Before describing the modelling of the V-belt it is important to give a full understanding of the terminology and descriptions used. Figure 8-1 shows the construction of the metal pushing V-belt and identifies a number of the main components.

V-BELT TERMINOLOGY

Primary Pulley	Pulley at input side of transmission
Secondary Pulley	Pulley at output side of transmission
Strut	Straight length of belt running between primary and secondary pulleys
Band Pack	Assembly of individual bands
Conventional Loading	Compression between segments occurs in the strut between exit of primary pulley and entrance of secondary pulley
Inverted Loading	Compression between segments occurs at the strut between exit of secondary pulley and entrance of primary pulley
Idle Tension Arc	Arc in which band tension does not change
Idle Compression Arc	Arc in which segment compression does not change
Active Tension Arc	Arc in which band tension changes
Active Compression Arc	Arc in which segment compression changes
Loading Pulley	Pulley on which segment compressive force increases in direction of rotation
Unloading Pulley	Pulley on which segment compressive force decreases in direction of rotation

This section of the thesis discusses each individual contributor to the torque losses for the whole transmission. A number of models for each component have been investigated and the merits and disadvantages of each are considered. Figure 8-2 shows a schematic diagram indicating the components in the transmission, which could result in possible loss mechanisms. A number of these component such as bearings and gears have been considered in detail by other authors, and are of a small significance when compared to the overall losses in the transmission. Therefore, these topics will only be touched upon later in this thesis, while the bulk of the modelling will concentrate on the two largest loss contributors, as discovered by the experimental work earlier in this thesis, the belt and the hydraulic pump. Of these two losses the belt is the least understood, in terms of function

_____

_____

and losses, and so most of the work detailed here will concentrate on understanding the fundamental mechanisms of the metal pushing V-belt.

8.1 The Belt

Figure 8-3 & Figure 8-4 show two flow diagrams of the expected losses through the belt variator system, in terms of torque and speed respectively. In modelling the CVT, initial conditions will be set as the output torque from the transmission and the input speed, or in vehicle terms wheel torque and engine speed. Considering Figure 8-3 in more detail, an initial output torque condition exists, while in the final drive a number of losses occur associated with seals, bearings and churning. Each of these losses can be calculated as a torque and added to the torque required at the output of the transmission. Similarly, in any gear mesh the torque will be multiplied by the ratio effect and a loss torque will be added, due to gear meshing losses and bearing losses. This methodology is repeated in the belt mechanism, where a (yet to be identified) torque loss is added at the secondary pulley, prior to torque multiplication by the belt ratio and addition of a similar torque loss at the primary pulley. Finally input shaft bearing and seal losses along with the hydraulic pump torque and clutch drag torque are added to determine the torque required at the input shaft of the transmission.

Referring to Figure 8-4 the initial input speed condition gives speed conditions for the primary pulley, clutch pack and hydraulic pump. Any primary pulley slip will result in a reduction of speed into the variator prior to the speed multiplication effect of the belt ratio. Similarly secondary pulley belt slip will result in a reduction of the ideal secondary pulley speed. Speeds through the final drive are then simply factored by the ratio associated with each of the gear meshes.

8.1.1 Belt Geometry

This section describes the geometry of the belt, which is necessary to develop the loss models. Figure 8-5 shows the idealised belt geometry; the radii indicated are those measured from the pulley centres to the rocking edges on the segments (Figure 8-1).
From Figure 8-5 it can be seen that, simple geometry gives an expression for the length of the belt as-

_____

_____

$$L = R_{pri}\beta_{pri} + R_{sec}\beta_{sec} + 2\sqrt{\left(X^2 - \left(R_{sec} - R_{pri}\right)^2\right)}$$ (1)

where-

$$\beta_{pri} = \pi - 2\alpha$$ (2)

$$\beta_{sec} = \pi + 2\alpha$$ (3)

and $$\sin\alpha = \frac{R_{sec} - R_{pri}}{X}$$ (4)

Since the length of the belt, L, is known, as is the distance between pulley centres X, the equation above can be implemented in an iterative program to find corresponding values of R_{pri} and R_{sec} and β_{pri} and β_{sec} for any value of belt ratio (I). In this work the belt ratio is defined in geometric terms, as output radius over input radius, as-

$$I = \frac{R_{sec}}{R_{pri}}$$ (5)

This is done to prevent confusion, as definitions based upon torque or speed ratios can be either ideal or actual depending upon the inclusion of associated losses. Figure 8-6 & Figure 8-7 shows the calculated pulley radii and angles of wrap about each pulley respectively for the complete range of ratios. Using the ratio definition described above a 'high ratio' or 'overdrive' condition is described by a ratio value (I) of less than one.

8.2 Identifying Locations for Losses

The initial stage of modelling was to consider where the losses are likely to occur in the variator system. For a power loss to occur relative motion has to exist between two or more components with a resistance force acting between them. Therefore a number of components within the variator system were identified where relative motion may occur. These were-

1. Between the segments and the band pack.
2. Between neighbouring bands within the band pack.
3. Between the segments and the pulley surfaces.
4. Between neighbouring segments

_____

_____

Each of these are possible sites for loss interactions between components, but it is necessary to identify conditions in the variator which may cause relative motion to occur. A number of conditions were highlighted and are investigated in the following sections of this thesis.

8.3 Relative Speeds Between Components

Consider first the relative movement between the band pack and the segments, and also between neighbouring bands within the band pack. Figure 8-8 shows the geometry of the band pack around a number of belt segments while travelling around a pulley wrap angle. The segments will be travelling at a rolling radius of R_{pri} and R_{sec} about the pulleys, such that the linear speed of each of the segments, V_{seg} may be calculated as follows.

$$V_{seg} = \omega_{pri}R_{pri} = \omega_{sec}R_{sec} \qquad\qquad (6)$$

With reference to Figure 8-8, let it be assumed that the segment will rock about a known point, the rocking edge (A), with the innermost band of the band pack touching the shoulder of the segment (B). The shoulder of the segment is located at a further radial distance (δ) from the rocking edge of the segment. This causes an inconsistency in the calculation of the band speed on each pulley, since-

$$\omega_{pri}\left(R_{pri} + \delta\right) \neq \omega_{sec}\left(R_{sec} + \delta\right) \qquad\qquad (7)$$

except for the special case when $\omega_{pri} = \omega_{sec}$ i.e. a ratio of 1:1.

The same inconsistency will also exist at every subsequent band interface within the band pack. The existence of this inconsistency indicates that for any ratio, other than unity, relative motion between band and segment and between each band within the band pack will exist at some point in the variator system. This raises the question as to what speed will be adopted by the band pack, and by each of the bands within the band pack.

First let the rolling radius of each of the bands be defined as their inner surfaces, such that for the innermost band.

_____

$$R_{pri}(1) = R_{pri} + \delta \qquad\qquad (8)$$

$$R_{sec}(1) = R_{sec} + \delta \qquad\qquad (9)$$

where 1 represents the band number with 1 being the innermost band. Similarly for each subsequent band the effective rolling radius may be calculated as-

$$R_{pri}(i) = R_{pri}(i-1) + t_{band} \qquad\qquad (10)$$

$$R_{sec}(i) = R_{sec}(i-1) + t_{band} \qquad\qquad (11)$$

where $i = 2....nband$ and t_{band} is the thickness of each band in the band pack. For each pulley a required absolute velocity ($Vreq$) can now be calculated such that no motion will occur between the band and segment in their respective arcs.

$$Vreq_{pri}(i) = R_{pri}(i)\omega_{pri} \qquad\qquad (12)$$

$$Vreq_{sec}(i) = R_{sec}(i)\omega_{sec} \qquad\qquad (13)$$

It is likely that the actual band speed adopted will lie somewhere between the limits of $Vreq_{pri}$ and $Vreq_{sec}$.

Considering the two extreme ratio conditions of the variator, then in low ratio $\omega_{pri} >> \omega_{sec}$ and hence from the relationship above $Vreq_{pri}(i) > Vreq_{sec}(i)$. Conversely in high ratio $\omega_{sec} >> \omega_{pri}$ and hence $Vreq_{sec}(i) > Vreq_{pri}(i)$.

Now considering in more detail the low ratio condition. In low ratio the bands will slide backwards relative to their inner partner on the primary pulley, and slide forwards relative to their inner partner on the secondary pulley. The bands will also slide ahead of their inner partner on the straight sections of the belt. It should be noted however that the absolute speed of each band is always higher than that of its innermost partner.

An arbitrary speed for each band (V_{band}) may now be adopted, which lies between the bounds described above, such that the relative velocities of the first band over the segments can be defined as follows for the three different situations that exist (strut, primary arc and secondary arc)-

$$\delta V_{strut}(1) = V_{band}(1) - V_{seg} \tag{14}$$

$$\delta V_{pri}(1) = V_{band}(1) - Vreq_{pri}(1) \tag{15}$$

$$\delta V_{sec}(1) = V_{band}(1) - Vreq_{sec}(1) \tag{16}$$

For each of the subsequent bands i.e. $i = 2....nband$ there will also be a required relative velocity such that no motion occurs between a band and its inner partner when they pass around the contact arcs, these are defined as-

$$\delta Vreq_{pri}(i) = Vreq_{pri}(i) - Vreq_{pri}(i-1) \tag{17}$$

$$\delta Vreq_{sec}(i) = Vreq_{sec}(i) - Vreq_{sec}(i-1) \tag{18}$$

Thus the sliding speed between each band in each of the three different locations may be calculated as follows.

$$\delta V_{strut}(i) = V_{band}(i) - V_{band}(i-1) \tag{19}$$

$$\delta V_{pri}(i) = \delta V_{strut}(i) - \delta Vreq_{pri}(i) \tag{20}$$

$$\delta V_{sec}(i) = \delta V_{strut}(i) - \delta Vreq_{sec}(i) \tag{21}$$

It is possible to correlate the adopted band speeds with the relative motions that occur between components and that were recorded on the variator test rig. The relative displacements (δx) between segments and the inner band and between individual bands were recorded experimentally for a number of belt revolutions.

The displacements per belt revolution of each component were calculated, for comparison with the experimental values, as follows. Firstly, the time of the belt is each sector of the variator may be calculated using the equations below-

$$t_{strut} = \frac{l_{strut}}{V_{seg}} \tag{22}$$

$$t_{pri} = \frac{R_{pri}\beta_{pri}}{V_{seg}} \tag{23}$$

$$t_{sec} = \frac{R_{sec}\beta_{sec}}{V_{seg}} \tag{24}$$

Thus the motion of each component relative to its partner may be calculated as follows

$$\delta x_{strut}(i) = 2t_{strut}\delta V_{strut}(i) \text{ (for both struts)} \qquad\qquad \textbf{(25)}$$

$$\delta x_{pri}(i) = t_{pri}\delta V_{pri}(i) \qquad\qquad \textbf{(26)}$$

$$\delta x_{sec}(i) = t_{sec}\delta V_{sec}(i) \qquad\qquad \textbf{(27)}$$

Hence the total motion between components per belt revolution is-

$$\delta x = \delta x_{strut} + \delta x_{pri} + \delta x_{sec} \qquad\qquad \textbf{(28)}$$

Typical experimental results for the relative motions per revolution of the belt are given in Table 8-1, along with comparative values obtained from the modelling. These results were achieved using adopted velocities within a few percent of the mean of the two pulley required velocities. This shows that the adoption of a mean speed between the two limits is a good approximation to the events that are occurring within the belt, and that the assumptions made in the band speed modelling are valid ones. It can be assumed that in the analysis that follows that the sliding between the components identified in this chapter is significant enough to discount it being accommodated elastically and that the friction forces occurring between the components can be modelled as sliding friciton.

8.4 Forces Acting on the Band Pack and Segment

Since a relative velocity has been identified between the bands and segments, it is now necessary to calculate the force acting at these interfaces, so as to calculate any possible power losses. Now consider what forces could be acting between the inner band and segments and at the segment to pulley interfaces. This is best achieved by developing a free body diagram of an individual segment and the portion of band interacting with that segment. Figure 8-9 shows such a diagram for a portion of band passing over a segment. Figure 8-10 & Figure 8-11 show the forces acting on an individual segment from a front and side view respectively.

The forces acting between the components and other quantities may be defined as follows:

C_X: The compressive force between segments.

_____

T: The band tension. (The total tension in both band packs.)

F_{rad}: The radial friction force acting between the pulley surface and the segment sides.

F_R: The friction force acting between band pack and segment or between neighbouring bands.

F_T: The tangential friction force acting between the pulley surface and the segment side.

M_{seg}: The mass of one belt segment.

N: The segment normal force. (The normal force acting between the pulley surface and the segment side, on each side of the segment.)

Q: The total normal force acting on the segment shoulder. Hence, each band pack subjects each shoulder to a normal load of Q/2.

R: The rolling radius of the belt segment

V: The velocity of the segment.

Z: Friction force acting on rocking edge

In the analysis performed here the force Z is assumed negligible (no radial movement occurs in this analysis) and it is also assumed that the locating pin and its preceding recess are a clearance fit so that no forces will occur between the two.

Considering the band as shown in Figure 8-9 and resolving forces in the x-direction gives-

$$(T + \delta T)\cos\phi - F_R = T\cos\phi$$

Hence simplifying to-

$$F_R = \delta T \cos\phi \tag{29}$$

Similarly resolving forces in the y-direction gives-

$$Q = (2T + \delta T)\sin\phi \tag{30}$$

Resolving forces acting on the segment in the tangential direction, Figure 8-11, gives-

$$F_T + C_X \cos\phi = (C_X + \delta C_X)\cos\phi + F_R$$

which may be simplified to-

$$F_T = \delta C_X \cos\phi + F_R \tag{31}$$

While in the radial direction the force balance gives-

$$Q = 2N\sin\theta + M_{seg}\frac{V^2}{R} + (2C_X + \delta C_X)\sin\phi - 2F_{rad}\cos\theta \tag{32}$$

_____

A substitution for the normal force acting on the segment side may be made to introduce the axial force acting on the segment (i.e. that acting in the direction of the pulley clamping pressures), $N = \dfrac{F_{AX,seg}}{\cos\theta}$, resulting in the following expression-

$$Q = 2F_{AX,seg}\tan\theta + M_{seg}\frac{V^2}{R} + (2C_X + \delta C_X)\sin\phi - 2F_{rad}\cos\theta$$

For small angles it is possible to make the following substitutions, $\sin\phi = \phi$ and $\cos\phi = 1 - \dfrac{\phi^2}{2}$ or since ϕ is very small $\cos\phi = 1$. From geometry it can be seen that

$$\sin\phi = \phi = \frac{0.5t}{R}$$

Hence, substituting the above approximations into the original Equation 29 to Equation 32 above gives-

$$F_R = \delta T \tag{33}$$

$$Q = \left(T + \frac{\delta T}{2}\right)\frac{t}{R} \tag{34}$$

$$F_T = \delta C_X + F_R \tag{35}$$

$$Q = 2F_{AX,seg}\tan\theta + M_{seg}\frac{V^2}{R} + (2C_X + \delta C_X)\frac{0.5t}{R} - 2F_{rad}\cos\theta$$

which can be rearranged as follows-

$$Q = 2F_{AX,seg}\tan\theta + M_{seg}\frac{V^2}{R} + \left(C_X + \frac{\delta C_X}{2}\right)\frac{t}{R} - 2F_{rad}\cos\theta \tag{36}$$

8.4.1 Analysing the Complete Wrap Angle

The analysis in the previous section (8.4) was performed on a small section of band and only one belt segment. Consider now the forces acting on a whole angle of wrap rather than a single segment. Each individual segment will have its own individual shoulder normal force, shoulder friction and compressive force loading. For the purpose of this

_____

modelling work the gross effects around the whole angle of wrap are required rather than a specific knowledge of the force mechanisms acting on each of the individual segments. Therefore an assumption is made that the shoulder friction force and shoulder normal forces can be approximated as the summation of a whole string of segments as shown in Figure 8-12. It should be noted that this is not resolving these forces into one, but it is simply summing the shoulder forces of all the segments, that results in a total effective normal force that acts in between the segment shoulders and the innermost band-

$$\hat{Q}_{pri} = \sum_{j=1}^{j=nseg,pri} Q \text{ and } \hat{Q}_{sec} = \sum_{j=1}^{j=nseg,sec} Q \qquad (37)$$

The segment thickness can be substituted by βR, the length of the contact arc, while the axial force per segment can be replaced by F_{AX} the total axial force applied by the pulley actuator. The number of segments engaged in each angle of wrap is defined as $n_{seg} = \dfrac{\beta R}{t}$. Hence, equation 36 may be rewritten as-

$$\hat{Q} = 2F_{AX}\tan\theta + M_{seg}\frac{\beta R}{t}\frac{V^2}{R} + \left(C_X + \frac{\delta C_X}{2}\right)\frac{\beta R}{R} - \sum_{j=1}^{j=nseg} 2F_{rad}\cos\theta$$

The above expression may be simplified and by setting the initial and final compression conditions of the wrap angle as $C_X=0$ and $\delta C_X = C_x$ results in-

$$\hat{Q} = 2F_{AX}\tan\theta + m_{belt}\beta V^2 + \frac{C_X}{2}\beta - \sum_{j=1}^{j=nseg} 2F_{rad}\cos\theta \qquad (38)$$

where m_{belt} is the mass of the belt per unit length and all other variables will take their appropriate values for either the primary or secondary pulleys. Similarly, performing the same substitutions on Equation 34 gives-

$$\hat{Q} = \left(T + \frac{\delta T}{2}\right)\beta \qquad (39)$$

Combining Equations 38 and 39 produces-

$$\left(T + \frac{\delta T}{2}\right)\beta = 2F_{AX}\tan\theta + m_{belt}\beta V^2 + \frac{C_X}{2}\beta - \sum_{j=1}^{j=nseg} 2F_{rad}\cos\theta \qquad (40)$$

As before the initial and final tension conditions around the wrap angle can be set as T_1 and T_2, which when rearranged gives the following expression.

$$\left(\frac{T_1 + T_2}{2}\right) = \frac{2F_{AX}\tan\theta}{\beta} + m_{belt}V^2 + \frac{C_X}{2} - \sum_{j=1}^{j=nseg} \frac{2F_{rad}\cos\theta}{\beta} \qquad (41)$$

_____

_____

However, C_X, the segment compressive force, is dependent on the output torque acting on the secondary pulley of the variator and the difference in belt tensions on either side of the secondary pulley. Figure 8-13 shows a general free body diagram of the forces acting on the secondary pulley. The band tensions in each strut T_1 and T_2, and the segment compression C_x may act through a range of angles depending on the ratio, and thus wrap angle, at which the belt is operating. A torque Tq_{sec} acts on the secondary pulley, which has a pulley specific axial clamping force F_{sec}. A simple force balance about the secondary pulley gives an expression for the segment compression, which holds for any angle of wrap-

$$C_x = \frac{Tq_{sec}}{R_{sec}} + T_2 - T_1 \tag{42}$$

It is important to maintain the sign convention for the definitions of T_1 and T_2. It can be seen that for a case where T_2 is larger than T_1, C_x will always be positive, but if T_1 is greater than T_2 and Tq_{sec} is small then C_x may be negative. This can only be interpreted as a compression force in the opposite strut. Substituting equation 42 into equation 41 results in-

$$\left(\frac{T_1 + T_2}{2}\right) = \frac{2F_{AX}\tan\theta}{\beta} + m_{belt}V^2 + \frac{Tq_{sec}}{2R_{sec}} + \frac{T_2}{2} - \frac{T_1}{2} - \sum_{j=1}^{j=nseg}\frac{2F_{rad}\cos\theta}{\beta} \tag{43}$$

which may be simplified to give a solution for T_1.

$$T_1 = \frac{2F_{AX}\tan\theta}{\beta} + m_{belt}V^2 + \frac{Tq_{sec}}{2R_{sec}} - \sum_{j=1}^{j=nseg}\frac{2F_{rad}\cos\theta}{\beta} \tag{44}$$

It can also be assumed that the radial friction force effect is negligible. This is for three reasons.

1. The radial friction force can be assumed small in comparison to other the other forces. The segment normal force must support the friction forces in both the tangential direction (F_T) and the radial friction force (F_{rad}) such that-

   $$\mu N = \sqrt{F_T^2 + F_{rad}^2}$$

   It can therefore be assumed that most of the force is generating the tangential force F_T and thus F_{rad} will be very small.

_____

_____

2. The net affect of F_{rad} around the contact arc is likely to me minimal as the force will act in opposite direction during belt entry (acting radially outwards) to that at belt exit (acting radially inwards).

3. The radial force has been shown to only be significant at entry and exit conditions Kanehara et al. **[23]**

Therefore neglecting F_{rad} terms-

$$T_1 = \frac{2F_{AX} \tan \theta}{\beta} + m_{belt}V^2 + \frac{Tq_{sec}}{2R_{sec}}$$ **(45)**

T_2 may then be calculated using the following equation-

$$T_2 = T_1 + \delta T$$

where $\delta T = F_R$ and F_R is approximated by $\mu\hat{Q}$ hence-

$$T_2 = T_1 + \mu\hat{Q}$$ **(46)**

8.4.2 Normal Force Acting Between Bands

The summation of the total normal force at the innermost band generates the gross tension in the band pack. However the next stage is to relate the gross tension of the band pack to the tensions in the individual neighbouring bands within the band pack. An important assumption made in this analysis is that all the bands must share the tension load evenly, such that no one band extends more than any of its neighbours. This can only be justified by considering the whole band pack acting as a self-regulating device to share load evenly between all the bands. If hypothetically, any one band was to carry more tension than any other band it will extend more thus increasing the tension in the other bands as they would have to expand in length by an identical amount.

Using this assumption the total normal force between subsequent bands for the whole angle of wrap can be calculated as follows-

$$\hat{Q}_{pri}(i) = \hat{Q}_{pri}(1) - \frac{(i-1)\hat{Q}_{pri}(1)}{nband} \text{ or simplifying } \hat{Q}_{pri}(i) = \hat{Q}_{pri}(1)\left[1 - \frac{(i-1)}{nband}\right]$$ **(47)**

$$\hat{Q}_{sec}(i) = \hat{Q}_{sec}(1) - \frac{(i-1)\hat{Q}_{sec}(1)}{nband} \text{ or simplifying } \hat{Q}_{sec}(i) = \hat{Q}_{sec}(1)\left[1 - \frac{(i-1)}{nband}\right]$$

_____

_____

The total normal force reduces by an equal amount at each interface towards the outside of the band pack. For the case of a band pack of 12 bands the total normal forces will be distributed such that the outer band has 1/12th of the innermost band loading.

8.4.3 Friction Force Acting Between Bands

Consideration will now be given to the effects of the total normal forces and the motion between each of the individual bands in an arc. There are two cases to consider, the first with the outer bands sliding ahead of the inner bands and the second case with the inner bands sliding ahead of the outer bands. The direction in which the sliding occurs will affect the direction in which the frictional forces between bands act.

The first case to consider is with the outer bands sliding ahead of the inner band as shown in Figure 8-14.

Consider an intermediate band in the band pack, band i, with a base tension T. A frictional force $F_R(i\text{-}1)$ acts on the inner surface, where $F_R(i-1) = \mu\hat{Q}(i-1)$ and on the outer surface a frictional force $F_R(i)$ acts where $F_R(i) = \mu\hat{Q}(i)$.

As discussed in the previous section (8.4.2), the total normal force at a bands inner surface is lower than that of its outer surface $(\hat{Q}(i) < \hat{Q}(i-1))$. Hence, if μ is constant between both interfaces, then the friction force acting on the outer surface of the band will be less than that acting on the inner surface ($F_R(i) < F_R(i-1)$)

Thus resolving the forces acting on the band gives
$$\delta T = F_R(i-1) - F_R(i)$$
Hence δT is always positive and the tension in the band will increase in the direction of belt motion.

Now consider the opposing case when the inner bands slide ahead of the outer bands, as shown in Figure 8-15-

_____

_____

Again consider a band i with a base tension T. A frictional force $F_R(i\text{-}1)$ acts on the inner surface, where $F_R(i-1) = \mu\hat{Q}(i-1)$ and on the outer surface a frictional force $F_R(i)$ acts where $F_R(i) = \mu\hat{Q}(i)$ as with the previous example.

As before, the resultant force at a bands outer surface is lower than that of its inner surface $(\hat{Q}(i) < \hat{Q}(i-1))$ and hence if μ is constant between both interfaces, then the friction force acting on the outer surface of the band will be less than that acting on the inner surface $(F_R(i) < F_R(i-1))$.

Resolving the forces on the band as before gives-

$$\delta T = F_R(i) - F_R(i-1)$$

Hence δT is always negative and the band tension will decrease in the direction of belt motion.

This theory agrees well with the experimental data shown by many authors especially Fujii et al. **[21 & 22]** that shows that on the smaller of the two pulleys the tension always decreases in the direction of belt motion.

8.4.4 Torque Losses due to Band Sliding

At each of the sliding interfaces there will be a power loss, which may be calculated and converted into an effective torque loss that is seen at the primary pulley of the transmission.

$$Tq_{loss}(i) = \frac{\mu\hat{Q}(i)\delta V(i)}{\omega_{in}}$$ **(48)**

Hence the total torque loss associated with the bands will be given by the expression

$$Tq_{loss,band} = \sum_{i=1}^{i=nband} \frac{\mu\hat{Q}_{pri}(i)\delta V_{pri}(i)}{\omega_{in}} + \sum_{i=1}^{i=nband} \frac{\mu\hat{Q}_{sec}(i)\delta V_{sec}(i)}{\omega_{in}}$$ **(49)**

8.4.5 Viscous Shear Approach

_____

_____

Some analysis of the inter-band interfaces was also performed by considering a fluid film undergoing viscous shear between each of the bands. This approach was discounted for modelling the contact around the arcs since the film thicknesses required to generate the tension differences in the arcs were too thin to be supported by the surface roughness measurements that were performed on the belt components. This analysis was also deemed unsuitable since the large difference in velocity gradient between the innermost band and the other band interfaces made it impossible to generate even band tension distributions with realistic oil film thickness distributions.

However, it is possible that some hydrodynamic lubrication may occur between the belt components in the strut sections of the belt when the normal force between the surfaces is minimal and thus a film may be able to form. If this is the case the effect of these films will be minimal, as none of the previous work has indicated significant changes in band tension or segment compression in the strut sections of the belt.

There is one other scenario in which hydrodynamic lubrication may occur between bands. The experimental data collected has shown that the torque loss due to the belt is considerably reduced when operating at 25°C. Under these conditions the lubricant viscosity in considerably increased, to the point where hydrodynamic 'lift off' might occur between the bands. This would result in a lower torque loss as shown experimentally, but would also result in smaller tension differences in the bands. Therefore phenomena such as inverted loading and slip measurements discussed later in this section would not occur. No experimental validation has been performed on this hypothesis. However it can be noted that experimental work by other authors, particularly Fujii et al., has always been performed at realistic operating temperatures (i.e. well in excess of 50°C). Therefore the analysis of the inter-band torque losses using a shear film analysis is included below for completeness.

Consider as before three bands in relative motion, but this time separated by an oil film of thickness h, as shown in Figure 8-16. The relative velocities of the outer band over the middle band and the middle over the inner are $\delta V(i+1)$ and $\delta V(i)$ respectively. The velocity gradient at each interface is-

$\dfrac{\delta V(i+1)}{h(i+1)}$ and $\dfrac{\delta V(i)}{h(i)}$ respectively.

_____

Considering the lower shear film only, the shear force due to each film is calculated as follows

$$F_{shear} = \eta BL \frac{\delta V(i)}{h(i)}$$

(50)

where B and L are the width and length of the shear film respectively. Hence the power loss due to shearing the oil film will be,

$$W_{shear} = \eta BL \frac{\delta V(i)^2}{h(i)}$$

(51)

The torque loss due to the viscous shear film when referred to the primary pulley will be,

$$Tq_{shear} = \eta BL \frac{\delta V(i)^2}{\omega_{in} h(i)}$$

(52)

The tension difference generated in the centre band (δT) is calculated by a simple force balance approach-

$$T + \eta BL \frac{\delta V(i)}{h(i)} = T + \delta T + \eta BL \frac{\delta V(i+1)}{h(i+1)}$$

Assuming B, L and η are constant for both interfaces the expression may be rearranged for δT-

$$\delta T = \eta BL \left[\frac{\delta V(i)}{h(i)} - \frac{\delta V(i+1)}{h(i+1)} \right]$$

(53)

8.5 Effect of Tension Differences

As discussed previously (section 2.1.1) a number of papers (Fujii et al. [22] Karam et al. [20]) have now been produced that both measure or model the distribution of band tensions and segment compressions throughout the belt variator system. A number of the authors have slightly conflicting views, but on the whole an agreement is achieved. Early work such as that by Micklem et al. [12] was based on uniform band tensions and had the compression force loading and unloading over the complete wrap angles. This is a fundamental flaw in the analysis of any slip mechanism as it has a significant implication on the compressive force distribution amongst the segments.

Therefore, this method needs to be improved, since the distribution of band tensions and segment compressions affects the torque transfer mechanisms between the two pulleys and the loading and unloading conditions that are seen on each pulley.

_____

8.5.1 Tension and Compression Force Distributions

Once the tensions T_1 and T_2 have been found for a desired output torque the maximum compressive force between segments may be calculated, using equation 12, derived in section 8.4.1-

$$C_x = \frac{Tq_{\text{sec}}}{R_{\text{sec}}} + T_2 - T_1$$

This then gives an input into the belt slip calculations as it describes the amount of loading that the segments must achieve within the active arc of the loading pulley. Figure 8-17 to Figure 8-19 show the expected variations in segment compressive force and band tensions for the variator system at the two extreme ratio conditions and in the low ratio case at both high and low output torques. The different modes under which torque is transferred add complexity to the simulation of the belt drive, as each individual condition requires a separate model.

Figure 8-17 & Figure 8-18 show the distribution of band tensions in high and low ratio respectively. As discussed in the literature review section (2.1.1) a number of authors, particularly Fujii et al. **[22]**, have measured experimentally that the band tension tends to decrease about the angle of wrap in the direction of belt travel on the smaller of the two pulleys. Thus in high ratio the tension T_2 is greater than T_1 and in low ratio the tension T_1 is greater than T_2. This has the effect of the band tensions impeding torque transfer in high ratio and aiding the transfer of torque in low ratio. This happens to such an extent that in low ratio for a range of lower torque levels the whole torque load is transferred by the band tensions alone. This has the effect that the segment compressive force can actually occur on the opposite side of the belt as shown in Figure 8-19. It should be noted that in each of the case highlighted below the values of C_x, T_1 & T_2 are not drawn to scale and should be used for illustrative purposes only.

8.6 Calculating Segment to Pulley Slip Speeds

If it is assumed that the band pack is assembled so that no clearances exist between the segments, then when the bands are loaded in tension they will stretch and if the segments are in compression they will reduce in thickness slightly. This will result in gaps existing

_____

_____

somewhere in the belt system. The only logical location for these gaps to exist is in the section of the belt where the segments are unloaded. The gaps by definition also have to disappear before compressive force can be loaded between the segments again. The logical location for the gaps to close up is on the loading pulley. For the gaps to close a slip speed must exist for the pulley surface over the segments in the active arc. This will bring the unloaded segments which are not slipping as fast relative to the pulley surface forward to meet the start of the active compression arc.

A higher slip speed will result in the gaps closing faster and thus the active arc will grow and the idle arc of the loading pulley will reduce. The increase in the active arc size will increase the number of segments in the arc and thus decrease the tractive force loading that each segment has to support.

As discussed at the start of this section, the gaps in the belt are developed by increases in band tension, which extend the bands and changes in compression force between segments which results in the segments reducing in thickness. Therefore an increase in output torque on the variator has a twofold effect on slip speed by increasing both the tractive force loading on segments and the gaps in the belt.

It is first necessary to define what is a positive slip and a negative slip speed. The definition used is that a positive slip speed results in a speed loss through the variator when compared to the ideal ratio due to belt geometry. Therefore at the primary pulley positive slip is defined as the primary pulley travelling faster than the belt, whereas at the secondary pulley positive slip is defined as the belt travelling faster than the secondary pulley. Conversely for each case negative slip is defined at the primary pulley as the belt travelling faster than the primary pulley and the secondary pulley travelling faster than the belt.

8.6.1 Calculating the Gaps in the Belt

As discussed in section 8.6, the gaps generated in the belt will always be present at the entrance to the loading pulley. Similarly, in section 8.5.1 it was shown that tension distributions in low ratio affect which side of the variator compression occurs on. Therefore at low torques in low ratio, negative slip situations can exist on the secondary and primary pulleys. At the point where the active compression arc changes pulleys (i.e. $C_x=0$) the slip

_____

_____

due to gaps will occur on the opposite pulley and be in the opposite direction. However, in high ratio only positive slip directions will occur.

Considering first the approach to slip calculations assuming that the slip occurs in the positive direction i.e. all conditions in high ratio and in low ratio at high torque loads. Therefore the slip due to gaps will occur at the primary pulley.

It is helpful to define two regions on the angle of wrap (β), in this case the primary pulley, called the active arc (ψ_{act}) and idle arc (ψ_{idle}). The active arc is the angle in which the compression force between neighbouring segments is generated, while the idle arc is the angle over which the gaps between segments are closed. By definition the segments must slip more in the active arc, than in the idle arc to close the gaps. The segments will not slip as much in the idle arc, but are instead moved forward at a gap slip speed relative to the segment in the active arc, thus closing the gaps.

The gaps due to band tension can be expressed by-

$$e_{band} = \frac{0.5(T_1 + T_2)L_{band}}{EA_{band}}$$
(54)

Similarly the gaps due to compression of segments can be defined as-

$$e_{segs} = \frac{|Cx|}{E}\left(\frac{L_{strut}}{A_{seg}} + \frac{0.5R_{pri}\psi_{act}}{A_{seg,arc}} + \frac{0.5R_{sec}\beta_{sec}}{A_{seg,arc}} \right)$$
(55)

or for the case when the compressive loading is inverted-

$$e_{segs} = \frac{|Cx|}{E}\left(\frac{L_{strut}}{A_{seg}} + \frac{0.5R_{sec}\psi_{act}}{A_{seg,arc}} + \frac{0.5R_{pri}\beta_{pri}}{A_{seg,arc}} \right)$$
(56)

The total gap in the belt can be defined as the sum of the segment compressions and the band extensions, plus any initial gaps present in the belt, which in this case is considered to be zero.

$$e_{belt} = e_{band} + e_{segs} + e_{init}$$
(57)

The cross sectional area of the bands was easy to measure, but the contact area between segments is harder to define, as it generally acts through a very small area near the rocking edge of the segment. This contact area is likely to be different in the contact arc to that in the straight strut section of the belt. To achieve accurate fit to the experimental slip data it became necessary to include a variable contact area between the segments which

_____

increases as the segment load increases, based upon the assumption of deformation around the rocking edge.

Micklem et al. **[12]** collected some experimental data in the form of compressive force vs. strain plots for a set of segments following an arc. These data were recalculated to give an effective change in cross sectional area of the segment and the results plotted as shown in Figure 8-21. A polynomial fit was then applied to the data to obtain an expression for the segment cross sectional area with respect to the segment compression force-

$$A_{seg,arc} = 1.74142x10^{-06} + 1.56364x10^{-09}|Cx| - 1.74032x10^{-13}|Cx|^2 \qquad \textbf{(58)}$$

8.6.2 Calculating the Forces Acting on the Segments

The routine for calculating the slip due to the gap phenomenon is described below. The sequence increments the number of segments engaged in the active arc until the tractive force loading on each segment is supported by a predicted coefficient of friction between the pulley and segment surface. The tractive force loading F_T must be generated by the predicted friction coefficient and the resultant normal force acting on the segment side. Such that-

$$F_T = \mu_{seg} 2N \qquad \textbf{(59)}$$

Where F_T the segment tractive loading is dependent on the segment compression force (δC_X) and the band friction on the shoulder of the segment (F_R) such that-

$$F_T = \delta C_X \pm F_R \qquad \textbf{(60)}$$

The directions of forces are dependent both on the direction of relative motion between segment and band and on the direction of loading of the segment. Hence a number of different loading and ratio conditions need to be defined as shown in Figure 8-22 to Figure 8-33.

Figure 8-22, Figure 8-25 and Figure 8-28 show the three permutations of belt geometry and gap location, while the force distributions on the segments in the active arcs and unloading arcs are shown in Figure 8-23, Figure 8-24, Figure 8-26, Figure 8-27, Figure 8-29, and Figure 8-30. Figure 8-31 to Figure 8-33 show similar force distribution diagrams for segments engaged in the idle arc and hence no compressive force loading exists.

_____

In low ratio and conventional loading situation (i.e. compressive strut is between exit of primary pulley and entrance to the secondary pulley) the tractive force per segment is-

$$F_T = \delta C_X + F_R$$

While at low ratio with an inverted loading situation it is-

$$F_T = \delta C_X - F_R$$

Similarly in high ratio conventional loading (inverted loading does not occur in high ratio) the tractive force per segment is given by-

$$F_T = \delta C_X - F_R$$

8.6.3 Calculating Segment Traction Coefficients

It is appropriate to consider first the case for conventional loading of the segments, i.e. that seen in low ratio with high output torques and in all high ratio situations. Once the number of segments required for the active arc has been found then the size of the active arc and idle arc may be calculated as shown below.

$$\psi_{act} = \frac{n_{seg,act} t_{seg}}{R_{pri}}$$
(61)

$$\psi_{idle} = \beta_{pri} - \psi_{act}$$
(62)

Once the idle arc angle has been found it is possible to calculate the time for the belt to travel from entry into the pulley to the start of the active angle.

$$\tau_{\psi,idle} = \frac{\psi_{idle} R_{pri}}{v_{belt}}$$
(63)

And thus the slip speed to close up the gaps is calculated as-

$$v_{slip,pri,gap} = \frac{e_{belt}}{\tau_{\psi,idle}}$$
(64)

This is the magnitude that the slip speed of the active arc is in excess of the slip speed on the idle arc. It will now be assumed that the slip speed in the other sectors of the belt will be proportional to the coefficient of traction required to support their respective tractive force loadings. As defined previously the coefficient of friction in the primary loading arc is-

$$\mu_{pri,act} = \frac{F_{T,pri,act}}{2N_{pri}}$$

_____

_____

The above expression can be redefined as a traction coefficient such that-

$$\lambda_{pri,act} = \frac{F_{T,pri,act}}{2N_{pri}}$$

(65)

Similarly the coefficient of traction required in the primary idle arc will be-

$$\lambda_{pri,idle} = \frac{F_{T,pri,idle}}{2N_{pri}}$$

(66)

Hence the slip speed in the primary idle arc will be-

$$v_{slip,pri,idle} = v_{slip,pri,gap} \frac{\lambda_{pri,idle}}{\lambda_{pri,act}}$$

(67)

And the total slip at the primary pulley will be the sum of the gap slip and the idle arc slip.

$$v_{slip,pri} = v_{slip,pri,gap} + v_{slip,pri,idle}$$

(68)

The results recorded on the variator test rig also indicated slip occurring on the unloading pulley as well as the loading pulley (Figure 6-8 & Figure 6-9). This is significant since this pulley does not have any gaps present. However a good approximation for the ratio of slip speeds between the two pulleys is achieved by looking at the ratio of tractive force loading to segment resultant force on each segment.

The corresponding required coefficient of traction to support the unloading at the secondary pulley is calculated as follows-

$$\lambda_{sec} = \frac{F_{T,sec}}{2N_{sec}}$$

(69)

Hence the slip speed at the secondary pulley may be defined as-

$$v_{slip,sec} = v_{slip,pri} \frac{\lambda_{sec}}{\lambda_{pri,act}}$$

(70)

The actual output speed of the secondary pulley can therefore be calculated as follows-

$$\omega_{sec} = \frac{v_{belt,act} - v_{slip,sec}}{R_{sec}}$$

(71)

where-

$$v_{belt,act} = \omega_{pri}R_{pri} - v_{slip,pri}$$

(72)

Hence the slip ratio through the transmission may be calculated as follows-

_____

_____

$$\%_{slip} = 100 \left(1 - \frac{\omega_{sec} I}{\omega_{pri}} \right)$$

(73)

where, I is the geometric ratio of the belt.

8.6.4 Segment to Pulley Slip Speeds During Inverted Loading

The analysis of the inverted compression case as shown in Figure 8-19 is very similar to that of the conventional case. However, in this situation the slip due to the gap closure occurs at the secondary pulley, and an idle arc also exits at the secondary pulley. As before the number of segments required to support the active arc is calculated and thus the size of the idle and active arc may be found.

$$\psi_{act} = \frac{n_{seg,act} t_{seg}}{R_{sec}}$$

$$\psi_{idle} = \beta_{sec} - \psi_{act}$$

Once the idle arc angle has been found it is possible to calculate the time for the belt to travel from entry into the pulley to the start of the active angle.

$$\tau_{\psi,idle} = \frac{\psi_{idle} R_{sec}}{v_{belt}}$$

And thus the slip speed to close up the gaps is calculated as-

$$v_{slip,sec,gap} = \frac{e_{belt}}{\tau_{\psi,idle}}$$

As defined previously the coefficient of friction required to support traction in the active arc is-

$$\mu_{sec,act} = \frac{F_{T,sec,act}}{2N_{sec}}$$

Which can be written as a coefficient of traction-

$$\lambda_{sec,act} = \frac{F_{T,sec,act}}{2N_{sec}}$$

The coefficient of traction required in the secondary idle arc will be-

$$\lambda_{sec,idle} = \frac{F_{T,sec,idle}}{2N_{sec}}$$

Hence the slip speed in the secondary idle arc will be-

_____

_____

$$v_{slip,\text{sec},idle} = v_{slip,\text{sec},gap} \frac{\lambda_{\text{sec},idle}}{\lambda_{\text{sec},act}}$$

In the conventional loading case at the primary pulley in low ratio the tractive force in the idle arc is positive, Figure 8-31, and hence the idle arc slip is positive and additional to the slip due to gap closure. However, on the inverted loading case the shoulder friction at the secondary pulley acts in the opposite direction to that at the primary pulley and hence in the idle arc, Figure 8-32, the tractive force component will negative. This negative tractive force will result in a negative idle slip speed. This negative speed will aid the closure of the gaps and thus the total slip at the secondary pulley will be reduced from the value indicated from the gap closure calculation. The direction of the tractive forces and thus slip speeds is accounted for in the definition of forces and as such the total secondary pulley slip speed is still described by-

$$v_{slip,\text{sec}} = v_{slip,\text{sec},gap} + v_{slip,\text{sec},idle}$$

At the primary pulley unloading will occur around the whole wrap angle such that-

$$\lambda_{pri} = \frac{F_{T,pri}}{2N_{pri}}$$

Hence the slip speed at the primary pulley may be defined as-

$$v_{slip,pri} = v_{slip,\text{sec}} \frac{\lambda_{pri}}{\lambda_{\text{sec},act}}$$

8.6.5 Torque Loss due to Segment Sliding Relative to a Pulley

Wherever there exists a relative motion between the belt segments and the pulley surface there will be an associated power loss and thus a torque loss. The torque loss referred to the primary pulley may be calculated as follows-

$$Tq_{slip} = \sum_{0}^{nseg} \left| \frac{v_{slip} F_{T}}{\omega_{in}} \right| \tag{74}$$

_____

_____

Hence a different torque loss due to slip will exist for each of the conditions described previously. For the primary pulley the torque loss due to segment sliding over the pulley is-

$$Tq_{slip,pri} = \sum_{0}^{nseg,pri,idle} \left| \frac{v_{slip,pri,idle} F_{T,pri,idle}}{\omega_{in}} \right| + \sum_{0}^{nseg,pri,act} \left| \frac{v_{slip,pri,act} F_{T,pri,act}}{\omega_{in}} \right| \qquad (75)$$

While at the secondary pulley the torque loss the loss is given by the following expression-

$$Tq_{slip,sec} = \sum_{0}^{nseg,sec,idle} \left| \frac{v_{slip,sec,idle} F_{T,sec,idle}}{\omega_{in}} \right| + \sum_{0}^{nseg,sec,act} \left| \frac{v_{slip,sec,act} F_{T,sec,act}}{\omega_{in}} \right| \qquad (76)$$

8.7 Comparing Slip Predictions to Measured Slip

This section of the thesis reviews results of correlation work between experimental and modelling results of belt slip. Figure 8-34 & Figure 8-35 show experimental results of belt slip measurement on the primary pulley and a typical model output of the same events respectively. With reference to Figure 8-34, typical results from the model are superimposed using solid lines in colours corresponding to the experimental results. Primary pulley slip speeds are shown plotted against variator output torque for a number of different secondary pressure conditions. In general trends seen experimentally are all reproduced in the model results. Best fit is achieved at higher pressure operating conditions, similar to those at which the transmission functions in real life (30 to 35 bar). Figure 8-35 shows the model results in more detail. The figure is annotated to show the effects of a number of parameters on the output of the model. The breakpoints where the slip mode changes are indicated as the points where C_x is zero (i.e. compression is at the point of swapping from inverted to conventional loading pattern). The position of these points can be adjusted by varying the friction coefficient between the bands. An increase in friction increases the difference in band tensions and thus the torque that is transferred by the bands increases and the $C_x=0$ points move to the right. Conversely a decrease in inter-band friction reduces the difference in band tensions and thus the torque transferred by them, so that the $C_x=0$ points move to the left. The value of inter-band friction also interacts with the torque loss model for the bands and thus the two interacting models can both be validated with separate experimental data increasing confidence in their combined validity. Also shown in Figure 8-35 is the effect of reducing the pulley to segment friction, this is also discussed in more detail later in this section. Decreasing the friction coefficient between the segments and the pulley results in an increase in the slip speed.

_____

Figure 8-36 & Figure 8-37 show similar results to those in Figure 8-34 & Figure 8-35 but for events occurring at the secondary pulley. Figure 8-36 shows the experimental slip data and typical modelling results superimposed. As with the case at the primary pulley, all the events measured experimentally are predicted by the model, although specific pressure conditions match the experimental data better. In both the primary and secondary slip case It may be possible to achieve a better fit to the experimental data by changing the characteristic of the segment compression function. The data used to describe these deflections in the model was derived from experimental work on a belt using an older style segment design. Good agreement between experimental and modelling results are achieved in terms of the break points at $C_x=0$. This indicates that the tension distributions in the variator are being modelled with a good degree of accuracy. Figure 8-37 shows the effect of model parameter variation on the slip loss results. The region of slip at low torques is negative (i.e. secondary pulley is sliding ahead of the segments), this region occurs due to gap closure phenomenon, whereas the slip at higher torques is referred from the slip due to gaps occurring on the primary pulley.

Figure 8-39 & Figure 8-39 show compiled results from modelling the primary and secondary belt slip indicating the effects of segment to pulley friction and input speed respectively. Best agreement with the measured slip results was achieved using a segment to pulley friction coefficient of 0.13. This value is similar to that predicted by a number of other authors, Ichihashi et al. **[45]** who have tended to work in the range of µ=0.10 to 0.15.

Figure 8-40 & Figure 8-41 show predicted belt slip results in high ratio at the primary and secondary pulleys respectively. Belt slip increases rapidly as the output torque on the variator increases. The results presented from the model are only shown up to an output torque of 40 Nm. At output torques in excess of 50 Nm the model predicts gross slip occurring, caused when the active arc on the primary pulley grows to be in excess of the primary pulley wrap angle. Under these conditions the incremental loop of the model is unable to converge at the desired coefficient of friction, and hence the model cannot run in its entirety.

8.8 Pulley Deflection Losses

Two further loss models are proposed here, based upon the knowledge that the pulleys deform both elastically and due to flexing in their mountings.

_____

Pulley deflection measurements were performed on the variator test rig using simple dial gauge arrangements to measure the axial pulley deflections at the maximum radius about each of the pulleys. The measurements were performed at a range of clamping pressures and in low and high ratio at a number of locations, see Figure 8-42. The compiled results from these measurements are shown in Figure 8-43. It appeared from the results that the pulley was effectively skewing on its axis and deforming elastically. The force distribution on the pulley is unusual as the hydraulic clamping force is effectively a uniformly distributed load, while the reaction force from the segments only acts over the angle of wrap on each of the pulleys.

Figure 8-43 shows a range of experimental deflection results collected from the variator test rig. The results are presented for low and high ratio conditions and in each case for the primary pulley and secondary pulley. For each of these cases the deflections are measured on both halves of the pulley (fixed half and actuated half), and then these results were used to calculate a change in axial clearance between the pulley surfaces, plotted in the third column. The results are plotted against distance across the pulley, as defined in Figure 8-42, with negative values on the x-axis indicating locations inwards of the pulley centres. Positive axial displacements are defined as deflections towards the bisecting line of the pulley halves.

In general all the deflections measured appear approximately proportional to the clamping pressure applied to the actuator (measurements were taken in 5 bar steps). Figure 8-43(a) shows the deflections of the secondary pulley in low ratio. Maximum deflection of the fixed pulley half was approximately 0.25 mm, while the actuated half deflected up to 0.5 mm. The fixed pulley deflected most at its external edge where force is applied to it via the segments. Conversely the actuated pulley half deflected most at the innermost edge where there are no segments to resist the force from the actuator. Results at the primary pulley, Figure 8-43(b), were unusual in that no deflection could be measured due to the pulley being against internal restraining end stops.

Figure 8-43(c) & Figure 8-43(d) show the deflections measured in high ratio at the secondary and primary pulleys respectively. Results were similar to those seen at the secondary pulley, with the pulley effectively splaying at its outer edge and pinching at its inner edges such that the belt is retained beyond its ideal operating radius. A typical

_____

_____

geometry after deflection due to loading is shown in Figure 8-44 it should be noted that this figure is not to scale and is only to show general trends.

Although the pulley deflection measurements were performed these indicated only large changes in pulley deflection at the outer radius of the pulleys, which was difficult to correlate to local pulley deflections. However, since both the proposed deflection losses are of a lower order of magnitude than those associated with the bands it was felt appropriate to approximate the pulley deflections as a simple function of clamping force and radius.

Such that-

$$\delta_{pri} = f\left(F_{pri}, R_{pri}\right) \tag{77}$$

$$\delta_{sec} = f\left(F_{sec}, R_{sec}\right)$$

It should be noted that this approach is limited as deflection data were only collected at the discrete conditions of high and low ratio, and a special case of zero deflection had to be adopted for the low ratio primary pulley condition.

It is important to first define the geometry of the deflected pulley, with reference to Figure 8-45, which shows a proposed ideal and actual belt trajectory around either pulley (primary pulley shown). As the pulley skews on its mounting bearings and deforms locally the belt will be able to penetrate into the rear of the wrap angle by distance (δ_{pen}) from its nominal radius (R_{pri}) to the penetrated radius (R_{pri}''). Similarly at entrance and exit the belt will remain in contact with the pulley by a radial distance (δ_{wedge}) to a radius (R_{pri}'). The wedge zone angle between ideal contact point (A) and actual contact point (B) is defined as (φ) where-

$$\varphi = \cos^{-1}\left(\frac{R_{pri}}{R'_{pri}}\right) \tag{78}$$

It should be noted that this angle, φ, is not associated in any way with ϕ, the angle of action between segments described in section 8.4.

_____

_____

8.8.1 Pulley Wedge Loss

This loss occurs at the entrance and exit of the pulley, due to deformation of the pulley, which results in the retention of the belt past its ideal exit point and contact between the belt and pulley before its ideal entry points. Therefore in the region radially outside the ideal contact points there will be a relative motion between the pulley and the belt segments engaged in the wedge zone. This is a similar loss to that proposed by Micklem et al. **[12 & 13]**, who developed an empirical model based on radial deflections of the belt at entry and exit.

The difference in radius (δ_{wedge}), as defined in Figure 8-45 can be found from geometry and the axial deflection of the pulley, as shown in Figure 8-46, such that-

$$\delta_{wedge,pri} = \frac{\delta_{pri}}{2\tan\theta}$$
(79)

And similarly at the secondary pulley-

$$\delta_{wedge,\sec} = \frac{\delta_{\sec}}{2\tan\theta}$$

While the exit and entrance radius on both pulleys is defined as-

$$R' = R + \delta_{wedge}$$
(80)

The analysis will now continue with reference specifically to the primary pulley although the events are also occurring at the secondary pulley, which is discussed later in this section.

Again with reference to Figure 8-46, the primary pulley is rotating with a rotational velocity ω_{pri} with the belt engaged at a radius R_{pri}. The belt is leaving the pulley at a velocity V_{belt} in the x direction, where-

$$V_{belt} = \omega_{pri}R_{pri}$$

In this case the effect of belt slip is neglected, and an ideal belt speed is used, since the difference between actual and ideal belt speed is small compared to the total belt velocity. However, this addition can be implemented if deemed necessary. It should also be noted that the co-ordinates x and y are orientated such that x is always in the tangential direction

_____

_____

and y is always radial from the ideal entrance/exit point and as such this analysis can be applied to the belt at any geometry.

There will be a deformation of the pulley and the segments engaged within the contact arc due to the axial compressive forces acting on each segment. Thus as the belt is removed from the pulley both components will begin to relax and lose their deformed states remaining in contact with the each other as they pass along the semi-chord a~b, Figure 8-46, until all the deformation is dissipated at a radius R_{pri}'.

As the belt passes along the semi-chord a~b there will be a relative velocity between the pulley surface and the segment sides.

Resolving speeds in the x direction-

$$V_{relx} = V_{pulleyx} - V_{belt} \tag{81}$$

And in the y direction-

$$V_{rely} = V_{pulleyy} \tag{82}$$

Where for any intermediate radius and angle-

$$V_{pulleyx} = r\omega\cos\varphi \tag{83}$$

And-

$$V_{pulleyy} = r\omega\sin\varphi \tag{84}$$

Hence-

$$V_{relx} = r\omega\cos\varphi - \omega_{pri}R_{pri} \tag{85}$$

$$V_{rely} = r\omega\sin\varphi \tag{86}$$

Therefore at the point b, where the belt exits the deformed pulley the relative speeds in the x and y directions will be-

$$V_{relx} = R_{pri}'\omega_{pri}\cos\varphi - \omega_{pri}R_{pri} \tag{87}$$

$$V_{rely} = R_{pri}'\omega_{pri}\sin\varphi \tag{88}$$

Since the angle φ is small it is appropriate to approximate $R_{pri} \approx R_{pri}'$. Resolving the above two equations results in-

_____

$$V_{rel,pri} = \sqrt{2R'_{pri}{}^2\omega_{pri}{}^2(1-\cos(\varphi))} \qquad (89)$$

An identical relative velocity will also exist between the belt and pulleys at the entrance to the primary pulley.

Similarly on the secondary pulley the belt will come into contact and leave contact with the deformed pulley at a larger radius (R'_{sec}) than that at which it will travel around the belt. Such that the relative velocity will be-

$$V_{rel,sec} = \sqrt{2R'_{sec}{}^2\omega_{sec}{}^2(1-\cos(\varphi))} \qquad (90)$$

Since there is a relative motion between the components in contact with each other there must be a frictional force absorbing energy. The number of segments engaged in the chord a~b is defined as-

$$n_{seg,wedge,pri} = \frac{R_{pri}\tan(\varphi)}{t_{seg}} \qquad (91)$$

While the mean resultant force on the segments in the wedge zone can be approximated to be half the segment normal force (N). Hence at the primary pulley the torque loss due to wedging losses at either the entrance or exit of the primary pulley will be-

$$Tq_{wedge,pri} = \frac{n_{seg,wedge,pri}V_{rel,pri}N_{pri}\mu_{pri}}{\omega_{in}} \qquad (92)$$

A similar loss will also exist at the secondary pulley entrance and exit, with a different number of engaged segments, relative speed and segment loading. This loss must be implemented at both entrance and exit and on both pulleys, such that the total torque loss due to the wedging effect will be-

$$Tq_{wedge,total} = 2\left[\frac{n_{seg,wedge,pri}V_{rel,pri}N_{pri}\mu_{pri}}{\omega_{in}}\right] + 2\left[\frac{n_{seg,wedge,sec}V_{rel,sec}N_{sec}\mu_{sec}}{\omega_{in}}\right] \qquad (93)$$

8.8.2 Pulley Penetration Loss

This is the second of the loss mechanisms associated with the deformation of the pulleys. It is caused by the segments of the belt penetrating into the pulley wedge angle and being forced out of the pulley wedge angle as the segment travels from inlet to exit, such that they take a non circular path as shown in Figure 8-45.

_____

The number of segments travelling past any fixed point, in the variator, per second $\dot{N}_{seg}$ can be defined as-

$$\dot{N}_{seg} = \frac{V_{belt}}{t_{seg}}$$

(94)

As with the pulley wedge loss the radial penetration of the belt δ_{pen} can be calculated from the axial deflection of the pulley-

$$\delta_{pen} = \frac{\delta}{2 \tan \theta}$$

(95)

The work done on sliding one segment into and out of the wedge angle by this depth is given by-

$$W_{pen,pri} = 2\delta_{pen,pri} \mu_{rad,pri} 2N_{pri}$$

(96)

And hence the torque loss is given by-

$$Tq_{pen,pri} = \frac{W_{pen,pri}\dot{N}_{seg}}{\omega_{in}}$$

(97)

Similar events also occur on the secondary pulley such that-

$$Tq_{pen,total} = \frac{W_{pen,pri}\dot{N}_{seg}}{\omega_{in}} + \frac{W_{pen,sec}\dot{N}_{seg}}{\omega_{in}}$$

(98)

8.9 Total belt torque loss

The total torque loss due to the belt can be calculated as the addition of all the individual belt torque loss mechanisms.

$$Tq_{loss,belt} = Tq_{wedge,total} + Tq_{pen,total} + Tq_{band,total} + Tq_{slip,total}$$

(99)

Figure 8-47 & Figure 8-48 show plots of the experimental belt torque losses vs. the modelled belt torque losses in low and high ratio respectively. Good agreement is achieved in both conditions when compared to the higher temperature experimental conditions (75°C & 95°C). As discussed previously (section 5.5.2) it is thought that the observed reduction in torque loss at the lower temperatures 25°C condition is due to hydrodynamic 'lift off' in the bands of the belt. This hydrodynamic 'lift off' theory is also supported by the 50°C result in high ratio, Figure 8-48, which shows the torque loss

_____

_____

diverging from the 75°C & 95°C results at high speeds, a condition under which band speeds are very high and likely to support lubrication film formation. The modelling of events under these proposed hydrodynamic conditions was not performed in detail, although it is an area highlighted as further work (Chapter 11), and the techniques to do so are discussed in section 8.4.5.

A breakdown of the modelled torque loss contributors is shown in Figure 8-49 & Figure 8-50 for low and high ratio respectively. The pressure data used to generate the model results is shown in Figure 8-51 & Figure 8-52 for low and high ratio respectively. It can be seen that in both cases the predominant loss mechanism is due to the band losses. The band losses generate nearly all of the characteristic shapes seen in the belt torque loss results. In low ratio the band losses increase rapidly with the changes in clamping pressure, Figure 8-51, while speed dependence appears minimal. Conversely in high ratio, where the clamping pressures are always within a 2 bar range, Figure 8-52, the torque loss due to the bands appears to be highly speed dependent. It should be noted that as the validation model was achieved by inputting the experimental clamping pressure data, which has a degree of variability between tests, there will be a degree of variation between measured and modelled results. By fine tuning the pressure data used an even better fit could be achieved. However, due to the large number of experimental variables used to calculate the belt loss data, it is felt that the accuracy of the model fit is highly acceptable.

Comparing the other predicted losses in Figure 8-49, it can be seen that in low ratio the entry and exit wedge losses are quite significant while the pulley penetration losses and segment slip losses are quite small components. In high ratio, Figure 8-50, the radial penetration loss increases considerably due to the greater number of segments passing around the pulley (higher belt speed), while the entry and exit wedge losses are of a similar magnitude to those seen in low ratio. Although the clamping pressures and thus pulley deflections are lower in high ratio, significant primary pulley deflection was measured in high ratio, while no primary pulley deflection is measured in low ratio (section 8.8).

Figure 8-53 shows the predicted belt torque losses in low ratio over a large range of output torque and clamping pressure conditions. This figure is supported by similar plots in Figure 8-54 & Figure 8-55, which show the variation in band losses and segment slip losses respectively over the same range of operating conditions. Both Figure 8-53 &

_____

_____

Figure 8-54 show a reduction in torque loss as initial output torque is increased on the variator. This is due to the reduction in band resultant force, and hence band friction, achieved as the segment compression force, C_x, first reduces under inverted loading and then begins to increase again under conventional loading conditions. This reduction in torque loss was also measured experimentally on the torque loss test rig, at which time no valid explanation was available. With reference to Figure 8-53 the diagonal white line represents the breakpoints, due to $C_x=0$, which changes with pulley clamping pressure. Figure 8-55 shows the torque loss due to segment sliding on both of the pulleys, this is characterised by a large torque in the low pressure, high output torque corner of the graph, where segment to pulley slip is greatest. On all the plots a number of meshes are layered over each over, each one representing a 500 rev/min increase in input speed, as noted on Figure 8-53. Hence the top layer represents 4000 rev/min while the bottom layer represents the 1000 rev/min operating condition. The lack of definition between the layers indicates the very small effect of input speed on the losses in low ratio. A small speed effect is seen in the band loss plot, Figure 8-54.

Similar plots to those described above are available for a range of high ratio operating condition. As before Figure 8-56, Figure 8-57 & Figure 8-58 represent the total belt torque loss, band loss and segment sliding loss respectively. In contrast to the low ratio test condition these results are obtained over a smaller range of clamping pressures (10~12 bar) and smaller range of output torques (max. 40 Nm). Figure 8-56 shows definite separation between each layer, thus indicating much more speed dependence of the losses, while pressure effects appear to be minimal and output torque loading does not show the characteristics of inverted loading as seen in low ratio.

8.10 Belt Loss Modelling Conclusions

A detailed investigation and analysis has been performed into the functioning of the pushing metal V-belt CVT. The models proposed have been validated with a range of experimental data from two test rigs, including torque loss data, belt slip data and pulley deflection information. The models proposed for belt slip and torque loss both interact in a number of ways and it is reassuring to note that the two interacting models both agree well with the experimental data under a significant range of operating conditions.

It is also significant that the models proposed have agreed in many respects with experimental finding published by other people working within this same field of research.

_____

_____

In particular the models proposed in this thesis predict similar phenomena to those described by Fujii et al. **[21 & 22]**, with regards to force distributions and Kobayashi et al. **[9]**, who proposed a slip due to gap theory. This project however has added further experimental finding to these previous publications and explained in some detail the fact that belt slip and torque transmission are highly inter-related.

A number of belt torque loss models were proposed in this thesis and they are all supported by a significant quantity of experimental data. The analysis of the interaction between bands and segments is the most significant and is validated both by the breakpoints in the belt slip data and the force distribution data proposed by others. It is also supported by the experimental segment deformation tests performed by Micklem et al. and a highly predictable elastic analysis of the band extensions under tension.

Pulley wedging losses and penetration losses were proposed, which at present are highly empirical, but supported by some significant measurements of deflection levels. With the deflection levels measured it would be hard to deny the existence of such losses even if the modelling of the deflection required some further analysis and quantification. This could possible be performed as further work by extending the fields of the experimental study into deflection or performing a theoretical analysis of the pulleys using a FEA package.

_____

	Low Ratio		High Ratio	
	Measured	Simulation	Measured	Simulation
Band 1 relative to segment	15 mm	16 mm	6 mm	7 mm
Subsequent bands relative to inner neighbour	1.5 mm	1.6 mm	1 mm	1.2 mm

Table 8-1 Experimental vs. Simulation Results of Belt Displacements
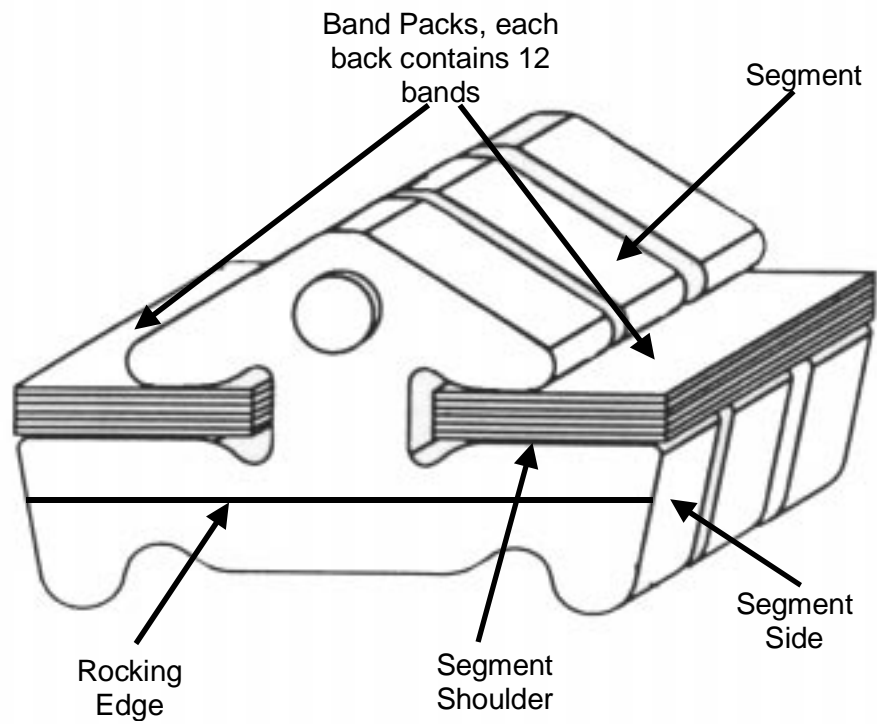
Figure 8-1 Components of the Metal V-Belt
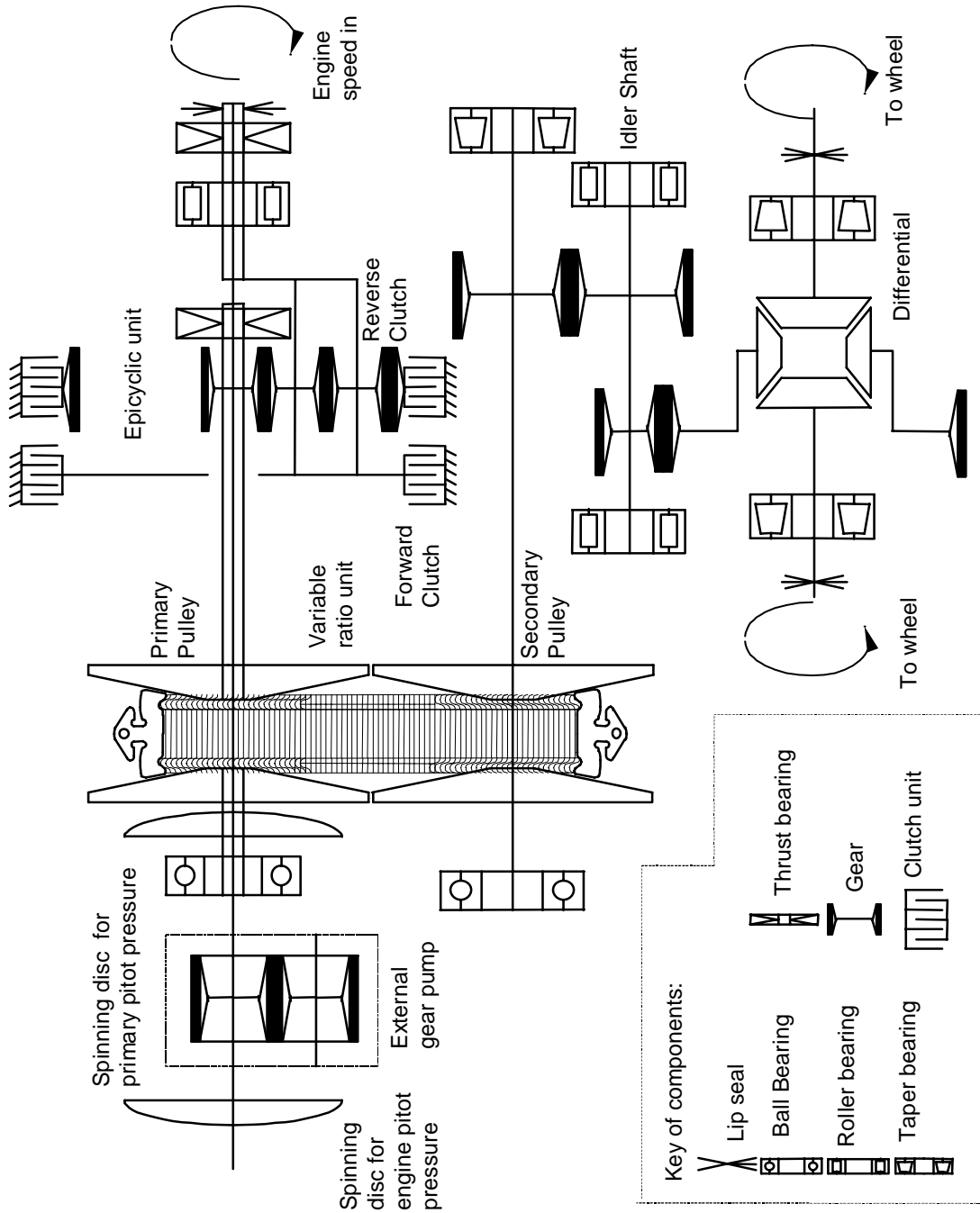
Figure 8-2 Mechanical Components in the Transmission
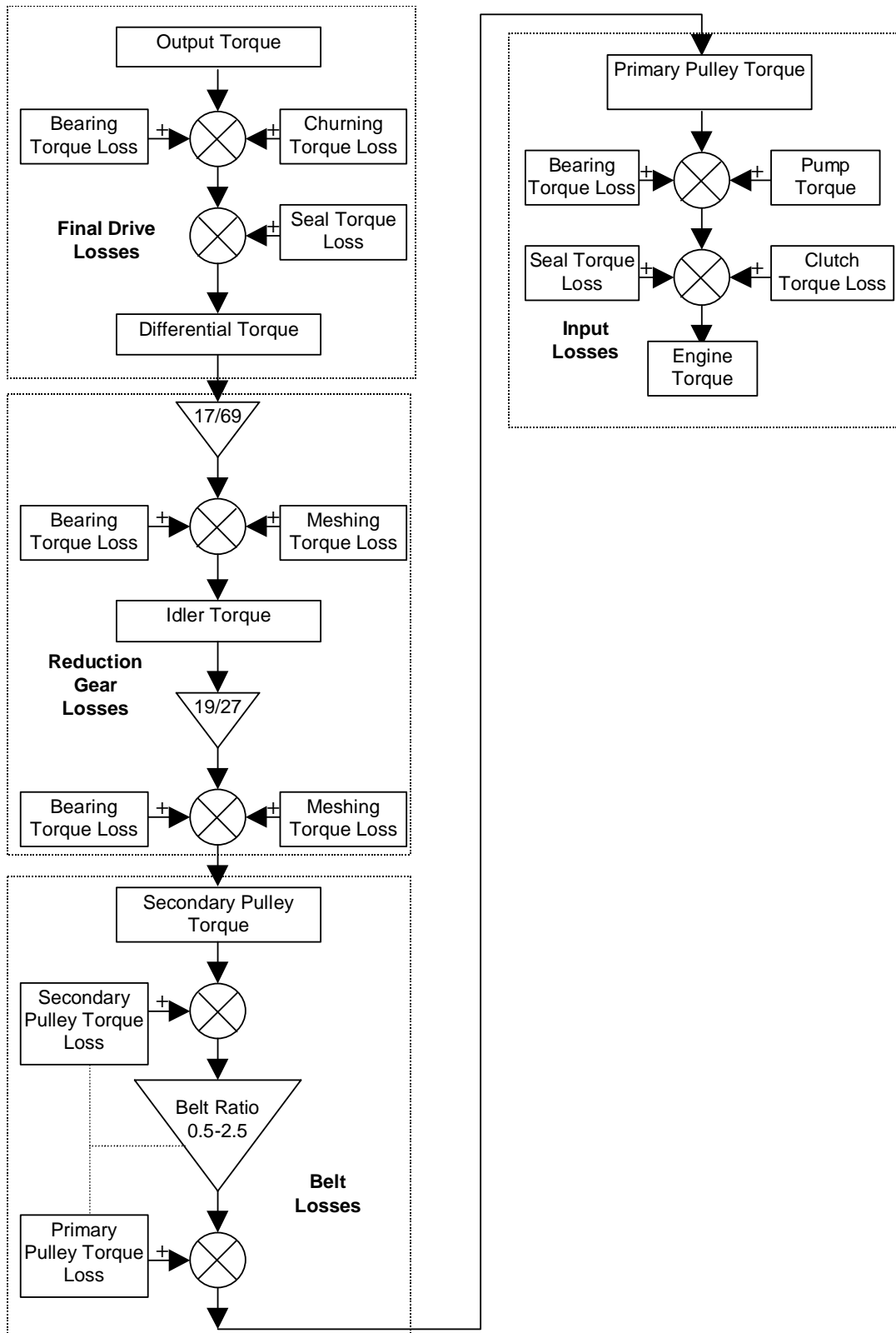
Figure 8-3 Flow Diagram of Torque Losses Through the Transmission
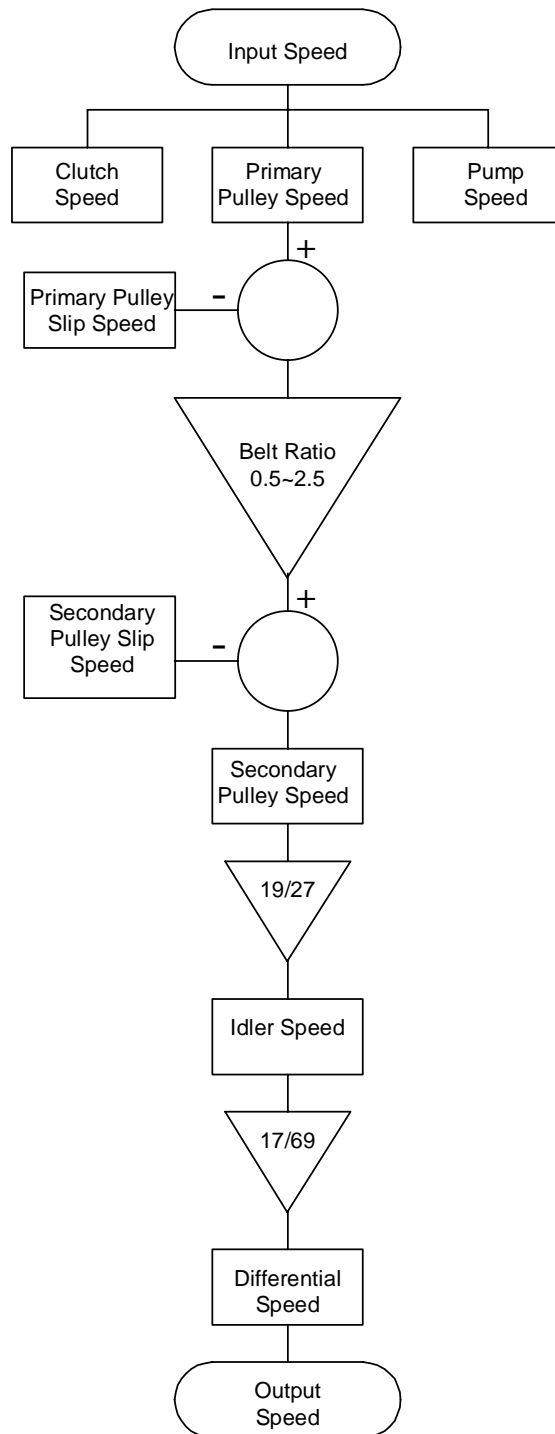
Figure 8-4 Flow Diagram of Speed Losses Through the Transmission
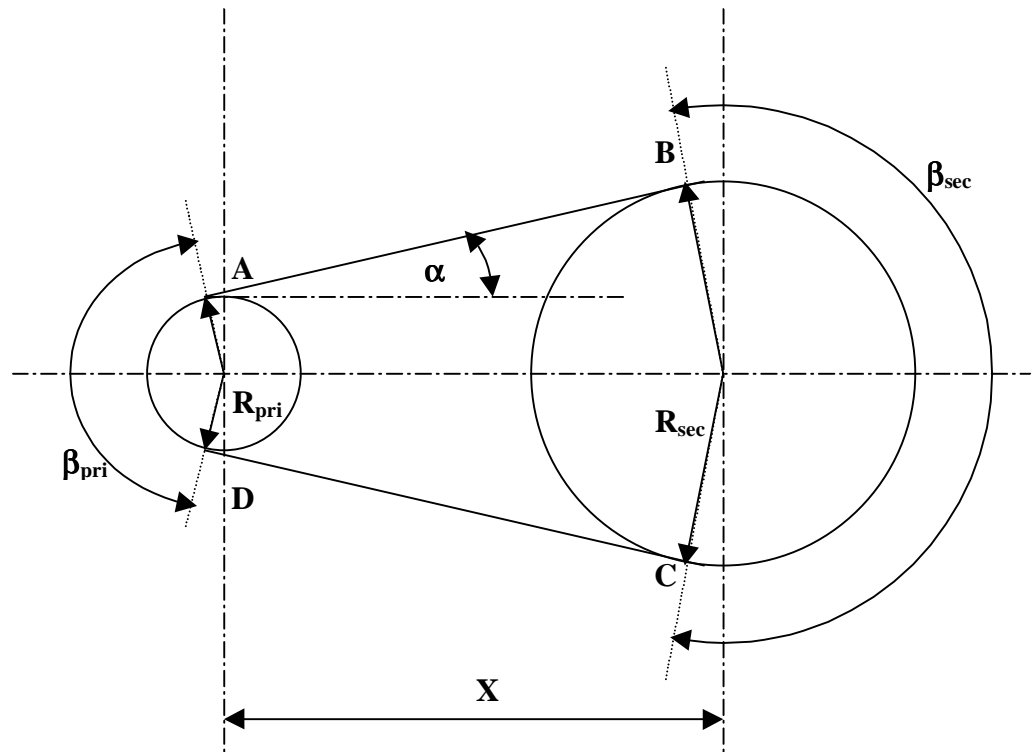
Figure 8-5 Geometry of the Belt
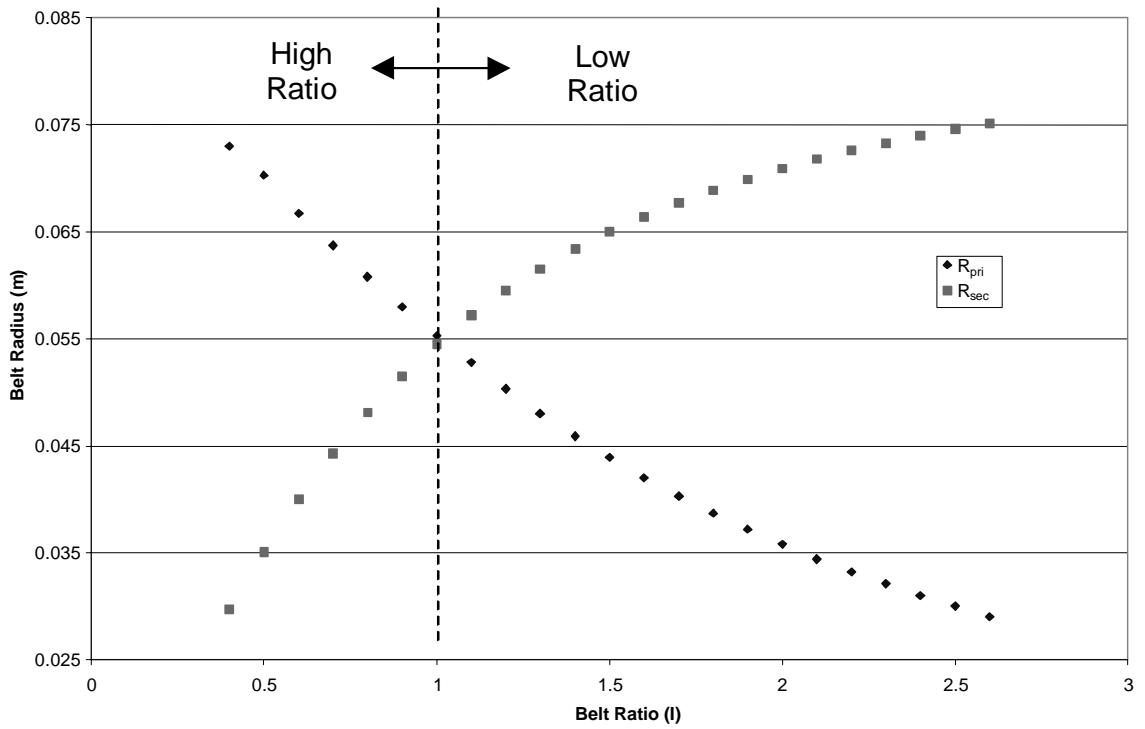
Figure 8-6 Calculated Belt Radii
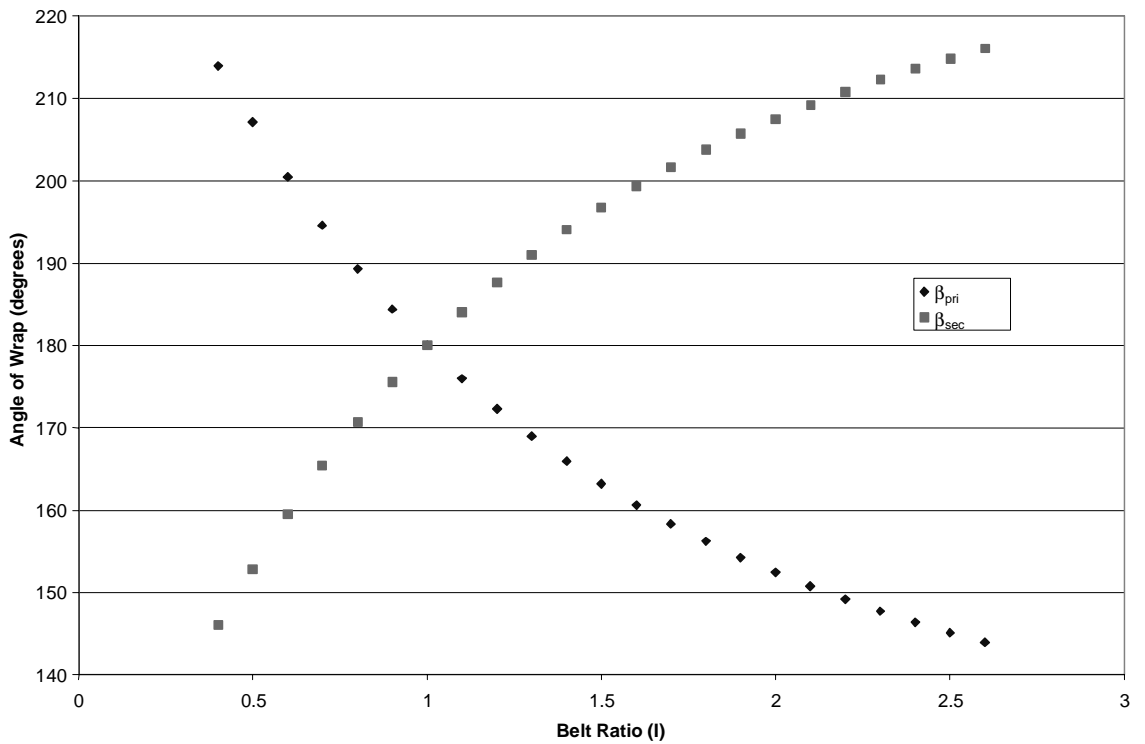
Figure 8-7 Calculated Variator Wrap Angles

_____
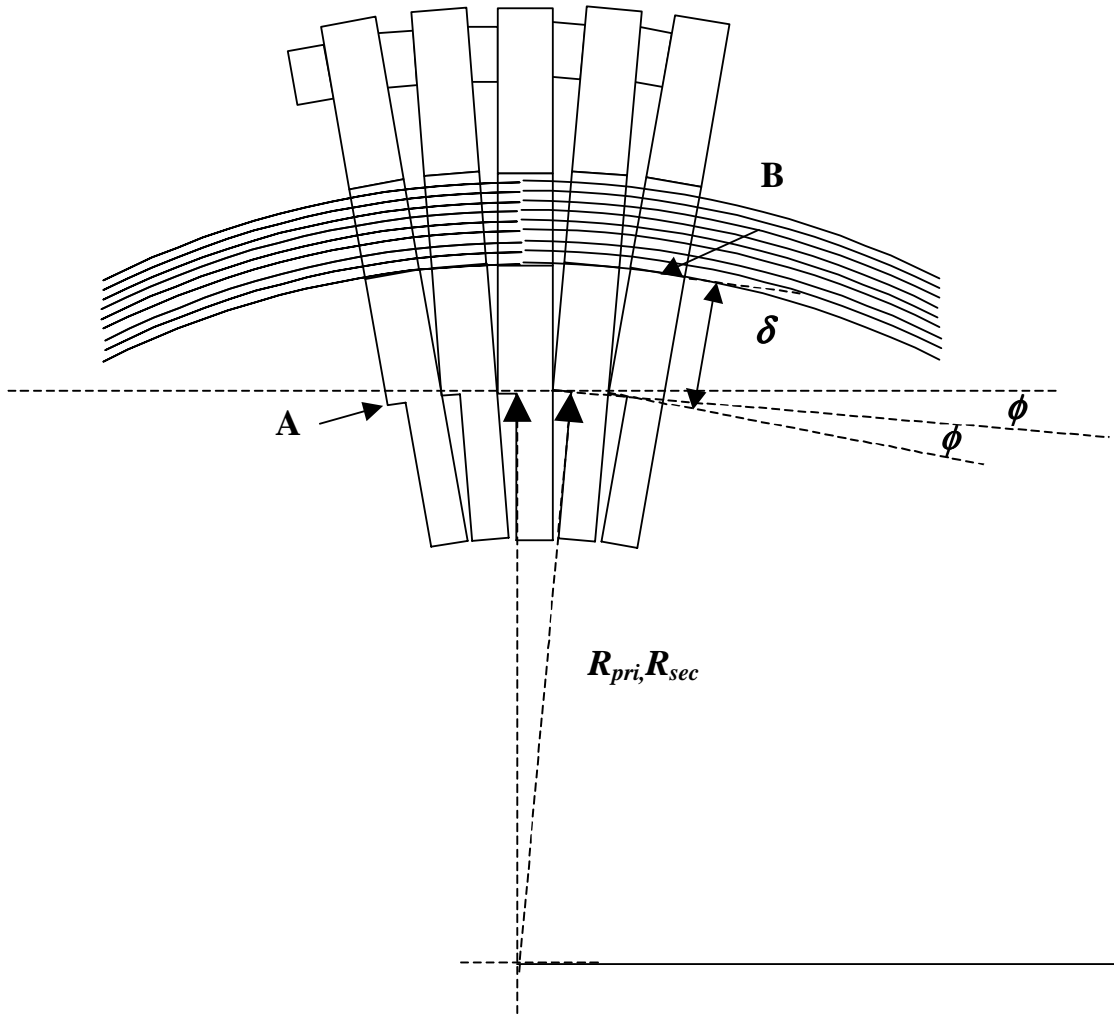
Figure 8-8 Geometry of Bands and Segments Travelling in a Wrap Angle
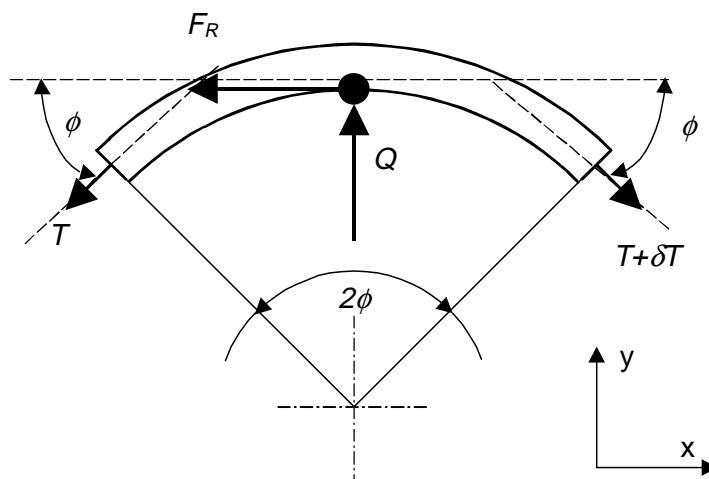
Figure 8-9 Free Body Diagram of Band Portion Around One Segment

_____

$Q/2$ $Q/2$

N N

θ

$M_{seg}V^2/R$

F_{rad} F_{rad} y

x in plane
of page
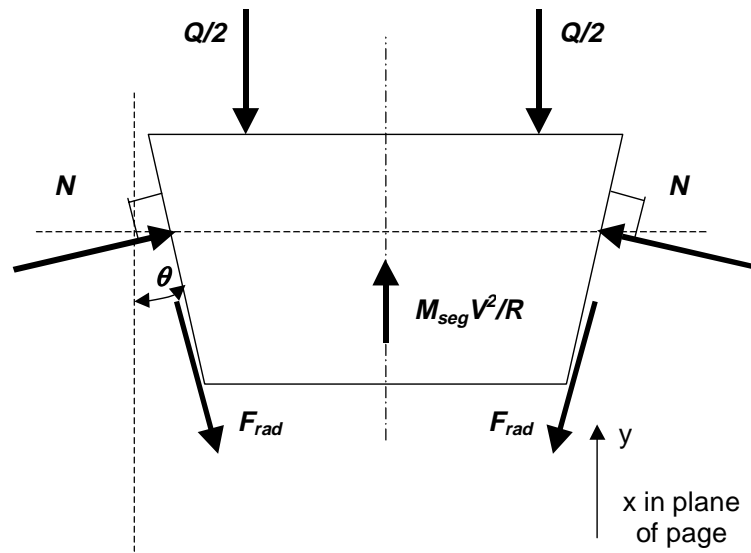
Figure 8-10 Free Body Diagram of One Segment, Radial Direction (Front View)

Q

F_R

$M_{seg}V^2/R$

Z

F_T

ϕ ϕ

$C_X + \delta C_X$ C_X y

$2F_{rad}cos\theta$ x
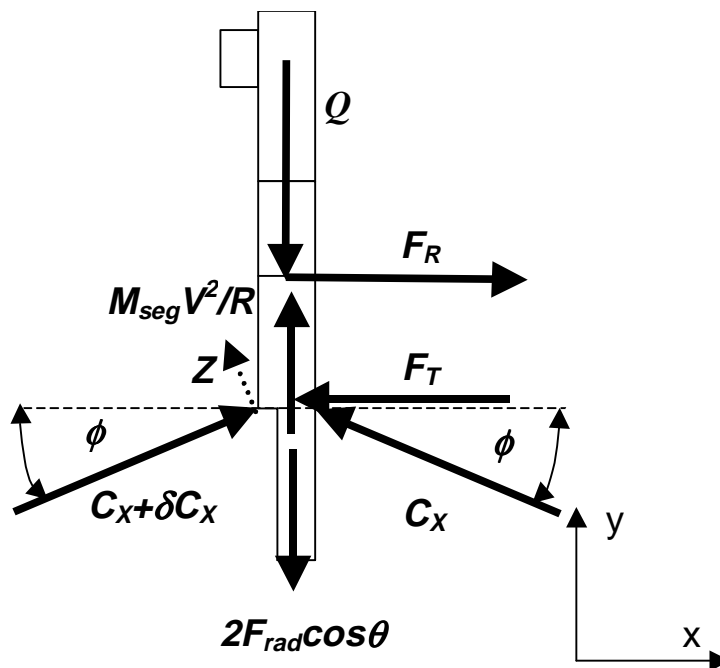
Figure 8-11 Free Body Diagram of One Segment, Tangential Direction (Side View)

_____
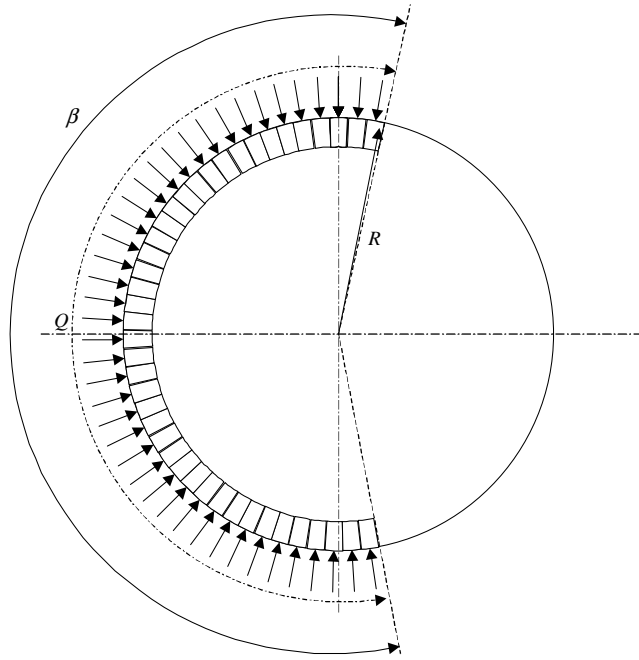
Figure 8-12 Individual Segment Shoulder Forces Contributing to Friction on Bands
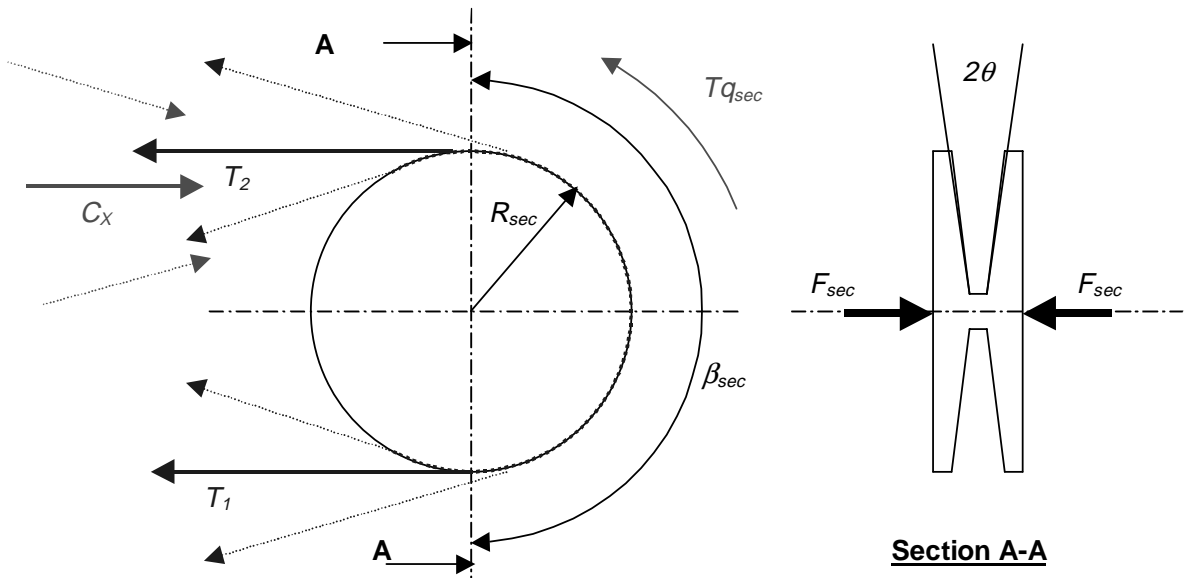
Figure 8-13 General Free Body Diagram of Forces Acting on the Secondary Pulley

_____

Direction of Motion

$i+1$

$F_R(i+1)$

i

$F_R(i)$ $\hat{Q}(i)$

$\delta V(i)$

$\delta V(i+1)$

T

$T+\delta T$

$i-1$

$F_R(i-1)$ $\hat{Q}(i-1)$
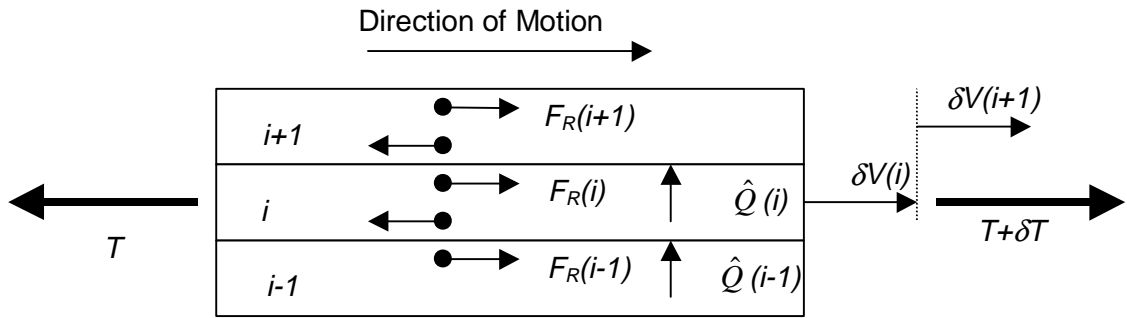
Figure 8-14 Outer Band Sliding Ahead of Inner Band

Direction of Motion

$i+1$

$F_R(i+1)$

i

$F_R(i)$ $\hat{Q}(i)$

$\delta V(i)$

$T+\delta T$

T

$i-1$

$F_R(i-1)$ $\hat{Q}(i-1)$

$\delta V(i-1)$
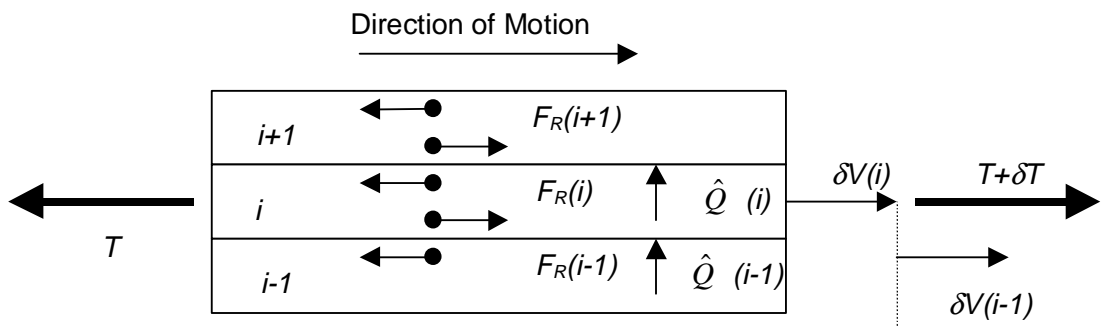
Figure 8-15 Inner Band Sliding Ahead of Outer Band

B

Direction of Motion

$i+1$

$\delta V(i+1)$

$h(i+1)$

$T+\delta T$

T

i

$\delta V(i)$

$h(i)$

$i-1$

$\delta V(i-1)$

L
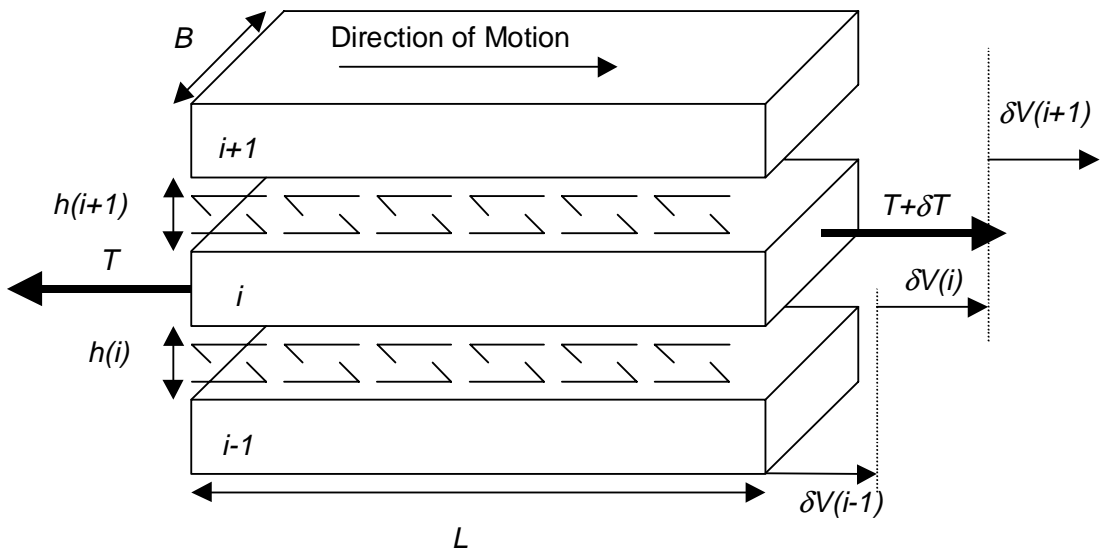
Figure 8-16 Bands Separated by a Lubrication Film

_____
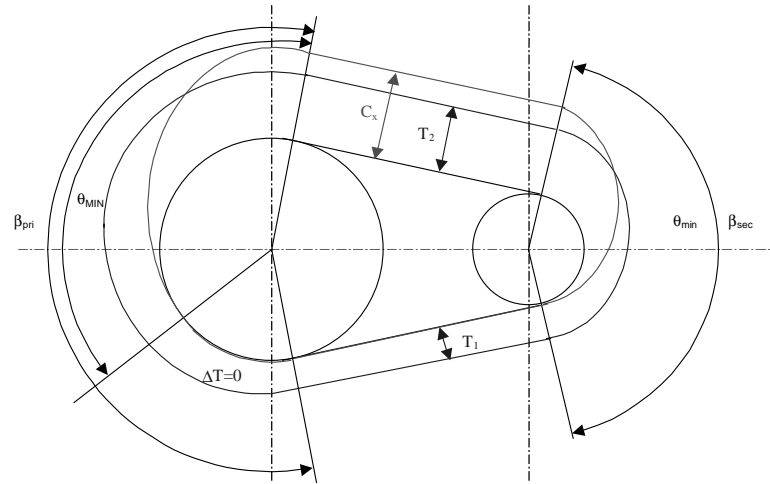
Figure 8-17 Distribution of Band Tensions and Belt Compression Forces in the Belt Mechanism in High Ratio
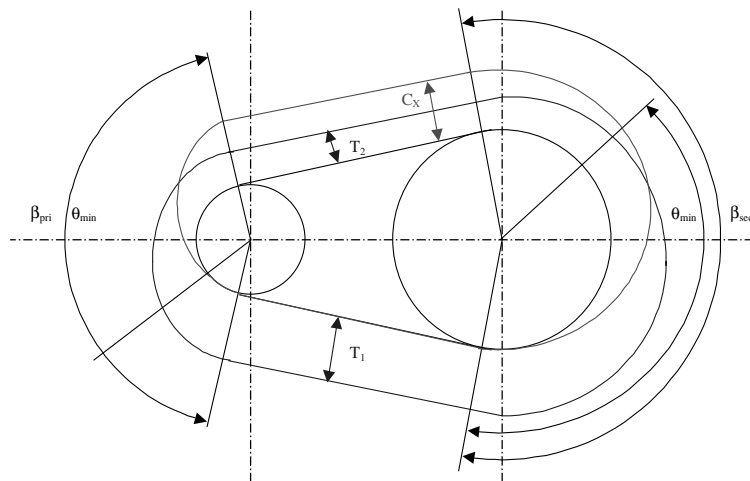
Figure 8-18 Distribution of Band Tensions and Belt Compression Forces in the Belt Mechanism in Low Ratio at High Torques
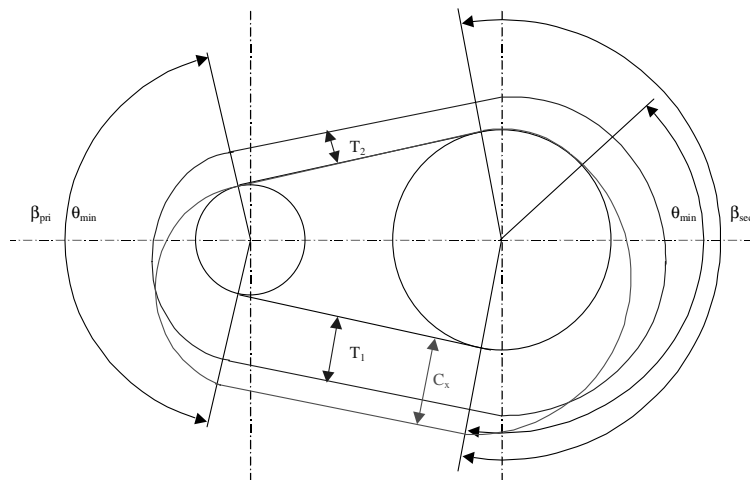
Figure 8-19 Distribution of Band Tensions and Belt Compression Forces in the Belt Mechanism in Low Ratio at Low Torques

_____

_____
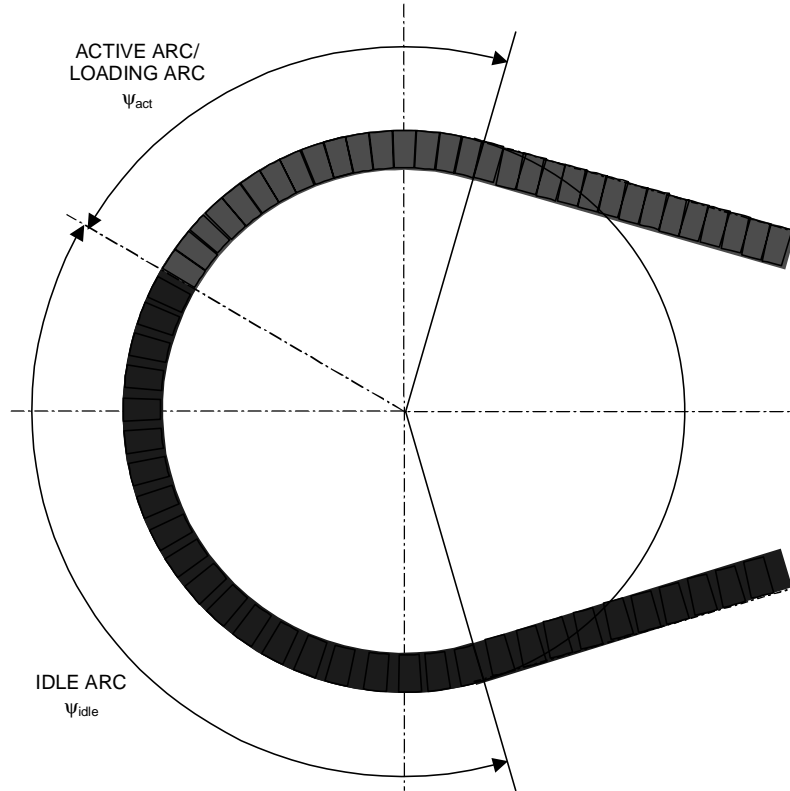
Figure 8-20 Definition of Active and Idle Compression Arcs
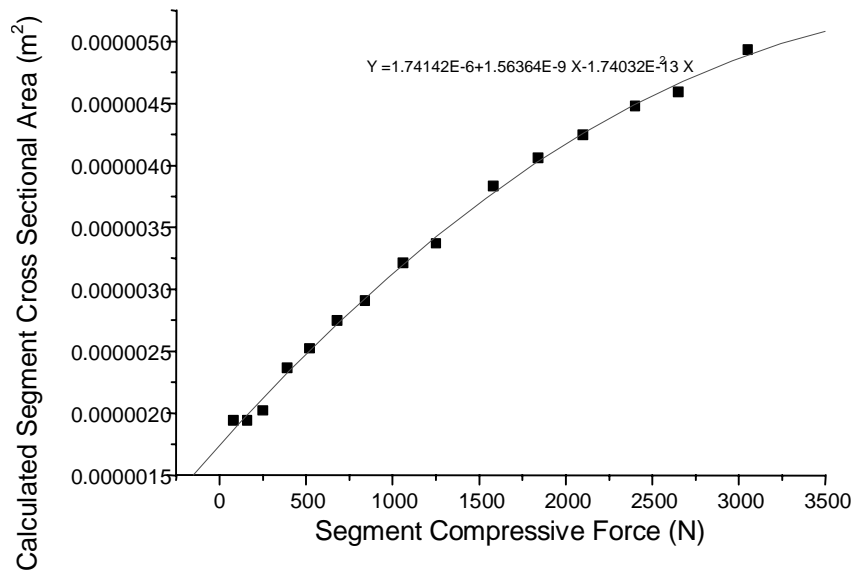
Figure 8-21 Calculated Segment Cross Sectional Area from Experimental Data [J.D. Micklem (1990)]

_____

Variator Function	Primary Pulley	Secondary Pulley
Figure 8-22 Gap location in low ratio high load	Figure 8-23 Low Ratio Primary Pulley Loading	Figure 8-24 Low Ratio Secondary Pulley Unloading
Figure 8-25 Gap location in low ratio low load	Figure 8-26 Low Ratio Primary Pulley Unloading	Figure 8-27 Low Ratio Secondary Pulley Loading
Figure 8-28 Gap location in high ratio all load	Figure 8-29 High Ratio Primary Pulley Loading	Figure 8-30 High Ratio Secondary Pulley Unloading

_____
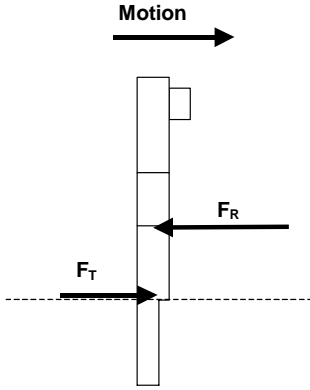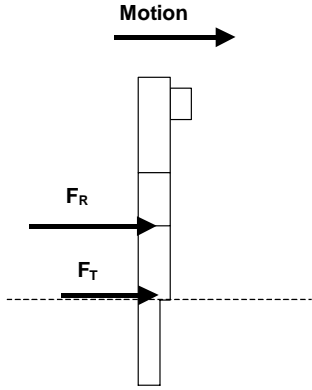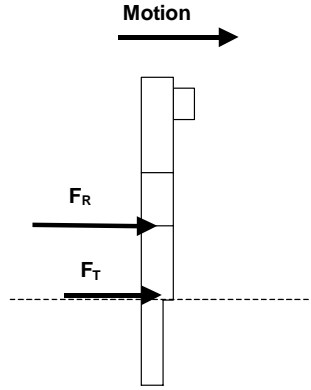
Motion →	Motion →	Motion →
F_R ← F_T →	F_R → F_T →	F_R → F_T →
Figure 8-31 Primary Pulley Idle Arc Low Ratio, High Load	Figure 8-32 Secondary Pulley Idle Arc Low Ratio, Low Load	Figure 8-33 Primary Pulley Idle Arc High Ratio, All Loads

_____
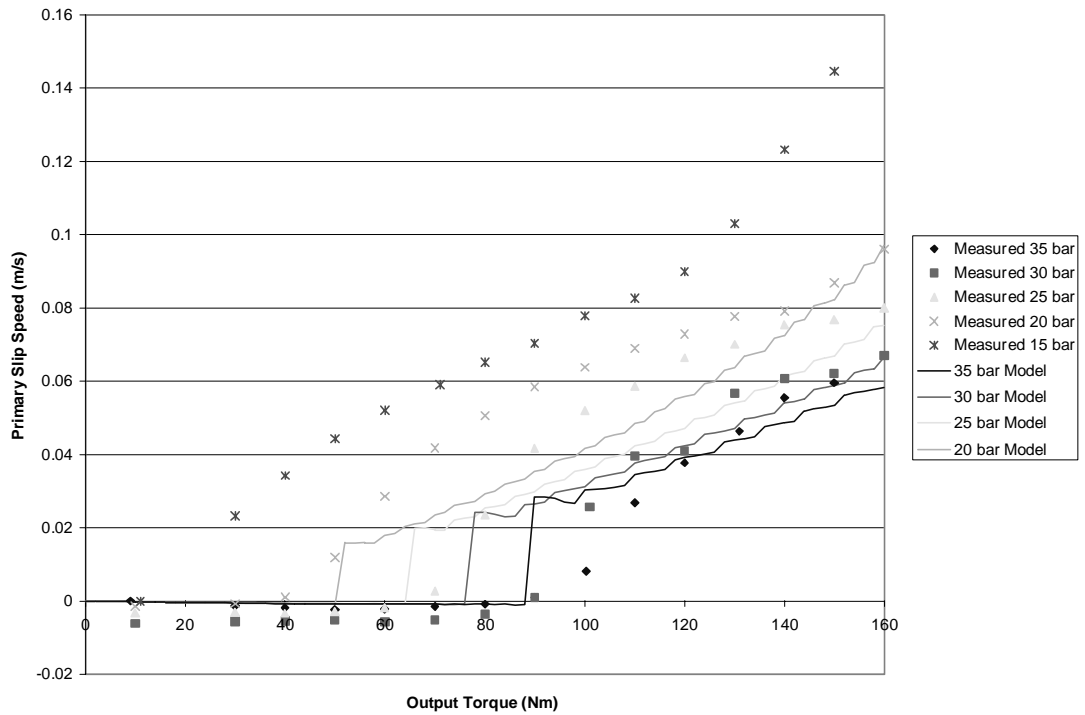
Figure 8-34 Primary Pulley Slip, Experimental Results vs. Simulation in Low Ratio
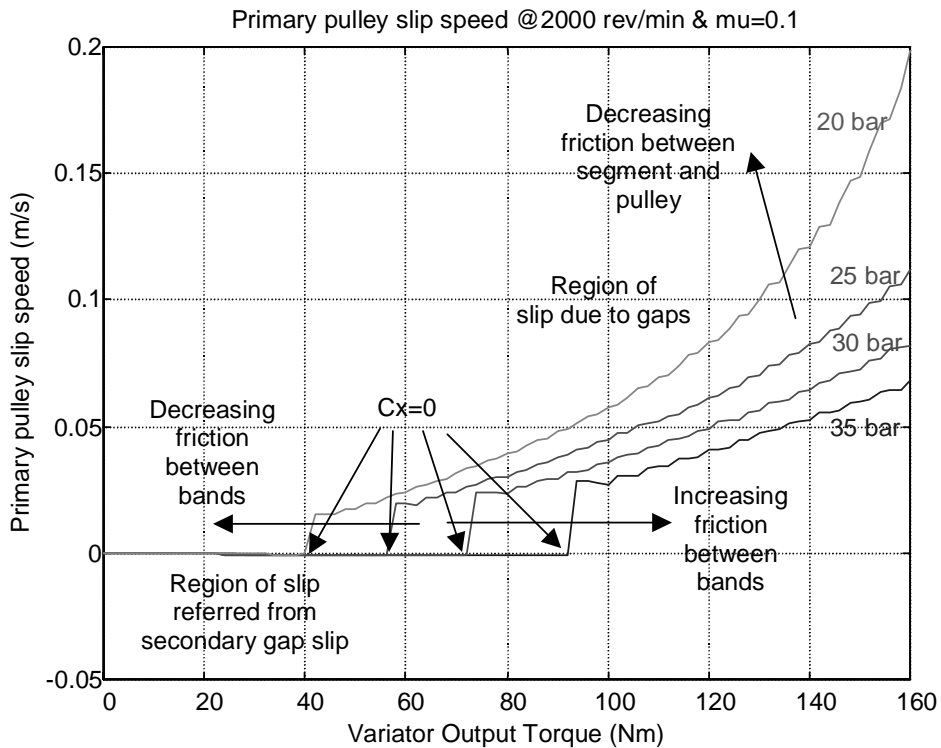
Figure 8-35 Effect of Parameter Variation on Primary Pulley Slip

_____

_____
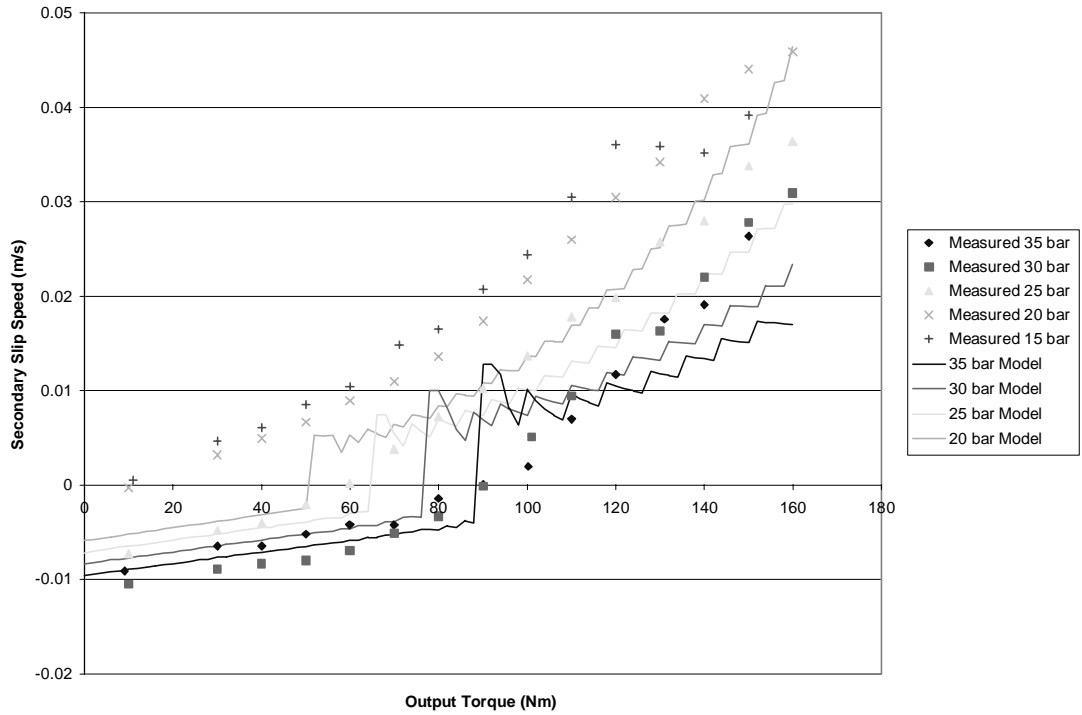
Figure 8-36 Secondary Pulley Slip, Experimental Results vs. Simulation in Low Ratio
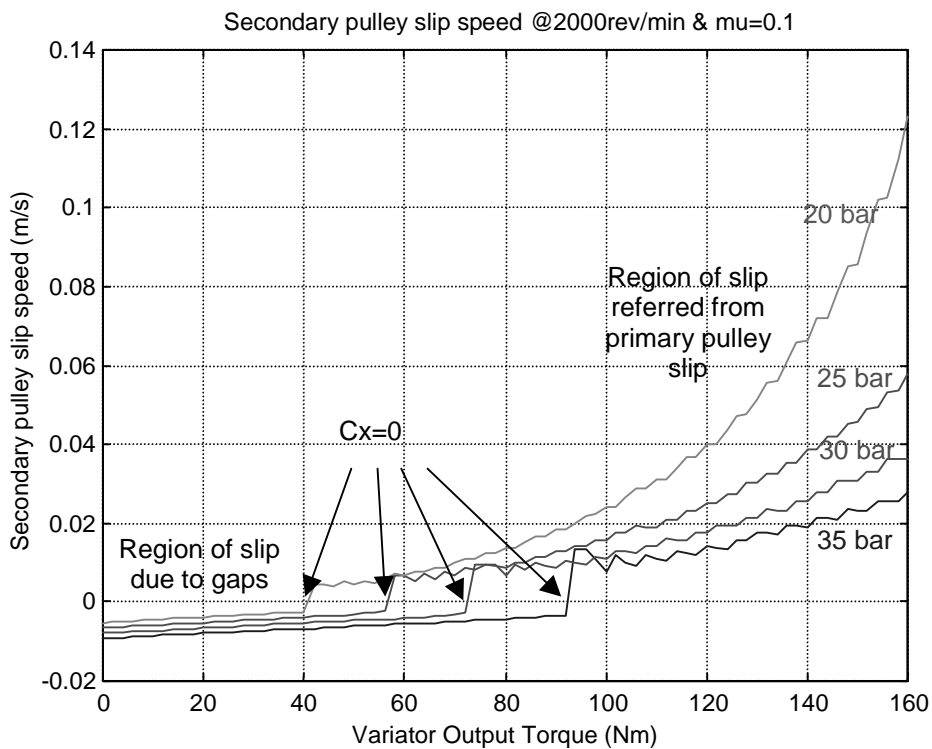
Figure 8-37 Effect of Parameter Variation on Secondary Pulley Slip

_____

_____
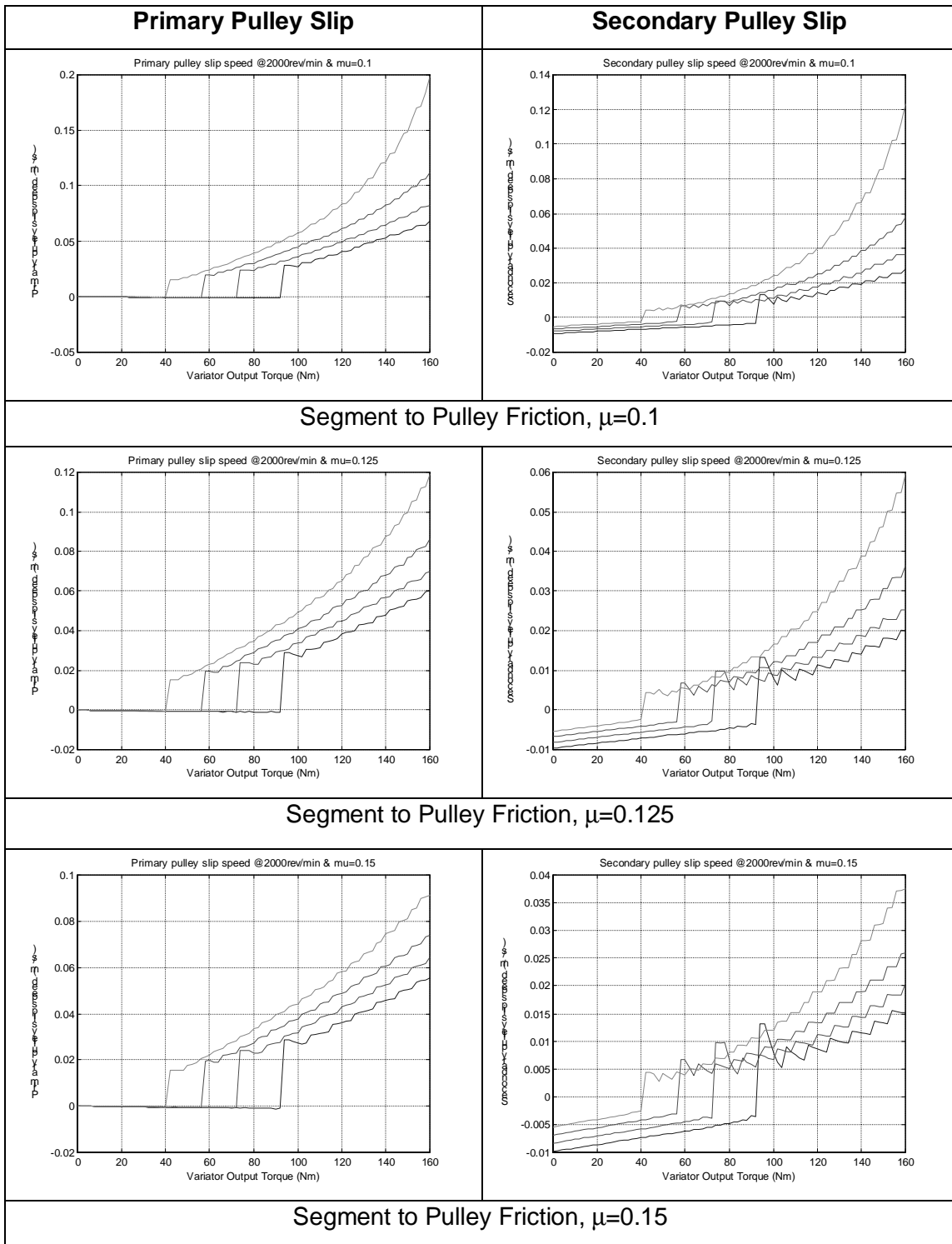
Figure 8-38 Effect of Segment to Pulley Friction on Belt Slip Speed at Primary and Secondary Pulleys

_____

Primary Pulley Slip	Secondary Pulley Slip
Primary pulley slip speed @1000rev/min & mu=0.125	Secondary pulley slip speed @1000rev/min & mu=0.125
Input Speed 1000 rev/min	
Primary pulley slip speed @2000rev/min & mu=0.125	Secondary pulley slip speed @2000rev/min & mu=0.125
Input Speed 2000 rev/min	
Primary pulley slip speed @3000rev/min & mu=0.125	Secondary pulley slip speed @3000rev/min & mu=0.125
Input Speed 3000 rev/min	

Figure 8-39 Effect of Input Speed on Belt Slip Speed at Primary and Secondary Pulleys
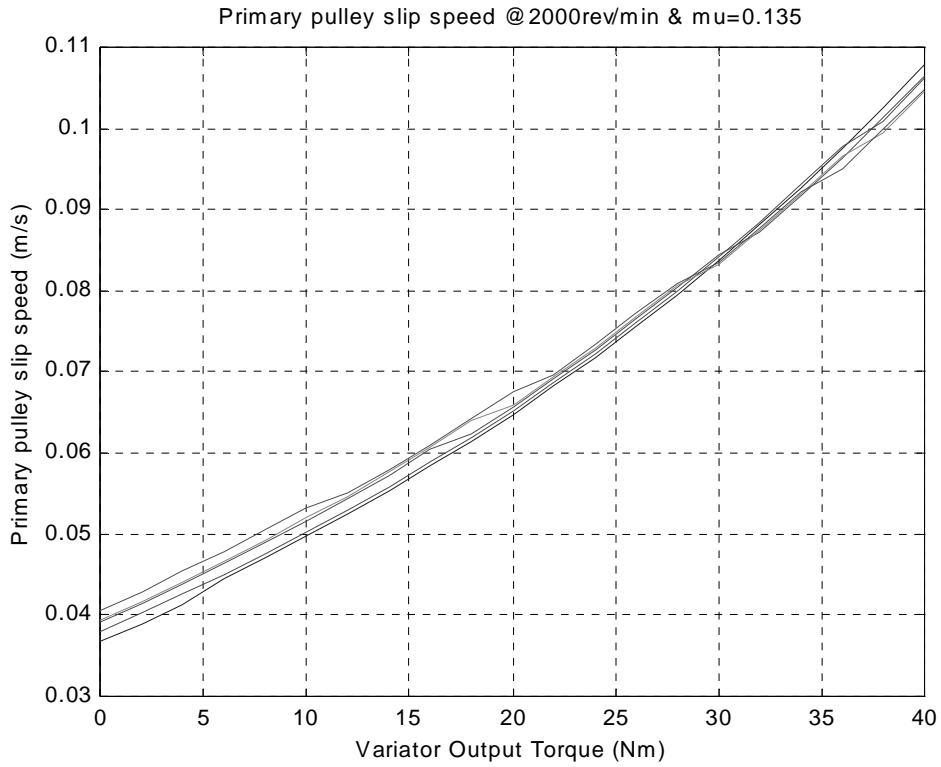
Figure 8-40 Primary Pulley Slip Speed Model Results in High Ratio
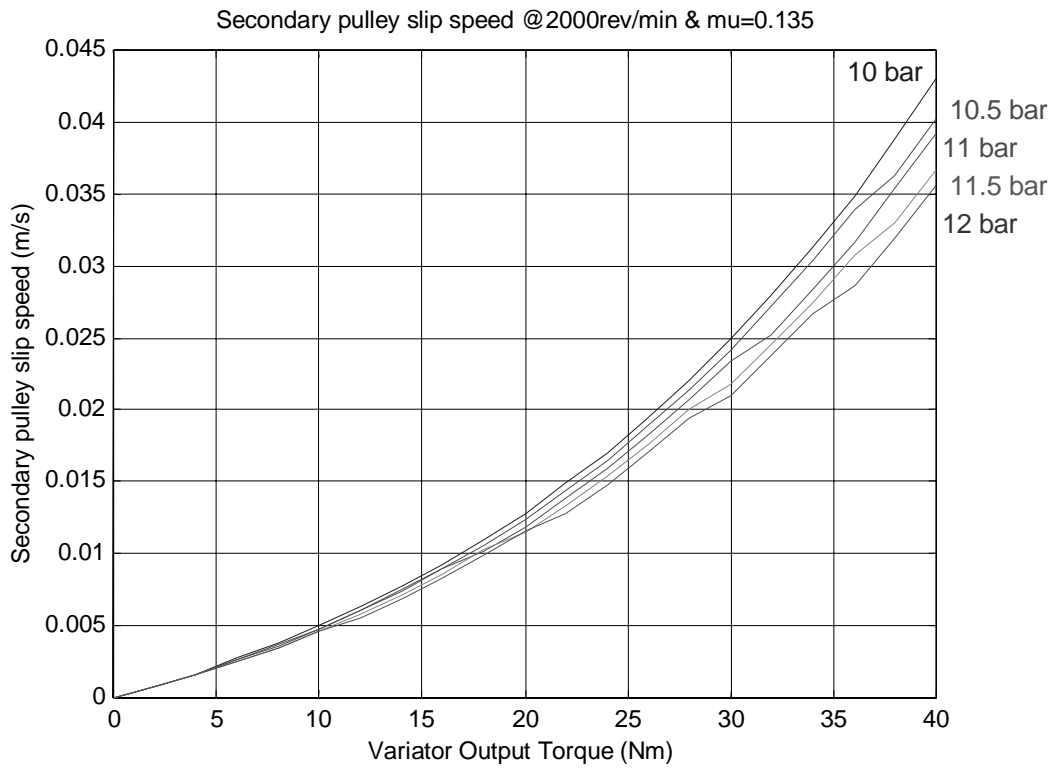
Figure 8-41 Secondary Pulley Slip Speed Model Results in High Ratio
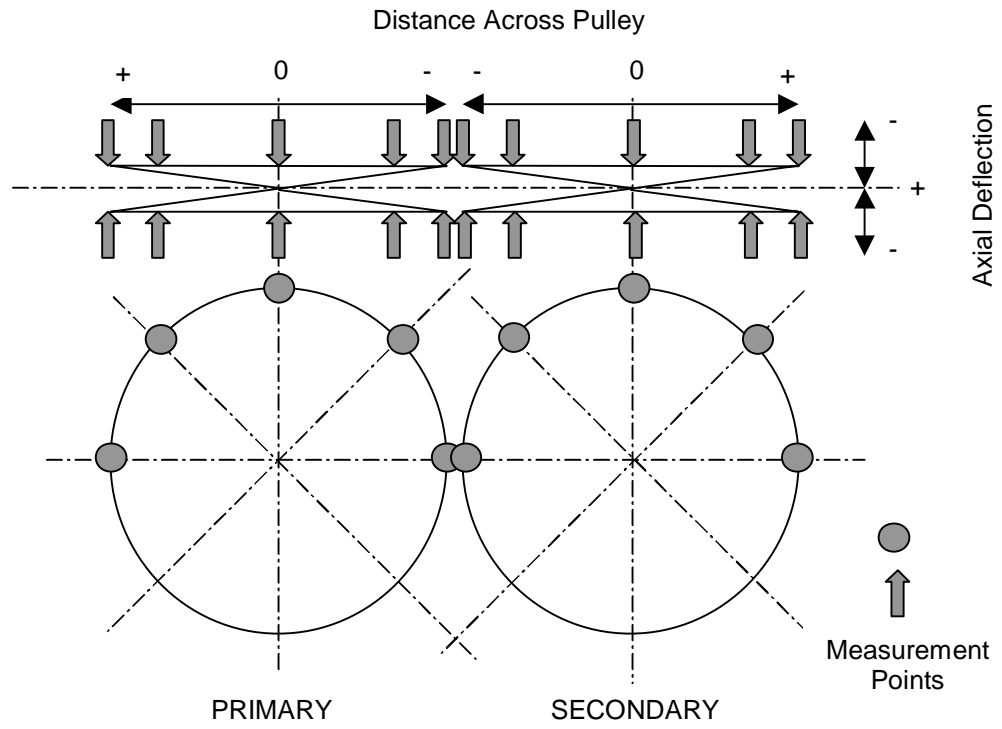
Figure 8-42 Locations and Definitions for Pulley Deflection Measurements

_____

Fixed Half	Actuated Half	Change in Clearance

(a) Low Ratio Secondary Pulley

No deflection	No deflection	N/A

(b) Low Ratio Primary Pulley

(c) High Ratio Secondary Pulley

(d) High Ratio Primary Pulley
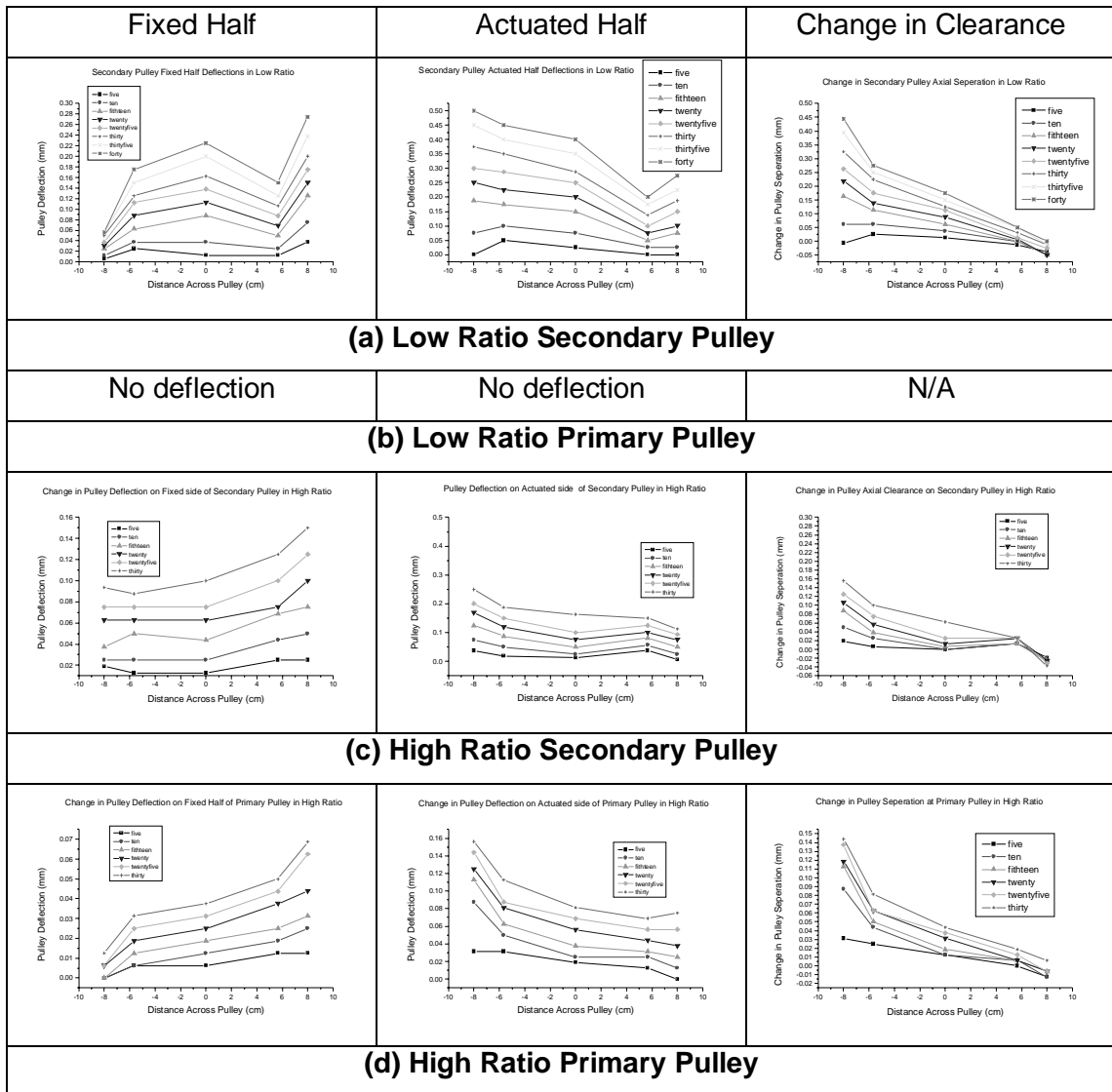
Figure 8-43 Measured Deflections and Calculated Changes in Clearance between Pulley Halves

Fixed Side

Actuated Side

Unloaded

Loaded
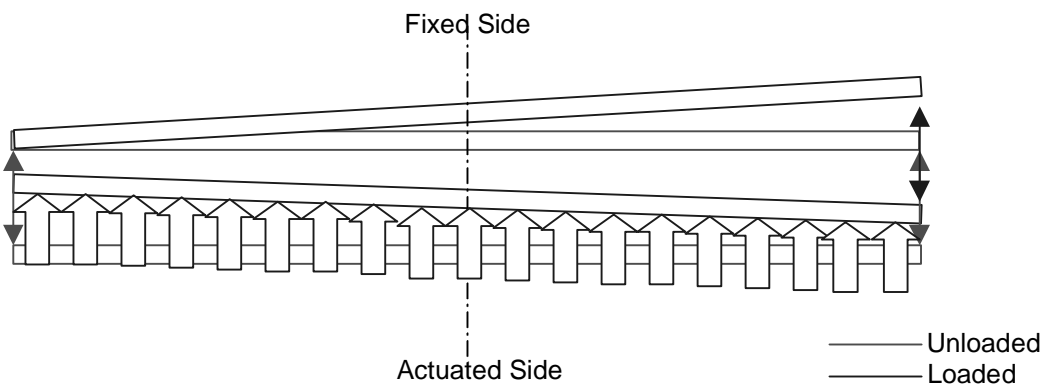
Figure 8-44 Typical Movement of Pulley Halves

_____
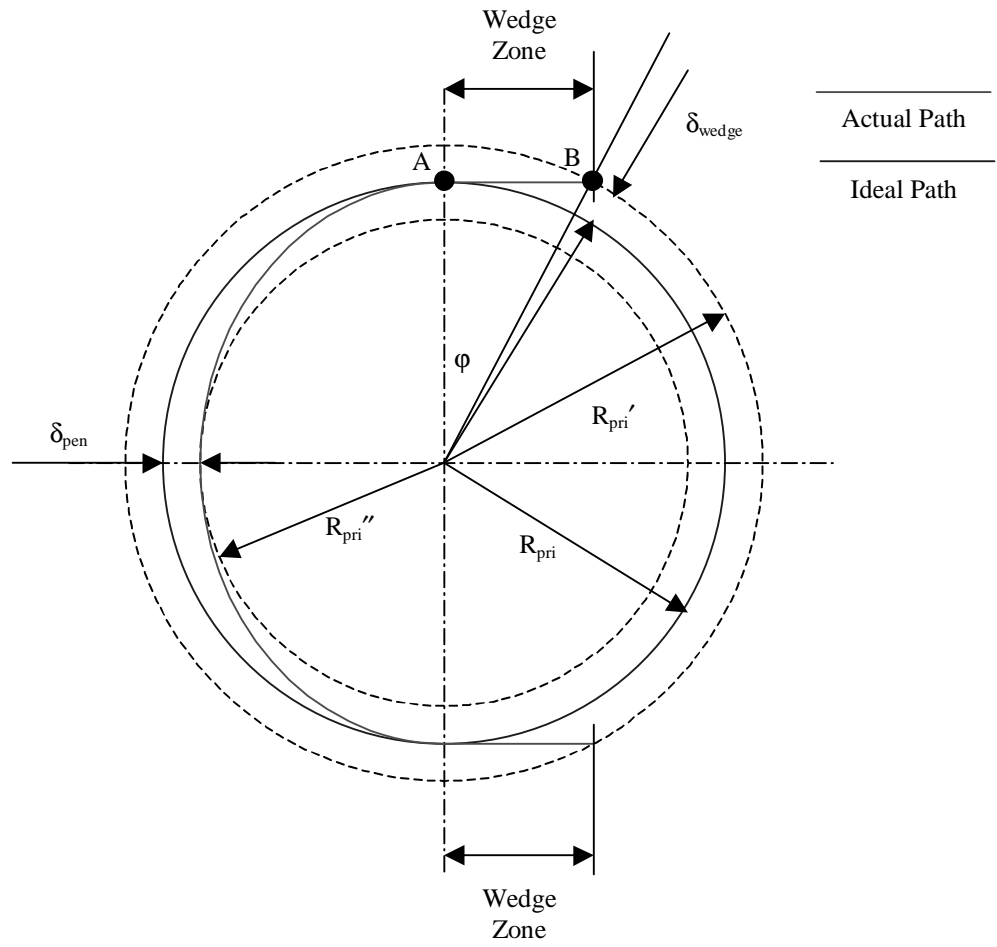
Figure 8-45 Geometry of a Deformed Pulley
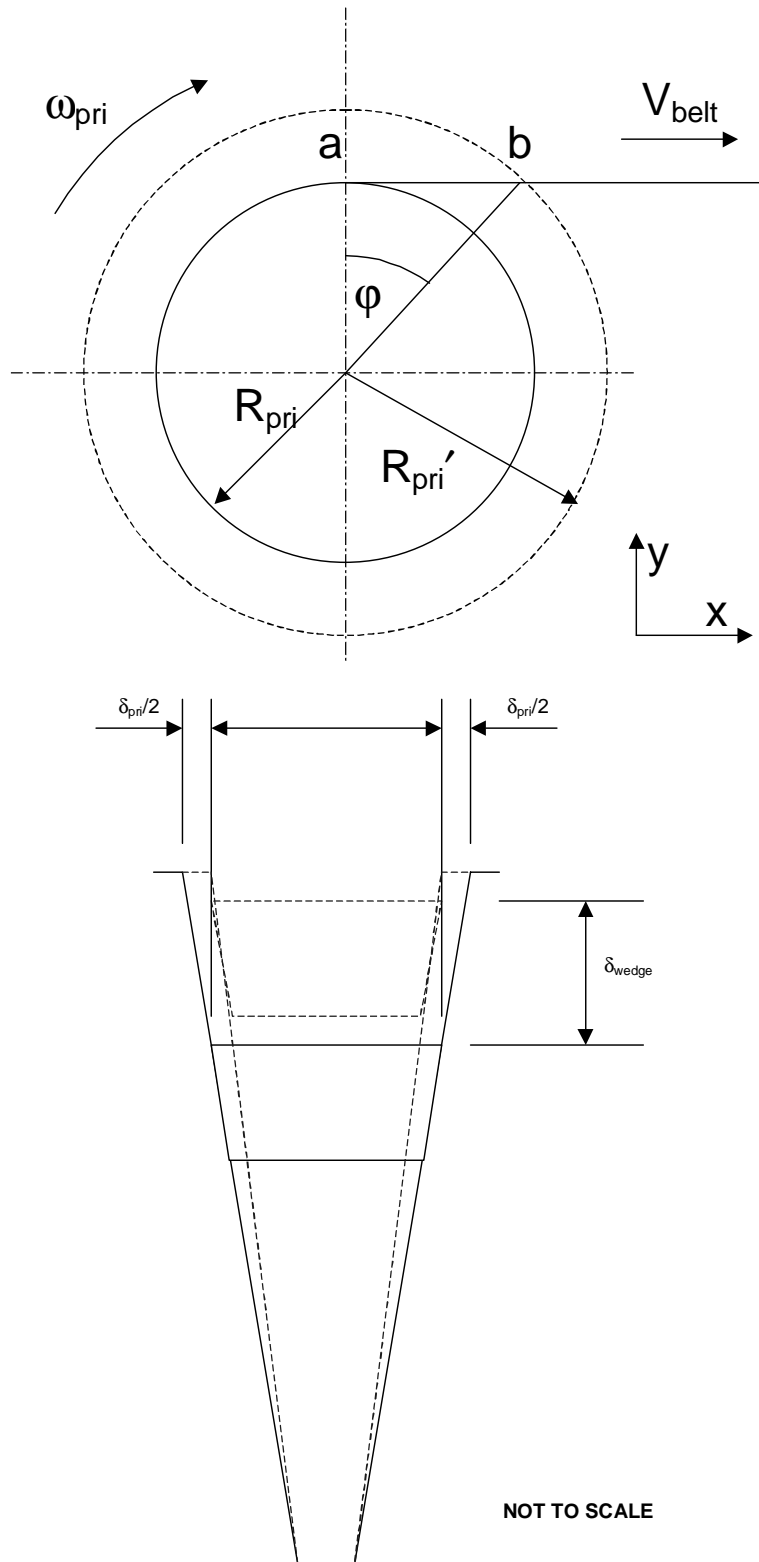
Figure 8-46 Belt Leaving Primary Pulley
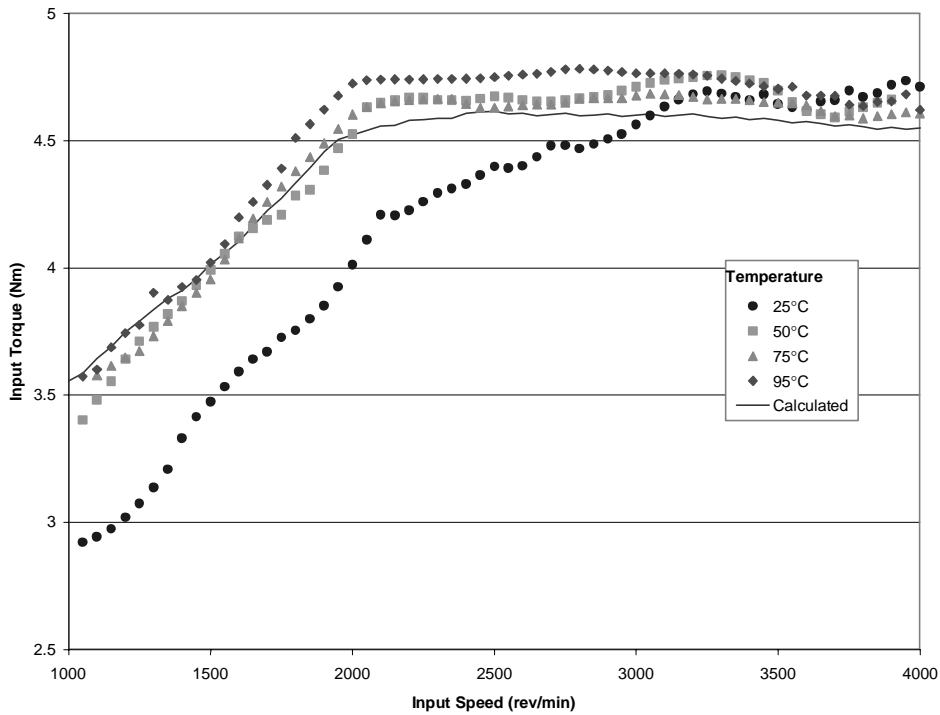
Figure 8-47 Experimental Measurements vs. Modelling Results of Belt Torque Loss in Low Ratio
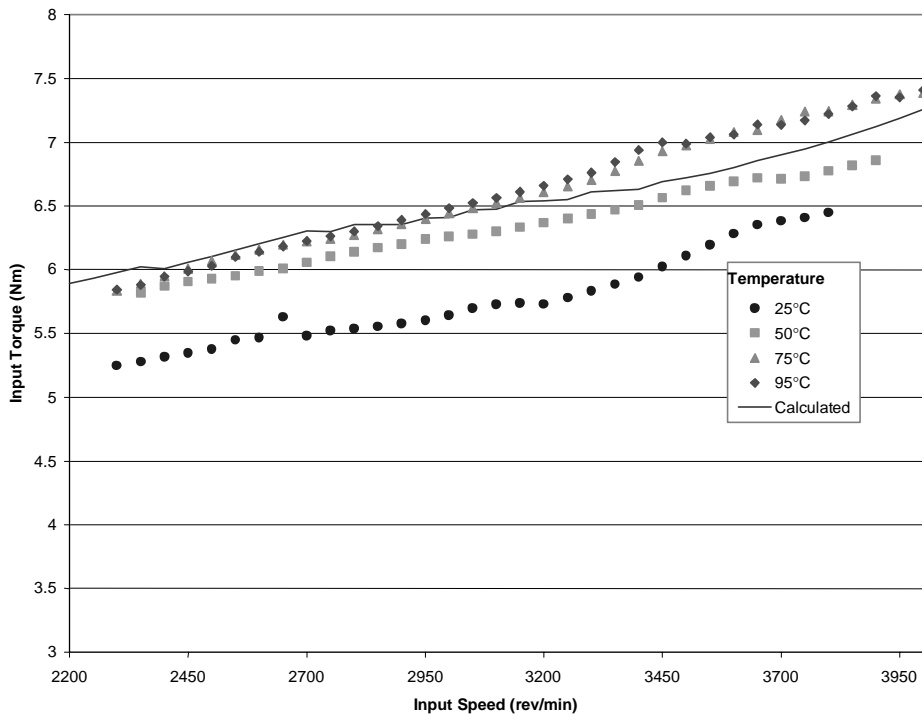
Figure 8-48 Experimental Measurements vs. Modelling Results of Belt Torque Loss in High Ratio
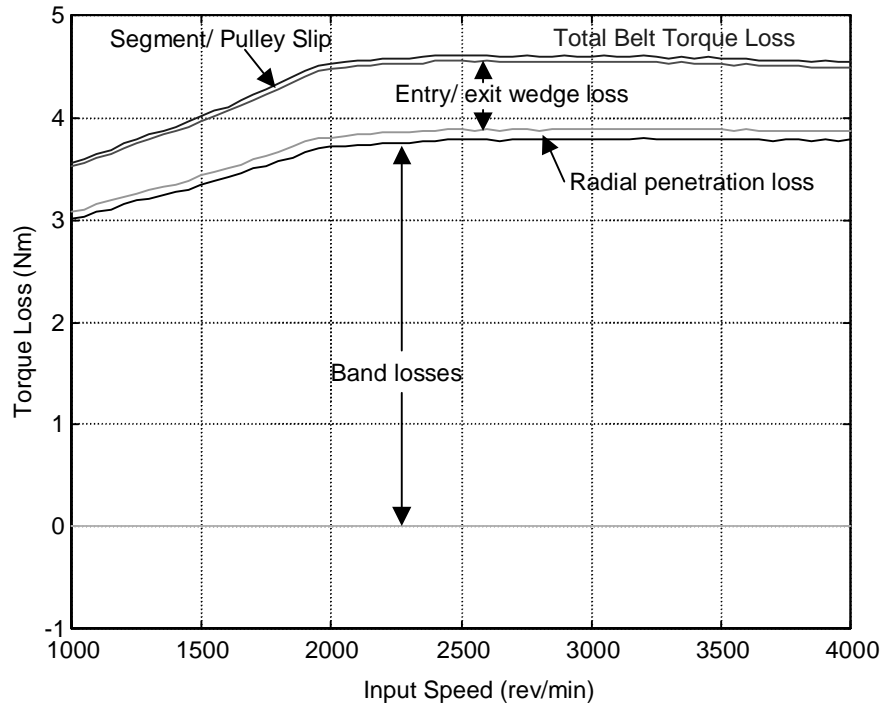
Figure 8-49 Modelled Belt Torque Loss Contributors in Low Ratio
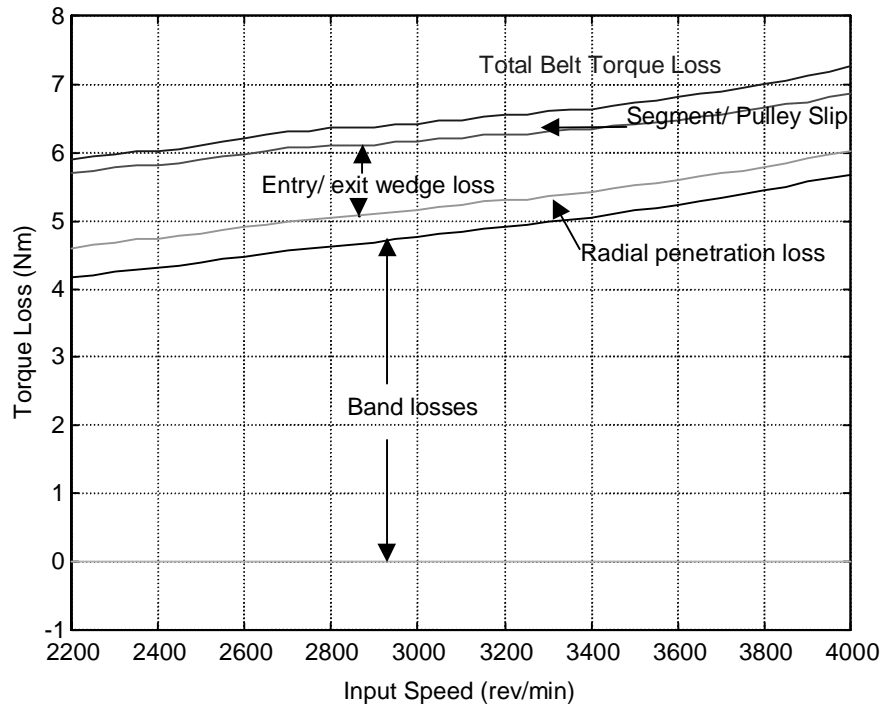
Figure 8-50 Modelled Belt Torque Toss Contributors in High Ratio
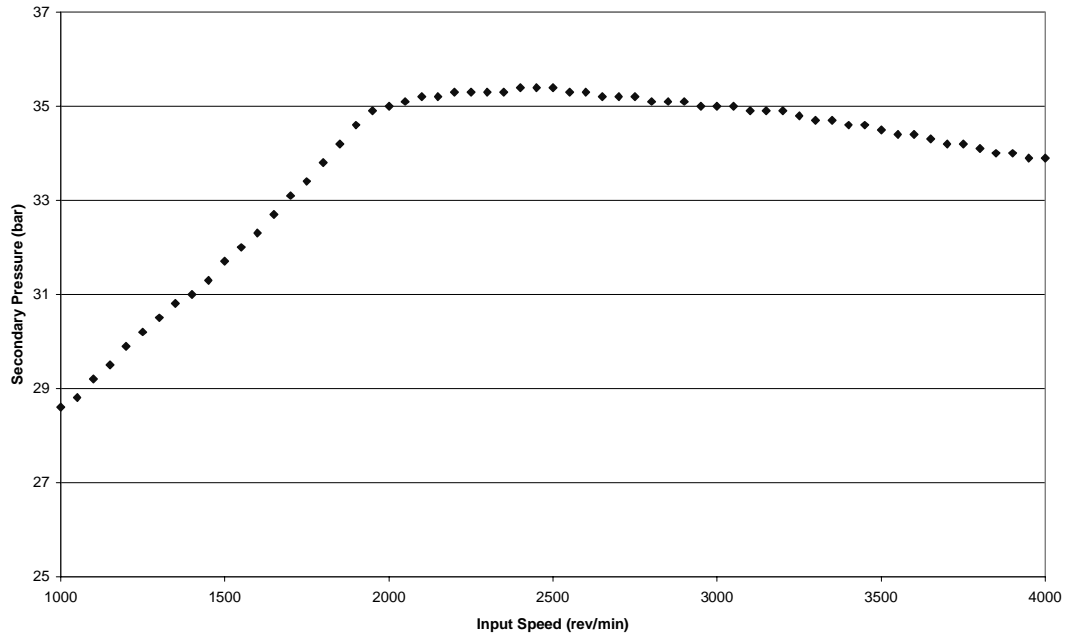
Figure 8-51 Secondary Pressure Validation Data, Low Ratio
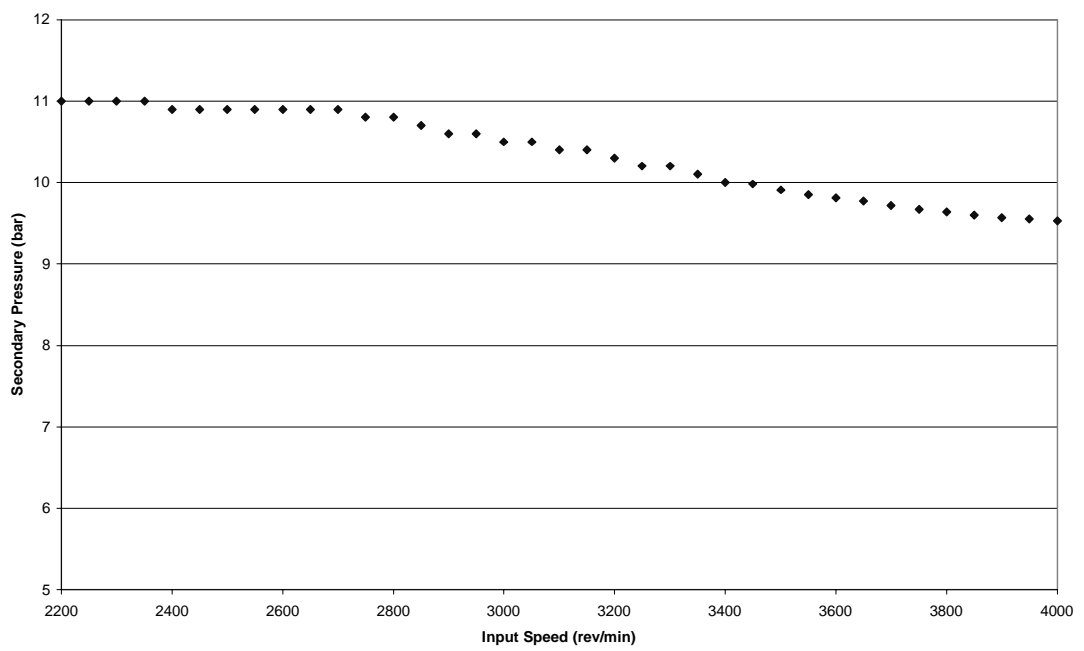
Figure 8-52 Secondary Pressure Validation Data, High Ratio

_____
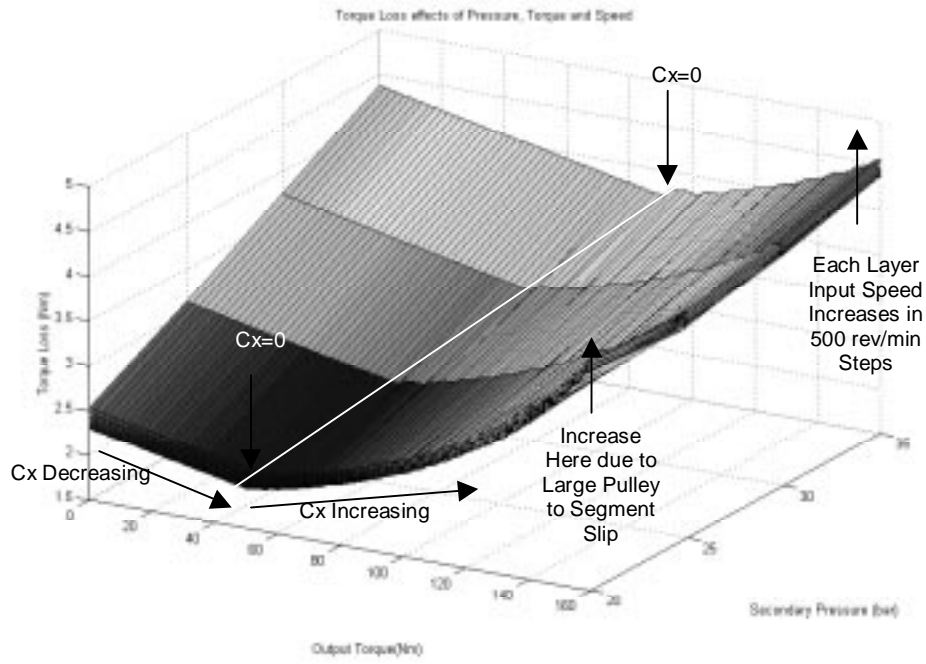
Figure 8-53 Total Belt Torque Loss Results in Low Ratio
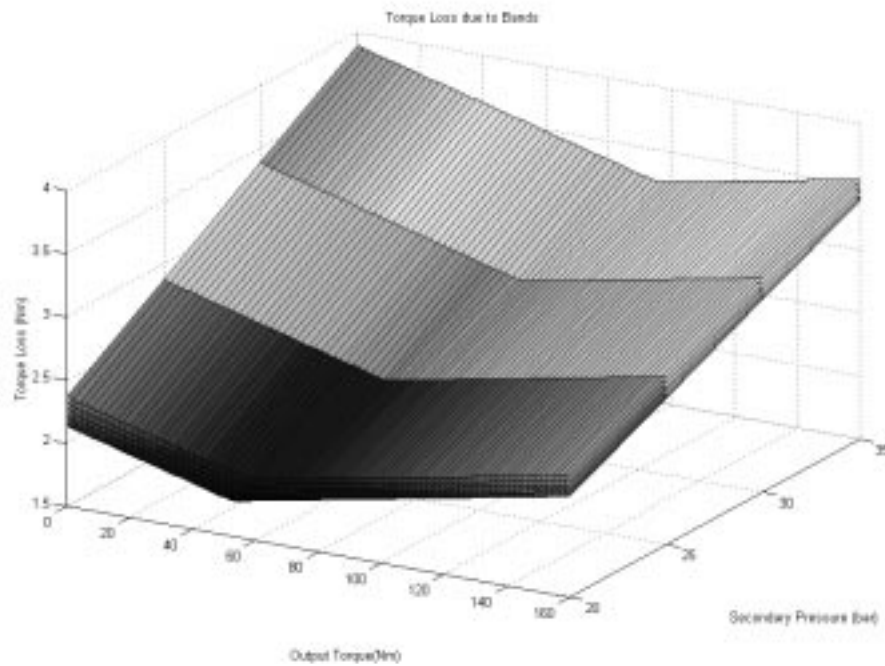
Figure 8-54 Torque Loss Results Due to Bands in Low Ratio

_____

_____
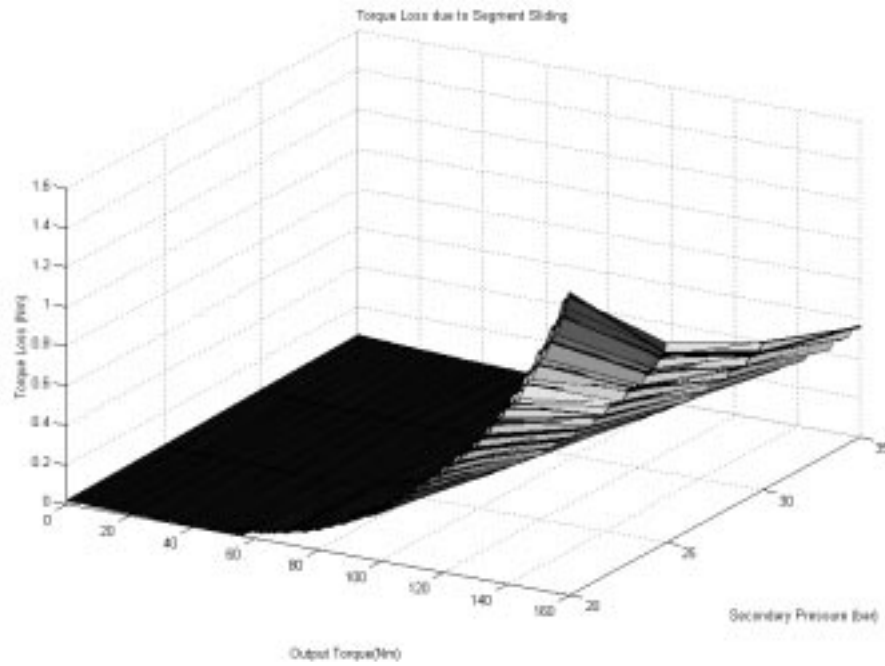
Figure 8-55 Torque Loss Results Due to Segment Slip in Low Ratio
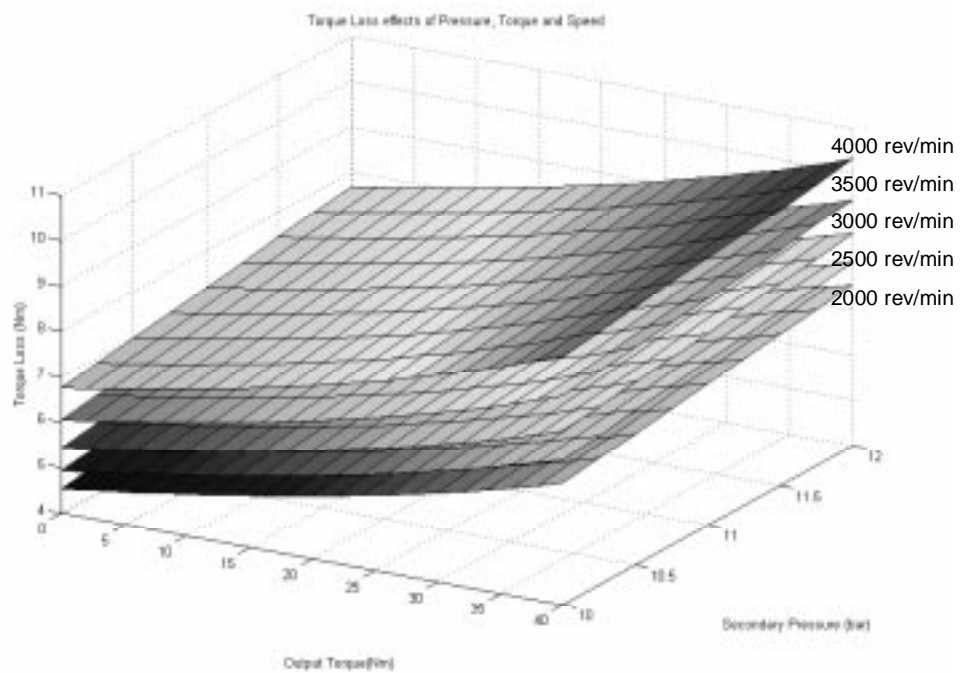
Figure 8-56 Total Belt Torque Loss Results in High Ratio

_____
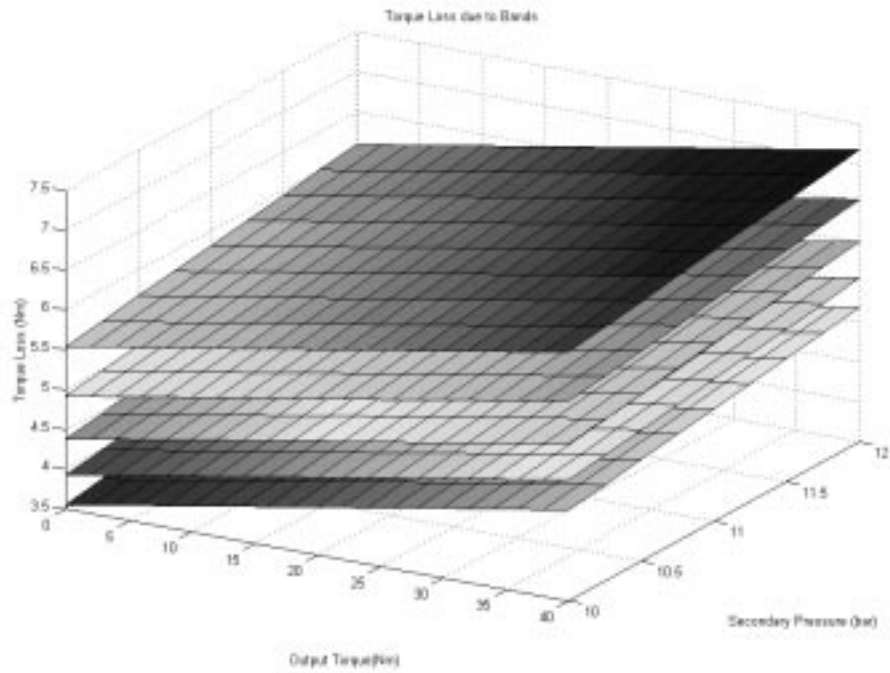
Figure 8-57 Torque Loss Results Due to Bands in High Ratio
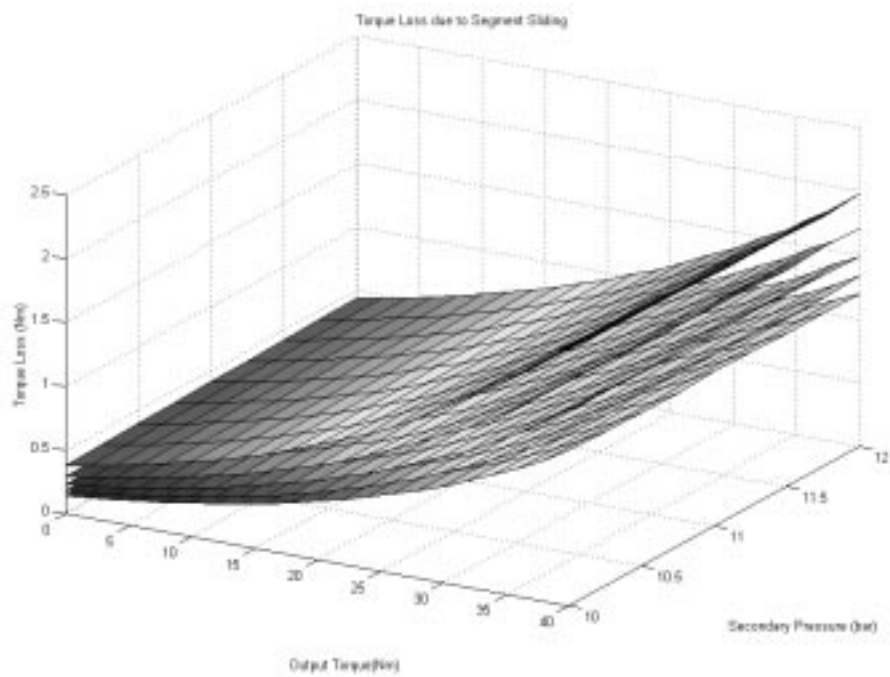
Figure 8-58 Torque Loss Results Due to Segment Sliding in High Ratio

9   Improving the Efficiency of the Belt Drive CVT

This chapter of the thesis introduces a number of proposals for improving the efficiency of the belt drive CVT. The analysis of the losses undertaken earlier in this thesis (chapters 7 & 8) have led to a number of methodologies being developed which could lead to improved efficiency of the belt drive transmission. Due to the significant magnitude of their respective losses this chapter will concentrate on the possible improvements to the losses in the hydraulic system and the belt variator itself. It is also noted that the performance of the transmission can be affected by changing the traction characteristics of the transmission lubricating fluid. However, any change in fluid traction properties has to be examined as a two-way trade-off. An increase in traction coefficient is likely to reduce belt slip, but at the same time sliding friction may be increased between the components. These lubricant property effects are however not considered in detail in this chapter, as they are considered a secondary effect to the changes discussed in the rest of this chapter.

9.1 Hydraulic System Improvements

The hydraulic pump losses were identified experimentally as a major contributor to the overall losses in the transmission (section 5.5). The losses due to the pump are either the largest loss (low ratio) or the second largest (high ratio). The primary design aim for optimising the efficiency of the hydraulic system should be the reduction of the pump flow or the system operating pressure. Both of these characteristics and the methods of achieving them interact with each other. For example system pressure could be reduced by applying larger actuators to each of the pulleys, but these actuators in turn would have a larger fill volume, due to their increased cross sectional area, requiring a larger displacement pump and hence at least some of the benefit would be lost.

One possibility of reducing the pump losses is in the design of the hydraulic pump or its operating system. This can be achieved with a system in which the hydraulic pump minimises its displacement to support the flow rates required for a given operating condition. Such systems could exist using either variable displacement hydraulic pumps or a dual pressure mode system using a dual cavity pump. Systems such as this are readily available, but often discounted by manufacturers due to increased costs.

The minimum design specification of the hydraulic system is to allow for rapid downshifts to be achieved in situations such as an emergency stop. Under these conditions the variator must reset to its lowest ratio so that a pull away can be performed when the vehicle moves off. The downshift must be completed before the vehicle wheels stop as rotational pulley motion is required to make the belt shift. A method for removing this constraint and thus down sizing the hydraulic pump is to use a clutch after the variator and before the final drive such that in stationary situations the variator is still being spun by the engine, and can thus change ratio. A system like this is used on the Honda Civic derivative of the belt drive CVT. The only restrictive design limit is the increased torque capacity required for the clutch to be moved to after the variator.

A trade-off occurs in the design of the controller that sets the clamping pressures for the transmission. There will be an optimal condition, which will maximise the efficiency of the transmission, and this will be a trade-off between pump losses, pulley deflection losses and belt slip which as discussed previously also incurs a torque loss.

The sizing of the actuator fill volume is dependent, as stated before, on the operating pressure and clamping force requirements of the system. In addition to this the fill volume is also dictated by the axial movement of the pulleys required to shift through the complete ratio range of the transmission. This in turn is dependent on the pulley wedge angle, and is discussed in more detail in section 9.2.1.

9.2 Belt Improvements

A number of changes can be envisaged to the design of the belt or pulleys that should improve the efficiency of the transmission. It should be noted however that these changes could have unforeseen effects on the performance of the belt and would require considerably more analysis than is performed here before they are implemented.

9.2.1 Reduce Pulley Wedge Angle

Reducing the pulley wedge angle has a two-fold effect on efficiency, see Figure 9-1. Firstly the change in geometry will result in a greater normal force acting on the sides of the segment for a similar clamping force. Hence the required force to support traction can be achieved with less pulley deflections, and lower clamping pressures and thus greater

_____

efficiency can be achieved. The second effect is due to the interaction of the pulley design with the hydraulic system. When the pulley angle is reduced a given radial belt displacement is achieved with a smaller axial displacement and hence less flow is required to shift the variator throughout its range. Therefore the flow capacity of the hydraulic system may be reduced. Thus reducing the pulley wedge angle can results in reducing the losses associated with the hydraulic system in terms of both flow and pressure requirements.

The change in geometry also reduces the component of pulley clamping force that acts vertically through the segment shoulders and thus the significant losses that occur at this interface will also be reduced. Similar changes to the pulley wedge angle have been discussed by Hendriks et al. **[2]**, although there is some concern over the effects of geometry changes may have on the stability of the variator mechanism in terms of a 'ratio hunting' effect. This would have to be analysed in more detail before proposing significant changes to the variator geometry.

9.2.2 Reduction of Segment Shoulder Friction

It may be possible to reduce the losses in the band pack by influencing the coefficient of friction between the shoulder of the segments and the innermost band. This could be achieved by applying a low friction coating with high wear resistance to both of the surfaces. It should however be noted that this will change the functioning of the transmission as the tension distribution effects in the band pack will be changed. This change in function is not thought to be detrimental to the overall performance of the belt. A change such as this is likely to result in torque losses such as those measured at 25°C (Figure 5-42 & Figure 5-45), where it is proposed a hydrodynamic oil film forms, reducing the friction between the bands and segments. Using the surface treatment method proposed these events would of course occur without the increased viscous losses occurring in the other components of the transmission at 25°C.

9.2.3 Reduce Band Pack Relative Velocity

The sliding velocity between the innermost band of the band pack and the segment shoulders may be reduced by decreasing the radial offset of the band pack from the rocking edge of the segments. This could be achieved by a radical redesign of the

_____

_____

segment such as that shown in Figure 9-2 below. Chapter 8 indicated that the most significant loss in the belt is due to the sliding losses between the individual bands and between the innermost band and the segment shoulder. The most significant of these is the latter, since it the most highly loaded of the contacts and the contact with the largest sliding speed, making up approximately 80-90% of the band losses. The proposal outlined below will reduce this loss significantly, although the losses between the individual bands will remain similar to the levels of the original design, since the thickness and number of bands has not been changed.

Figure 9-3 shows simulation results for the proposed modifications to the segment, for a range of band to rocking edge radial offsets and for both low and high ratio. Figure 9-3(a) shows the results for a standard segment with 3 mm offset between the rocking edge of the segment and the band shoulders in low ratio. While model results for reduced offsets of 2 and 1 mm are shown in Figure 9-3(b) and Figure 9-3(c) respectively. A similar set of results for high ratio conditions are shown in Figure 9-3(d) to Figure 9-3(f). All the results show each of the individual modelled loss mechanisms, as shown in Figure 8-49 & Figure 8-50. The total torque loss is the blue line and the band losses the black line, as marked in Figure 9-3(a). All the other losses should remain constant. The effect of the proposed segment modification is significant, in low ratio band losses reduce from ~3.75 Nm (standard) to ~2.75 Nm (2 mm offset) and 2.0 Nm (1 mm offset). Similarly in high ratio losses reduce from ~5.75 Nm to ~4.25 Nm (2 mm offset) and 3.5 Nm (1 mm offset). It was noted that reducing the radial offset of the bands much beyond 1 mm had minimal effect on the belt losses. It was also considered sensible to maintain some offset so that the primary purpose of the bands (to prevent buckling of the compressed belt) is not compromised.

Significantly this system will not alter the forces acting between the components, but simply reduce the power losses. Therefore the belt as a whole will still function in a similar manner to that achieved with the original segment design. A number of other parameter variations were performed, including changing band numbers and band thickness to maintain the same cross sectional area, although these were found to have no significant benefit. Reducing the overall band cross sectional area also had a minimal effects although this also compromised the belt slip behaviour by allowing larger gaps to develop.

_____

9.2.4 Pulley Stiffness

Improving the overall pulley stiffness will reduce both the pulley wedging losses and pulley penetration losses described in chapter 8. A significant reduction in the global movement of the pulley halves will result in these losses becoming minimal and associated only with the very small elastic deflections of the pulley and belt structures.

The stiffness of the pulley structure has to be considered in three key areas; namely pulley elastic stiffness, bearing/mounting stiffness, and the stiffness of the axially moveable pulley half relative to the pulley shaft. It should be noted however that significant changes in this area could result in a weight penalty, more significant than the deflection losses.

_____

Force Distributions   **Segment Geometry**

NOT TO SCALE
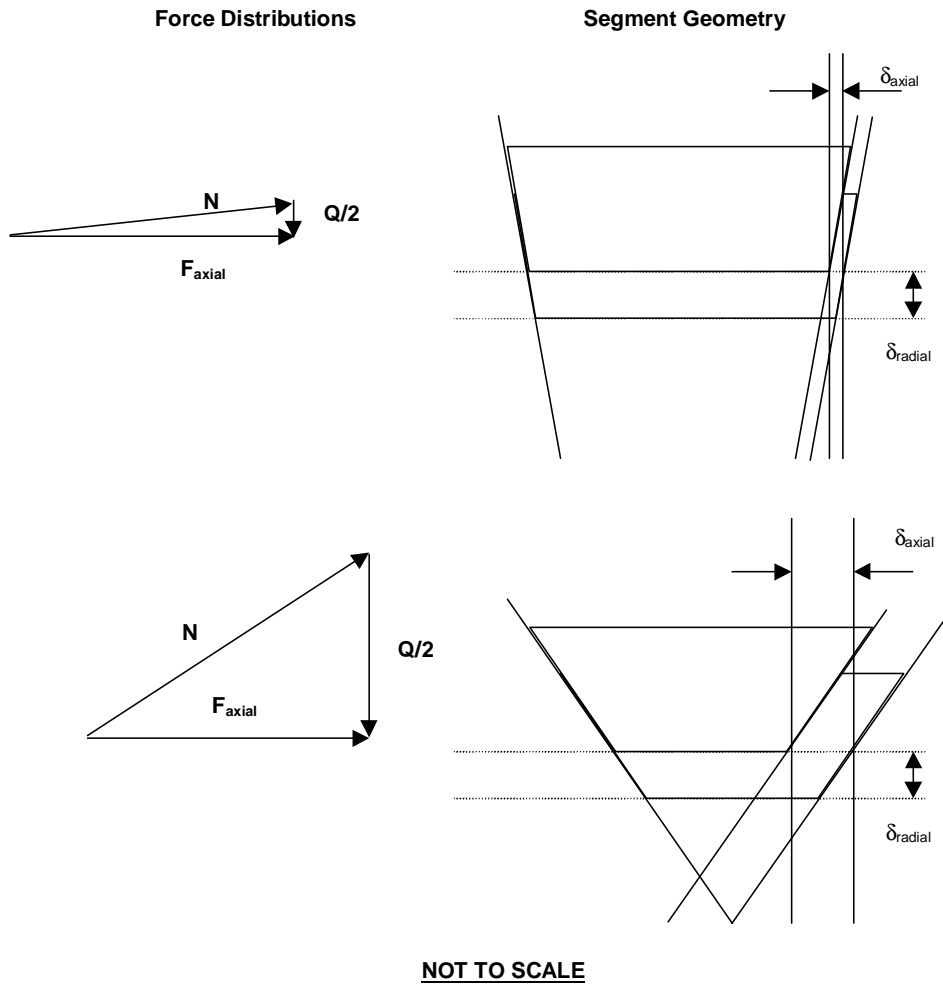
Figure 9-1 Effect of Changing Pulley Wedge Angle Geometry

NOT TO SCALE
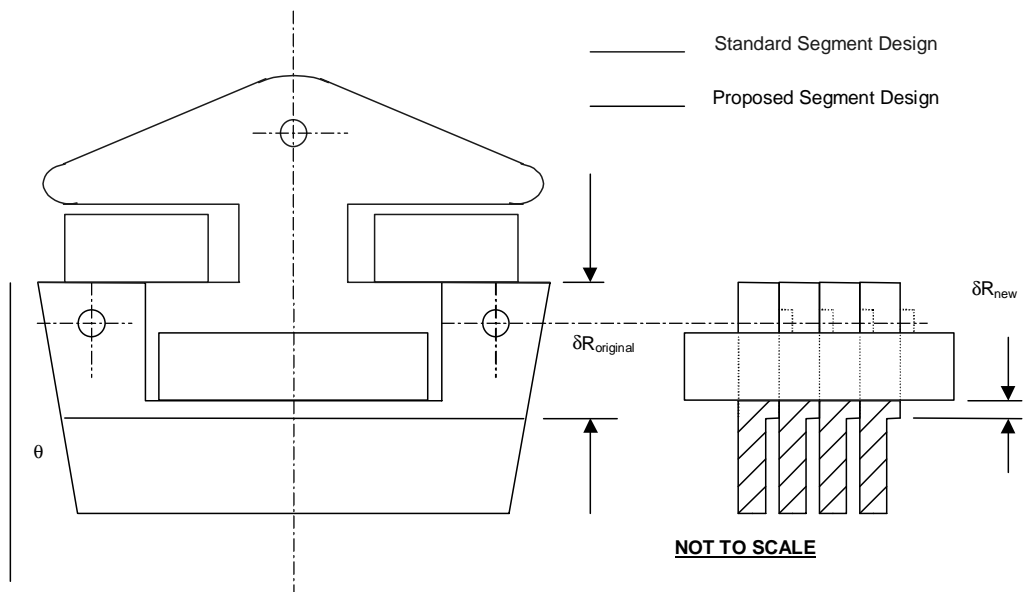
Figure 9-2 New Segment Design for Reduced Sliding Between Inner Band and Segment Shoulder

_____

_____
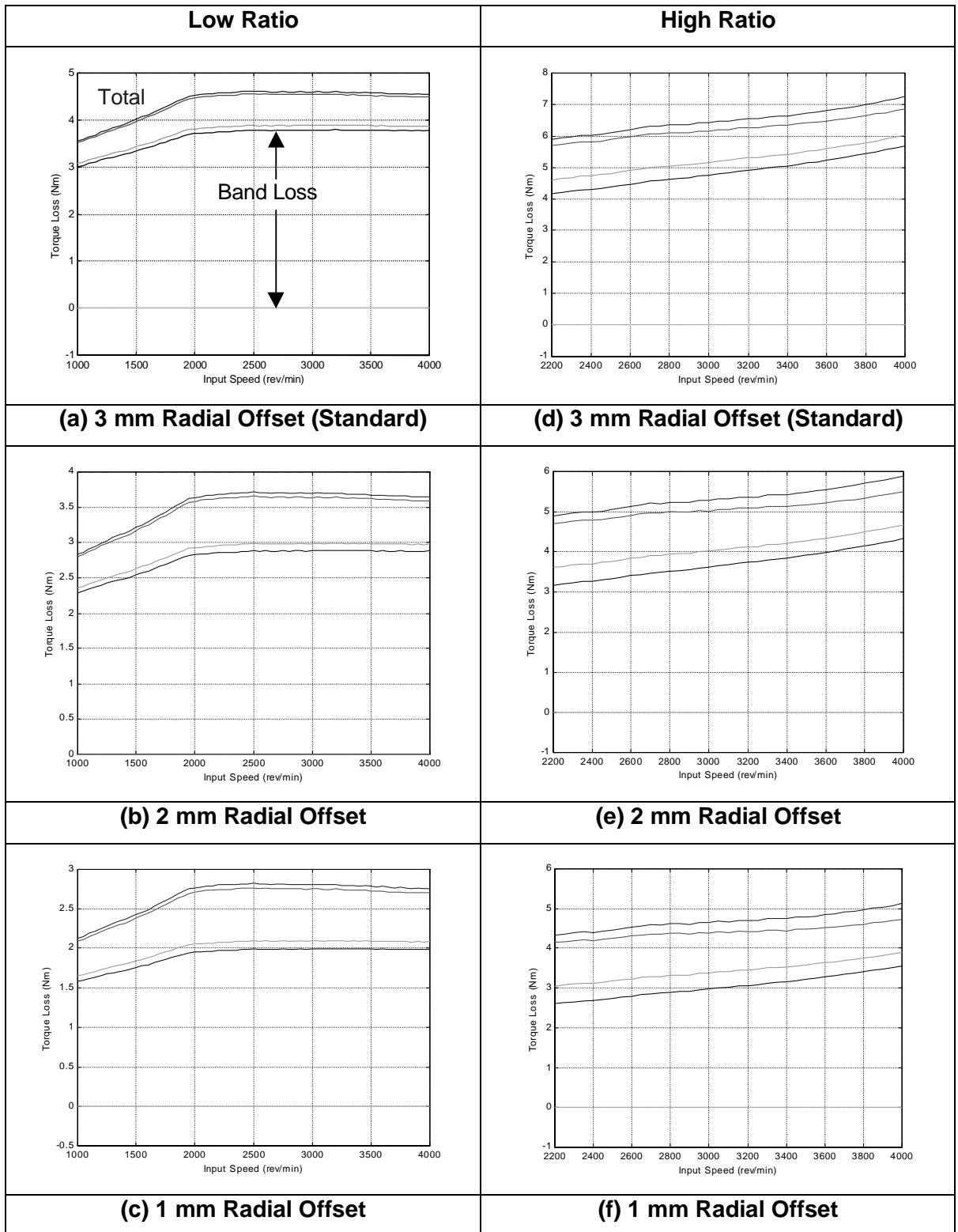
Figure 9-3 Effect of Reducing Segment Shoulder to Rocking Edge Distance

_____

_____

10 Conclusions

This chapter of the thesis represents a brief summary of all the experimental results and finding from this research. It highlights specific areas where this work has contributed new ideas to the modelling and understanding of how the pushing metal V-belt functions.

Initial testing of a CVT equipped vehicle was performed on a chassis dynamometer facility indicating poor efficiency of the belt drive CVT when compared to a manual transmission. Experimental data from the chassis dynamometer also indicated very slow warm up periods for the belt drive CVT. This testing also indicated poor performance of the CVT equipped vehicle under low load urban manoeuvres, where the parasitic losses are high. However during the high speed sections of the drive cycle the efficiency of the transmission was improved over the manual transmission due to the increased ratio range of the CVT.

Two test rigs were developed specifically to measure low load torque losses through the transmission and belt slip losses through the belt variator at higher torque levels. Accurate experimental measurements of torque losses throughout the belt drive CVT were performed at a range of lubricant temperature conditions. In particular these measurements concentrated on isolating the torque loss associated with each component within the transmission. Detailed loss measurements associated with the belt variator were acquired, indicating significant changes in losses occurring in the belt at different lubricant temperatures. Belt slip in the variator was also measured experimentally, with a high degree of accuracy that allowed the slip speed terms at both the primary pulley and secondary pulley to be isolated. The belt slip work was novel in that it identified a ratio drift phenomenon not previously identified and isolated the slip occurring on each pulley.

The speed of the bands relative to the segments and to neighbouring bands was derived by measuring the relative displacements of each of the bands to a specific segment over a number of belt revolutions. Suspected deflections of the belt pulleys were also measured using simple dial gauge arrangements to measure deflections at different angular positions and on each of the pulley halves.

Mathematical modelling was performed to describe the torque loss mechanisms within the belt drive. The model was based upon a number of sub models predicting losses between bands and at the band to segment interface. Two further loss models were developed to

_____

_____

describe losses as the segments travel around the pulley contact arc. These losses were due to the measured pulley deflections causing the segments to contact the pulley past ideal exit and entry points (wedge loss) and to penetrate further into the pulley than the ideal radius of the belt (penetration loss). The wedge loss is similar to an earlier empirical model (Micklem [12]) although the addition of pulley deflection information and re-modelling has added significantly to its validity.

The main torque loss event is proposed to occur between the bands and segment and in between individual bands. A novel model of band velocity was adopted based upon the bands adopting the mean speed of both pulleys. The belt displacement results validated this assumption. Equations were then developed to describe the total normal force acting through the bands around a complete wrap angle, and to describe the base tension in the band packs. The motion between the bands under the action of these forces was then proposed to cause the tension differences in the bands that had been observed by others (Fujii et al. [22]). These tension distributions were validated by both the torque losses that they caused and by their interaction with the belt slip model, which was developed simultaneously.

Further mathematical modelling was performed to describe the belt slip measurements at both the primary and secondary pulleys. These models were based upon the theory of gap closure, originally proposed by Kobayashi et al. [9], although they were expanded significantly to take account of the many varied loading conditions which occur about each of the contact arcs. The belt slip that occurs also incurs a torque loss effect due to the sliding over the pulley surfaces. Both mathematical models were validated using the previously collected experimental data. A good degree of accuracy between experimental and theoretical results was achieved. Improved confidence in the individual models was gained by the considerable interactions occurring between all the models.

Based upon the models, a number of proposals were introduced to improve the efficiency of the metal V-belt CVT based upon the findings of the experimental and theoretical analyses. In particular it was proposed that a reduction in the height of the bands relative to the segment rocking edge would result in a significant reduction in the losses of the variator without any detrimental effect on its function.

_____

_____

11 Proposed Further Work

This chapter introduces some proposals for future work to expand on that already performed during this investigation. While a considerable amount of the work here has been validated, some of the models are still semi-empirical and there are a number of avenues of future work which could improve the quality of some models and/ or generate a greater range of validation conditions.

These areas for proposed future work are:

1. Investigate in more detail and at other intermediate ratio conditions both slip and torque losses simultaneously on the variator only rig as described in chapter 6 of this thesis, but using improved torque loss measurement equipment similar to that used on the original transmission test rig (chapter 4).

2. Fluid testing, using one non-ATF based product with a predictable low coefficient of friction and one high traction fluid such as Santotrac 50, to increase validation data at the extreme conditions of friction likely to be seen between components.

3. More detailed modelling and validation of proposed hydrodynamic lubrication between bands (section 8.4.5) and new belt models for the lower temperature operating conditions (typically 25°C). The fluid testing proposed above could provide useful validation material by adopting test fluids with higher viscosities tests could be performed at standard temperatures rather than requiring low temperature test facilities.

4. FEA modelling of pulley and segment and band deflections similar to that described by Shimizu et al. **[31]**. However, this is likely to be highly individual to the build of each transmission and in no way a generic solution to the prediction of deflection losses for all belt drives.

5. More detailed modelling and testing of the proposed segment redesign (section 9.2.3) to ascertain more accurately any likely improvements in efficiency.

_____

12 References

1. **Lubomyr O. H.,** "Automotive Traction Drive CVTs – An Overview", *SAE Paper 861355, SAE Passenger Car Meeting & Exposition. (conference code 09031), Dearborn, MI, USA, 1986*

2. **Hendriks E., ter Heegde P., van Prooijen T.,** "Aspects of a metal Pushing V-Belt for Automotive CVT Application", *SAE Paper 881734, presented at the SAE passenger Car Meeting and Exposition, Dearborn, Michigan, Nov 1988*

3. **Hendriks E.,** "Qualitative and Quantitative Influence of a Fully Electronically Controlled CVT on Fuel Economy and Vehicle Performance", *SAE Transactions 1993 Paper 930668*

4. **Simner D.,** "The Contribution of Transmissions to Vehicle Fuel Economy", *presented at IMechE AUTOTECH 95 conference, C498/34/135*

5. **Brace C. J.,** "Transient Modelling of a DI TCi Diesel Engine", *University of Bath, School of Mech. Eng. PhD. Thesis 1996*

6. **Rover Group,** "Autocourse 92, Continuously Variable Transmissions", *Bulletin 4-C592 Rover Product Update*

7. **Ide T.,** "Effect of Power Losses of Metal V-belt CVT Components on the Fuel Economy", *Int. Congress on Continuously Variable Power Transmission CVT'99. Eindhoven, September 16-17, 1999, pp. 93-98*

8. **Abo K., Hideaki T.,** "Heat Generation of a Metal V-belt for CVTs", *Int. Congress on Continuously Variable Power Transmission CVT'99. Eindhoven, September 16-17, 1999, pp. 148-152*

9. **Kobayashi D., Mabuchi Y., Katoh Y.,** "A Study of the Torque Capacity of a Metal Pushing V-Belt for CVTs" *SAE Paper, 980822, 1998*

10. **Gerbert G.,** "Metal V-belt mechanics", *ASME paper 84-DET-227, presented at .Design Engineering Technology Conference. (conference code 05902). 1984*

11. **Becker H. J.,** "Mechanik des Van Doorne CVT- Schubgliederbandes", *Antiebstechnik 26, 1987, No. 8, pp. 47-52*

12. **Micklem J. D., Longmore D. K., Burrows C. R.,** "Modelling of the Steel Pushing V-belt Continuously Variable Transmission", *Proceedings Inst. Mech. Engineers Vol. 208 Part C: pp. 13-27*

13. **Micklem J. D., Longmore D. K., Burrows C. R.,** "Belt Torque Losses in a Steel V-belt Continuously Variable Transmission", *Proceedings Inst. Mech. Engineers Vol. 208 Part D: pp. 91-97*

14. **Micklem J. D., Longmore D. K., Burrows C. R.,** "The Magnitude of the Losses in the Steel Pushing V-belt Continuously Variable Transmission", *Part D: Journal of Automobile Engineers, IMechE 1996, Vol. 210, pp. 57-62*

15. **Guebeli M.,** "Optimum Efficiency Control of the CTX Powertrain", *University of Bath, School of Mech. Eng. PhD. Thesis 1993*

16. **Guebeli M., Micklem J. D., Burrows C. R.,** "Maximum Transmission Efficiency of a Steel Belt Continuously Variable Transmission", *DE-Vol.43-1, International Power Transmission and Gearing Conference – Volume 1 ASME 1992, pp. 329-334*

17. **Vaughan N. D., Guebeli M., Burrows C. R.,** "Fuel Economy Benefits with Effective Powertrain Control", *C481/023/94 IMechE 1994*

18. **Liebrand N. J.,** "Future developments in push belts for CVT applications", *SAE Paper 925063, 1992*

19. **Asayama H., Kawai J., Tonohata A., Adachi M.,** "Mechanism of metal pushing belt", *JSAE Review, volume 16, (1995), pp. 137-143*

20. **Karam A., Play D.,** "A Discrete Analysis of Metal V-Belt Drive", *ASME 1992, International Power Transmission and Gearing Conference DE- Vol. 43-1, pp. 319-327*

21. **Fujii T., Kurokawa T., Kanehara S.,** "A Study of a Metal Pushing V-Belt type CVT, Part 1: Relationship between Transmitted Torque and Pulley Thrust", *SAE Transactions 1993, Paper 930666, pp. 989-999*

22. **Fujii T., Kurokawa T., Kanehara S.,** "A study of a Metal Pushing V-Belt Type CVT-Part 2: Compression Force Between Metal Blocks and Ring Tension", *SAE Transactions 1993, Paper 930667, pp. 1000-1009*

23. **Kanehara S., Fujii T., Kitagawa T., ,** "A study of a Metal Pushing V-Belt Type CVT-(Part 3: What Forces Act on Metal Blocks?", *SAE Transactions 1994, Paper 940735, pp. 942-952*

24. **Kitagawa T., Fujii T., Kanehara S.,** "A study of a Metal Pushing V-Belt Type CVT-(Part 4: Forces Act on Metal Blocks when the Speed Ratio is Changing", *SAE Transactions 1995, Paper 950671, pp. 1344-1353*

25. **Kuwabara S., Fujii T., Kanehara S.,** "Power Transmitting Mechanism of CVT Using a Metal V-Belt and Load Distribution in the Steel Ring" *SAE Paper, 980824*

26. **Kim H., Lee J.,** "Analysis of Belt Behaviour and Slip Characteristics for a Metal V-Belt CVT", *Mechanism & Machine Theory, Vol. 29, No. 6, pp. 865-876, 1994*

27. **Lee H., Kim H.,** "Analysis of Primary and Secondary Thrust for a metal CVT Part 1: New Formula for Speed Ratio-Torque-Thrust Relationship Considering Band Tension and Block Compression" *SAE Paper, 2000-01-0841, SAE special publication (SP-1522), transmission and driveline synposium 2000, pp. 117-125*

28. **Sato T., Kato T.,** "A study of the Torque-transmitting Mechanism in the Steel Pushing V-belt CVT", *Int. Congress on Continuously Variable Power Transmission CVT'99. Eindhoven, September 16-17, 1999, pp. 52-57*

29. **Kanehara S., Fujii T., Oono S.,** "A study on a Metal Pushing V-Belt Type CVT Macroscopic Consideration for Coefficients of Friction between Belt and Pulley", *SAE Transactions Paper 9636277, International Conference on Continuously Variable Transmissions, CVT'96, Yokohama National University, Yokohama, Japan, September 11-12, 1996, pp. 15-22*

_____

30. **Fujimura O., Okubo K., Fujii T., Kanehara S.,** "Shifting Mechanism and Variation of Frictional Coefficients for CVT using Metal Pushing V-Belts", *SAE Paper 2000-01-0840, SAE special publication (SP-1522), transmission and driveline synposium 2000, pp. 107-116*

31. **Shimizu H., Kobayashi D., Kawashima J., Kato Y.,** "Development of 3-D Simulation for Analyzing the Dynamic Behavior of a Metal Pushing V-Belt for CVTs", *SAE Paper, 2000-01-0828, SAE special publication (SP-1522), transmission and driveline synposium 2000, pp. 31-36*

32. **Robertson A.J., Tawi K.B.,** "Misalignment equation for the Van Doorne metal pushing V-belt continuously variable transmission", *Proc. IMechE Vol. 211 Part D, 1997* pp. 121-128

33. **Sorge F.,** "Influence of Pulley Bending on Metal V-Belt Mechanics", *SAE Paper 9636268, International Conference on Continuously Variable Transmissions, CVT'96, Yokohama National University, Yokohama, Japan, September 11-12, 1996, pp. 9-14*

34. **Sattler H.,** "Efficiency of a Metal Chain and V-belt CVT", *Int. Congress on Continuously Variable Power Transmission CVT'99. Eindhoven, September 16-17, 1999, pp. 99-104*

35. **Gerbert G.,** "Skew V-belt pulleys", *SAE Paper 9636259 International Conference on Continuously Variable Transmissions, CVT'96, Yokohama National University, Yokohama, Japan, September 11-12, 1996.*

36. **Gerbert G.,** "Traction Belt Mechanics", *Machine and Vehicle Design Chalmers University of Technology, 1999, ISBN 91-630-7885-6*

37. **Park D. H., Seo T. S., Lim D. G., Cho H. B.,** "Theoretical Investigation on Automatic Transmission Efficiency", *SAE Paper 960426, 1996*

38. **Kluger M. A., Greebaum J. J.,** "Automatic Transmission Efficiency Characteristics and Gearbox Torque Loss Data Regression Techniques" *SAE Paper, 930907, 1993*

39. **van Dongen L. A. M.,** "Efficiency Characteristics of Manual and Automatic Passenger Car Transaxles", *SAE Paper 820741, 1982*

40. **Roulet B., Briec A.,** "Modelling of Power Losses in Mechanical Gearbox", *E.A.E.C The European Automotive Industry meets the Challenge of the Year 2000. Paper SIA9506A19*

41. **Tuplin W. A.,** "Gear Design", *The Machinery Publishing Co. Ltd.*

42. **Buckingham E.,** "Analytical Mechanics of Gears", *Dover Publications Inc. ISBN 486-61073-X*

43. **Fewkes R., Gunsing J., Sumiejski J. L.,** "Lubricant as a Construction Element in the VDT Push-Belt CVT System", *SAE Paper 932848, 1993*

44. **Ishikawa T., Murakami Y., Yauchibara R., Sano A.,** "The Effect of Belt-Drive CVT Fluid on the Friction Coefficient Between Metal Components", *SAE Special Publication, Paper 972921, Conference Code 47262, pp. 11-18.*

45. **Ichihashi T., Deshimaru J., Yamaguchi Y.,** "Performance of Lubricants for new generation V-Belt CVTs", *Int. Congress on Continuously Variable Power Transmission CVT'99. Eindhoven, September 16-17, 1999, pp. 178-183*

46. **Peiffer R., Kraneburg P.,** "Functionality of New CVTs – the Fluid Question", *Int. Congress on Continuously Variable Power Transmission CVT'99. Eindhoven, September 16-17, 1999, pp. 172-176*

47. **Watts R. F., Richards K. M.,** "Development of High Performance Lubricants for Non-traction CVTs", *Int. Congress on Continuously Variable Power Transmission CVT'99. Eindhoven, September 16-17, 1999, pp. 184-189*

48. **Chan C.,** "Parasitic Losses in Belt Drive Continuously Variable Transmissions", *University of Bath Final Year Project Report ME6/96*

49. **Valenta R.,** "Parasitic Losses in Belt Drive Continuously Variable Transmissions", *University of Bath Final Year Project Report ME6/96*

50. **SKF Catalogue**

51. **Esso,** "Esso CVT Fluid Product Data Sheet", *Esso Report No. r33/91/500*

52. **Bishop J. S.,** "Proposed Efficiency Rating for an Optimised Automatic Transmission", *Southwest Research Institute Paper, 96MJA042, 1996*

53. **Kluger M. A., Fussner D. R., Roethler R.,** "A Performance Comparison of Various Automatic Transmission Pumping Systems" *Southwest Research Institute Paper, 96MJA041, 1996*

54. **McCandlish D., Dorey R.,** "Steady State Losses in Hydrostatic Pumps and Motors", *6th International Fluid Power Symposium, Apr. 8-10 1981, paper C3, pp. 133-144*

55. **Harris T. A.,** "Roller Bearing Analysis", *John Wiley & Sons, Inc.*

56. **Palmgren A.,** "Ball and Roller Bearing Engineering"

57. **Fish R. L.,** "Using the SAE #2 Machine to Evaluate Wet Clutch Drag Losses", *SAE Transactions 1991 Paper 910803, volume 100, Sect 6, (1991), pp. 1041-1054*

58. **Lloyd F. A.,** "Parameters Contributing to Power Loss in Disengaged Wet Clutches", *SAE Paper 740676, 1974*

59. **Vahabzadeh H., Linzell S. M.,** "Modelling, Simulation, and Control Implementation for a Split Torque, Geared Neutral, Infinitely Variable Transmission", *SAE Paper 910409, SAE Transactions, volume 100, Sect 6, (1991), pp. 546-557*

APPENDIX A

RESULTS OF TRANSMISSION WARM UP EXPERIMENTS OVER COMBINED ECE15 + EUDC DRIVE CYCLE TESTING

This appendix contains a complete set of the transmission warm up data collected during the chassis dynamometer test program discussed in chapter 3 of this thesis. Results presented give transmission sump temperature, engine sump temperature and the oil temperatures to and from the transmission cooler. Test results are produced at –10, 0, 10, 25 and 40°C for both soak and warm conditions. The temperatures are plotted against test time along side a trace of the vehicle speed during the cycle.
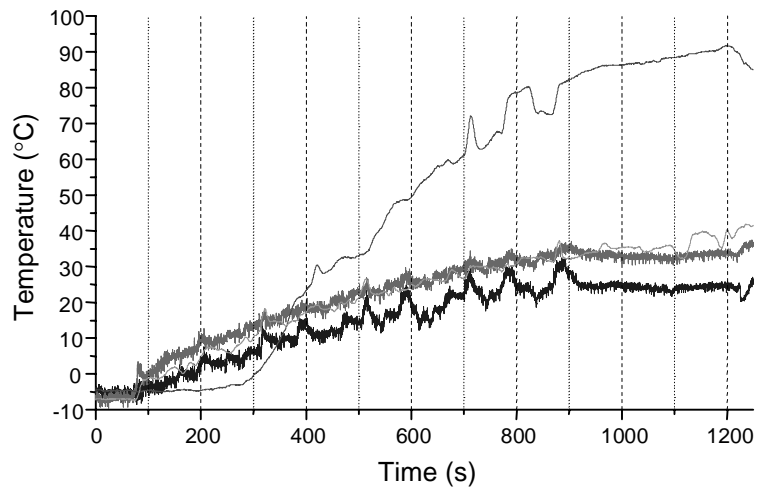
Figure A-1 Soak Test at –10°C Ambient
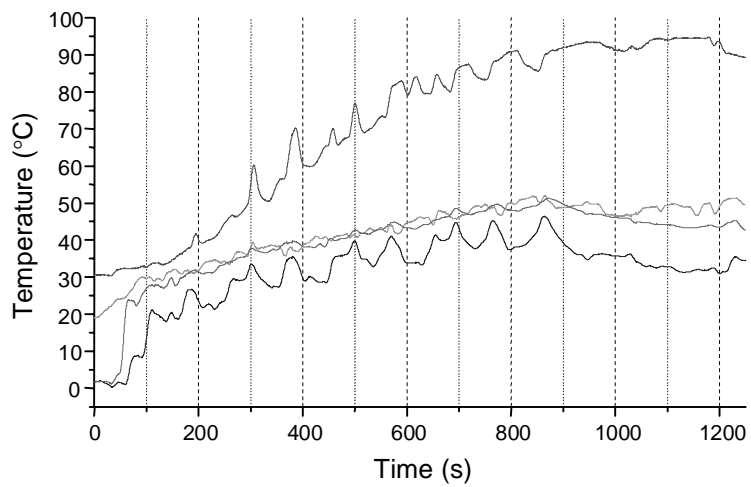
Figure A-2 Warm Test –10°C Ambient
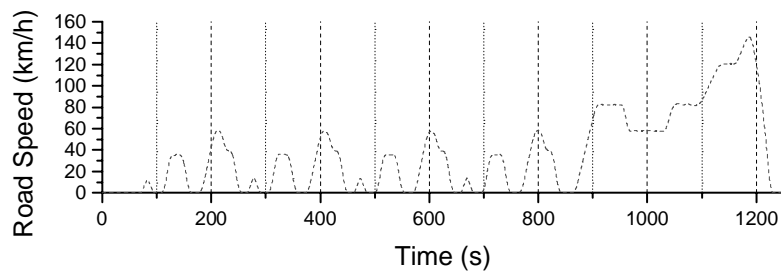
——Engine Sump ——CVT Sump ——To Cooler ——From Cooler

_____
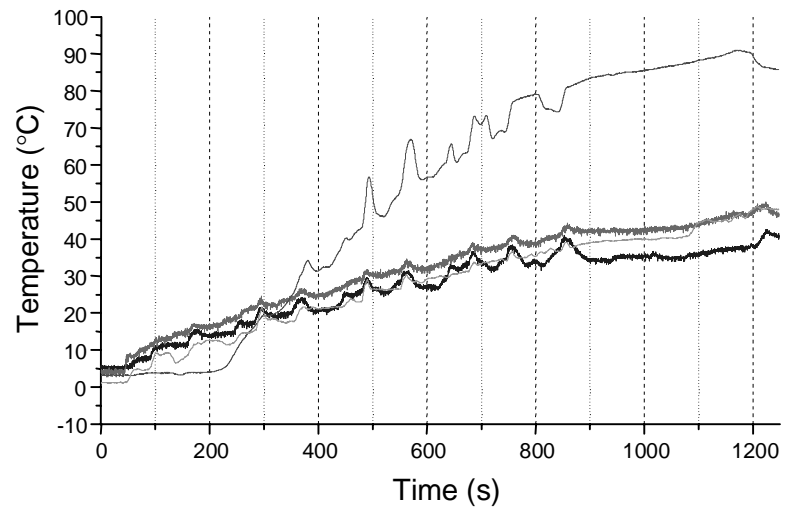
Figure A-3 Soak Test at 0°C Ambient
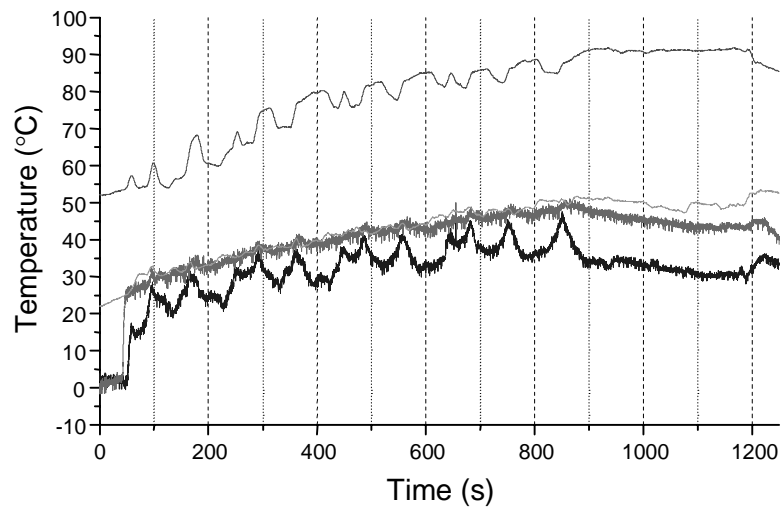
Figure A-4 Warm Test 0°C Ambient
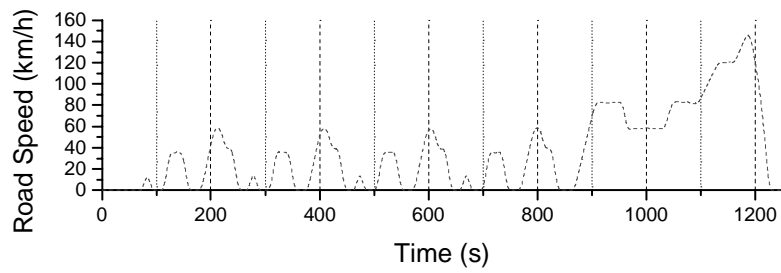
——Engine Sump ——CVT Sump ——To Cooler ——From Cooler

_____
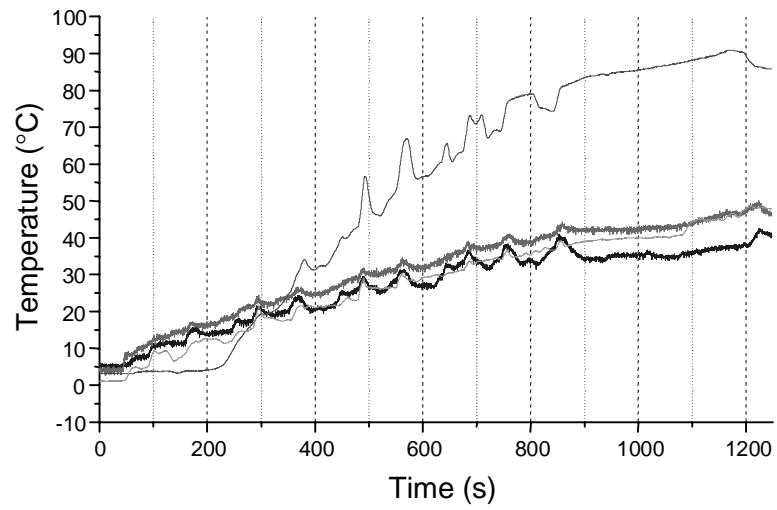
Figure A-5 Soak Test at 10°C Ambient
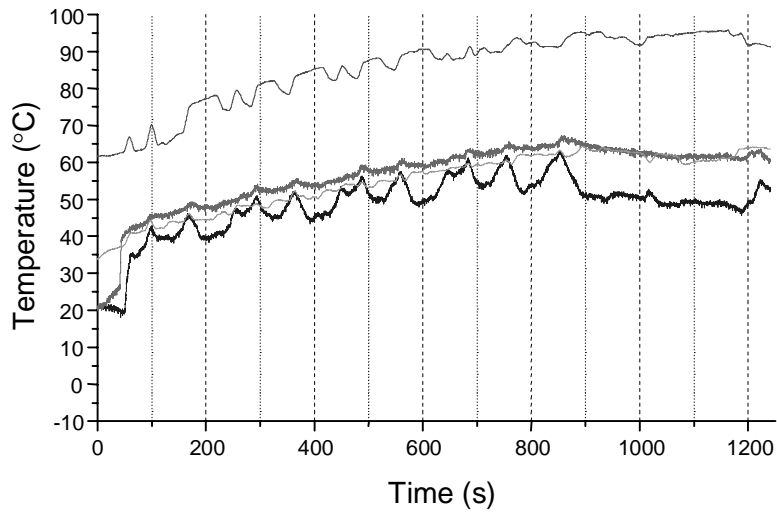
Figure A-6 Warm Test at 10°C Ambient
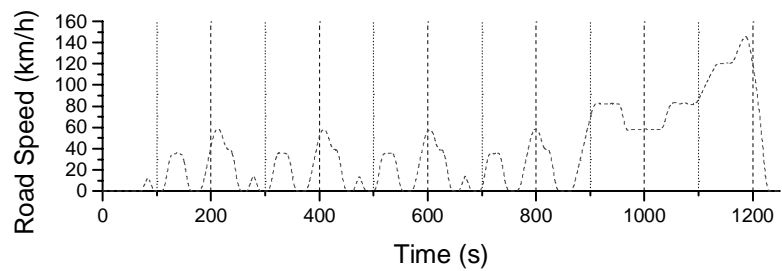
——Engine Sump ——CVT Sump ——To Cooler ——From Cooler
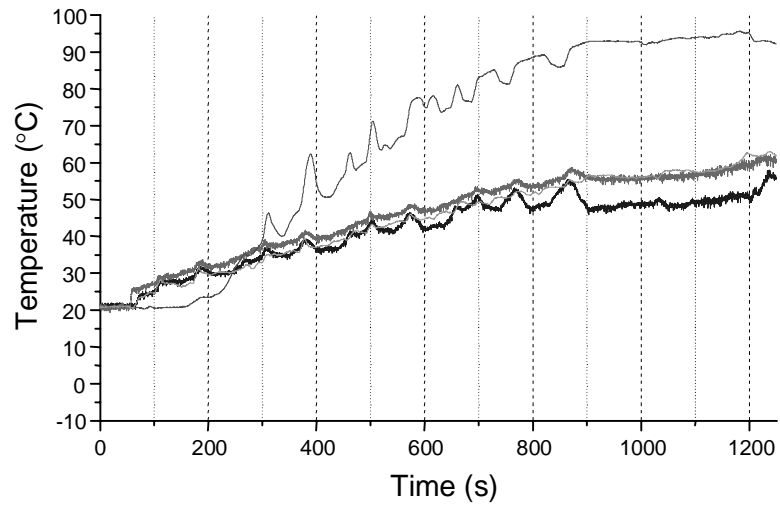
Figure A-7 Soak Test at 25°C Ambient
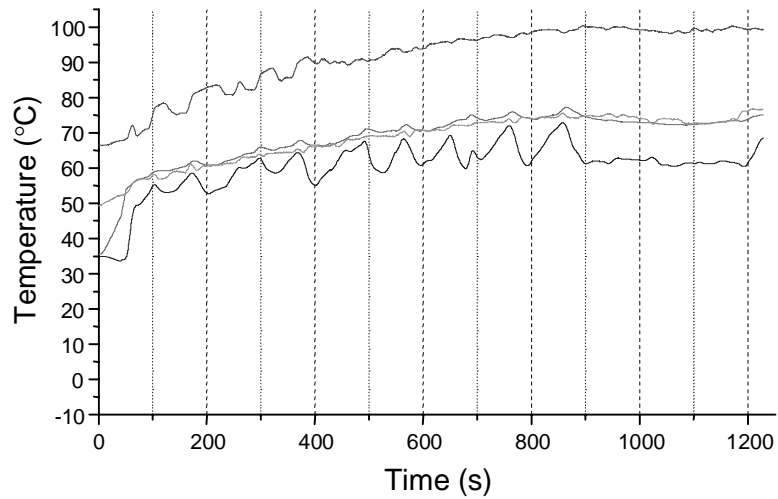
Figure A-8 Warm Test 25°C Ambient
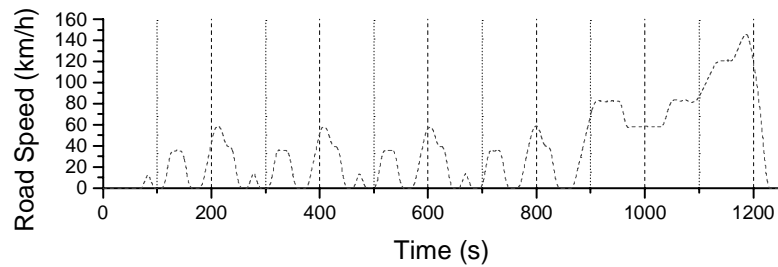
——Engine Sump ——CVT Sump ——To Cooler ——From Cooler

_____
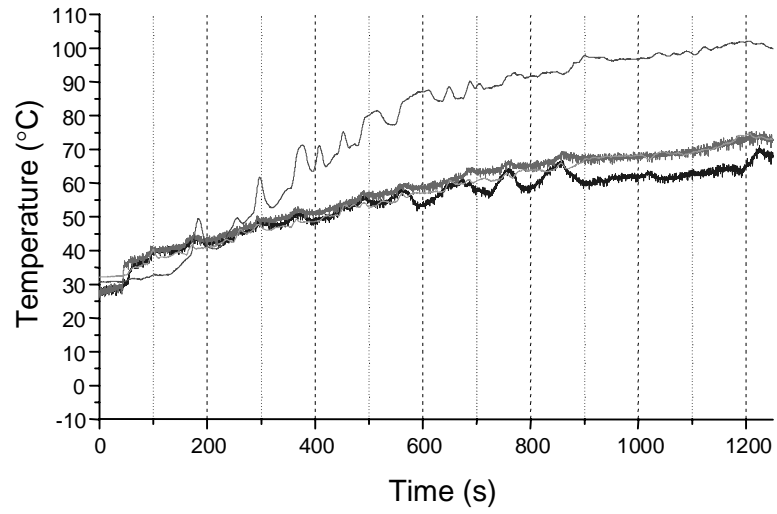
Figure A-9 Soak Test at 40°C Ambient
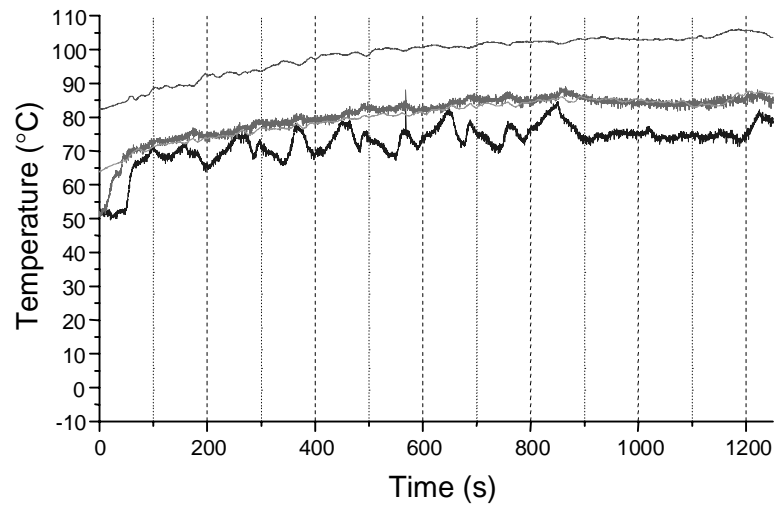
Figure A-10 Warm Test at 40°C Ambient
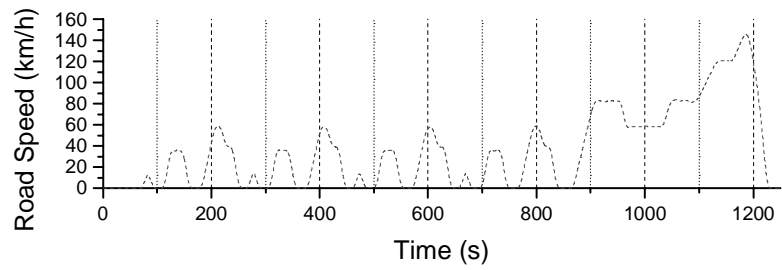
——Engine Sump ——CVT Sump ——To Cooler ——From Cooler

APPENDIX B

EMISSIONS RESULTS FOR ROVER 216 CVT VEHICLE TESTING DURING COMBINED ECE15 + EUDC DRIVE CYCLES

This appendix contains a complete set of the vehicle emissions data collected during the chassis dynamometer test program discussed in chapter 3 of this thesis. Results presented give exhaust gas O_2, CO_2,. CO, NOx and THC. Test results are produced at – 10, 0, 10, 25 and 40°C for both soak and warm conditions. The temperatures are plotted against test time along side a trace of the vehicle speed during the cycle.
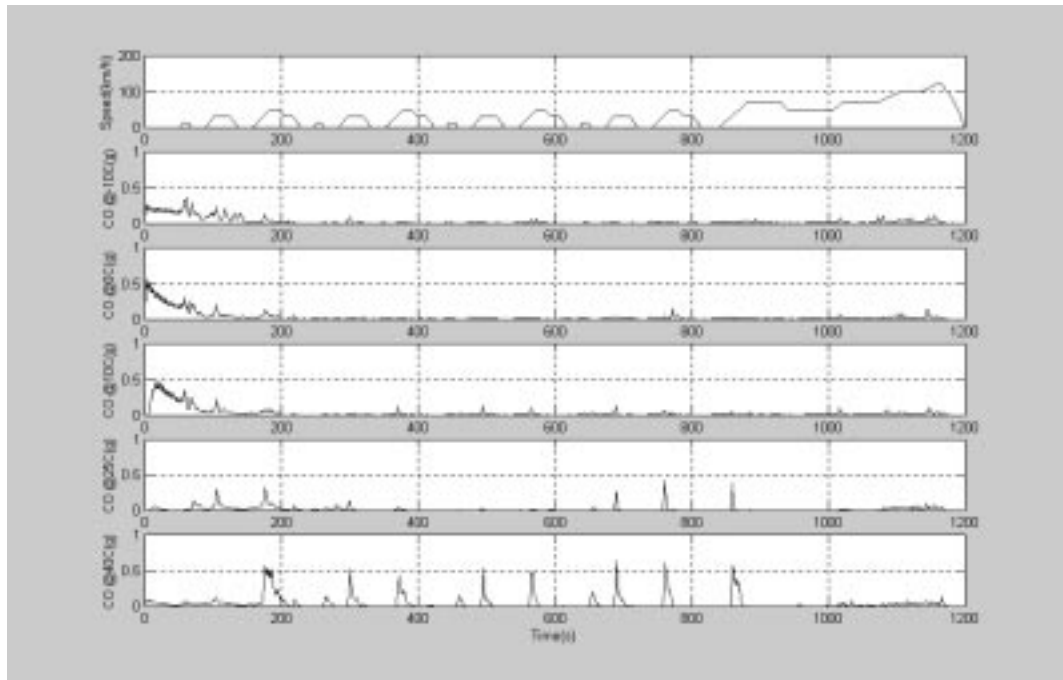
Figure B-1 CO Production for Soak Test Conditions
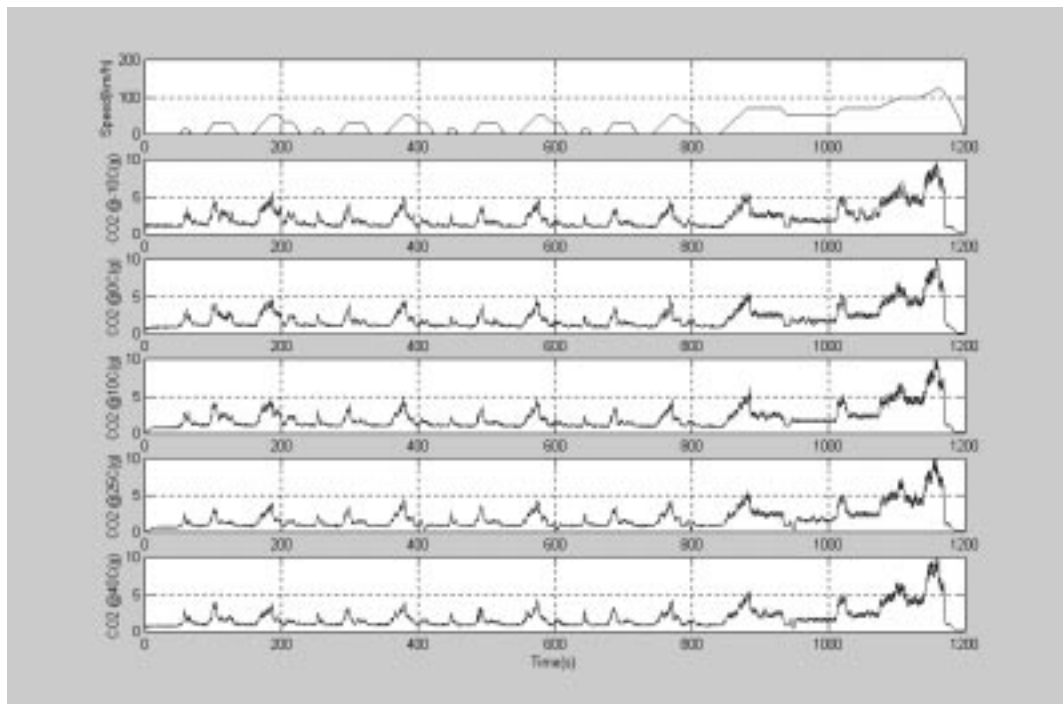
Figure B-2 CO2 Production for Soak Test Conditions
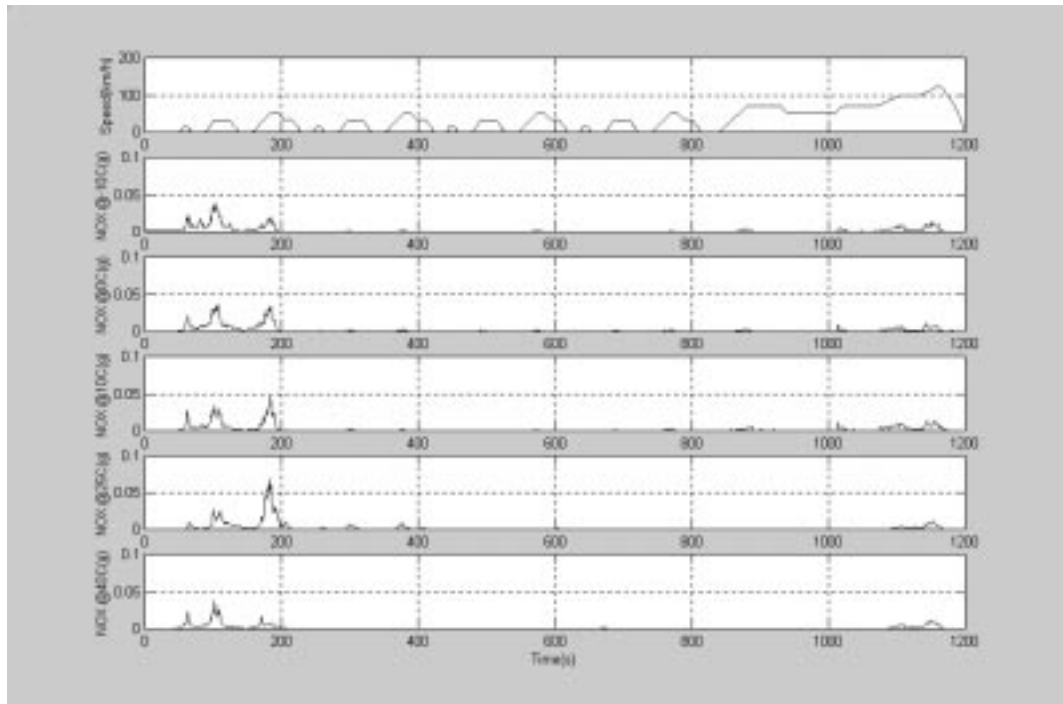
Figure B-3 NOx Production for Soak Test Conditions
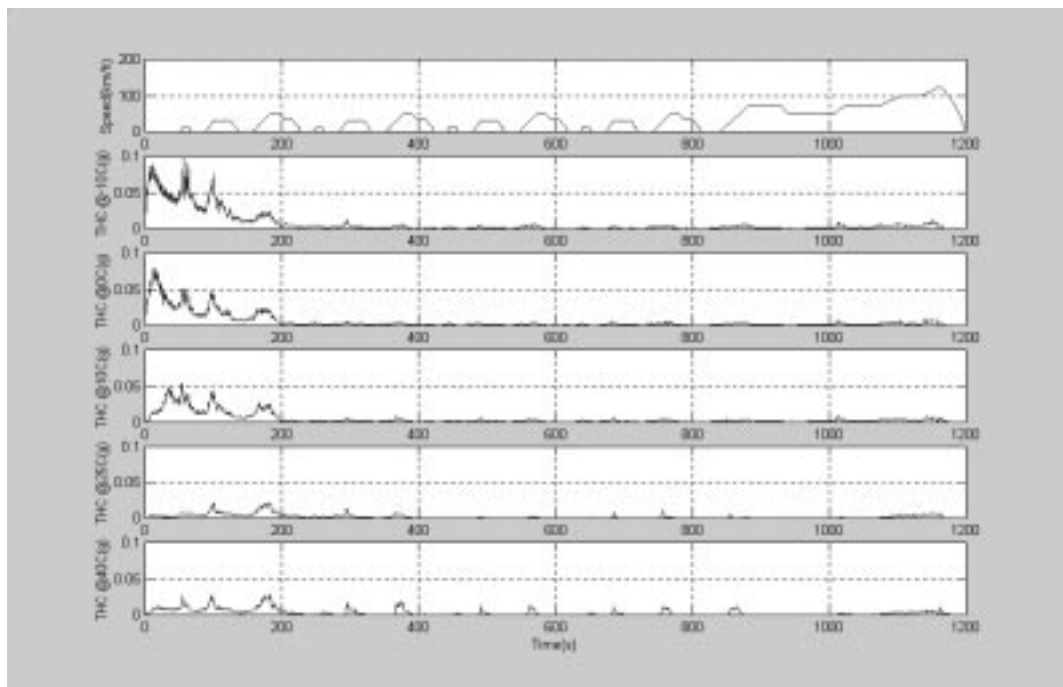
Figure B-4 THC Production for Soak Test Conditions
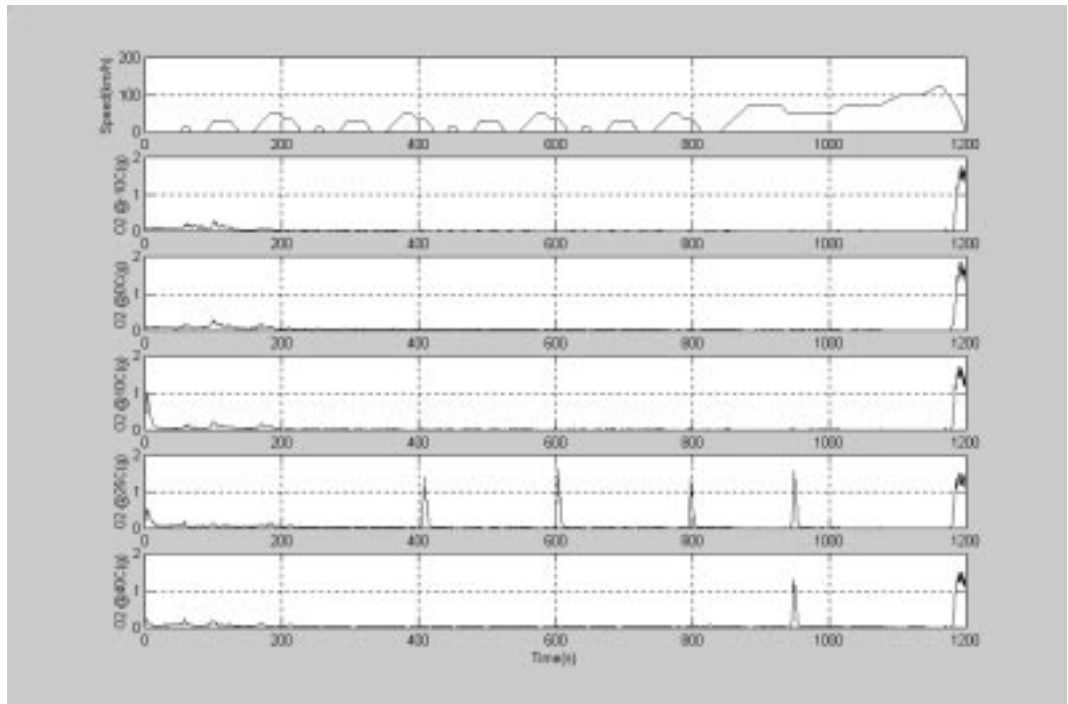
Figure B-5 O2 Production for Soak Test Conditions
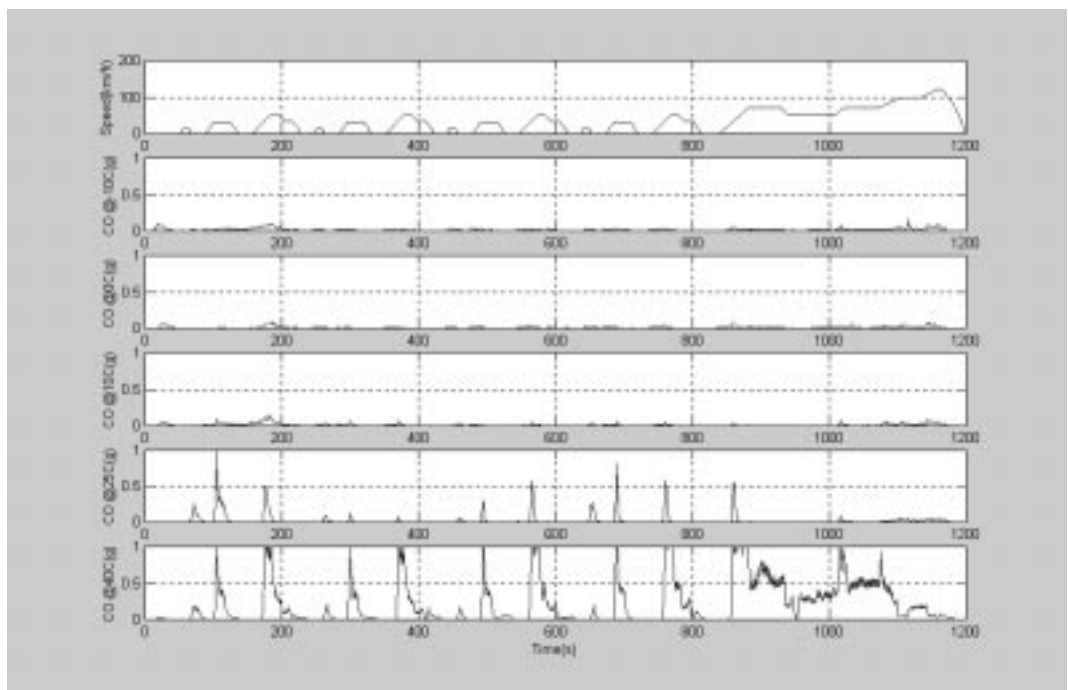
Figure B-6 CO Production for Warm Test Conditions
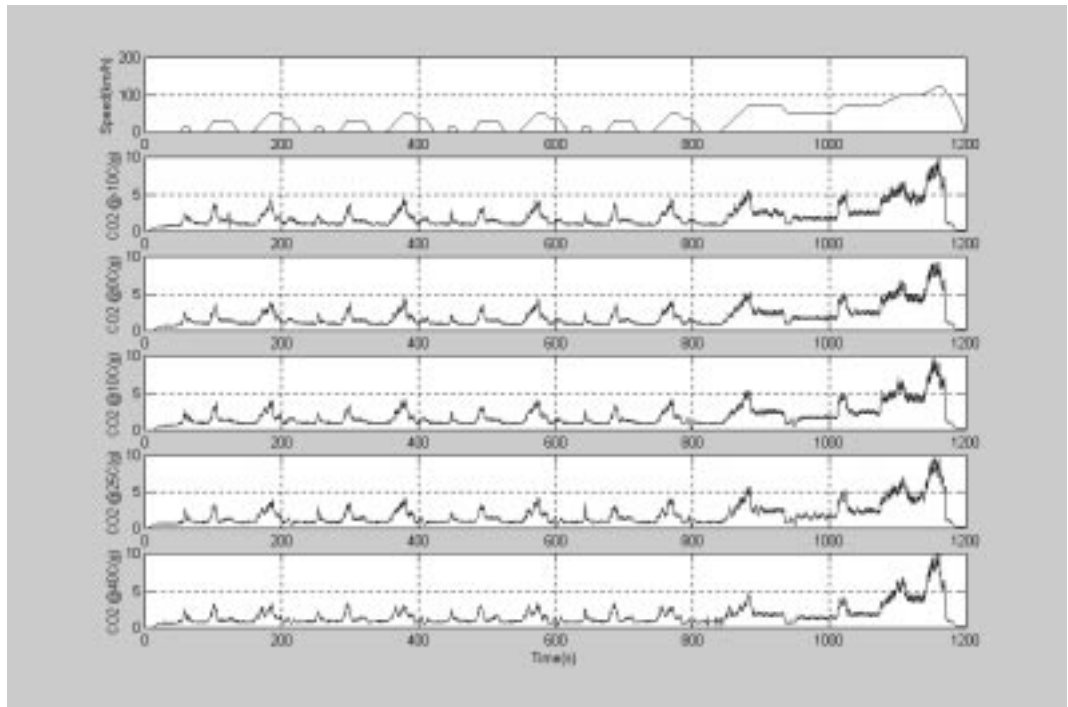
Figure B-7 CO2 Production for Warm Test Conditions
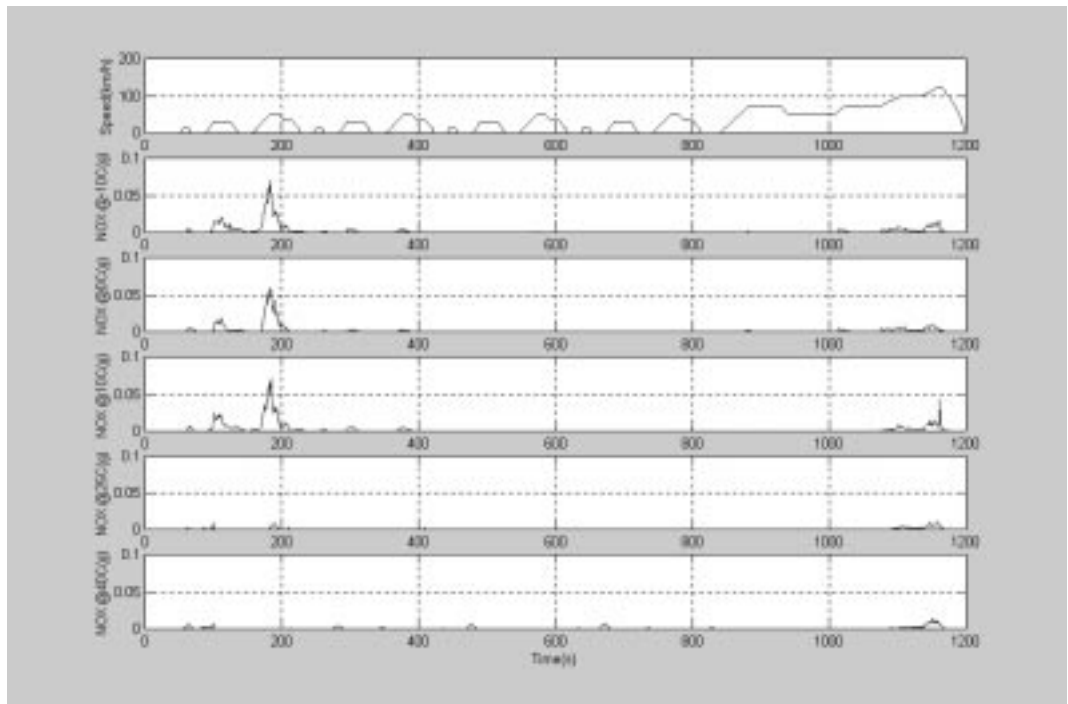
Figure B-8 NOx Production for Warm Test Conditions
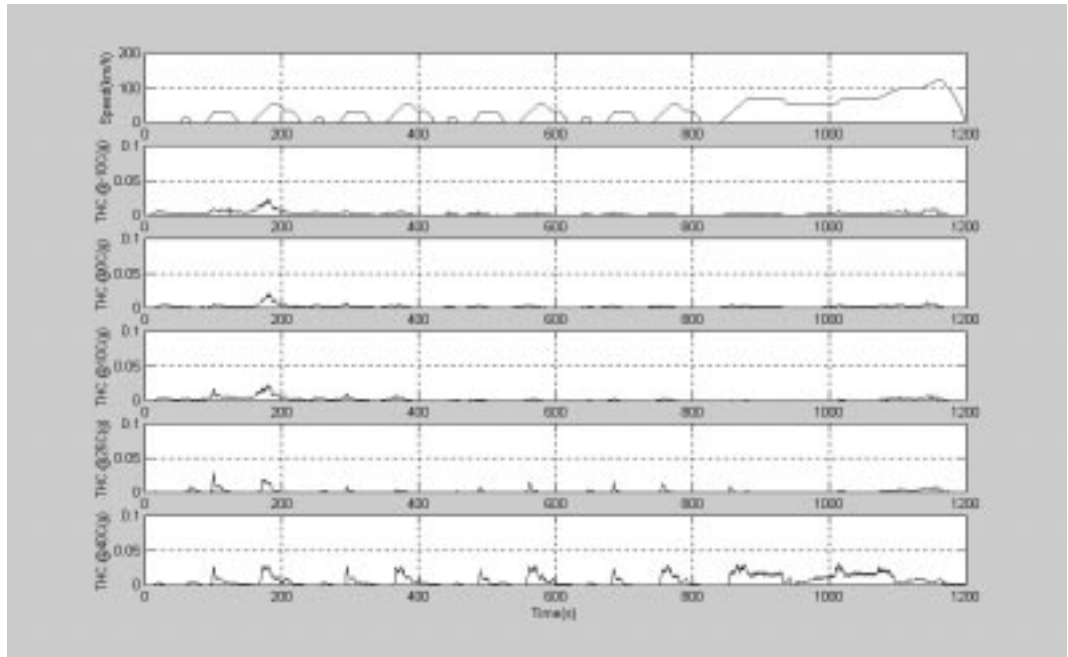
Figure B-9 THC Production for Warm Test Conditions
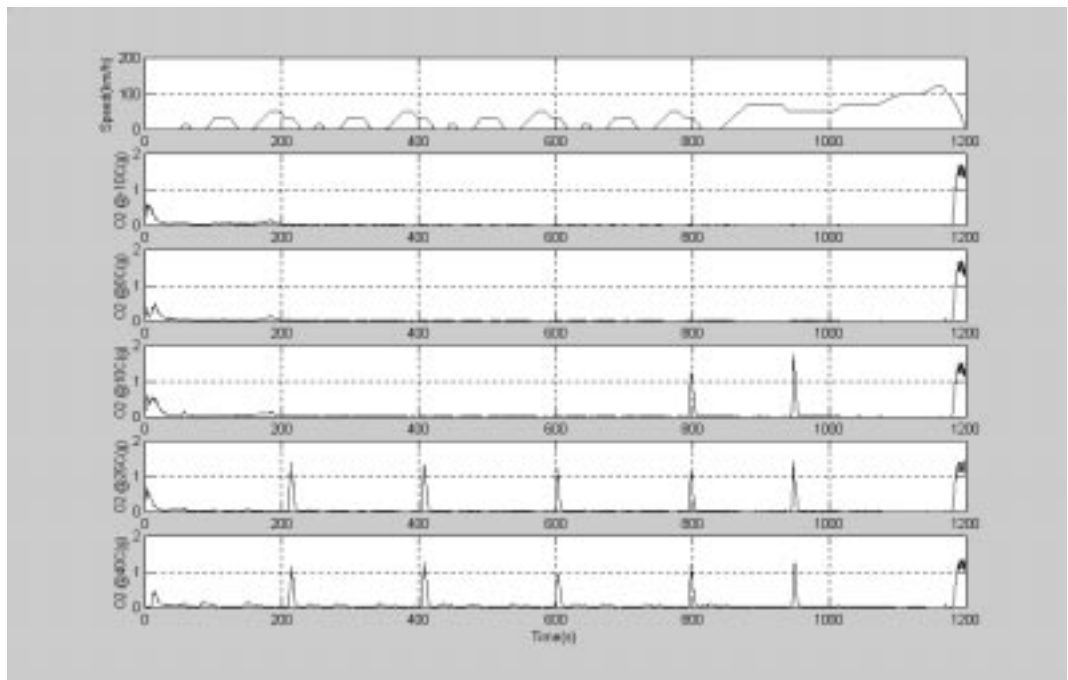
Figure B-10 O2 Production for Warm Test Conditions

APPENDIX C

MATLAB MODELLING CODE FOR

BELT LOSS PREDICTIONS

This appendix contains a typical MATLAB m file of the code used to describe all the belt torque loss mechanisms and belt slip.

```
%%%%%%%%%%%%%%%%%%%%%%%%%%%%%%%%%%%%%%%%%%%%%%%%%%%%%%%%%
%%%%% Belt program models geometry of belt for given ratio and
%%%%% calculates torque losses based upon pulley deflection
%%%%%% model, relative motion between bands and segments and belt
%%%%%% slip theory based upon existance of gaps
%%%%%% Written By Sam Akehurst
%%%%%%%%%%%%%%%%%%%%%%%%%%%%%%%%%%%%%%%%%%%%%%%%%%%%%%%%%


% Data input
close all;
clear all;
bratio=0.5;                             % Set ratio condition
all=[];
RPMIN=[];
STASH=[];
for rpmin=2000:500:4000;                % Set Input Speed Range as an array
  VSLIPRI=[];                           % Initialise empty matrices for filling
  TQ_BAND_PRI=[];
        TQ_BAND_SEC=[];
        TLOSS_SLIDE_PRI=[];
        TLOSS_SLIDE_SEC=[];
        SEG_CSA=[];
        MU_SET=[];
        CX=[];
        EXT_BAND=[];
        COM_SEG=[];
        VSLISEC=[];
        TQ_WEDGE=[];
        TQ_RADIAL=[];
        PRESS=[];


        x=155e-03;                      % Centre distance between pulleys
        tseg=1.46e-03;                  % Segment thickness
        lact=0.6486;                    % Length of Belt
        theta=(11/180)*pi;              % Half Pulley Wedge Angle
        diff=5;
        rsec=0.08;                      % Preliminary guess of rsec for iterative loop to find ratio
        n=1;


        % Itteraive loop to find pulley radii and wrap angles from belt length and ratio
        while diff > 0.0001;
                rpri=rsec./bratio;
                alpha=asin((rsec-rpri)/x);
                betap=pi-2*alpha;
                betas=pi+2*alpha;
                lnew=rpri.*betap+rsec.*betas+2.*sqrt(x^2-(rsec-rpri).^2);
                diff=lnew-lact;
                rsec=rsec-.1*diff;
                diff=abs(diff);
```

_____

```
            n=n+1;
        end
    lstrut=sqrt(x^2-(rsec-rpri).^2);   %length of belt strut running between pulleys
    betamin=min(betap,betas);
    win=rpmin*2*pi/60;
    wpri=win;
    wsec=wpri/(rsec/rpri);                          %Ideal secondary pulley speed

    areas=0.97190e-02;                              % CSA of secondary actuator
Fspring=750;                                        % Secondary pulley spring force

    vel=wpri*rpri;
    vbelt=vel;
    vseg=vbelt;
    massb=1.039/0.6486;                             %belt mass in kg/m
    vbelt_seg=vbelt/tseg;                           %belt speed in segments per second

    % Calculate Tension distribution in bands

    nband=12;                                       %number of bands
    tband=0.217e-03;                                %band thickness
    band_width=20e-3;                               %width of both band packs
    drad=3e-03;                                     %radial offset of band 1 relative to rocking edge
    rpri_band(1)=rpri+drad;
    rsec_band(1)=rsec+drad;

    vband_req_sec(1)=rsec_band(1)*wsec;
    vband_req_pri(1)=rpri_band(1)*wpri;
    vband_adopt(1)= (vband_req_pri(1)+vband_req_sec(1))/2;


    rel_vband_req_pri(1)=vband_req_pri(1)-vbelt;
    rel_vband_req_sec(1)=vband_req_sec(1)-vbelt;

    rel_vband_strut(1)=vband_adopt(1)-vbelt;
    rel_vband_pri(1)=rel_vband_strut(1)-rel_vband_req_pri(1);
    rel_vband_sec(1)=rel_vband_strut(1)-rel_vband_req_sec(1);


%Calculate relative speed between all band members

    for i=2:nband

    rpri_band(i)=rpri_band(i-1)+tband;
    rsec_band(i)=rsec_band(i-1)+tband;
    vband_req_pri(i)=rpri_band(i)*wpri;             % primary band speeds required due to geometry
    vband_req_sec(i)=rsec_band(i)*wsec;             % secondary band speeds required due to geometry
    rel_vband_req_pri=vband_req_pri(i)-vband_req_pri(i-1); %required difference in relative speed for no motion
    rel_vband_req_sec=vband_req_sec(i)-vband_req_sec(i-1); %required difference in relative speed for no motion
```

```matlab
        vband_adopt(i)=(vband_req_pri(i)+vband_req_sec(i))/2;  % Adopted  band  speed  (mean  of  geometric
requirements)
        rel_vband_strut(i)=vband_adopt(i)-vband_adopt(i-1);         %calculate relative motion between bands in struts
        rel_vband_pri(i)=rel_vband_strut(i)-rel_vband_req_pri;
        rel_vband_sec(i)=rel_vband_strut(i)-rel_vband_req_sec;

    end

%%%%%%%%%%%%%%%%%%%%%%%%%%%%%%%%%%%%%%%%%%%%%%%%%%%%%%%%%%%%%%%%
%%%%
%%%% CHECK BELT MOTION ACHIEVED WITH ADOPTED VELOCITIES
%%%%%%%%%%%%%%%%%%%%%%%%%%%%%%%%%%%%%%%%%%%%%%%%%%%%%%%%%%%%%%%%

        time_belt_lap=lact/vbelt;
        timestrut=lstrut/vbelt;
        time_pri=rpri*betap/vbelt;
        time_sec=rsec*betas/vbelt;
        check=time_belt_lap-(2*timestrut)-time_pri-time_sec;
        strut_motion=(2*timestrut)*rel_vband_strut;
        pri_motion=time_pri*rel_vband_pri;
        sec_motion=time_sec*rel_vband_sec;
        total_motion=strut_motion+sec_motion+pri_motion;
%%%%%%%%%%%%%%%%%%%%%%%%%%%%%%%%%%%%%%%%%%%%%%%%%%%%%%%%%%%%%%%%

        for press=10e05:0.25e05:12e05
            Vslippri=[];
            Vslipsec=[];
            Tqout=[];
            COMP=[];
            Tq_band_pri=[];
            Tq_band_sec=[];
            FTRACT_pri=[];
            FTRACT_sec=[];
            FTRACT_pri_idle=[];
            FTRACT_sec_idle=[];
            TLOSS_slide_pri=[];
            TLOSS_slide_sec=[];
            Vslip_pri_idle=[];
            Vslip_sec_idle=[];
            Vslip_pri_gap=[];
            Vslip_sec_gap=[];
            Seg_csa=[];
            Mu_set=[];
            DELTAT=[];
            Tq_radial=[];
            Tq_wedge=[];
            K=[];
            J=[];
            Com_seg=[];
            Ext_band=[];
```

```
for TOUT=0:1:10
        % Fixed information

            force=(press*areas)+Fspring;
            Faxial_sec=force;
            Faxial_pri=Faxial_sec*betap/betas;

%%%%%%%%%%%%%%%%%%%%%%%%%%%%%%%%%%%%%%%%%%%%%%%%%%%%%%%%%%%%%%
%%%%
%%%% CALCULATE BAND LOSSES IN ARCS AND TENSION DISTRIBUTIONS
%%%%%%%%%%%%%%%%%%%%%%%%%%%%%%%%%%%%%%%%%%%%%%%%%%%%%%%%%%%%%%
            error=2;
            Cx=10000;
            z=0;
            mu_band=0.13

    end

    while error>1
            cx=Cx;
            z=z+1;
            resultant_pri(1)=2*Faxial_pri*tan(theta)+massb*betap*vbelt^2+abs(Cx)*betap/2;
            resultant_sec(1)=2*Faxial_sec*tan(theta)+massb*betas*vbelt^2+abs(Cx)*betas/2;
            T1=resultant_pri(1)*(1/betap-mu_band/2);
            T2=resultant_pri(1)*(1/betap+mu_band/2);
                    if bratio>1
                    deltaT=T2-T1;
                    elseif bratio<1
                    deltaT=T1-T2;
                    end

              Cx=(TOUT/rsec)-deltaT;
            error=abs(Cx-cx);
    end

    for i=2:nband
    resultant_pri(i)=resultant_pri(1)-((i-1)*resultant_pri(1)/nband);
    resultant_sec(i)=resultant_sec(1)-((i-1)*resultant_sec(1)/nband);
            end

     if bratio>1
            friction_pri=resultant_pri*mu_band;
            friction_sec=resultant_sec*mu_band*betap/betas;

            elseif bratio<1
            friction_pri=resultant_pri*mu_band*betas/betap;
            friction_sec=resultant_sec*mu_band;
```

```
            end

            torque_loss_pri_band=abs(friction_pri(1:nband).*rel_vband_pri/win);

            torque_loss_sec_band=abs(friction_sec(1:nband).*rel_vband_sec/win);
            torque_loss_arc_band=sum(abs(torque_loss_sec_band)+abs(torque_loss_pri_band));
            for i=1:9
                    deltaT_pri(i)=friction_pri(i)-friction_pri(i+1);
                    deltaT_sec(i)=friction_sec(i)-friction_sec(i+1);
            end

            deltaT_pri(10)=friction_pri(10);
            deltaT_sec(10)=friction_sec(10);
```

%%
%%%%This part of program calculates belt slip based upon gaps and ouptut torque
%%

```
            if abs(Cx)<30
        Cx=30;
        elseif abs(Cx)>30
        Cx=Cx;
        end
            gap_init=0;
            band_csa=nband*20e-03*0.217e-03;
            Esteel=206e09;
            ext_band=0.5*(T1+T2)*lact/(Esteel*band_csa);

            seg_csa=1.74142E-6+1.56364E-9*abs(Cx)-1.74032E-13*abs(Cx)^2;   %FROM   MICKLEM
DATA
            seg_csa_strut=10e-06;
            mu_set=0.125;        %set design coefficient for pulley contact

            nseg_pri=rpri*betap/tseg;;
            nseg_sec=betas*rsec/tseg;

            Fseg_pri=2*Faxial_pri/nseg_pri;

            Fseg_sec=2*Faxial_sec/nseg_sec;

            Rseg_pri=Fseg_pri/cos(theta);

            Rseg_sec=Fseg_sec/cos(theta);
            mseg=massb*tseg;
            Seg_csa=[Seg_csa seg_csa];
            nseg_sec_act=betap*rsec/tseg;
            nseg_pri_act=betas*rpri/tseg;
            if bratio>1
```

```
                                    dTseg_pri=deltaT/nseg_pri;
                                    dTseg_sec=deltaT/nseg_sec_act;


                    elseif bratio<1
                    dTseg_pri=deltaT/nseg_pri_act;
                    dTseg_sec=deltaT/nseg_sec;
                    end


                    if Cx>=0 %define gap slip to occur at primary pulley and primary pulley to be compressive
loading arc

                    k=0;
                    mu=mu_set+0.1;
                            while mu>mu_set

                            k=k+1;
                            Ftract_pri=Cx/k+dTseg_pri;     %tractive force in low at primary is Cx + dT
                            mu=Ftract_pri/Rseg_pri;
                            end


                    ang_act_pri=k*tseg/rpri;
                    ang_idle_pri=betap-ang_act_pri; %calculate size of idle angle

         com_seg=(abs(Cx)*(0.5*k*tseg+0.5*(rsec*betas)))/(Esteel*seg_csa)+lstrut*abs(Cx)/(Esteel*seg_csa_strut);        %
CALCULATE COMPRESSION OF STRUT OF SEGMENTS
                                    tot_gap=gap_init+ext_band+com_seg;
                                    time_idle_pri=ang_idle_pri*rpri/vbelt;
                                    vslip_pri_gap=tot_gap/time_idle_pri;
                                    nseg_act_pri=k;               %segments in the active arc of the belt
                                    nseg_idle_pri=nseg_pri-k;      %segments in the idle arc of the belt

                                    Ftract_sec=(Cx/nseg_sec)+dTseg_sec;

                                    mupri=mu;
                                    Ftract_pri_idle=dTseg_pri;
                                    mu_pri_idle=Ftract_pri_idle/Rseg_pri;
                                    vslip_pri_idle=vslip_pri_gap*abs(mu_pri_idle/mupri);
                                    musec=Ftract_sec/Rseg_sec;

                                            vslip_pri=vslip_pri_gap+vslip_pri_idle;
                                            vslip_sec=vslip_pri*abs(musec/mupri);
                                            vslip_sec_gap=0;
                                            K=[K k];
                                            FTRACT_pri=[FTRACT_pri Ftract_pri];
                                            FTRACT_pri_idle=[FTRACT_pri_idle Ftract_pri_idle];
                                            FTRACT_sec=[FTRACT_sec Ftract_sec];
                                            Vslip_pri_idle=[Vslip_pri_idle vslip_pri_idle];
                                            Vslip_sec_idle=[Vslip_sec_idle 0];
                                            Vslip_pri_gap=[Vslip_pri_gap vslip_pri_gap];
                                            Vslip_sec_gap=[Vslip_sec_gap 0];
                    elseif Cx<0 % Define gap slip to occur at secondary pulley
```

```
j=0;
mu=mu_set+0.1;

        while mu>mu_set

        j=j+1;
        Ftract_sec=-dTseg_sec+abs(Cx)/j;
        mu=Ftract_sec/Rseg_sec;


        end

ang_act_sec=j*tseg/rsec;
ang_idle_sec=betas-ang_act_sec; %calculate size of idle angle

com_seg=(abs(Cx)*(0.5*j*tseg+0.5*(rpri*betap)))/(Esteel*seg_csa)+lstrut*abs(Cx)/(Esteel*seg_csa_strut);        %
CALCULATE COMPRESSION OF STRUT OF SEGMENTS
                tot_gap=gap_init+ext_band+com_seg;

time_idle_sec=ang_idle_sec*rsec/vbelt;
vslip_sec_gap=tot_gap/time_idle_sec;
nseg_act_sec=j;                 %segments in the active arc of the belt
nseg_idle_sec=nseg_sec-j;       %segments in the idle arc of the belt
musec=mu;
Ftract_sec_idle=-dTseg_sec;
mu_sec_idle=Ftract_sec_idle/Rseg_sec;
vslip_sec_idle=vslip_sec_gap*mu_sec_idle/musec;
Ftract_pri=abs(Cx)/nseg_pri-dTseg_pri;

        mupri=Ftract_pri/Rseg_pri;

        J=[J j];
        vslip_sec=-(vslip_sec_gap+vslip_sec_idle);
        vslip_pri=-((mupri/musec)*vslip_sec);
        vslip_pri_gap=0;
        FTRACT_sec=[FTRACT_sec Ftract_sec];
        FTRACT_pri=[FTRACT_pri Ftract_pri];
        FTRACT_sec_idle=[FTRACT_sec_idle Ftract_sec_idle];
        Vslip_sec_idle=[Vslip_sec_idle vslip_sec_idle];
        Vslip_pri_idle=[Vslip_pri_idle 0];
        Vslip_sec_gap=[Vslip_sec_gap vslip_sec_gap];
        Vslip_pri_gap=[Vslip_pri_gap 0];
end


if Cx>0
Tloss_slide_pri=abs(vslip_pri*Rseg_pri*nseg_act_pri*mupri/win);
Tloss_slide_sec=abs(vslip_sec*Rseg_sec*nseg_sec*musec/win);
```

```
elseif Cx<0
Tloss_slide_pri=abs(vslip_pri*Rseg_pri*nseg_pri*mupri/win);
Tloss_slide_sec=abs(vslip_sec*Rseg_sec*nseg_act_sec*musec/win);
end
Mu_set=[Mu_set mu_set];
```

```
%%%%%%%%%%%%%%%%%%%%%%%%%%%%%%%%%%%%%%%%%%%%%%%%%%%%%%%%%%%%%%%%
%%%%
%%%% This section of the program will describe pulley geometry changes and
%%%% the associated losses
%%%%%%%%%%%%%%%%%%%%%%%%%%%%%%%%%%%%%%%%%%%%%%%%%%%%%%%%%%%%%%%%
```

```
%information described here for pulley deflections
delta_pri=rpri*Faxial_pri/0.6e7;          %primary pulley deflection
delta_sec=rsec*Faxial_sec/5e7;            %secondary pulley deformation

mu_seg_pri=0.13;
mu_seg_sec=0.13;

drad_pri=(delta_pri/2)/(tan(11*pi/180)); %Calculate radial movement to escape
drad_sec=(delta_sec/2)/(tan(11*pi/180));

rpri_exit=rpri+drad_pri;
rsec_exit=rsec+drad_sec;

phi_pri=acos(rpri/rpri_exit);
phi_sec=acos(rsec/rsec_exit);

vrel_pri=((2*(rpri_exit)^2)*wpri^2*(1-cos(phi_pri)))^0.5;
vrel_sec=((2*(rsec_exit)^2)*wsec^2*(1-cos(phi_sec)))^0.5;
eta_pri=atan((rpri_exit*wpri*sin(phi_pri))/(rpri_exit*wpri*cos(phi_pri)-wpri*rpri_exit));
eta_sec=atan((rsec_exit*wsec*sin(phi_sec))/(rsec_exit*wsec*cos(phi_sec)-wsec*rsec_exit));


chord_pri=rpri*tan(phi_pri);
chord_sec=rsec*tan(phi_sec);

nseg_wedge_pri=chord_pri/tseg;
nseg_wedge_sec=chord_sec/tseg;

Rseg_mean_pri=Rseg_pri/2; %mean resultant force in wedge
Rseg_mean_sec=Rseg_sec/2;
pow_loss_wedge_pri=nseg_wedge_pri*vrel_pri*Rseg_mean_pri*mu_seg_pri;
pow_loss_wedge_sec=nseg_wedge_sec*vrel_sec*Rseg_mean_pri*mu_seg_sec;

% Calculate pulley wedge torque loss

Tq_loss_pri=pow_loss_wedge_pri/win;
Tq_loss_sec=pow_loss_wedge_sec/win;
```

_____

```
                      Tloss_wedge_TOT=(Tq_loss_pri)+(Tq_loss_sec);


                      % Torque loss from radial penetration calcs


                      rad_pen_pri=rpri*Faxial_pri/0.6e7;
                      rad_pen_sec=rsec*Faxial_sec/5e7;


                      rad_move_pri=2*rad_pen_pri;
                      rad_move_sec=2*rad_pen_sec;


                      mu_rad_pri=0.13;
                      mu_rad_sec=0.13;


                      frict_seg_pri=mu_rad_pri*Rseg_pri;
                      frict_seg_sec=mu_rad_sec*Rseg_sec;


                      work_seg_pri=frict_seg_pri*rad_move_pri;
                      work_seg_sec=frict_seg_sec*rad_move_sec;


                      pow_seg_pri=vbelt_seg*work_seg_pri;
                      pow_seg_sec=vbelt_seg*work_seg_sec;


                      Tq_rad_pri=pow_seg_pri/win;
                      Tq_rad_sec=pow_seg_sec/win;


                      Tq_total_radial_pen=Tq_rad_pri+Tq_rad_sec;



                      Vslippri=[Vslippri vslip_pri];
                      Vslipsec=[Vslipsec vslip_sec];
                      Tqout=[Tqout TOUT];
                      COMP=[COMP Cx];
                      Com_seg=[Com_seg com_seg];


                      Ext_band=[Ext_band ext_band];


                      DELTAT=[DELTAT deltaT];
                      Tq_band_pri=[ Tq_band_pri sum(torque_loss_pri_band)];
                      Tq_band_sec=[ Tq_band_sec sum(torque_loss_sec_band)];
                      Tq_radial=[ Tq_radial Tq_total_radial_pen];
                      Tq_wedge=[ Tq_wedge Tloss_wedge_TOT];
                      TLOSS_slide_pri=[TLOSS_slide_pri Tloss_slide_pri];
                      TLOSS_slide_sec=[TLOSS_slide_sec Tloss_slide_sec];
                      end
              TLOSS_SLIDE_PRI=[TLOSS_SLIDE_PRI; TLOSS_slide_pri];
              TLOSS_SLIDE_SEC=[TLOSS_SLIDE_SEC; TLOSS_slide_sec];
              VSLIPRI=[VSLIPRI;Vslippri];
              CX=[CX;COMP];
              COM_SEG=[COM_SEG;Com_seg];
```

```
                    EXT_BAND=[EXT_BAND;Ext_band];
                    SEG_CSA=[SEG_CSA;Seg_csa];
                    MU_SET=[MU_SET;Mu_set];
                    VSLISEC=[VSLISEC;Vslipsec];
                    TQ_BAND_PRI=[TQ_BAND_PRI;Tq_band_pri];
                    TQ_BAND_SEC=[TQ_BAND_SEC;Tq_band_sec];
                    TQ_RADIAL=[TQ_RADIAL;Tq_radial];
                    TQ_WEDGE=[TQ_WEDGE;Tq_wedge];


        TQ_TOTAL=TQ_BAND_PRI+TQ_BAND_SEC+TQ_WEDGE+TQ_RADIAL+TLOSS_SLIDE_PRI+TLOSS_SLIDE
_SEC;
                    PRESS=[PRESS press];


                    end
        STASH= [ STASH TQ_TOTAL];
        RPMIN=[RPMIN,rpmin];
        figure (1);
        hold on
        surf(Tqout,PRESS/1e05,TQ_TOTAL)
        grid on
        view(30,30);
        xlabel('Output Torque(Nm)');
        ylabel('Secondary Pressure (bar)');
        zlabel('Torque Loss (Nm)');
        title('Torque Loss effects of Pressure, Torque and Speed');
        figure (2);
        hold on
        surf(Tqout,PRESS/1e05,TQ_WEDGE);
        grid on
        view(30,30);
        xlabel('Output Torque(Nm)');
        ylabel('Secondary Pressure (bar)');
        zlabel('Torque Loss (Nm)');

        title('Torque Loss due to pulley wedge')
        figure (3);
        hold on
        surf(Tqout,PRESS/1e05,TQ_RADIAL);
        grid on
        view(30,30);
        xlabel('Output Torque(Nm)');
        ylabel('Secondary Pressure (bar)');
        zlabel('Torque Loss (Nm)');
        title('Torque Loss due to pulley radial penetration')

        figure (4);
        hold on
        surf(Tqout,PRESS/1e05,TQ_BAND_PRI+TQ_BAND_SEC);
        grid on
        view(30,30);
```

```
        xlabel('Output Torque(Nm)');
        ylabel('Secondary Pressure (bar)');
        zlabel('Torque Loss (Nm)');
        title('Torque Loss due to Bands')

        figure (5);
        hold on
        surf(Tqout,PRESS/1e05,TLOSS_SLIDE_PRI+TLOSS_SLIDE_SEC);
        grid on
        view(30,30);
        xlabel('Output Torque(Nm)');
        ylabel('Secondary Pressure (bar)');
        zlabel('Torque Loss (Nm)');
        title('Torque Loss due to Segment Sliding')



        figure
        plot (Tqout,VSLIPRI)
        grid on
        rpm=num2str(rpmin);
        fric=num2str(mu_set);
        samthing=strcat('Primary pulley slip speed @',rpm,'rev/min & mu=',fric);
        title(samthing);
        xlabel('Variator Output Torque (Nm)');
        ylabel('Primary pulley slip speed (m/s)')
        figure
        plot(Tqout,VSLISEC)
        grid on
        samthing=strcat('Secondary pulley slip speed @',rpm,'rev/min & mu=',fric);

        title(samthing);
        xlabel('Variator Output Torque (Nm)');
        ylabel('Secondary pulley slip speed (m/s)');
        end

q=0;
NO_LOAD_LOSS_TOT=[];
for q=1:size(RPMIN,2)
NO_LOAD_LOSS_TOT=[NO_LOAD_LOSS_TOT STASH(:,1+((q-1)*size(Tqout,2)))]
end
plot(RPMIN,[NO_LOAD_LOSS_TOT]);
grid on

xlabel('Input Speed (rev/min)');
ylabel('Torque Loss (Nm)');
```